

**Calibration of a Building Energy Model Using Measured Data for a Research
Center**

Andreea Mihai

A Thesis
in
The Department
of
Building, Civil & Environmental Engineering

Presented in Partial Fulfillment of the Requirements
for the Degree of Master of Applied Sciences (in Building Engineering)
at
Concordia University
Montreal, Quebec, Canada

January 2014

© Andreea Mihai, 2014

ABSTRACT

Calibration of a Building Energy Model Using Measured Data for a Research Center

Andreea Mihai

This thesis proposes an evidence-based bottom-up methodology to calibrate a building energy model starting at the zone level, and finishing with the whole building level. The calibration is based as much as possible on measurements taken from the existing Building Automation System (BAS). This study presents the calibration at the zone and air handling unit level.

First a literature review is presented, followed by the evidence-based bottom-up methodology. Next, the case study building is described, along with the extraction and analysis of the monitored data. Then the building model is created and calibrated at the zone level based on the supply air flow rate to each zone. The calibration at the air handling unit level is based on: i) the supply air flow rate leaving the air handling unit; ii) the supply air temperature and iii) the cooling coil load. The evaluation of the calibration quality is proposed to be performed in three stages: i) graphical representation; ii) statistical indices (RMSE, CV-RMSE, NMBE); and iii) paired difference statistical hypothesis testing.

A sensitivity analysis is performed and it is found that the energy model is not sensitive to changes in the building envelope parameters, but rather to variations in internal loads.

Two approaches for representing the schedules of internal loads are compared and the proposed approach, where the internal loads are derived from measured cooling load in each zone, is recommended.

ACKNOWLEDGMENTS

First, I would like to thank my supervisor, Dr. Radu G. Zmeureanu, for his help, support and for teaching me to be patient. His joyful character and knowledge in the domain of building energy simulation have helped me enormously to understand and pass this challenge in my life. I also need to give special thanks to my godfather, Ovidiu Parvulescu, for making mathematics seem like a piece of cake and to my teacher from “Tudor Vianu” high school, Ioana Stoica, for making me understand and like physics.

I would like to acknowledge the financial support from NSERC Smart Net-Zero Energy Building Strategic Research Network and the Faculty of Engineering and Computer Science of Concordia University. This thesis could not have been completed without the collaboration of the Concordia Facilities Management, Stephan Drolet, Yves Gilbert, Steven Troughon, Luc Lagace and Mathieu Laflamme. I would like to thank Mr. Christian Houle, from Siemens, for taking the time to collaborate with us regarding the measured data.

Special thanks to my friends and colleagues from the undergraduate and graduate programs at Concordia University. I enjoyed every moment spent together, and I need to thank you all so much, for putting up with me through my best and worst days. I wish you success and happiness in your careers and life.

Lastly, I appreciate the constant support from my brother Alexandru-Cezar and from my parents, Gavrilă and Dumitru Mihai. I am so grateful for having such a great, loving family.

This thesis is dedicated to my godfather, Ovidiu Parvulescu.

Thank you for teaching me to believe in myself!

Table of Contents

LIST OF FIGURES	IX
LIST OF TABLES	XXI
CHAPTER 1 INTRODUCTION	1
1.1 PROBLEM STATEMENT	1
1.2 SCOPE	2
CHAPTER 2 LITERATURE REVIEW	3
2.1 SCOPE OF CALIBRATION	3
2.2 PUBLICATIONS AND STUDIES.....	7
2.3 GUIDELINES FOR VERIFICATION AND VALIDATION OF CALIBRATION.....	21
2.4 CONCLUSIONS FROM LITERATURE REVIEW	25
CHAPTER 3 METHODOLOGY	26
3.1 OBJECTIVE	26
3.2 EVIDENCE-BASED BOTTOM-UP CALIBRATION APPROACH.....	26
CHAPTER 4 MONITORED DATA AT THE CENTRE FOR STRUCTURAL AND FUNCTIONAL GENOMICS BUILDING	29
4.1 DESCRIPTION OF THE BUILDING	29
4.2 DESCRIPTION OF THE HVAC SYSTEM	30
4.2.1 Air side system	30
4.2.2 Water side system	34
4.2.3 Heat recovery system.....	37
4.3 MONITORED DATA ANALYSIS AND EXTRACTION.....	38
CHAPTER 5 CALIBRATION OF THE EQUEST MODEL FOR SUPPLY AIR FLOW RATES TO ZONES	59
5.1 PRELIMINARY CALIBRATION OF SUPPLY AIR FLOW RATE TO ZONES	59
5.2 EVALUATION OF THE CALIBRATION QUALITY	70
5.2.1 Graphical representation	70
5.2.2 Statistical indices	74
5.2.3 Hypothesis testing	77
5.3 IMPROVEMENT OF PRELIMINARY CALIBRATION	85
CHAPTER 6 CALIBRATION OF THE EQUEST MODEL OF THE AIR HANDLING UNIT	92
6.1 AIR HANDLING UNIT MODEL INPUTS.....	92
6.2 ANALYSIS OF THE SUMMATION OF AIR FLOW RATES TO ZONES	96
6.3. RESULTS OF THE CALIBRATION OF THE AIR HANDLING UNIT SUPPLY AIR FLOW RATE	106
6.3.1 Graphical representation.....	106
6.3.2 Statistical indices analysis.....	110
6.3.3 Hypothesis testing.....	111
6.4 CALIBRATION OF THE SUPPLY AIR TEMPERATURE IN THE AIR HANDLING UNIT.....	113
6.4.1 Graphical representation.....	113
6.4.2 Statistical indices analysis	117
6.4.3 Hypothesis testing.....	117
6.5 CALIBRATION OF THE COOLING COIL LOAD IN THE AIR HANDLING UNIT.....	119

6.5.1 Graphical representation.....	119
6.5.2 Statistical indices	124
6.5.3 Hypothesis testing.....	124
6.5.4 Analysis of cooling coil load based on fraction of fresh air entering the building	126
6.5.5 Cooling coil load based on measured mixed air enthalpy measured on site	139
CHAPTER 7 SENSITIVITY ANALYSIS	147
CHAPTER 8 IMPACT OF THE REPRESENTATION OF INTERIOR LOADS ON THE CALIBRATION AT THE ZONE LEVEL	159
8.1 ZONE AIR TEMPERATURE ANALYSIS.....	165
8.1.1 Graphical representation	166
8.1.2 Statistical indices	167
8.1.3 Hypothesis testing	168
8.2 ANALYSIS OF SUPPLY AIR FLOW RATE TO EACH ZONE	168
8.2.1 Graphical representation	169
8.2.1 Statistical indices	171
8.2.3 Hypothesis testing	174
8.3 ANALYSIS OF COOLING LOAD IN EACH ZONE	177
8.3.1 Graphical representation	177
8.3.2 Statistical indices	178
3.3.3 Hypothesis testing	179
CHAPTER 9 CONCLUSIONS.....	181
REFERENCES	187
APPENDICES	193
APPENDIX A: CALIBRATION RESULTS AT THE ZONE LEVEL	193
APPENDIX B: HISTOGRAMS OF THE DIFFERENCE BETWEEN PREDICTED AND MEASURED SUPPLY AIR FLOW RATE TO EACH ZONE	238
APPENDIX C: HISTOGRAMS FOR THE DIFFERENCE BETWEEN THE PREDICTED AND MEASURED SUMMATION OF AIR FLOW RATES SUPPLIED TO ZONES	244
APPENDIX D: RESULTS OF PREDICTIONS FOR EACH ZONE WITH APPROACH A AND B FROM 18 TH TO 20 TH JULY 2012	245

List of Figures

Figure 3.1: Calibration phases of the bottom-up approach	27
Figure 4.1: Air handling units 101 and 102	31
Figure 4.2: General Evacuation (System VE1/VE2-103-400).....	32
Figure 4.3: Heating water loop in Genomic Research Center	35
Figure 4.4: Cooling water loop	36
Figure 4.5: Heat recovery system	38
Figure 4.6: Zone locations in the Genomic research center, Concordia University	40
Figure 4.7: Hourly indoor air temperature variation with time for zone 2.4 SW from 18-20 July	44
Figure 4.8: Hourly indoor air temperature variation with time for zone 2.4 SW for the summer period	44
Figure 4.9: Daily indoor air temperature variation with time for zone 2.4 SW for the summer period	44
Figure 4.10: Hourly supply air flow rate variation with time for zone 2.4 SW from 18-20 July ..	45
Figure 4.11: Hourly supply air flow rate variation with time for zone 2.4 SW during the summer period	45
Figure 4.12: Daily supply air flow rate variation with time for zone 2.4 SW during the summer period	46
Figure 4.13: Hourly cooling load variation with time for zone 2.4 SW from 18-20 July.....	46
Figure 4.14: Hourly cooling load variation with time for zone 2.4 SW for the summer period....	47
Figure 4.15: Daily cooling load variation with time for zone 2.4 SW for the summer period	47
Figure 4.16: Measured hourly indoor air temperature signature for the summer period for zone 2.4 SW	48
Figure 4.17: Measured daily indoor air temperature signature for the summer period for zone 2.4 SW	48
Figure 4.18: Measured hourly supply air flow rate signature for zone 2.4 SW for the summer period	49
Figure 4.19: Measured daily supply air flow rate signature for zone 2.4 SW for the summer period	49
Figure 4.20: Measured hourly outdoor air temperature variation with time for the whole summer period at Loyola	53
Figure 4.21: Measured daily outdoor air temperature variation with time for the whole summer period	54
Figure 4.22: Measured hourly outdoor air temperature variation with time from the 18th-20th July.....	54
Figure 5.1: Measured vs. predicted hourly supply air flow rate in zone 1.6 NE over three days in June 2012, with constant thermostat set-point.....	63
Figure 5.2: Measured vs. predicted hourly supply air flow rate in zone 1.6 NE over three days in June 2012, with thermostat setup during unoccupied hours	63
Figure 5.3: Measured vs. predicted hourly supply air flow rate in zone 2.4 SW over three days in June 2012, with constant thermostat set-point temperature.....	64
Figure 5.4: Measured vs. predicted hourly supply air flow rate ion zone 2.4 SW over three days in June 2012, with thermostat setup during unoccupied hours	64
Figure 5.5: Schedule for internal loads in zone 1.4 SW	65

Figure 5.6: Schedule for internal loads in zone 3.1 NE	65
Figure 5.7: Measured vs. predicted air flow rate for zone 1.4 SW with CWEC and Montreal 2012 weather files, for three days in July 2012	68
Figure 5.8: Measured vs. predicted air flow rates for zone 1.6 NE, without and with fins, overhangs and building shades, for three days in July 2012.....	69
Figure 5.9: Research Centre for Structural and Functional Genomics of Concordia University...	70
Figure 5.10: Predicted vs. measured hourly supply air flow rate to zone 1.6 NE, 18-20 July 2012	71
Figure 5.11: Predicted vs. measured hourly cooling load for the zone 1.6 NE, 18-20 July 2012..	72
Figure 5.12: Measured vs. predicted air flow rate for zone 1.6 NE.....	72
Figure 5.13: Measured vs. predicted cooling load for zone 1.6 NE.....	72
Figure 5.14: Histogram for the difference between hourly predicted and measured air flow rate for zone 1.6 NE.....	80
Figure 5.15: Histogram for the difference between hourly predicted and measured air flow rate for zone 3.1 NE.....	80
Figure 5.16: Predicted vs. measured air flow rate for zone 2.5 SE, for the entire summer period	82
Figure 5.17: Histogram of measured air flow rate for zone 3.1 NE.....	87
Figure 5.18: Histogram of predicted air flow rate for zone 3.1 NE.....	87
Figure 5.19: Histogram of the difference between predicted and measured air flow rates for zone 3.1 NE	88
Figure 6.1: Coil bypass conditions that are needed to calculate the coil bypass factor	94
Figure 6.3: Cold deck air temperature vs. outdoor air temperature	96
Figure 6.4: Measured vs. predicted hourly summation of air flow rates supplied to zones for the summer period	97
Figure 6.5: Hourly measured and predicted air flow rates supplied to zones vs. outdoor air temperature	98
Figure 6.6: Measured vs. predicted hourly summation of air flow rates supplied to zones from July 18 th to 20 th	99
Figure 6.7: Measured vs. predicted air flow rate signatures (supplied to zones) from July 18 th to 20 th	99
Figure 6.8: Measured vs. predicted hourly summation of air flow rates supplied to zones from August 14 th to 16 th	100
Figure 6.9: Measured vs. predicted air flow rate signatures (supplied to zones) from August 14 th to 16 th 2012	100
Figure 6.10: Measured vs. predicted daily summation of air flow rates supplied to zones for the summer period.	101
Figure 6.11: Measured vs. predicted daily air flow signatures (supplied to zones) for the summer period	102
Figure 6.12: Histogram of the difference between predicted and measured summation of air flow rates supplied to the zones for the summer period.....	103
Figure 6.13: Hourly measured supply airflow rate leaving the air handling unit vs. summation of measured airflow rates to zones for the summer period	105
Figure 6.14: Daily measured supply airflow rate leaving the air handling unit vs. summation of airflow rates to zones for the summer period.....	105

Figure 6.15: Measured vs. predicted air flow rate supplied by the air handling unit from the 18 th to the 20 th of July.....	106
Figure 6.16: Measured vs. predicted air flow rate supplied by the air handling unit from the 14 th to the 16 th of August.....	106
Figure 6.17: Hourly measured vs. predicted airflow rate leaving the AHU for the summer period	107
Figure 6.18: Daily measured vs. predicted airflow rate leaving the AHU for the summer period	107
Figure 6.19: Measured vs. predicted air handling unit supply air flow rate signatures from the 18 th to the 20 th of July.....	108
Figure 6.20: Measured vs. predicted air handling unit supply air flow rate signatures from the 14 th to the 16 th of August.....	108
Figure 6.21: Hourly signatures of measured and predicted airflow rate for the summer period .	108
Figure 6.22: Daily signatures of measured and predicted airflow rate for the summer period....	109
Figure 6.23: Measured vs. predicted hourly supply air flow rate leaving the AHU for the summer period	109
Figure 6.24: Measured vs. predicted daily supply air flow rate leaving the AHU for the summer period	110
Figure 6.25: Histogram of the difference between predicted and measured hourly airflow rates	111
Figure 6.26: Histogram of the difference between predicted and measured daily airflow rates..	111
Figure 6.27: Hourly measured vs. predicted supply air temperature from 18-20 July	113
Figure 6.28: Hourly measured vs. predicted supply air temperature from 14-16 August.....	114
Figure 6.29: Hourly measured vs. predicted supply air temperature from the air handling unit for the summer period.....	114
Figure 6.30: Daily measured vs. predicted supply air temperature from the air handling unit....	114
Figure 6.31: Hourly predicted vs. measured supply air temperature signature for the summer period	115
Figure 6.32: Hourly measured and predicted supply air temperature signatures from 18 th -20 th July 2012	116
Figure 6.33: Hourly measured and predicted supply air temperature signatures from 14 th -16 th August 2012.....	116
Figure 6.34: Daily predicted vs. measured supply air temperature signature for the summer period 2012	116
Figure 6.37: Histogram of the hourly difference between the predicted and measured supply air temperature for the summer season	118
Figure 6.38: Histogram of the daily difference between the predicted and measured supply air temperature for the summer season	118
Figure 6.39: Hourly predicted vs. measured cooling coil load in the AHU from 18 th -20 th July 2012	119
Figure 6.40: Hourly predicted vs. measured cooling coil load in the AHU from 14 th -16 th August 2012	120
Figure 6.41: Hourly predicted vs. measured cooling coil load in the AHU for the summer period	120
Figure 6.42: Daily predicted vs. measured cooling coil load in the AHU	120
Figure 6.43: Predicted vs. measured hourly cooling coil load signatures from 18-20 July	121

Figure 6.44: Predicted vs. measured hourly cooling coil load signatures from 14-16 August	121
Figure 6.45: Predicted vs. measured hourly cooling coil load signatures for the summer period	122
Figure 6.46: Predicted vs. measured daily cooling coil load signatures for the summer period..	122
Figure 6.47: Measured vs. predicted hourly cooling coil load for the summer period	123
Figure 6.48: Measured vs. predicted cooling coil load for the summer period.....	123
Figure 6.49: Histogram of the difference between predicted and measured hourly cooling coil load.....	125
Figure 6.50: Histogram of the difference between predicted and measured daily cooling coil load.....	125
Figure 6.51: Measured vs. predicted outdoor air enthalpy for the periods when 100% return air is used for mixing	127
Figure 6.52: Measured vs. predicted outdoor air temperature for the periods when 100% return air is used for mixing	127
Figure 6.53: Measured vs. predicted mixed air enthalpy for the periods when 100% return air is used for mixing	128
Figure 6.54: Measured vs. predicted cold deck air enthalpy during the periods when 100% outdoor air is used for mixing.....	128
Figure 6.55: Measured vs. predicted cooling coil load for the periods when 100% return air is used for mixing	129
Figure 6.56: Measured vs. predicted enthalpy difference across the cooling coil during the periods when 100% return air is used for mixing	129
Figure 6.57: Measured vs. predicted outdoor air enthalpy when a portion of return air is mixed with a portion of fresh air to ventilate the building.....	131
Figure 6.58: Measured vs. predicted outdoor air temperature when a portion of return air is mixed with a portion of fresh air to ventilate the building.....	131
Figure 6.59: Measured vs. predicted mixed air enthalpy when a portion of return air is mixed with a portion of fresh air to ventilate the building.....	131
Figure 6.60: Measured vs. predicted cold deck air enthalpy when a portion of return air is mixed with a portion of fresh air to ventilate the building.....	132
Figure 6.61: Measured vs. predicted cooling coil load when a portion of return air is mixed with a portion of fresh air is used to ventilate the building	132
Figure 6.62: Measured vs. predicted enthalpy difference across the cooling coil when a portion of return air is mixed with a portion of fresh air to ventilate the building	132
Figure 6.63: Measured vs. predicted outdoor air enthalpy when 100% fresh air is used to ventilate the building	134
Figure 6.64: Measured vs. predicted outdoor air temperature when 100% fresh air is used to ventilate the building.....	135
Figure 6.65: Measured vs. predicted mixed air enthalpy when 100% fresh air is used to ventilate the building	135
Figure 6.66: Measured vs. predicted cold deck air enthalpy when 100% fresh air is used to ventilate the building.....	135
Figure 6.67: Measured vs. predicted cooling coil load when 100% fresh air is used to ventilate the building	136
Figure 6.68: Measured vs. predicted enthalpy difference across the cooling coil when 100% fresh air is used to ventilate the building	136

Figure 6.69: Histogram for the difference between measured and predicted cooling coil load when 100% return air is used to ventilate the building	137
Figure 6.70: Histogram for the difference between measured and predicted cooling coil load when a portion of return air is mixed with a fraction of fresh air to ventilate the building.....	138
Figure 6.71: Histogram for the difference between measured and predicted cooling coil load when 100% fresh air is used to ventilate the building.....	138
Figure 6.72: Measured vs. predicted hourly cooling coil load based on mixed air enthalpy measured on site.....	139
Figure 6.73: Measured vs. predicted daily cooling coil load based on mixed air enthalpy measured on site.....	139
Figure 6.74: Measured vs. predicted hourly cooling coil load signature (based on mixed air enthalpy measured on site).....	140
Figure 6.75: Measured vs. predicted daily cooling coil load signature (based on mixed air enthalpy measured on site).....	140
Figure 6.76: Measured vs. predicted hourly cooling coil load (based on mixed air enthalpy measured on site)	141
Figure 6.77: Measured vs. predicted daily cooling coil load (based on mixed air enthalpy measured on site)	141
Figure 6.78: Histogram for the difference between measured and predicted hourly cooling coil load (based on mixed air enthalpy measured on site)	143
Figure 6.79: Histogram for the difference between measured and predicted daily cooling coil load (based on mixed air enthalpy measured on site)	143
Figure 8.1: Diversity factors for weekdays and weekend days used for simulation of the zone 1.6 NE with approaches A and B.....	165
Figure 8.2: Diversity factors for weekdays and weekend days used for simulation of zone 3.4 SW with approaches A and B.....	165
Figure 8.3: Measured vs. predicted indoor air temperature in zone 1.6 NE when using equivalent step-change schedules and when using the RP-1093 schedule, for the entire summer period	166
Figure 8.4: Measured vs. predicted indoor air temperature in zone 3.4 SW when using equivalent step-change schedules and when using the RP-1093 schedule, for the entire summer period	166
Figure 8.5: Measured hourly supply air flow rate vs. predictions using approach A and B for zone 1.6 NE for the summer period.....	169
Figure 8.6: Measured hourly supply air flow rate vs. predictions using approach A and B for zone 3.4 SW for the summer period.....	170
Figure 8.7: Measured hourly supply air flow rate vs. prediction using approach A and B for zone 1.6 NE from 18-20 July	171
Figure 8.8: Measured hourly supply air flow rate vs. predictions using approach A and B for zone 3.4 SW from 18-20 July.....	171
Figure 8.9: Hourly measured cooling load vs. predictions using approach A and B, for zone 1.6 NE, for the entire summer.....	178
Figure 8.10: Hourly measured cooling load vs. predictions using approach A and B, for zone 3.4 SW, for the entire summer	178

APPENDIX A

Figure A. 1: Predicted vs. measured hourly indoor air temperature for zone 1.3 NW from 18-20 July 2012..... 193

Figure A. 2: Predicted vs. measured hourly supply air flow rate to zone 1.3 NW from 18-20 July 2012 193

Figure A. 3: Predicted vs. measured hourly indoor air temperature for zone 1.3 NW, for the summer 2012..... 194

Figure A. 4: Predicted vs. measured hourly supply air flow rate to zone 1.3 NW, for the summer 2012 194

Figure A. 5: Predicted vs. measured hourly supply air flow rate signature for zone 1.3 NW for summer 2012..... 195

Figure A. 6: Predicted vs. measured daily supply air flow rate signature for zone 1.3 NW for summer 2012..... 195

Figure A. 7: Predicted vs. measured hourly indoor air temperature for zone 1.4 SW, from 18-20 July 2012..... 196

Figure A. 8: Predicted vs. measured hourly supply air temperature to zone 1.4 SW, from 18-20 July 2012..... 196

Figure A. 9: Predicted vs. measured hourly indoor air temperature for zone 1.4 SW, for summer 2012 197

Figure A. 10: Predicted vs. measured hourly supply air flow rate to zone 1.4 SW, for summer 2012 197

Figure A. 11: Predicted vs. measured hourly supply air flow rate signature for summer 2012... 198

Figure A. 12: Predicted vs. measured daily air flow rate signature for summer 2012..... 198

Figure A. 13: Predicted vs. measured hourly indoor air temperature for zone 1.5 SE, from 18-20 July 2012..... 199

Figure A. 14: Predicted vs. measured hourly supply air flow rate to zone 1.5 SE, from 18-20 July 2012 199

Figure A. 15: Predicted vs. measured hourly indoor air temperature for zone 1.5 SE, for summer 2012 200

Figure A. 16: Predicted vs. measured hourly supply air flow rate to zone 1.5 SE, for summer 2012 200

Figure A. 17: Predicted vs. measured hourly supply air flow rate signature for zone 1.5 SE, for summer 2012..... 201

Figure A. 18: Predicted vs. measured daily supply air flow rate signature for zone 1.5 SE, for summer 2012..... 201

Figure A. 19: Predicted vs. measured hourly indoor air temperature for zone 1.6 NE, from 18-20 July 2012..... 202

Figure A. 20: Predicted vs. measured hourly supply air flow rate to zone 1.6 NE, from 18-20 July 2012 202

Figure A. 21: Predicted vs. measured hourly indoor air temperature for zone 1.6 NE, for summer 2012 203

Figure A. 22: Predicted vs. measured hourly supply air flow rate to zone 1.6 NE, for summer 2012 203

Figure A. 23: Predicted vs. measured hourly supply air flow rate signature for zone 1.6 NE, for summer 2012..... 204

Figure A. 24: Predicted vs. measured daily supply air flow rate signature for zone 1.6 NE, for summer 2012..... 204

Figure A. 25: Predicted vs. measured hourly indoor air temperature for zone 2.1 NE, from 18-20 July 2012..... 205

Figure A. 26: Predicted vs. measured hourly supply air flow rate for zone 2.1 NE, from 18-20 July 2012.....	205
Figure A. 27: Predicted vs. measured hourly indoor air temperature for zone 2.1 NE, for summer 2012	206
Figure A. 28: Predicted vs. measured hourly supply air flow rate to zone 2.1 NE, for summer 2012	206
Figure A. 29: Predicted vs. measured hourly supply air flow rate signature for zone 2.1 NE, for summer 2012.....	207
Figure A. 30: Predicted vs. measured daily supply air flow rate signature for zone 2.1 NE, for summer 2012.....	207
Figure A. 31: Predicted vs. measured hourly indoor air temperature for zone 2.3 NW, from 18-20 July 2012.....	208
Figure A. 32: Predicted vs. measured hourly supply air flow rate to zone 2.3 NW, from 18-20 July 2012.....	208
Figure A. 33: Predicted vs. measured hourly indoor air temperature for zone 2.3 NW, for summer 2012	209
Figure A. 34: Predicted vs. measured hourly indoor supply air flow rate for zone 2.3 NW, for summer 2012.....	209
Figure A. 35: Predicted vs. measured hourly supply air flow rate signature for zone 2.3 NW, for summer 2012.....	210
Figure A. 36: Predicted vs. measured daily supply air flow rate signature for zone 2.3 NW, for summer 2012.....	210
Figure A. 37: Predicted vs. measured hourly indoor air temperature for zone 2.4 SW, from 18-20 July 2012.....	211
Figure A. 38: Predicted vs. measured hourly supply air flow rate to zone 2.4 SW, from 18-20 July 2012	211
Figure A. 39: Predicted vs. measured hourly indoor air temperature for zone 2.4 SW, for summer 2012	212
Figure A. 40: Predicted vs. measured hourly supply air flow rate to zone 2.4 SW, for summer 2012	212
Figure A. 41: Predicted vs. measured hourly supply air flow rate signature for zone 2.4 SW, for summer 2012.....	213
Figure A. 42: Predicted vs. measured daily supply air flow rate signature for zone 2.4 SW, for summer 2012.....	213
Figure A. 43: Predicted vs. measured hourly indoor air temperature for zone 2.5 SE, from 18-20 July 2012.....	214
Figure A. 44: Predicted vs. measured hourly supply air flow rate to zone 2.5 SE, from 18-20 July 2012	214
Figure A. 45: Predicted vs. measured hourly indoor air temperature for zone 2.5 SE, for summer 2012	215
Figure A. 46: Predicted vs. measured hourly supply air flow rate to zone 2.5 SE, for summer 2012	215
Figure A. 47: Predicted vs. measured hourly supply air flow rate signature for zone 2.5 SE, for summer 2012.....	216
Figure A. 48: Predicted vs. measured daily supply air flow rate signature to zone 2.5 SE, for summer 2012.....	216
Figure A. 49: Predicted vs. measured hourly indoor air temperature for zone 2.6 NE, from 18-20 July 2012.....	217

Figure A. 50: Predicted vs. measured hourly supply air flow rate to zone 2.6 NE, from 18-20 July 2012	217
Figure A. 51: Predicted vs. measured hourly indoor air temperature for zone 2.6 NE, for summer 2012	218
Figure A. 52: Predicted vs. measured hourly supply air flow rate to zone 2.6 NE, for summer 2012	218
Figure A. 53: Predicted vs. measured hourly supply air flow rate signature for zone 2.6 NE, for summer 2012.....	219
Figure A. 54: Predicted vs. measured daily supply air flow rate signature for zone 2.6 NE, for summer 2012.....	219
Figure A. 55: Predicted vs. measured hourly indoor air temperature for zone 3.1 NE, from 18-20 July 2012.....	220
Figure A. 56: Predicted vs. measured hourly supply air flow rate for zone 3.1 NE, from 18-20 July 2012.....	220
Figure A. 57: Predicted vs. measured hourly indoor air temperature for zone 3.1 NE, for summer 2012	221
Figure A. 58: Predicted vs. measured hourly supply air flow rate to zone 3.1 NE, for summer 2012	221
Figure A. 59: Predicted vs. measured hourly supply air flow rate signature for zone 3.1 NE, for summer 2012.....	222
Figure A. 60: Predicted vs. measured daily supply air flow rate signature for zone 3.1 NE, for summer 2012.....	222
Figure A. 61: Predicted vs. measured hourly indoor air temperature for zone 3.2 SW, from 18-20 July 2012.....	223
Figure A. 62: Predicted vs. measured hourly supply air flow rate to zone 3.2 SW, from 18-20 July 2012	223
Figure A. 63: Predicted vs. measured hourly indoor air temperature for zone 3.2 SW, for summer 2012	224
Figure A. 64: Predicted vs. measured hourly supply air flow rate to zone 3.2 SW, for summer 2012	224
Figure A. 65: Predicted vs. measured hourly supply air flow rate signature for zone 3.2 SW, for summer 2012.....	225
Figure A. 66: Predicted vs. measured daily supply air flow rate signature for zone 3.2 SW, for summer 2012.....	225
Figure A. 67: Predicted vs. measured hourly indoor air temperature for zone 3.3 NW, from 18-20 July 2012.....	226
Figure A. 68: Predicted vs. measured hourly supply air flow rate to zone 3.3 NW, from 18-20 July 2012.....	226
Figure A. 69: Predicted vs. measured hourly indoor air temperature for zone 3.3 NW, for summer 2012	227
Figure A. 70: Predicted vs. measured hourly supply air flow rate for zone 3.3 NW, for summer 2012	227
Figure A. 71: Predicted vs. measured hourly supply air flow rate signature for zone 3.3 NW, for summer 2012.....	228
Figure A. 72: Predicted vs. measured daily supply air flow rate signature for zone 3.3 NW, for summer 2012.....	228
Figure A. 73: Predicted vs. measured hourly indoor air temperature for zone 3.4 SW, from 18-20 July 2012.....	229

Figure A. 74: Predicted vs. measured hourly supply air flow rate for zone 3.4 SW, from 18-20 July 2012.....	229
Figure A. 75: Predicted vs. measured hourly indoor air temperature for zone 3.4 SW, for summer 2012	230
Figure A. 76: Predicted vs. measured hourly supply air flow rate for zone 3.4 SW, for summer 2012	230
Figure A. 77: Predicted vs. measured hourly supply air flow rate signature for zone 3.4 SW, for summer 2012.....	231
Figure A. 78: Predicted vs. measured daily supply air flow rate signature for zone 3.4 SW, for summer 2012.....	231
Figure A. 79: Predicted vs. measured hourly indoor air temperature for zone 3.5 SE, from 18-20 July 2012.....	232
Figure A. 80: Predicted vs. measured hourly supply air flow rate to zone 3.5 SE, from 18-20 July 2012	232
Figure A. 81: Predicted vs. measured hourly indoor air temperature for zone 3.5 SE, for summer 2012	233
Figure A. 82: Predicted vs. measured hourly supply air flow rate to zone 3.5 SE, for summer 2012	233
Figure A. 83: Predicted vs. measured hourly supply air flow rate signature for zone 3.5 SE, for summer 2012.....	234
Figure A. 84: Predicted vs. measured daily supply air flow rate signature for zone 3.5 SE, for summer 2012.....	234
Figure A. 85: Predicted vs. measured hourly indoor air temperature for zone 3.6 NE, from 18-20 July 2012.....	235
Figure A. 86: Predicted vs. measured hourly supply air flow rate to zone 3.6 NE, from 18-20 July 2012	235
Figure A. 87: Predicted vs. measured hourly indoor air temperature for zone 3.6 NE, for summer 2012	236
Figure A. 88: Predicted vs. measured hourly supply air flow rate to zone 3.6 NE, for summer 2012	236
Figure A. 89: Predicted vs. measured hourly supply air flow rate signature for zone 3.6 NE, for summer 2012.....	237
Figure A. 90: Predicted vs. measured daily supply air flow rate signature for zone 3.6 NE, for summer 2012.....	237

APPENDIX B

Figure B. 1: Histogram for the difference between hourly predicted and measured supply air flow rate to zone 1.3 NW for the summer period.....	238
Figure B. 2: Histogram for the difference between hourly predicted and measured supply air flow rate to zone 1.4 SW for the summer period	238
Figure B. 3: Histogram for the difference between hourly predicted and measured supply air flow rate to zone 1.5 SE for the summer period.....	239
Figure B. 4: Histogram for the difference between hourly predicted and measured supply air flow rate to zone 1.6 NE for the summer period	239
Figure B. 5: Histogram for the difference between hourly predicted and measured supply air flow rate to zone 2.1 NE for the summer period	239
Figure B. 6: Histogram for the difference between hourly predicted and measured supply air flow rate to zone 2.3 NW for the summer period.....	240

Figure B. 7: Histogram for the difference between hourly predicted and measured supply air flow rate to zone 2.4 SW for the summer period	240
Figure B. 8: Histogram for the difference between hourly predicted and measured supply air flow rate to zone 2.5 SE for the summer period.....	240
Figure B. 9: Histogram for the difference between hourly predicted and measured supply air flow rate to zone 2.6 NE for the summer period.....	241
Figure B. 10: Histogram for the difference between hourly predicted and measured supply air flow rate to zone 3.1 NE for the summer period.....	241
Figure B. 11: Histogram for the difference between hourly predicted and measured supply air flow rate to zone 3.2 SW for the summer period	241
Figure B. 12: Histogram for the difference between hourly predicted and measured supply air flow rate to zone 3.3 NW for the summer period	242
Figure B. 13: Histogram for the difference between hourly predicted and measured supply air flow rate to zone 3.4 SW for the summer period	242
Figure B. 14: Histogram for the difference between hourly predicted and measured supply air flow rate to zone 3.5 SE for the summer period	242
Figure B. 15: Figure B. 14: Histogram for the difference between hourly predicted and measured supply air flow rate to zone 3.6 NE for the summer period.....	243

APPENDIX C

Figure C. 1: Histogram of the difference between hourly predicted and measured summation of air flow rates supplied to zones from 18-20 July	244
Figure C. 2: Histogram of the difference between hourly predicted and measured summation of air flow rates supplied to zones from 14-16 August	244
Figure C. 3: Histogram of the difference between predicted and measured daily summation of air flow rates to zones for summer period.....	244

APPENDIX D

Figure D. 1: Measured vs. predicted indoor air temperature in zone 1.3 NW when using equivalent step-change schedules and when using the RP-1093 schedule, from 18 th to 20 th of July 2012	245
Figure D. 2: Measured vs. predicted supply air flow rate in zone 1.3 NW when using equivalent step-change schedules and when using the RP-1093 schedule, from 18 th to 20 th of July 2012 .	245
Figure D. 3: Measured vs. predicted cooling load in zone 1.3 NW when using equivalent step-change schedules and when using the RP-1093 schedule, from 18 th to 20 th of July 2012.....	246
Figure D. 4: Measured vs. indoor air temperature in zone 1.4 SW when using equivalent step-change schedules and when using the RP-1093 schedule, from 18 th to 20 th of July 2012.....	246
Figure D. 5: Measured vs. predicted supply air flow rate in zone 1.4 SW when using equivalent step-change schedules and when using the RP-1093 schedule, from 18 th to 20 th of July 2012 .	247
Figure D. 6: Measured vs. predicted cooling load in zone 1.4 SW when using equivalent step-change schedules and when using the RP-1093 schedule, from 18 th to 20 th of July 2012.....	247
Figure D. 7: Measured vs. predicted indoor air temperature in zone 1.5 SE when using equivalent step-change schedules and when using the RP-1093 schedule, from 18 th to 20 th of July 2012 .	248
Figure D. 8: Measured vs. predicted supply air flow rate to zone 1.5 SE when using equivalent step-change schedules and when using the RP-1093 schedule, from 18 th to 20 th of July 2012 .	248

Figure D. 9: Measured vs. predicted cooling load in zone 1.5 SE when using equivalent step-change schedules and when using the RP-1093 schedule, from 18th to 20th of July 2012.....	249
Figure D. 10: Measured vs. predicted indoor air temperature in zone 1.6 NE when using equivalent step-change schedules and when using the RP-1093 schedule, from 18th to 20th of July 2012.....	249
Figure D. 11: Measured vs. predicted supply air flow rate in zone 1.6 NE when using equivalent step-change schedules and when using the RP-1093 schedule, from 18th to 20th of July 2012 .	250
Figure D. 12: Measured vs. predicted cooling load in zone 1.6 NE when using equivalent step-change schedules and when using the RP-1093 schedule, from 18th to 20th of July 2012.....	250
Figure D. 13: Measured vs. predicted indoor air temperature in zone 2.1 NE when using equivalent step-change schedules and when using the RP-1093 schedule, from 18th to 20th of July 2012.....	251
Figure D. 14: Measured vs. predicted supply air flow rate to zone 2.1 NE when using equivalent step-change schedules and when using the RP-1093 schedule, from 18th to 20th of July 2012 .	251
Figure D. 15: Measured vs. predicted cooling load in zone 2.1 NE when using equivalent step-change schedules and when using the RP-1093 schedule, from 18th to 20th of July 2012.....	252
Figure D. 16: Measured vs. predicted indoor air temperature in zone 2.3 NW when using equivalent step-change schedules and when using the RP-1093 schedule, from 18th to 20th of July 2012.....	252
Figure D. 17: Measured vs. predicted supply air flow rate to zone 2.3 NW when using equivalent step-change schedules and when using the RP-1093 schedule, from 18th to 20th of July 2012 .	253
Figure D. 18: Measured vs. predicted cooling load in zone 2.3 NW when using equivalent step-change schedules and when using the RP-1093 schedule, from 18th to 20th of July 2012.....	253
Figure D. 19: Measured vs. predicted indoor air temperature in zone 2.4 SW when using equivalent step-change schedules and when using the RP-1093 schedule, from 18th to 20th of July 2012.....	254
Figure D. 20: Measured vs. predicted supply air flow rate to zone 2.4 SW when using equivalent step-change schedules and when using the RP-1093 schedule, from 18th to 20th of July 2012 .	254
Figure D. 21: Measured vs. predicted cooling load in zone 2.4 SW when using equivalent step-change schedules and when using the RP-1093 schedule, from 18th to 20th of July 2012.....	255
Figure D. 22: Measured vs. predicted indoor air temperature in zone 2.5 SE when using equivalent step-change schedules and when using the RP-1093 schedule, from 18th to 20th of July 2012.....	255
Figure D. 23: Measured vs. predicted supply air flow rate to zone 2.5 SE when using equivalent step-change schedules and when using the RP-1093 schedule, from 18th to 20th of July 2012 .	256
Figure D. 24: Measured vs. predicted cooling load in zone 2.5 SE when using equivalent step-change schedules and when using the RP-1093 schedule, from 18th to 20th of July 2012.....	256
Figure D. 25: Measured vs. predicted indoor air temperature in zone 2.6 NE when using equivalent step-change schedules and when using the RP-1093 schedule, from 18th to 20th of July 2012.....	257
Figure D. 26: Measured vs. predicted supply air flow rate in zone 2.6 NE when using equivalent step-change schedules and when using the RP-1093 schedule, from 18th to 20th of July 2012 .	257
Figure D. 27: Measured vs. predicted cooling load in zone 2.6 NE when using equivalent step-change schedules and when using the RP-1093 schedule, from 18th to 20th of July 2012.....	258

Figure D. 28: Measured vs. predicted indoor air temperature in zone 3.1 NE when using equivalent step-change schedules and when using the RP-1093 schedule, from 18th to 20th of July 2012.....	258
Figure D. 29: Measured vs. predicted supply air flow rate in zone 3.1 NE when using equivalent step-change schedules and when using the RP-1093 schedule, from 18th to 20th of July 2012 .	259
Figure D. 30: Measured vs. predicted cooling load in zone 3.1 NE when using equivalent step-change schedules and when using the RP-1093 schedule, from 18th to 20th of July 2012.....	259
Figure D. 31: Measured vs. predicted indoor air temperature in zone 3.2 SW when using equivalent step-change schedules and when using the RP-1093 schedule, from 18th to 20th of July 2012.....	260
Figure D. 32: Measured vs. predicted supply air flow rate in zone 3.2 SW when using equivalent step-change schedules and when using the RP-1093 schedule, from 18th to 20th of July 2012 .	260
Figure D. 33: Measured vs. predicted cooling load in zone 3.2 SW when using equivalent step-change schedules and when using the RP-1093 schedule, from 18th to 20th of July 2012.....	261
Figure D. 34: Measured vs. predicted indoor air temperature in zone 3.3 NW when using equivalent step-change schedules and when using the RP-1093 schedule, from 18th to 20th of July 2012.....	261
Figure D. 35: Measured vs. predicted supply air flow rate in zone 3.3 NW when using equivalent step-change schedules and when using the RP-1093 schedule, from 18th to 20th of July 2012 .	262
Figure D. 36: Measured vs. predicted cooling load in zone 3.3 NW when using equivalent step-change schedules and when using the RP-1093 schedule, from 18th to 20th of July 2012.....	262
Figure D. 37: Measured vs. predicted indoor air temperature in zone 3.4 SW when using equivalent step-change schedules and when using the RP-1093 schedule, from 18th to 20th of July 2012.....	263
Figure D. 38: Measured vs. predicted supply air flow rate in zone 3.4 SW when using equivalent step-change schedules and when using the RP-1093 schedule, from 18th to 20th of July 2012 .	263
Figure D. 39: Measured vs. predicted cooling load in zone 3.4 SW when using equivalent step-change schedules and when using the RP-1093 schedule, from 18th to 20th of July 2012.....	264
Figure D. 40: Measured vs. predicted indoor air temperature in zone 3.5 SE when using equivalent step-change schedules and when using the RP-1093 schedule, from 18th to 20th of July 2012.....	264
Figure D. 41: Measured vs. predicted supply air flow rate in zone 3.5 SE when using equivalent step-change schedules and when using the RP-1093 schedule, from 18th to 20th of July 2012 .	265
Figure D. 42: Measured vs. predicted cooling load in zone 3.5 SE when using equivalent step-change schedules and when using the RP-1093 schedule, from 18th to 20th of July 2012.....	265
Figure D. 43: Measured vs. predicted indoor air temperature in zone 3.6 NE when using equivalent step-change schedules and when using the RP-1093 schedule, from 18th to 20th of July 2012.....	266
Figure D. 44: Measured vs. predicted supply air flow rate in zone 3.6 NE when using equivalent step-change schedules and when using the RP-1093 schedule, from 18th to 20th of July 2012 .	266
Figure D. 45: Measured vs. predicted cooling load in zone 3.6 NE when using equivalent step-change schedules and when using the RP-1093 schedule, from 18th to 20th of July 2012.....	267

List of Tables

Table 2.1: Acceptable differences for different energy end-uses (Kaplan et al. (1990)).....	22
Table 4.1: Construction of the envelope for the Genomic Research Center.....	30
Table 4.2: Daily average and standard deviation (SD) of measured air temperature, air flow rate and cooling load for all zones, for the month of June 2012.....	41
Table 4.3: Daily average and standard deviation (SD) of measured air temperature, air flow rate and cooling coil load for all zones, for the month of July 2012.....	41
Table 4.4: Daily average and standard deviation (SD) of measured air temperature, air flow rate and cooling coil load for all zones, for the month of August 2012.....	42
Table 4.6: Areas of various conditioned thermal zones.....	43
Table 4.6: Surface area and supply air flow rate for all zones in the building.....	50
Table 4.7: Average zone air return temperature and standard deviation (SD).....	51
Table 4.9: Monthly average and standard deviation (SD) values of outside air temperature and relative humidity, supply air flow rate and temperature of AHU, cold deck and mixed air temperature for each month of year 2012.....	53
Table 5.1: Schedules of equivalent internal loads.....	66
Table 5.2: Internal load and supply air flow rate for all the zones.....	68
Table 5.3: Summary of figures presented in Appendix A.....	74
Table 5.4: CV-RMSE of the difference between predicted and measured air flow rate.....	75
Table 5.5: NMBE of the difference between predicted and measured air flow rate.....	77
Table 5.6: Hourly coefficient of variation for all the zones in the building for the summer period.....	81
Table 5.7: Hourly, daily and monthly coefficient of variation for zones 1.3 NW to 2.5 SE.....	83
Table 5.8: Hourly, daily and monthly coefficient of variation for zones 2.6 NE to 3.6 NE.....	84
Table 5.9: Mean indoor air temperatures for all zones for the occupied hours for all summer period (Run 4) and for all summer period except weekend days (Run5).....	88
Table 5.10: Corrected internal loads for all zones for all runs.....	89
Table 5.11: Coefficient of variation values for all zones for the entire summer period, based on hourly values.....	89
Table 5.12: CV values for all zones, for the entire summer period, based on daily values.....	90
Table 6.1: Mean measured supply air flow rate in the air handling unit from the 11th of June until the 31st of August.....	93
Table 6.2: Measured cold deck reset temperatures.....	96
Table 6.3: Statistical indices for comparing the measured and predicted summation of air flow rates supplied to zones.....	103
Table 6.4: The t-statistic value for comparing the measured and predicted summation of air flow rates supplied to zones.....	104
Table 6.5: Statistical indices for the difference between the predicted and measured supply air flow rate leaving the air handling unit.....	110
Table 6.6: The t-statistic for hourly and daily difference between measured and predicted supply air flow rate.....	112
Table 6.7: Measured vs. predicted supply air temperature for three days in July and for the entire summer period.....	115

Table 6.8: Statistical indices for the difference between predicted and measured supply air temperature	117
Table 6.9: T-statistic value for the difference between predicted and measured supply air temperature	118
Table 6.10: Statistical indices for hourly and daily difference between predicted and measured cooling coil load.....	124
Table 6.11: The t-statistic value using hourly and daily averaged values for the calibration of the cooling coil load.....	125
Table 6.12: Statistical indices and t statistic hypothesis testing for the three cases.....	137
Table 6.13: Statistical indices for the calibration of the cooling load based on mixed air enthalpy measured on site.....	142
Table 7.1: Changes to inputs.....	149
Table 7.2: Changes of internal loads [kW] for all zones.....	150
Table 7.3: Mean output values for each variation in window's U value	151
Table 7.4: Mean output values for each variation in walls' U value	151
Table 7.5: Mean output values for each variation in blinds solar heat gain multiplier	151
Table 7.6: Mean output values for each variation in infiltration rate multiplier.....	152
Table 7.7: Mean output values for each variation in internal loads	152
Table 7.8: Sensitivity coefficient SC1 based on average values over the summer	153
Table 7.9: Sensitivity coefficient SC2 based on average values over the summer	153
Table 7.10: Maximum values of outputs for each variation in windows' U value.....	154
Table 7.11: Maximum values of outputs for each variation in walls' U value.....	154
Table 7.12: Maximum values of outputs for each variation in blinds solar heat gain multiplier.....	154
Table 7.13: Maximum values of outputs for each variation in infiltration rate multiplier	155
Table 7.14: Maximum values of outputs for each variation in interior loads	155
Table 7.15: Sensitivity coefficient SC1 based on maximum values over the summer	156
Table 7.16: Sensitivity coefficient SC2 based on maximum values over the entire summer	156
Table 7.17: Statistical indices for the supply air flow rate and cooling load sensitivities when various inputs are changed.....	157
Table 8.1: Combined lights and receptacles profiles for medium buildings for weekdays and weekend days from ASHRAE RP-1093	163
Table 8.2: Hourly RMSE, CV-RMSE and NMBE for temperature differences between measurements and predictions with approaches A and B for the summer period	167
Table 8.3: The t-statistic values for the difference between measured indoor air temperature and predictions using approach A and B for the summer period using hourly values	168
Table 8.4: Hourly statistical indices for the difference between measured and predicted supply air flow rate using approaches A and B for all zones and for the entire summer period	172
Table 8.5: Hourly statistical indices for the difference between measured supply air flow rate and predictions using approaches A and B for all zones from 18-20 July	173
Table 8.6: Hourly statistical indices for the difference between measured supply air flow rate and predictions using approaches A and B for all zones from 14-16 August.....	174
Table 8.7: The hourly t-statistic value for the difference between measured supply air flow rate and predictions using approaches A and B for all zones for the entire summer	175
Table 8.8: The t-statistic values for the difference between measured supply air flow rates and predictions with approach A and B for all zones, using hourly values, from 18-20 July	176

Table 8.9: The hourly t-statistic values for the difference between measured supply air flow rates and predictions with approach A and B for all zones, from 14-16 August.....	177
Table 8.10: Statistical indices for the difference between the hourly measured cooling load and predictions using approach A and B for the entire summer.....	179
Table 8.11: The hourly t-statistic value for the difference between measured cooling loads and predictions using approaches A and B for the entire summer	180

Chapter 1 Introduction

1.1 Problem Statement

World energy use has increased considerably in the past decades. In a study conducted by the International Energy Agency, the world energy consumption has been analyzed from the year 1984 until 2004. The results show that primary energy has grown by 49%, with an average annual increase of 2%. According to Perez-Lombard et al. (2008), the HVAC systems energy use has considerably increased, accounting for 50% of the building energy consumption or 20% of total energy consumption of the United States.

As the fossil fuel resources decrease and the impact of greenhouse gases on the climate is rising, it is important to design buildings with reduced loads, high efficiency and using as much as possible renewable energy sources. Employing energy modeling programs can help the user analyze various energy conservation measures; find the best combinations of building features, in order to optimize the building performance.

Waltz (2000) discussed how whole building energy simulation tools have been used since the early 1960's in the design phase to analyze thermal behavior and energy consumption of buildings, in order to find the optimum design of envelope and HVAC systems. It is recently that they started being used in post occupancy stage for commissioning and evaluation of energy conservation measures.

Energy simulation programs have constantly been updated and changed considerably with the evolution of technology. Their complexity and accuracy have improved over the years, and users need to have a very good understanding not only of the

simulation tool, but also the building physical characteristics and HVAC systems, in order to create a model that simulates reality closely.

There are many studies that analyze the capabilities and accuracies of energy simulation programs, but there are not many publications about the calibration of models for practical purposes.

1.2 Scope

The objective of this study is to develop a calibration methodology of a building energy model, and to verify the proposed methodology when it is applied to eQuest program (Department of Energy (DOE) (2006)) along with data measured in a new building, the Genomic Research Center of Concordia University.

The eQuest (Quick Energy Simulation Tool) energy analysis program was selected for this purpose because of its large use in consulting companies and being the core of the next CAN-QUEST program (N.R.C. (2013)), which complies with the National Energy Code of Canada for Buildings (N.R.C. (2011)) or the Model National Code for Buildings (N.R.C. (1997)). eQuest is a DOE-2 based software that was approved by the California Energy Commission in 2004. It is currently widely used in simulating whole building performance and in analyzing energy efficiency measures to be implemented.

Chapter 2 Literature Review

2.1 Scope of calibration

Calibrating a simulation is the process of obtaining outputs that are very close to selected measured data, for instance the energy usage. This can be done by varying some inputs and recording the changes in outputs, in this fashion identifying which parameters have a big impact on the output results, in order to minimize the difference between measurements and simulation results. Calibration of an energy model implies changing the inputs in a reasonable range to make the simulation results more accurate. For a model to be accurate, it is important not only to closely match the predicted total energy use to the real energy use, but also to account for all the sources and uses of energy and to follow the same seasonal variations in energy use in a building as the real seasonal variations.

Many papers analyzed the development of building energy calculation tools, from manual calculation methods (degree day, bin method) to computer simulation programs. Models are composed of three main components: 1) input variables, 2) system structure and parameters and 3) output variables or results. The system structure is contained in the simulation core or engine, while the input values have to be inserted in the software by the user.

In general, there are two approaches used for the development of building energy simulation models: forward or classical approach and inverse or data-driven approach. Forward modeling uses a physical model to predict the behavior of a system. It requires input variables along with system structure and parameters in order to calculate the output variables. Most simulation programs use the forward approach in the design process or the analysis of impact of energy conservation techniques. This approach is more flexible for

applications, however, it might lead to less accurate results when compared with measurements in an existing building, if not correct calibration process is undertaken. The inverse approach uses measurements in a building to develop a model (e.g. a correlation-based model) that is representative to that building. Hence the model is less flexible for application to other buildings; however, it is more accurate in its predictions.

ASHRAE (2001) defined forward modeling or direct/classical approach as a method of estimating output variables starting from a model with known input variables, structure and parameters. Its advantage is that it can be used even when the physical system is not built yet, therefore it could be a very good candidate for preliminary design and analysis stage or for performing renovations/changes in an existing system.

In the past, simulation programs, including DOE-2 and eQuest, were based on loads-system-plants sequence, because it is a fast approach that does not need a lot of computation resources. The main disadvantage is in the lack of feedback between those three blocks; the room air temperature (simulated in the load blocks) does not change if the cooling coil of the air handling unit (simulated in the systems blocks) is too small.

The advanced software nowadays, for instance EnergyPlus (Department of Energy (DOE) (2013)) made it possible for the simultaneous simulations of loads, system and plants. In the simultaneous solutions approach, unmet loads and unbalances cannot occur, because the calculations at the plant are immediately reflected to the secondary system and so on, which forces them to readjust instantaneously. It is true that it demands more computing resources, but this obstacle is becoming of no importance with the evolution of today's technology.

The software selected to perform the energy simulation is eQuest (QUick Energy Simulation Tool) (Department of Energy (DOE) (2006)), a DOE-2 based program, which is constantly updated and improved. eQuest has four simulation subprograms called LOAD, SYSTEMS, PLANT, and ECONOMICS. In terms of thermodynamics, a building has flows of energy through its surfaces and spaces, which leads to a series of integral-differential equations with complex initial and boundary conditions. The simulation approach used by eQuest is to solve the set of equations, first calculating the heat balance for all zones with the LOADS simulator, then calculating the energy demand through the SYSTEMS program, thirdly determining the on-site and off-site energy use by primary equipment through the PLANT subprogram, and lastly it calculates the costs associated with fuel and electricity demand through the ECONOMICS subprogram. In eQuest, the calculation of heat conduction through surfaces is done by solving a one dimensional diffusion equation for each hour, and using the response factor method. The space extraction or addition of heat is done based on the space loads and using the weighting factors method.

Since there are various building energy modeling tools on the market nowadays, some that require less user expertise, others that are more complicated to use, simulation has become readily accessible to various types of users.

Calibrated energy models are very useful in commissioning, measurement and verification (M&V) protocols of building retrofits, and in predicting savings from energy conservation measures.

Bronson et al. (1992) showed that energy models are used to analyze building retrofits and to calculate the savings obtained from employing energy conservation

measures. It could happen that the predicted savings from employing certain energy conservation measures do not reflect the reality at all, because the energy simulation model is not accurate or due to poor engineering judgment. The end result is an underestimate or an overestimate of the real building energy consumption. A calibrated model is a model that matches closely the real building performance, therefore a model that is calibrated will give better estimates of energy conservation measures along with the savings involved, than a non-calibrated model.

Another useful application of calibrated models is that they can be used to predict, find problems and improve HVAC system performance, because the differences between expected and actual energy use can be analyzed to find where a certain component is not performing as well as expected.

Bordass et al. (2001) discussed the issue that buildings are handed over after commissioning without any feedback from the actual measured operational performance or comparison with the calibrated simulated intended performance. This leaves the designer with no real proof of the effects of improvements, if any, in a system, and no evidence that the simulated model is calibrated. Calibrated simulation and continuous feedback from the comparison to measured operational performance should become a prerequisite/standard for designing high performing buildings for the future.

Owners can benefit from having a calibrated building energy model because it can provide the thermal/electrical load shapes and the functional distribution of energy end-use, instead of having only the utility bill data, as explained by Sonderegger et al. (2001). It can also help predict the impact of load control measures on the electrical load, using the breakdown of baseline, cooling and heating energy use, as discussed by Mayer et al.

(2003). It is also very helpful to energy auditors in the process of evaluating the feasibility and cost effectiveness of Energy Conservation Measures (ECMs).

Bazjanac (2005) explained that the construction industry is the only sector in which it is common practice to deliver a product without fully testing it. Designing a building should go hand in hand with calibrated building energy simulation, as one can verify, if the design calculations match the results of the simulation.

2.2 Publications and studies

The time needed to calibrate an energy simulation can vary drastically, from a few minutes, usually for fully automated inputs, which might lead to a superficial calibration, to several weeks or months depending on the scale of the project and the budget invested in it.

Generally, calibrating a model implies comparing simulation results to utility data, but there is not a specified method to do so. The most common graphical approaches that have been used in the past are: 1) monthly percent difference time-series graph, 2) bar charts, and 3) monthly x-y scatter plots. Measurement technology has become less expensive, which allows for measurements of energy usage and environmental data (climatic data) over long periods of time and at sub-hourly intervals. Having a much bigger set of data, developing new techniques to compare data became imminent, as the previous methods, such as 2D plots, became obsolete, as too many data points have to be analyzed. It has become common in the engineering community to compare hourly simulation results to hourly measured data. New advanced methods for comparing the two sets of data include

the following: weather day-type analysis, carpet plots, and comparative 3D time-series plots.

There are various papers dealing with the subject of sensitivity analysis of models results to inputs, some for different purposes than calibration of energy simulation, but nevertheless still important in understanding the effects caused by changes in them.

The most used methods to define the relationship between measured input variables and predicted output variables are sensitivity analyses and mathematical regression techniques. An exact relationship cannot be expressed analytically, as the interactions between input variables, sub-systems, system and the output variables are too complex. Therefore the purpose of sensitivity analysis is to establish the impact of each input variable on the output variables of the simulation. There are two types of input variables: 1) static variables (envelope overall thermal resistance), and 2) dynamic variables; that vary according to the way the building is operated (internal loads, control settings) and the variation of weather conditions.

Diamond et al. (1985) conducted a sensitivity analysis of the human factor in building energy simulation, in which six contractors were asked to perform three simulations for four buildings with three different levels of inputs: uncontrolled, refined and set inputs. The results show a decrease in the scatter range from 63% to 19% between the uncontrolled and refined inputs, and 48% to 22% going from refined to the set inputs.

Kaplan et al. (1990) attained tuning tolerances of about 10% for the whole building energy use on an annual basis. They have achieved this by monitoring several end-uses individually during short periods of time and doing calibration for those periods only and

not the whole year. They recommend using one month during the cold season, one month during the hot season and one month in between. This concept is later supported by Lunneberg (1999), who stated that it is of critical importance to monitor key-short term end-use internal loads in order to obtain more realistic operational schedules.

Corson (1992) conducted a study on the effect of changes in certain inputs, in which two buildings, a small retail and a large office building, were investigated using five different software packages. The results lead to the conclusion that the inputs with the least effect on building performance are the envelope and lighting, while the inputs with more impact were found to be occupancy, weather, air supply, HVAC systems and plants. Two different results were obtained: one for conformed output, meaning that user has full decision on what inputs to use; one for conformed input, in which specified inputs are given. The results show that the differences between conformed output and conformed input are higher in the case of the large office building compared to the small retail building.

Kaplan et al. (1992) discussed the impact of simulation inputs on the results, and gave suggestion to analyst on how to minimize the errors. The main parameters that modelers should pay attention to are: 1) on the load side: zoning of the building, infiltration, window U values, thermal mass, interior walls, weather files, internal loads and 2) on the HVAC side: selection of the type of HVAC system, specification of control operation, simulation of multi-zone systems and fan schedules.

Bronson et al. (1992) found that using the default day type profiles from DOE-2, for a simulation performed over half a year, leads to 26% error in electricity use when compared to real measurements. Three other day-types were analyzed in this study: profiles

that depend on occupancy and electric load factors, profiles that resulted from two weeks of measured data and profiles based on a procedure developed by Katipamula et al. (1991) The analysis of the results was mostly based on graphical and statistical techniques, with the help of two-dimensional and three dimensional plotting programs, which proved to be very valuable in detecting the small differences in profiles. The first day type gave the best estimate of overall monthly energy use but did not closely match the hourly profile. The second profile followed closely the actual profile, but the overall goodness of the fit of the electricity use decreased. The third profile was the best overall profile, but unlike the first one, it did not give an accurate monthly profile.

Chou et al. (1993) developed multiple linear regressions that describe the relationship between the effect of different design parameters on building performance.

Zmeureanu et al. (1995) performed a comparative study of three energy analysis programs in which they predicted the energy and cost savings in a large existing office building. The verification and validation of the simulation results consisted in comparing the predictions with the energy performance of the building as given by the utility bills. The simulation performed with three different energy analysis tools resulted in a variety of results. The BESA-design program led to the simulated annual energy consumption to be within 3.5 to 6.5% of the utility bills. The model simulated with MICRO-DOE2 presented an annual energy consumption between 2.8 and 4.5% of the utility bills while the simulation performed with PC-BLAST predicted the annual energy consumption within 3.7% of utility bills. These results were obtained after individual calibrations which were based on the capabilities of each software.

Kaplan et al. (1990), Bronson et al. (1992), and Clarke et al. (1993) recommended the use of hourly data, if available, for calibration. Another technique implied the use of 3-D graphs to visualize the difference between measured hourly data and predicted results (Bronson et al. (1992), and Haberl et al. (1998)).

Developers of building simulation programs have been aware of the lack of compatibility between the various software, but nowadays, having different output files that can be further used as input files in simulation programs, these software have increasing ease of use. The gap between designers of software and the users, mentioned in papers by Sornay (1985) and Clarke et al. (1993), is decreasing considerably due to the advancement of technology. Gathering weather data is still a problem for the analyst in charge of calibrating the building energy model. If the simulation is done before the building is constructed, then it will be based on past weather files and any predicted future building performance will be based on them as well. If on the other hand, the building was already constructed, the simulation should integrate actual weather files of the year that the simulation needs to be done. Some newer buildings even have their own “weather station” meaning that outdoor conditions are measured locally at a selected time step. The accuracy of the simulation results would be greatly increased if these local outdoor conditions could be input in the software. In general, the weather data files are based on measurements near the airport, but the temperature could vary by a few degrees in a different location in the city.

Lam et al. (1996) performed an elaborate study on 60 input parameters that were changed at a time, and observed that the building envelope is less influential than occupancy schedules, weather, air supply and system and plant. They discussed the

importance of sensitivity analysis in the process of determining how responsive the building thermal loads, energy consumption and demand are to changes in various input parameters such as material properties, design of building envelope, capacity and operation of HVAC system components. They developed a methodology to determine sensitivity coefficients for input parameters. They proposed that a base case reference with its description be formulated first, then the parameters of interest be selected and the corresponding base case values be extracted. Then the analyst must determine which simulation outputs are to be investigated. The next step is to introduce perturbations to the selected parameters about their base case values one at a time and to study the corresponding effect of these perturbations on the outputs and lastly to determine the sensitivity coefficients for each parameter.

The results of the building energy model depend considerably on a number of factors: i) the user's experience with the simulation program; ii) the time allocated for the calibration; iii) the modelling capabilities of the selected software; and iv) the user's knowledge of design and operation of the building and HVAC systems.

The need for reliable identification of energy savings and demand reducing measures and confidence in monitoring and verification processes led to the development of calibrated building energy simulation models.

Many techniques have been explored over the years to calibrate building energy models. In the past, the trial and error calibration approach was widely used, but it was time consuming and not always reliable. According to Troncoso (1997), a big problem is that in order to perform model calibration, the analyst has to adjust the input data without sufficient evidence on which data should be modified or to what extent. In general, an

energy simulation program will have as outputs electrical demand and consumption data, which has to be compared to monitored data. If the simulation results and measured data are very different, then the user has to adjust inputs and operating parameters on a trial-and-error basis, until the percent difference is satisfactory, but the fact that these parameters are continuously changed, reduces drastically the liability of the calibrating process. Gathering the information about the building could be a tedious and long process, and it often happens that the information is too complex for the model input; therefore the analyst is forced to base himself on his engineering knowledge and experience related to those particular circumstances, leading to the results to be user-specific. Troncoso (1997) presented some steps to perform calibration of building simulation, that are based on definition of the parameters that most affect the main electric end-uses of a building. Calibration methodology is composed of six stages: definition of power and schedules of constant loads, simulation of design days for thermal loads analysis, sensitivity analysis over input parameters related to significant heat gain/loss, adjustment of input values of high level of influence and uncertainty, whole year simulation and final adjustments.

Stein (1997) proposed a four step methodology based on sub-metering as well as hourly whole building data. The first step is to collect data: whole building hourly electric data, weather data, building characteristics and equipment data, site visits to gather nameplate data and inventory significant loads in the building, and on site measurements of major electric loads. At this step, instantaneous measurements of lighting, fans, and pumps can be used, as well as plug loads, internal air temperatures and primary equipment such as chillers, pumps and fans. These last measurements need to be performed only for a few days, as their purpose is only to verify that the operating schedules are accurate. Step

2 implies entering data and running the simulation, but some input parameters will probably still not be available, therefore the author proposes using the best guess estimate or the default values registered in the software. The third step is comparing the simulation model output to whole building data by using graphical plots and statistical indices. Lastly, the analyst must decide if the desired accuracy has been achieved, and if not changes in the input parameters will follow.

In general, the calibration is performed for the whole building energy use, by comparing the simulation results with some monthly utility bills or measurements (Haberl et al. (1998)). The calibration could also be performed for any available measurements from the Building Automation System (BAS).

Yoon et al. (1999) developed a six steps approach to calibrate energy simulation as follows:

- 1) base case modeling (gathering building data, utility bills, weather data and as built drawings, where attention must be paid to building zoning);
- 2) using monitored data from several end-uses during a week, comparison between simulation and measurements in the base load is performed;
- 3) fine tuning simulation is then performed during the mid-season when heating and cooling loads are low;
- 4) additional visits to the site are required in order to refine power densities of lighting and equipment, schedules and number of occupants;
- 5) calibration is performed for the heating and or cooling season; and

6) analysis of calibration accuracy is done by using statistical indices and graphical plots;

Waltz (2000) described in more detail the process of calibrating simulation. Compared to the report by Stein (1997), he breaks down each step into discrete steps that are explained in more detail. He proposed a new concept: in addition to analyzing the difference between utility bills and results of the simulation for an entire year for both electricity and gas, he suggested that the simulation results at the cooling and heating loads level to be scrutinized during peak days.

Mottillo (2001) presented the results of sensitivity analysis by building type, on five Canadian locations, using the DOE-2 software. Fourteen parameters are varied, one at a time, in order to determine the annual energy change. The results did not match any of the previous studies, as it was found that the most influential component for houses is the thermal resistance of the walls, roof and fenestration, followed by installed lighting power density, minimum outdoor air flow rate, pump type, efficiency of heating equipment and temperature set-point schedules. The least important factors were the thermal mass, building orientation, service water heating equipment efficiency, supply air flow rate, average monthly ground temperature and cooling equipment efficiency. She concluded that the environmental/climatic data can change the order of influence of these parameters on the performance of buildings.

The ASHRAE Guideline 14 (ASHRAE (2002)) contains a methodology for performing calibrated simulation. In short, the followings steps are proposed: 1) produce a calibrated simulation plan, 2) collect data, 3) input data into simulation software and run model, 4) compare simulation model outputs to measured data, 5) refine model until an

acceptable calibration is achieved, 6) produce baseline and post-retrofit models, 7) estimate savings, and 8) report on observations and savings.

Pedrini et al. (2002) suggested a three-step methodology that involves using as-built drawings, walk through visits, and electrical and thermal measurements. They achieved an impressive reduction from 20% errors resulted from the first calibration to 1% for the final calibration.

Liu et al. (2005) proposed an environment to calibrate whole-building energy models without manual adjusting the input model parameters. The calibration process was divided into two steps: 1) to define the parameters that affect the building cooling or heating load and 2) to tune the capacities, efficiencies and part-load performance of HVAC systems in order to match predicted energy consumption. Both steps are based on an error minimization process.

Reddy (2006) categorized the sources of errors or uncertainties into four different categories: 1) improper input parameters due to user related lack of experience and improper specification of material properties and system structure; 2) improper model assumptions and simplifications due to usage of semi-empirical models or even perhaps weaknesses in the physical modeling; 3) inaccurate numerical algorithms; and 4) errors in the simulation code.

In the research project RP-1051, Reddy et al. (2007) developed a fractional factorial analysis to quantify the effect of different input variables. For the study, data was collected from three office buildings with central cooling plants and VAV systems. The results are presented below in decreasing order of effect of each factor on the energy consumption

and demand: 1) thermal mass; 2) wall insulation thickness; 3) glazing U value; 4) solar heat gain coefficients; 5) lighting power density; 6) equipment power density; 7) supply fan static pressure; 8) supply air temperature; 9) hot water supply temperature; 10) hot water temperature difference; 11) chiller coefficient of performance; 12) chilled water return temperature; and 13) chilled water temperature difference.

Raftery et al. (2009) proposed a new methodology for calibrating building energy simulation (BES) models using an evidence-based decision-making using measurements from the building automation systems (BAS) and detailed simulation modeling. The following steps are proposed: (1) obtain data & information, use of the building integrated model (BIM) is preferred; (2) perform physical survey in order to validate the accuracy of the information gathered; (3) the data is analyzed and split into two categories: inputs and outputs; (4) evidence based decision-making is performed, meaning that any changes should be performed based on a clear hierarchy of priority; (5) various inputs are updated: geometry and construction, HVAC and plant operating set-points and schedules, redefining the thermal zones in order to eliminate inaccuracies (smaller zones rather than one big zone); (6) the model is then run and outputs are compared to utility level measurement; (7) the outputs are reviewed using (a) visualization techniques such as carpet or surface plots (Baumann (2004)), scatter plots and matrices of dependent scatter plots; (b) CV-RMSE analysis on a yearly, monthly and daily basis; (c) sensitivity analysis is performed in order to investigate possible sources of discrepancies and to determine which changes have a significant impact; in order to find out which changes are minor or trivial, the values should be modified within a reasonable range to check if the change has a significant effect; (d)

after the model is updated and in good agreement with measurements, the analysis of energy conservation measures (ECMs) is performed.

Raftery et al. (2009) encouraged keeping a history of changes along with the evidence of change, through using version control software. This basically creates a new version of the model when changes are performed, but it also stores all of the previous versions, along with a change log. He also suggests using sensitivity analysis in order to determine which changes in parameters have a significant effect and determine which changes are minor.

Guiterman et al. (2011) conducted a study over thirty low-income housing units in which he compared the energy savings predicted by the calibrated simulation to the savings predicted by two simpler methods: the temperature based method, which correlates energy use to outdoor air temperature, and the degree day method, which correlates the energy use to heating degree days. The calibrated simulation method was conducted by following the ASHRAE guideline 14 and the results are within 5% of the utility data, with the CV-RMSE coefficients of variation of the root mean squared error are of less than 15%. For one-bedroom units, the temperature based method under-predicted savings relative to the degree-day method and the calibrated simulation by 2% and 10% respectively. For two-bedroom units, the temperature based method and the degree-day method over-predicted savings relative to calibrated simulation by 4% and 6% respectively. For three-bedroom unit the temperature based method and the degree-day method, both over-predicted savings relative to calibrated simulation approach by 6%. Therefore, the calibrated simulation approach is preferred, as it provides the most accurate results.

Liu et al. (2011) recommended the use of calibration signature and characteristic signature to better understand the source of differences between predictions and measurements, and suggest inputs to be changed.

Millette et al. (2011) discussed the development of assisted calibration that uses monthly utility bills, engineering rules and optimization algorithms. They have developed a simplified common interface for DOE2.1E, DOE2.2 and EnergyPlus, called SIMEB. They discuss the possibility (in future versions of SIMEB) of using the hourly metered data of typical days for calibration of parameter values and schedules, in which the typical days are determined by using a clustering analysis method. They mention that while calibrating, the user often troubleshoots control strategies or faulty components, therefore the assisted calibration can be used as a benchmarking, retrofit assessment or commissioning tool.

Errors in calibrating of building energy simulation models are not only the result of bad modeling, but also of measurement errors. Plourde (2011) discussed the influence of the accuracy of measurement devices. The detection of data quality problems should be done at the level of sub-metering devices through validation routines; they should be corrected manually or automatically, either case, the changes made should be recorded. Properly testing, evaluating and calibrating metering devices, before putting them in use, can reduce these errors, as well as properly training the technicians in charge.

Kelsey et al. (2011) discussed procedures for energy audits using onsite measurements. There are two types of measurement devices: devices in which measurements are taken at one point in time and those that log the data over a period of time. In the case of single point measurements, the advantage is that they are fairly inexpensive and accurate, but the any variations need to be estimated. Data loggers are a

lot more expensive and the problem with them is that they are not very accurate and have calibration issues. Also storage data capacity is limited, therefore storing too many trends can cause slow communication infrastructures.

Eley et al. (2011) discussed the impact of information about the building operation on the energy simulation. The variation with time of energy performance or change of equipment should not be disregarded since most of the equipment that produces non-regulated energy use such as plug loads, refrigeration, mechanical escalators, elevators, cooking, fume hoods, freezers, have a short life. Therefore the modeling assumptions need to include all energy end-uses and be as realistic as possible. Office equipment is quite problematic since it is very short lived and the operation of it cannot be known, because it is not a scheduled activity; the solution would be to conduct surveys in order to assume the operation period. Another important issue is that the elevators, escalators and moving walkways are not currently addressed by energy efficiency codes and these are not usually readily available in energy simulation software. New equipment is introduced at a very high rate and the only thing the user could do is to try to model it as accurately as possible, but again this process relies on user's judgment and assumptions. A simple solution could be to require that any such equipment to be labeled in order to know the energy use.

Bertagnolio et al. (2012) proposed an evidence-based calibration of a simplified dynamic hourly model that uses technical specifications, measurements, sensitivity and uncertainty analysis to predict the whole building energy use.

Love et al. (2013) performed a signature-based calibration for an EnergyPlus model of a school, using measured hourly data and the characteristic signatures developed by Claridge et al. (2003). The calibration addressed adjustments first of weather-independent

factors, then on a group of weather-dependent factors and finally on the weather-independent electric demand parameters. The comparison of results with measurements show a MBE of 0.55% and a CV-RMSE of 7% for electricity use, using daily data, and 5% and 9%, respectively, for gas use using with weekly data. It should be noted that The ASHRAE Guideline 14 suggest limits only for hourly and monthly data.

2.3 Guidelines for verification and validation of calibration

The methods used in calculations vary from one software to another, some results overestimating the real values, while others underestimating them. In the case of DOE-2 program (the engine used by eQuest), a verification project was conducted at Los Alamos National Laboratory in which the monthly simulation results are compared to manual calculations and field measurements of existing buildings. Among the first verification studies, one could mention “DOE-2 Verification Project, Phase I, Interim Report” (Diamond et al. (1981)) and “DOE-2 Verification project, Phase I, Final Report” (Diamond et al. (1986)); they concluded that the predicted results follow closely enough the utility data. Many other verification and validation studies have followed, however, it is beyond the purpose of this thesis to focus on this direction.

Kaplan et al. (1990) suggested different values for various energy end-uses such as lighting, fans, heating, cooling, etc. as seen in Table 2.1. Nonetheless, there are no references for calibrating a building energy model for the supply air flow rates to zones.

Kaplan et al. (1992) have established a benchmark for maximum allowable difference between predicted and monitored data. They have proposed that a difference of 15-25% of monthly average and 25-35% of daily average is acceptable when simulating

HVAC systems, while for interior loads, differences of 5% of monthly and 15% of daily are satisfactory.

Haberl et al. (1998) considered their results are acceptable with an hourly CV-RMSE of 23.1%.

Table 2.1: Acceptable differences for different energy end-uses (Kaplan et al. (1990))

End-Use	Tuning Period Weather Type	Monthly End- Use Tolerances	Daytype Profile Tolerances
Interior light	All	± 5%	± 15%
Exterior light	All	± 5%	± 15%
DHW	All	± 5%	± 15%
Receptacles	All	± 5%	± 15%
Heating	Cold	± 15%	± 25%
Heating	Temperature	± 25%	± 35%
Cooling	Hot	± 15%	± 25%
Cooling	Temperature	± 25%	± 35%
Fans	Hot, cold	± 15%	± 25 %
Fans	Temperature	± 25%	± 35%
Building total	All	± 10%	± 15%

ASHRAE Guideline 14 (ASHRAE (2002)) provides methods for analyzing energy and demand savings from retrofits, as well as instructions on how to use calibrated simulation, but it does not give a detailed methodology on how to calibrate a simulation. It proposes of few steps to be followed for doing the calibration but it does not give explanations on how to achieve each step.

The most common method for assessing the calibration agreement is to compare the monthly energy use values to the corresponding utility bills. The problem with this approach is that the positive and negative differences, regardless of their magnitude, could cancel out, giving the impression that there is no difference between simulated and

measured values. Therefore it is not recommended to express the results only in terms of a mean and a percent difference; other statistical indices should be used to report calibrated results. The ASHRAE Guideline-14 (ASHRAE (2002)) requires the use of two different statistical indices to comply with the “Whole Building Calibrated Simulation” path: CV-RMSE and NMBE. The root mean squared error (RMSE) is used to estimate the magnitude of the error of the model, or how much spread exists in the difference between measured and predicted values (Reddy (2011)):

$$RMSE = \sqrt{\frac{\sum(M-P)^2}{n-1}} \quad (2.1)$$

where:

RMSE= root mean squared error;

P= Predicted value;

M= Measured value;

n= number of values.

Another way to represent the measured squared errors between measured and predicted values is by using the dimensionless quantity called coefficient of variation of the root mean squared error (CV-RMSE). This coefficient quantifies the relative error as well, but is a normalized measure, which is often more appropriate for model evaluation as suggested by Reddy (2011):

$$CV - RMSE = \frac{RMSE}{\mu} \times 100\% \quad (2.2)$$

where:

μ = Mean measured value.

The mean biased error (MBE) represents the difference between the measured values and predicted values (Reddy (2011)):

$$NMBE = \frac{\sum(M-P)}{(n-1) \times \mu} \times 100\% \quad (2.3)$$

ASHRAE Guideline 14 (ASHRAE (2002)) indicated that CV-RMSE of maximum 15% and NMBE of maximum 5% on a monthly basis, or 30% and 10%, respectively, on an hourly basis should guarantee a calibrated model when the whole building energy use is compared. It is uncertain whether these values are based on experimental work or some statistical analysis. The same values are prescribed by the Federal Energy Management Program (FEMP) (DOE (2008)). The International Performance Measurement & Verification Protocol (IPMVP-Committee (2002)) suggested a CV-RMSE of maximum 5% on monthly basis or 20% on hourly basis for whole building energy use.

In the research project RP-1051, Reddy et al. (2006) acknowledged that there are no specific guidelines published on how to perform a calibration using detailed simulation programs. They propose a methodology that deals with sensitivity analysis, numerical optimization and uncertainty analysis.

According to Bertagnolio et al. (2008), there are three guidelines and protocols to validate whether a building is calibrated: ASHRAE Guideline 14 (ASHRAE (2002)), the International Performance Measurement and Verification Protocol (IPMVP-Committee (2002)), the Federal Energy Measurement Program (FEMP) (DOE (2008)). However, these guidelines do not give a methodology to perform the calibration and there still is no accepted standard methodology. Often, there is not a set of complete measured data available for calibration, which forces the analyst to simulate the building performance for a very short period of time, which could lead to discrepancies over the long run simulation.

Differences between the predicted and measured values are mostly due to uncertainty in inputs (e.g. defaults, assumptions), experimental errors, mathematical models limitations, and user knowledge of HVAC systems and experience with the software (Monfet et al. (2009)). Users are often forced to assume or predict certain input parameters, but a small variation could lead to considerable change in simulated energy consumption.

Raftery et al. (2011) recommended a reduction in the acceptable hourly CV-RMSE from 30% to 20%.

2.4 Conclusions from literature review

In conclusion, the trial and error approach and the optimization approach should be used when no sufficient reliable measured data exist. Although an experienced user can predict the annual or monthly overall building energy use within a few percentages of utility bills, he/she might not achieve the calibration of systems or components models. By using monthly or daily averaged values, the fluctuations with time are lost due to the integration effect.

The evidence-based calibration approach will be explored in this study, and a calibration sequence for building energy models of existing institutional buildings using data available from the Building Automation system (BAS) will be proposed. The changes made to the input parameters are based as much as possible on data measured on site. Once the evidence-based calibrated model is obtained, the energy modeler could explore further the calibration with the uncertainty analysis and finally validate the model with statistical indices.

Chapter 3 Methodology

3.1 Objective

The objective of this study is to develop a model calibration methodology of an energy analysis program and verify the proposed methodology with data measured at the Genomic Research Center of Concordia University in Montreal, and recorded by the Building Automation System (BAS). The eQuest energy analysis program was selected for this purpose because of its large use in consulting companies and being the base of the next canQuest program.

3.2 Evidence-based bottom-up calibration approach

The hourly calibration should correspond to the main blocks of detailed building energy models: Loads, Secondary HVAC Systems and Primary Systems, instead of limiting the comparison to the annual or monthly whole building energy use (Figure 3.1). The measurements are recorded by BAS with a time interval of 15 minute, from which the hourly average values are calculated, and compared with hourly predictions from eQuest.

The proposed bottom-up approach has the following sequence:

1. Selection of measurement points available in the BAS and transfer of data to the user's database;
2. Verification of data quality and treatment such as removal of missing data, outliers, and abnormal operation data;

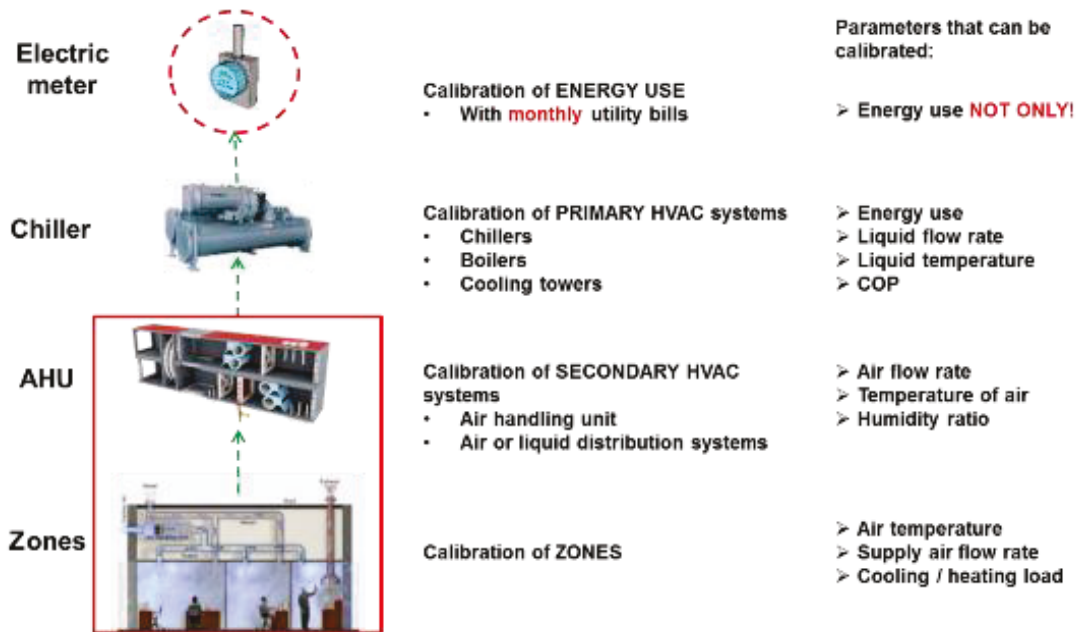


Figure 3.1: Calibration phases of the bottom-up approach

3. Data mining to extract the values of operation variables that would become inputs in the energy analysis program; only a few examples are presented here:

- average, maximum and minimum air temperatures in each thermal zone to assess the thermostat set point under regular operation, and night or week-end set-up or set-back;
- maximum supply air flow rate in each room and minimum flow ratio, in case of VAV system;
- derived measured cooling load in each space from measurements of supply air flow rate, and room-to-supply temperature difference;
- derived equivalent schedule of operation (lights, equipment, people) in each room;
- derived schedule of operation of air-handling unit (AHU);
- maximum supply air flow rate and minimum flow ratio at AHU;

- cold-deck temperature reset in terms of outdoor air temperature (T_{outdoor});
 - ratio between the outdoor air flow rate and supply air flow rate versus T_{outdoor} ;
 - switch-over temperature of economizer;
 - supply air flow rate signature versus T_{outdoor} ;
 - cooling coil load signature versus T_{outdoor} .
4. Development of the initial building model using design specifications, drawings, information from the commissioning and operation teams, and information from data mining. An equivalent step-change internal thermal load is defined for each zone, based on derived measured space cooling load and derived schedules of operation;
 5. Calibration for the supplied air flow rate and the indoor air temperature, at the zone level; it is important that the variation with time of predictions follow closely the measured profile;
 6. Calibration of the air-handling unit (AHU) for the supply air flow rate and temperature;
 7. Calibration at AHU for the heat flow rate of the hydronic or DX cooling coil, and hydronic or electric heating coil load;
 8. Calibration at AHU for the electric input;
 9. Calibration at the chilled/hot water loop level, including the water flow rate, and electric input and energy use for primary equipment (e.g., chillers and boilers); and
 10. Whole building model calibration for energy use and electric demand.

This thesis covers the items 1 to 7.

Chapter 4 Monitored data at the Centre for Structural and Functional Genomics building

4.1 Description of the building

The case study is the Research Centre for Structural and Functional Genomics in the Loyola campus of Concordia University. The Centre was built in 2011, is four stories high plus a basement, and with a total floor area of 3000 m².

The construction of the walls and roof is presented in Table 4.1. The values have been extracted from the as-built architectural drawings. The overall resistance of the walls is 3.55 m² K / W, while the roof's thermal resistance is 5.11 m² K / W. There are two types of glazing: the double low-e glazing is the one used for the doors, while the double clear glazing is used for the windows. Their properties are also presented in Table 4.1 and it should be noted that the glazing code represents the reference number for that specific glazing as it is found in "DOE2-Glass Library" file of eQuest.

The Genomic Research Center (GE building) has a variety of zones: forty-eight offices, three conference room on the first floor, a kitchen/lounge and restrooms on each floor, culturing room, environmental room and laboratories only on the 2nd and 3rd floors.

The ventilation system has special requirements, for example the laboratories that deal with chemicals have to be at negative pressure relative to the corridors or adjacent office spaces, in order for the contaminated air not to leak to the other spaces. They also have several fume hoods, through which the pollutants and contaminated air is directly evacuated to the outside.

Table 4.1: Construction of the envelope for the Genomic Research Center

Wall		
Construction	Thickness (m)	R value (m ² K / W)
Brick	0.09	0.18
Air	0.04	0.17
Insulation	0.1	2.99
Cement block	0.19	0.21
	Total R value	3.55
Roof		
Construction	Thickness (m)	R value (m ² K / W)
Membrane	-	-
Supporting channel	0.02	0.53
Insulation	0.07	3.03
Concrete	-	1.55
	Total R value	5.11
Glazing		
	SHGC	R value (m ² K / W)
Double low E (code 2600 in eQuest)	0.02	2.85
Double clear (code 2004 in eQuest)	0.02	2.73

4.2 Description of the HVAC system

4.2.1 Air side system

There are two main air handling units for air supply: 101 and 102 (Figure 4.1), which operate in parallel and distribute air throughout the building, to the labs and offices, except the mechanical room on the 4th floor, for which the system 111 is used. The main AHUs consist of the following components: pre filters, preheating coils (SC2-101-400 & SC2-102-400), pre-filters and filters, heating coils (SC1-101-400, SC1-102-400),

humidifiers, cooling coils (SF1-101-400 & SF1-102-400), followed by two supply fans in parallel for each unit (VA1-101-400, VA2-101-400 & VA1-102-400 & VA2-102-400). Two fans (VR1-101-400 and VR1-102-400) are used for the return air.

There is another system, called 103 (Figure 4.2), built entirely for evacuation of stall air from the ventilation hoods from all three floors, which has a heat recovery coil, in which glycol transfers heat between the recovery coil (SR1-103-400) and the two preheat coils from system 101 and 102 (SC2-101-400 & SC2-102-400).

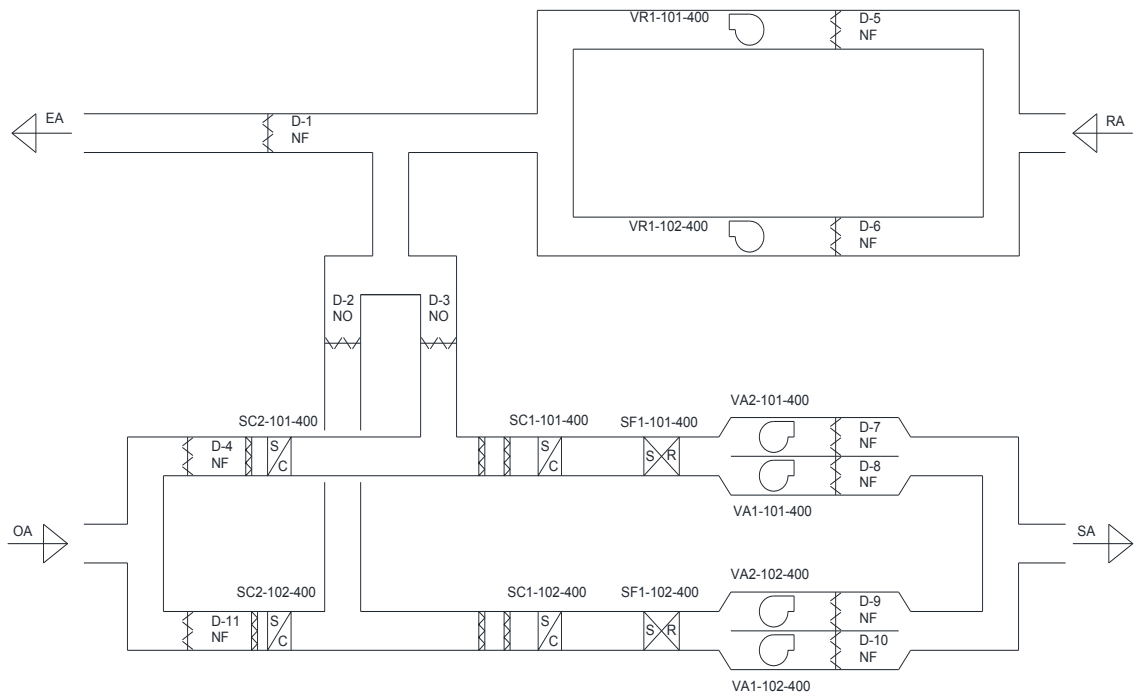


Figure 4.1: Air handling units 101 and 102

The systems for laboratories and offices have variable flow and constant temperature and they are supposed to be functioning all the time and in unison. The supply air temperature leaving the AHUs is done through the temperature sensor, which controls the heating coil's valve, the cooling coil's valve and the dampers of the mixing box; it

controls the position of outdoor air dampers to maintain the mixing temperature, when it is possible around 13 °C.

There are different types of systems for different types of spaces. The different spaces are: (i) offices in the core zone and in the perimeter zones, (ii) laboratories without ventilation hoods, (iii) laboratories with ventilation hoods, and (iv) spaces with autonomous cooling fan-coils.

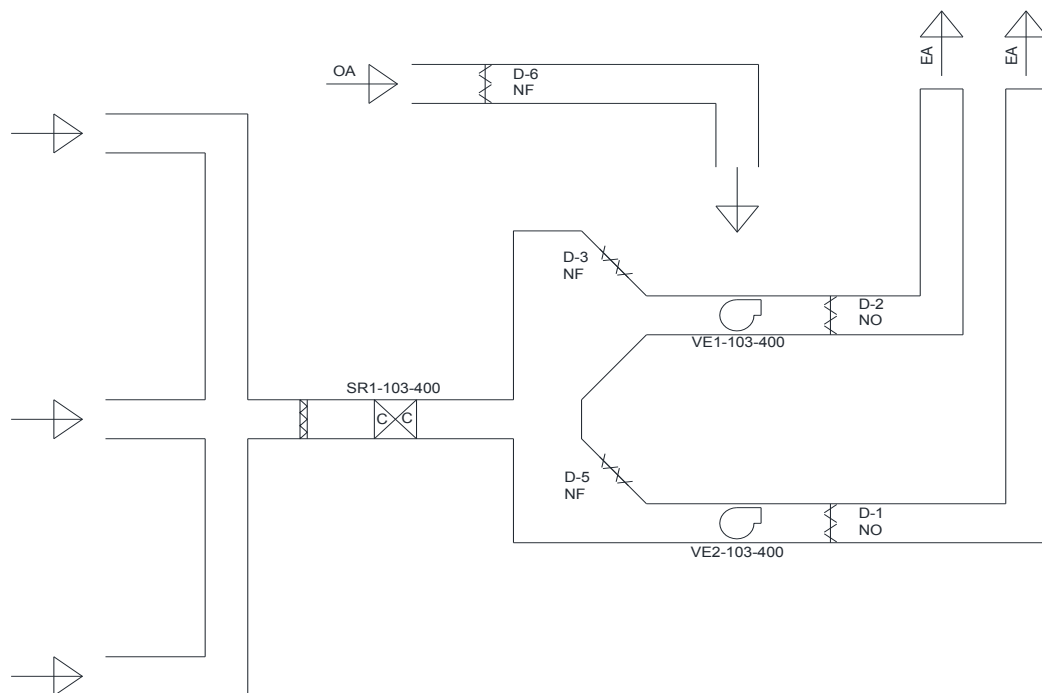


Figure 4.2: General Evacuation (System VE1/VE2-103-400)

Offices in the core zone and in the perimeter zones

The system is composed of variable air flow supply boxes with hot water reheat terminal coils and evacuation boxes. The ambient temperature is maintained at its set-point by modulating the supply air flow rate through a damper in the VAV box, and the reheating through the valve of the reheat coil. There are three operation modes for this kind of system:

1. Occupied period with a design supply air flow rate of 10 air changes per hour (ACH);
2. Unoccupied periods during the day with a design supply air flow rate of 6 air changes per hour (ACH); and
3. Unoccupied periods during the night with a design supply air flow rate of 3 air changes per hour (ACH).

Laboratories with no evacuation hoods

These rooms are equipped with the same devices like the offices. The operation modes are identical to those for the offices, with the only difference being that these laboratories are depressurized, by controlling the difference between the supply and the evacuation air flow rates.

Laboratories with evacuation hoods

In addition to the systems presented for other spaces, these systems have variable flow ventilation hoods. If the air flow rate evacuated by the ventilation hoods increases, then the air flow rate of the evacuation unit is reduced proportionally, up to the minimum, if necessary. If the difference between the supply and evacuation airflow rates is less than desired, then the supply air flow rate is increased until this difference is reduced.

The variable volume hoods are working permanently, however at reduced extraction rate when they are not in use, in order to maintain the laboratory under lower pressure than the surrounding spaces.

Spaces with fan-coils

There are two operation modes: occupied and unoccupied. In the occupied mode, the ventilator is turned on and the ambient temperature is maintained at its set-point by modulating the cooling valve of the autonomous cooling unit. During the unoccupied

mode, the ventilator stops, but the autonomous cooling unit can still be turned on in order to maintain the set-point for the unoccupied mode. An alarm is sent to central control when the temperature is higher than 27 °C.

4.2.2 Water side system

Heating water loop

In order to accommodate heating demands the heating water loop has been connected with the heating water loop of the existing Science building (SP). Two pumps were added to the hydronic circuit for circulating the hot water: PO6-CBT-611 and PO7-CBT-611, situated in the SP building on the 6th floor. In addition, two electric furnaces have been added in the central plant: a 1030 kW electric steam boiler and a 1020 kW electric water boiler. The heating water loop includes two plate heat exchangers, EC5-GLC-400 and EC6-GLC-400, which are used to transfer heat from the hot water to the glycol, which is transported to two heating coils, SC1-101-400 and SC1-102-400, which are part of the main air handling unit (Figure 4.3). The hot water loop also supplies all the reheat terminal on all four floors, including the basement.

The variable speed pumps run constantly as long as the exterior temperature is less than 16 °C and they operate alternately. The pumps stop if the exterior temperature is higher than 18 °C. If the return temperature of glycol is less than 18 °C, an alarm is sent to the central control and the pumps are stopped. The transmitter of the differential pressure DPTE-2 modulates the variable speed in sequence, in order to maintain the pressure at its set-point. The valve VP-1 is controlled in order to maintain the hot water temperature 3°C below the set-point of the hot water loop.

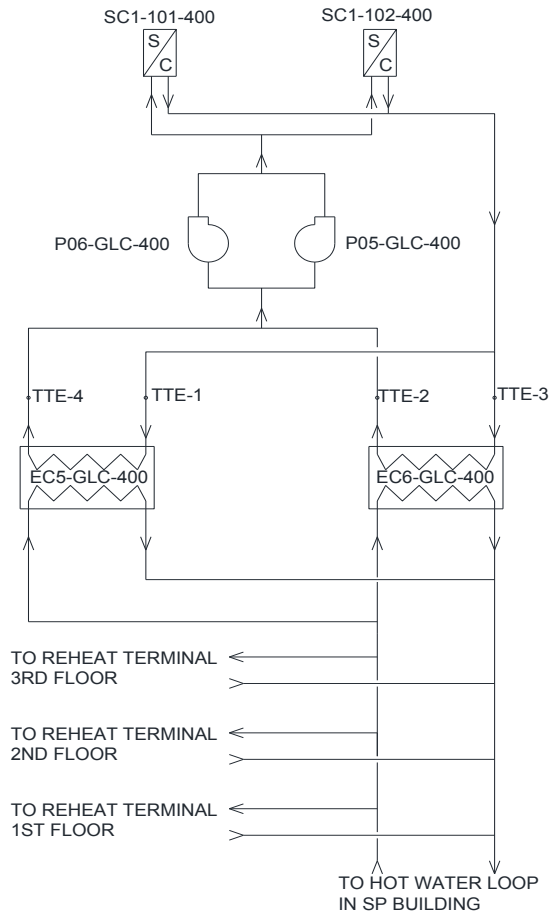


Figure 4.3: Heating water loop in Genomic Research Center

Cooling water loop

There are two individual cooling water loops: a main loop, placed in the mechanical room on the 4th floor, that supplies all the floors; and a separate loop situated in the basement of the building, designed specifically for the freezing and the server rooms.

The main chilled water loop is connected to the loop in the SP building, but it could act independently as well. This loop consists of a 1758 kW (500 tons) chiller (RF5-ERP-400) connected to a cooling tower (TR3-ETR-400), both located in the mechanical room on the 4th floor (Figure 4.4). There are two 352 kW (100 tons) chillers (RF4-ERP-612 & RF3-ERP-612) in the SP building that are connected to the circuit, as well as two 3165 kW

(900 tons) chillers (RF1-ERP-RF1 & RF2-ERP-RF1) in the central plant. If the cooling demand is low, and the two 900 tons chillers in the central plant can accommodate this demand, in addition to the demand of other buildings, then they will supply both the SP building and the GE building. Usually, in spring, the 500 tons chiller is turned off and the central plant supplies the chilled water loop. In winter, only the two 100 tons chillers supply the GE building. In the summer of whenever the demand increases, the 500 tons chiller should be activated. The chilled water is distributed to the cooling coils installed in the air handling units (SF1-101-400 and SF1-102-400) (Figure 4.4) and to the fan coil units situated on different floors.

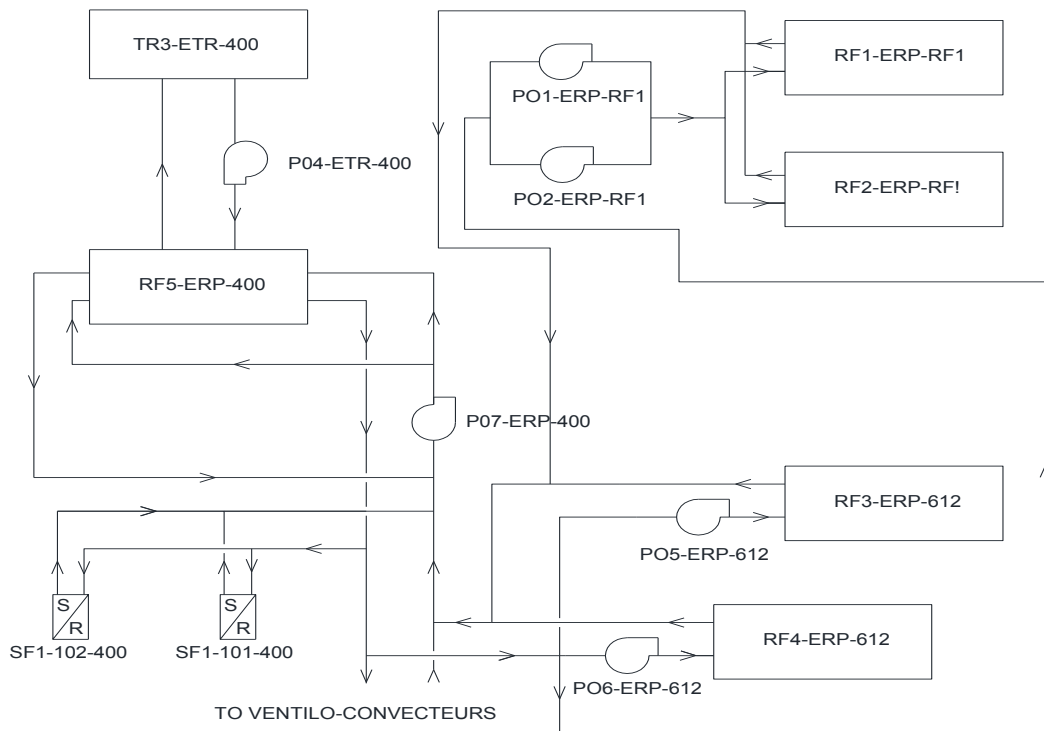


Figure 4.4: Cooling water loop

The second water loop, which is installed in the basement, is composed of three 60 tons chillers (RF6-120-S120, RF7-120-S120 & RF8-120-S120) connected to three liquid cooling units (RL1-GLC-TT, RL2-GLC-TT & RL3-GLC-TT). There are also eight LIEBERT air cooling units in the basement, six of them are used for the server room and the fridge rooms. The other two units are used to cool the mechanical room in the basement.

At the startup of a chiller, the valves open and the pumps are turned on. After receiving the confirmation of pumps running, the chiller is activated. There is a delay of minimum 1 hour when an additional chiller is started.

In normal operation, if there is a cooling demand, one of the two 100 tons chillers is authorized to start. If the chiller that is operating is at 85% of its maximum capacity and the supply water temperature is below its set-point, then the second 100 tons chiller is authorized to start. If the supply temperature cannot be satisfied, then a first 900 tons chiller is authorized to start. When the system receives confirmation that this chiller works, the two 100 tons chillers are stopped.

When the exterior temperature is less than 4 °C and for a period of 45 minutes, the system is said to be in “winter” mode under these conditions. Alternatively, when the exterior temperature is higher than 13 °C, the system is in “summer” mode.

4.2.3 Heat recovery system

The heat recovery system is composed of a loop in which glycol is being pumped by pump P03-GLR-400 in order to extract heat from the evacuated air through the recovery coil SR1-103-400 and use it to preheat the air in the two main air handling units, through the preheating coils SC2-101-400 and SC2-102-400 (Figure 4.5).

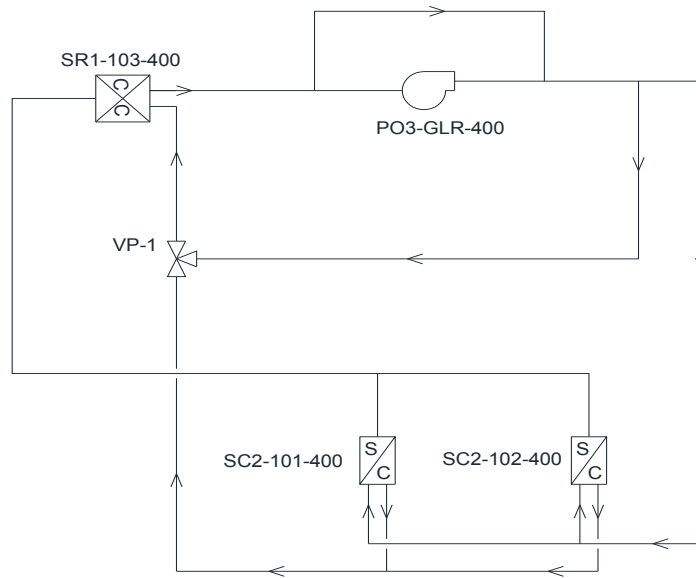


Figure 4.5: Heat recovery system

4.3 Monitored data analysis and extraction

This section discusses the methodology used to select and analyze the measurements and presents the observations found from the analysis. The measured data points are obtained from the Building Automation System (BAS), through the collaboration of the Physical Plant of the Loyola campus of Concordia University.

First, a set of 305 points are extracted from the Siemens Insight program, which is used as the data logging system. Secondly, some data points of interest for this study are selected. These are the temperatures of supply from and return to the two air handling units, the volumetric air flow rate supplied by each air handling unit, the volumetric flow rate of air supplied to each room, the return air temperature from each zone, and outdoor air temperature and relative humidity.

Third, a working file is created with all the measured values recorded every fifteen minutes for the months of June, July and August 2012. From this file, hourly, daily and

monthly averages values are calculated. A series points that present abnormal operation have been removed from this set of data, such as the period from 1st to the 10th of June inclusively.

The various rooms in the building are grouped in different thermal zones, for which the following notation was used (Tables 4.2 to 4.4): **Zone x.y z**; where: x is the floor number; y is the zone number; z is the orientation. The daily average, the standard deviation and peak values of zone air temperatures and volumetric air flow rate for each zone are listed from measurements. Figure 4.6 presents the location of thermal zones for the eQuest model of the Genomic Research building, while Table 4.5 shows the area of each thermal zone.

By knowing the measured airflow rate supplied to a zone and the return and supply air temperatures, the formula (4.1) is used to derive the heating/cooling load for each thermal zone, listed in Tables 4.2 to 4.4:

$$Q_{zone} = \frac{V_a}{1000} \times \rho_a \times c_{p,a} \times (T_{RA} - T_{SA}) \quad (4.1)$$

where:

Q_{space} = the derived thermal load [W];

V_a = the measured volumetric airflow rate for each zone [l/s];

ρ_a = the density of air, $\rho_a = 1.1225 \text{ kg/m}^3$;

$c_{p,a}$ = the specific heat of air, $c_{p,a} = 1.050 \text{ kJ/kg } ^\circ\text{C}$;

T_R = the return air temperature [$^\circ\text{C}$];

$T_{S/A}$ = the average supply air temperature [$^\circ\text{C}$].

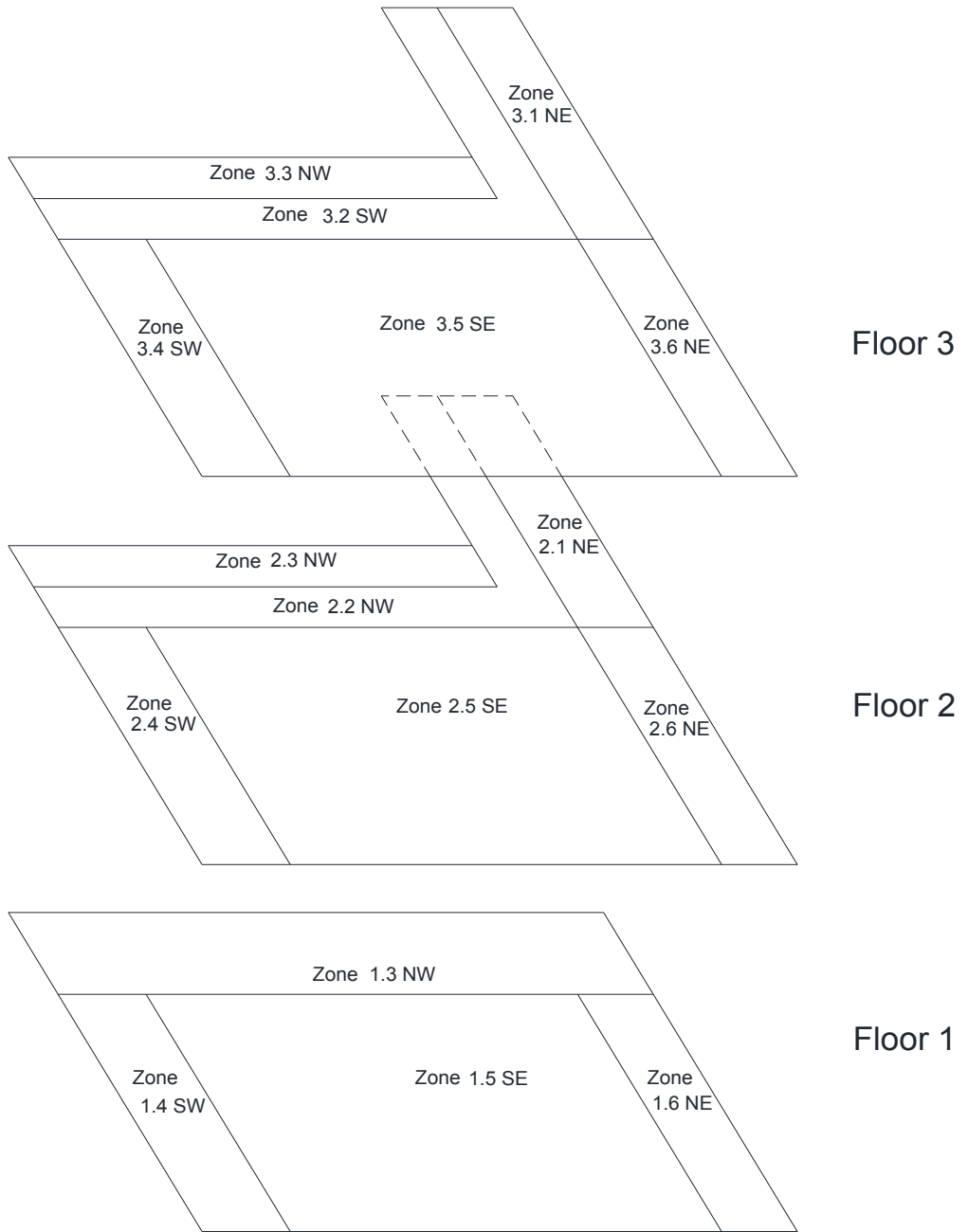


Figure 4.6: Zone locations in the Genomic research center, Concordia University

Table 4.2: Daily average and standard deviation (SD) of measured air temperature, air flow rate and cooling load for all zones, for the month of June 2012

Month	Zone	T zone [C]		Peak T zone [C]	Air flow rate [l/s m ²]		Peak air flow rate [l/s m ²]	Cooling load [W/ m ²]		Peak cooling load [W/ m ²]	
		Mean	SD		Mean	SD		Mean	SD		
June	Floor 1	1.3 NW	21.5	0.2	22.8	1.6	0.1	1.8	9.3	2.1	13.2
		1.4 SW	24.3	1.7	29.9	1.6	2.1	8.5	13.6	18.7	122.9
		1.5 SE	23.4	0.9	26.3	1.7	0.3	3.7	14.6	3.6	48.7
		1.6 NE	24.0	0.7	26.1	5.4	4.0	13.9	49.5	38.6	190.5
	Floor 2	2.1 NE	22.5	0.5	25.1	4.5	1.5	9.0	32.2	13.2	120.4
		2.3 NW	23.9	0.5	26.3	0.5	0.6	3.1	3.8	5.1	30.3
		2.4 SW	22.5	0.9	27.1	6.6	2.4	13.5	47.6	22.9	183.2
		2.5 SE	22.9	0.2	24.0	8.1	1.3	11.4	61.5	13.7	168.5
	Floor 3	2.6 NE	22.4	0.9	25.4	5.1	1.0	8.2	36.4	11.6	140.2
		3.1 NE	23.2	0.7	25.2	3.2	1.1	6.1	25.7	10.5	93.2
		3.2 SW	23.2	0.5	25.6	2.8	0.5	4.2	22.4	6.3	52.6
		3.3 NW	23.1	0.9	27.2	0.9	0.6	2.9	6.9	4.8	35.9
		3.4 SW	22.6	1.0	26.8	6.1	1.8	11.3	45.3	18.8	175.6
	3.5 SE	22.9	0.3	24.9	8.0	1.0	10.2	61.2	12.6	154.0	
	3.6 NE	22.4	0.9	25.6	5.0	0.9	8.7	35.4	11.4	120.5	

Table 4.3: Daily average and standard deviation (SD) of measured air temperature, air flow rate and cooling coil load for all zones, for the month of July 2012

Month	Zone	T zone [C]		Peak T zone [C]	Air flow rate [l/s m ²]		Peak air flow rate [l/s m ²]	Cooling load [W/ m ²]		Peak cooling load [W/ m ²]	
		Mean	SD		Mean	SD		Mean	SD		
July	Floor 1	1.3 NW	21.5	0.2	23.6	1.6	0.0	1.6	9.8	1.1	17.1
		1.4 SW	25.1	1.5	30.8	1.7	2.2	8.6	16.8	21.6	93.3
		1.5 SE	23.6	0.9	26.4	1.7	0.2	3.2	15.1	3.5	35.6
		1.6 NE	24.1	0.6	26.4	5.8	4.2	11.0	56.3	41.9	147.7
	Floor 2	2.1 NE	22.4	0.4	24.7	4.6	1.6	9.2	34.5	14.1	103.1
		2.3 NW	24.2	0.6	26.7	0.4	0.5	2.5	3.8	4.8	31.7
		2.4 SW	22.7	0.9	26.0	6.5	2.4	12.8	51.9	23.6	124.6
		2.5 SE	22.8	0.1	24.4	7.8	1.1	11.0	62.2	10.7	130.7
	Floor 3	2.6 NE	22.9	0.9	26.8	5.2	1.1	8.7	42.6	14.7	119.2
		3.1 NE	23.6	0.5	25.4	3.1	1.1	6.7	27.9	10.4	76.2
		3.2 SW	23.4	0.5	25.4	2.8	0.7	6.3	24.5	6.7	77.2
		3.3 NW	23.7	0.9	27.8	0.8	0.5	3.0	7.5	4.4	33.8
		3.4 SW	22.8	0.9	26.3	6.3	1.9	11.9	50.1	19.8	147.2
	3.5 SE	23.0	0.2	25.5	7.9	1.1	10.5	64.3	11.3	133.0	
	3.6 NE	22.9	0.8	26.3	4.9	0.9	9.0	40.1	11.6	87.2	

Table 4.4: Daily average and standard deviation (SD) of measured air temperature, air flow rate and cooling coil load for all zones, for the month of August 2012

Month	Zone	T zone [C]		Peak T zone [C]	Air flow rate [l/s m ²]		Peak air flow rate [l/s m ²]	Cooling load [W/ m ²]		Peak cooling load [W/ m ²]	
		Mean	SD		Mean	SD		Mean	SD		
June	Floor 1	1.3 NW	21.5	0.3	22.8	1.6	0.2	1.7	9.6	1.6	20.5
		1.4 SW	24.7	1.5	30.5	1.7	2.1	7.9	16.7	20.6	84.2
		1.5 SE	23.4	0.8	25.9	1.6	0.3	3.3	14.2	3.4	30.5
		1.6 NE	23.7	0.5	25.1	5.4	3.9	11.6	49.4	37.0	155.1
	Floor 2	2.1 NE	22.3	0.3	23.9	4.5	1.6	9.3	32.6	13.5	91.7
		2.3 NW	24.0	0.8	26.5	0.6	0.8	4.2	5.8	6.8	36.9
		2.4 SW	22.8	0.9	26.6	6.7	2.7	12.7	53.6	26.8	138.3
		2.5 SE	22.8	0.1	23.4	8.4	1.7	11.1	66.4	14.9	145.9
	Floor 3	2.6 NE	22.8	0.9	25.0	5.4	1.3	8.7	43.2	16.1	103.7
		3.1 NE	23.5	0.5	25.4	3.0	1.1	6.2	26.2	10.5	62.9
		3.2 SW	23.2	0.5	25.4	3.0	0.6	4.2	24.7	5.0	50.3
		3.3 NW	23.6	0.8	27.4	0.7	0.4	2.9	6.5	3.6	34.0
		3.4 SW	22.9	1.1	27.7	6.2	2.2	11.1	50.8	22.6	131.4
	3.5 SE	22.8	0.2	24.1	8.2	1.5	10.4	64.1	13.2	146.7	
	3.6 NE	22.6	0.8	24.5	5.0	1.1	8.5	38.6	13.4	82.1	

From Tables 4.2 to 4.4 one can conclude that there is no significant variation of listed variables from June to August 2012. For example, zone 3.4 SW has a mean airflow rate between 6.12 – 6.25 l/s per m² for the three months of summer, a standard deviation between 1.8-2.15 l/s m², and a peak air flow rate between 11.09-11.91 l/s per m². For the same zone, the derived mean cooling load is between 45.27- 50.82 W/ m², standard deviation is between 18.82-22.55 W/m², while the peak cooling load is between 131.36 – 175.55 W/m². It should be noted that the mean values presented in tables 4.2 to 4.4 have been averaged over each month, for each hour. Since the measurements are taken every 15 minutes, the values of each hour are an average of these 4 periods of 15 minutes.

As a first approach, the calibration is performed for three consecutive days of each month, which were selected as the days with the highest outdoor air temperature being recorded for each month: 8th-10th June, 18th-20th July and 14th-16th August 2012. The scope

of this is twofold: (i) to reduce the number of data points to be analyzed, as the total number of points is about 8000 over the summer; and (2) to verify if the calibration could be performed over a smaller number of days, instead of using the whole summer period. Figure 4.7 presents, as an example, the hourly indoor air temperature variation with time in zone 2.4 SW for the three days in July. The indoor air temperature varies for this particular interval from 21 °C to 24.5 °C. Figure 4.8 presents the hourly indoor air temperature variation with time in zone 2.4 SW for the summer period and it can be seen that the temperature varies between 21 °C and 27 °C.

Table 4.5: Areas of various conditioned thermal zones

Thermal zone	Area [m ²]
1.3 NW	335.75
1.4 SW	100.15
1.5 SE	489.41
1.6 NE	226.31
2.1 NE	126.16
2.3 NW	96.61
2.4 SW	100.15
2.5 SE	489.41
2.6 NE	100.15
3.1 NE	126.16
3.2 SW	239.13
3.3 NW	96.61
3.4 SW	100.15
3.5 SE	489.41
3.6 NE	100.15

Figure 4.9 presents the daily indoor air temperature variation with time in zone 2.4 SW for the summer period. Because the temperature was averaged over each day, the values do not fluctuate as much as with hourly average values. The daily temperature in zone 2.4 SW varies from 22 °C to 24 °C.

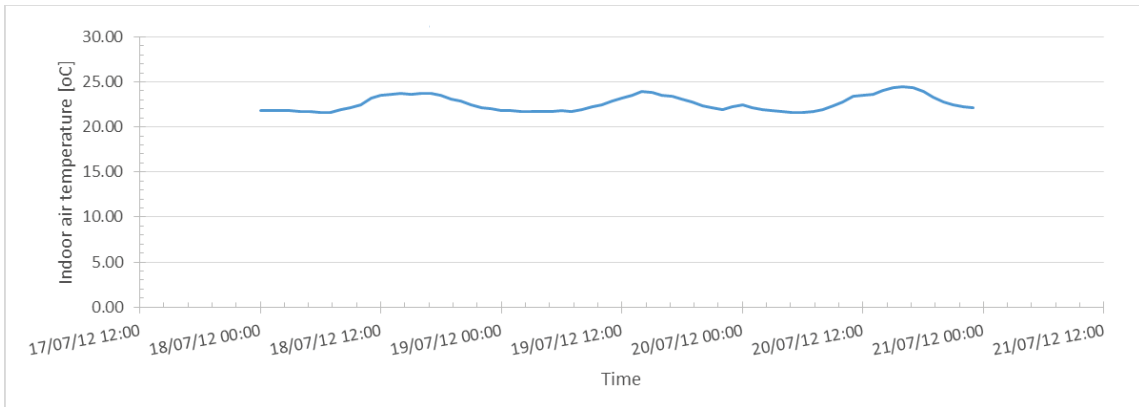


Figure 4.7: Hourly indoor air temperature variation with time for zone 2.4 SW from 18-20 July

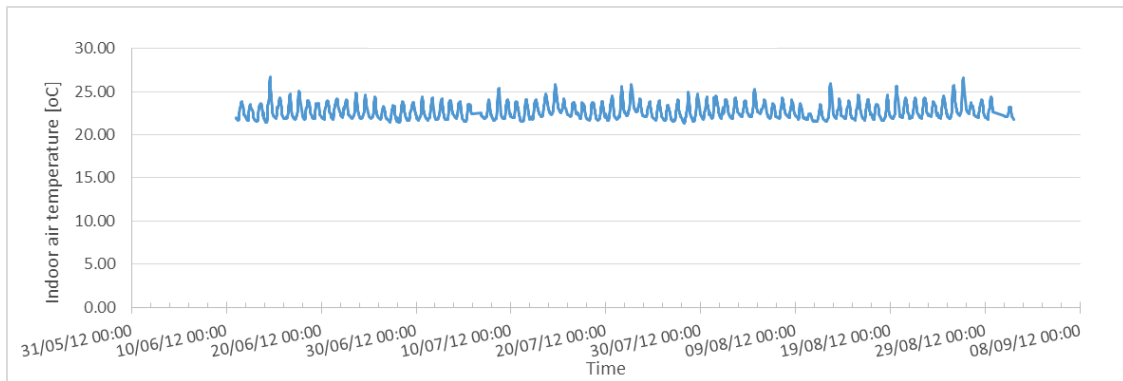


Figure 4.8: Hourly indoor air temperature variation with time for zone 2.4 SW for the summer period

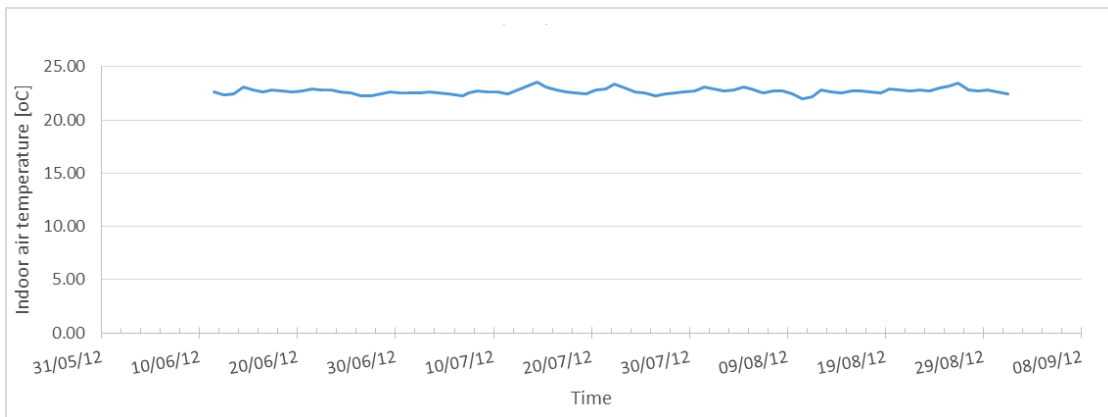


Figure 4.9: Daily indoor air temperature variation with time for zone 2.4 SW for the summer period

Figure 4.10 presents the variation of the supply air flow rate to zone 2.4 SW for the three days in July and it can be noticed that during the occupied periods the supply air flow

rate peaks around noon, having a maximum value of about 1.3 m³/s. During the unoccupied periods, the supply air flow rate varies between about 0.5 and 0.9 m³/s.

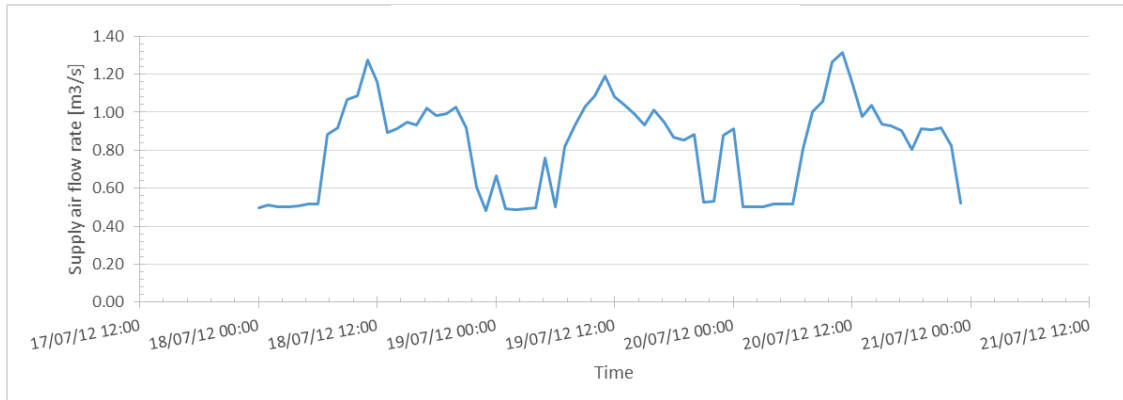


Figure 4.10: Hourly supply air flow rate variation with time for zone 2.4 SW from 18-20 July

Figure 4.11 presents the hourly variation with time of the supply air flow rate to zone 2.4 SW for the summer period. The supply air flow rate varies between about 0.5 m³/s during unoccupied periods to about 1.3 m³/s during the occupied periods.

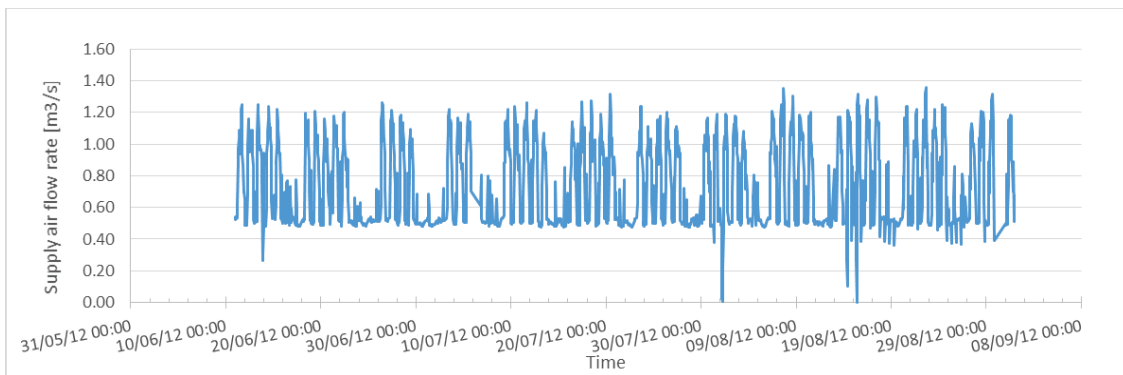


Figure 4.11: Hourly supply air flow rate variation with time for zone 2.4 SW during the summer period

Figure 4.12 presents the daily variation with time of the supply air flow rate to zone 2.4 SW for the summer period. The supply air flow rate varies from about 0.5 m³/s during the weekends to 0.85 m³/s during the week days.

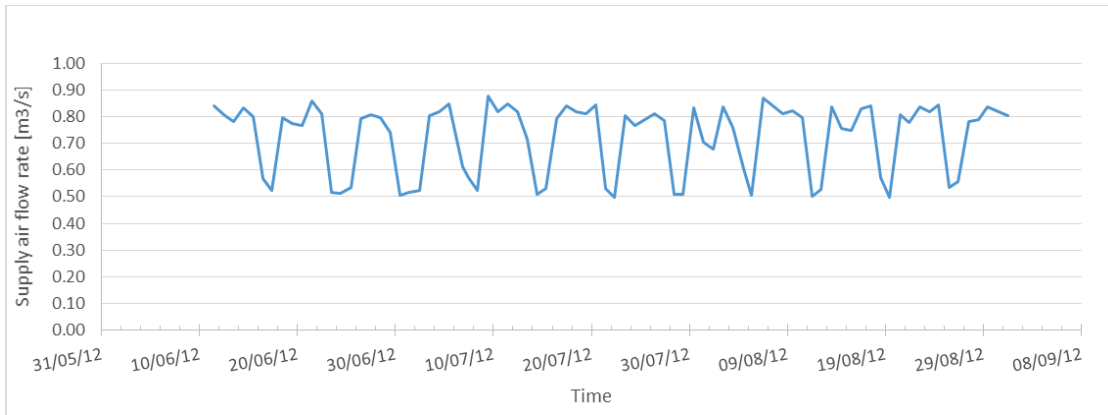


Figure 4.12: Daily supply air flow rate variation with time for zone 2.4 SW during the summer period

Figure 4.13 presents as an example, from the 18th to the 20th July the cooling load variation with time for zone 2.4 SW. The cooling load varies from about 3.75 kW during the unoccupied hours to about 10 kW during occupied hours for these particular three days.

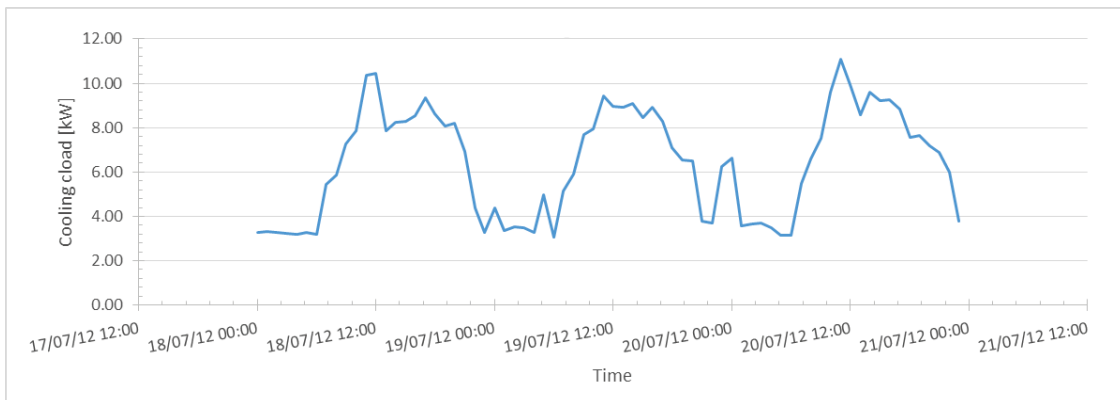


Figure 4.13: Hourly cooling load variation with time for zone 2.4 SW from 18-20 July

Figure 4.14 shows the variation with time of the cooling load for zone 2.4 SW for the summer months and it can be noticed that the cooling load varies from about 3 to 12 kW for unoccupied and occupied hours, respectively.

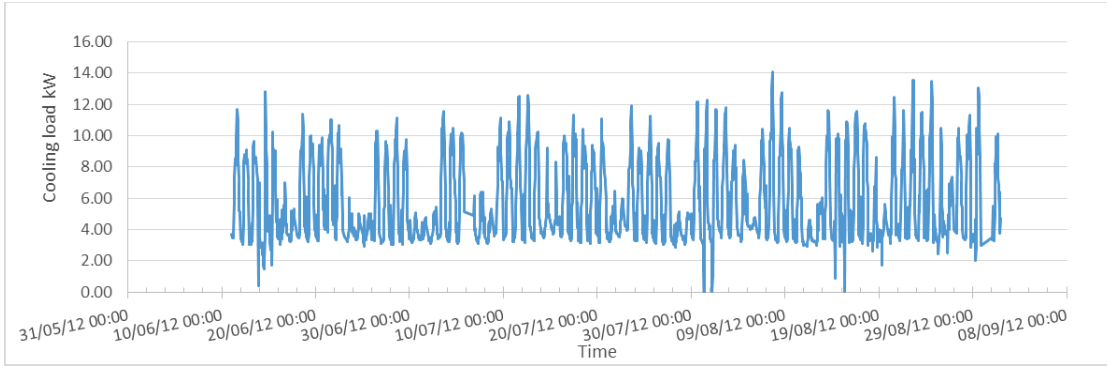


Figure 4.14: Hourly cooling load variation with time for zone 2.4 SW for the summer period

For the same zone, the daily variation of the cooling load with time is presented in Figure 4.15. When using daily averaged values, the cooling load varies from about 3.5 to 7.5 kW for weekend and week days periods respectively.

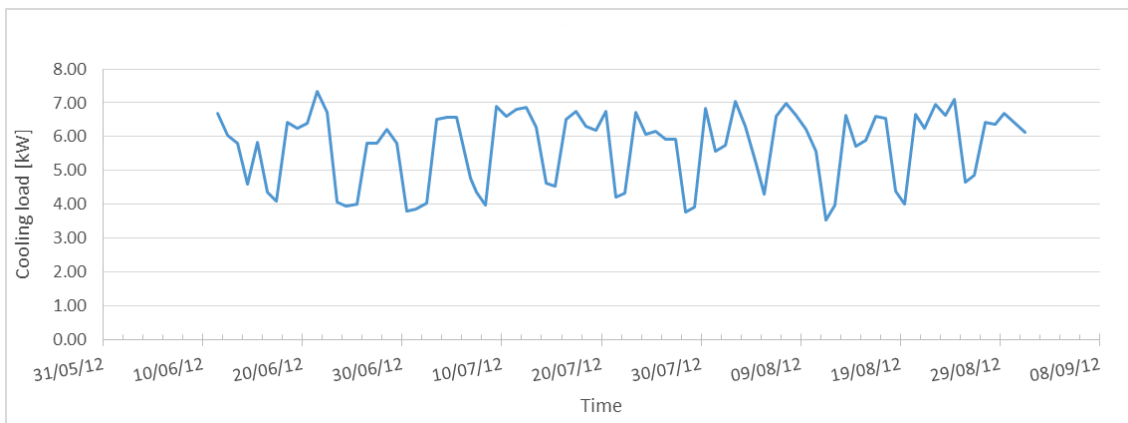


Figure 4.15: Daily cooling load variation with time for zone 2.4 SW for the summer period

Apart from analyzing the data as plots of variations with time, other graphical representations have been developed: the signatures of temperature, supply air flow rate and cooling loads versus the outdoor air temperature, as a useful approach for the study of weather dependency. Some examples will follow, for the same selected zone 2.4 SW. The signatures have been developed using hourly and daily averaged values over the summer period. The hourly measured indoor air temperature signature (Figure 4.16) presents a

small increase with the increase of outdoor air temperature; the best fit of linear regression is $T_{in} = 0.17 T_{out} + 18$ ($R^2 = 0.5924$); hence for each 1 °C of increase of outdoor temperature, the indoor air temperature increases by 0.17 °C. In the case of daily values (Figure 4.17), the linear regression is $T_{in} = 0.15 T_{out} + 21$ ($R^2 = 0.2317$), with a slope of 0.15 °C.

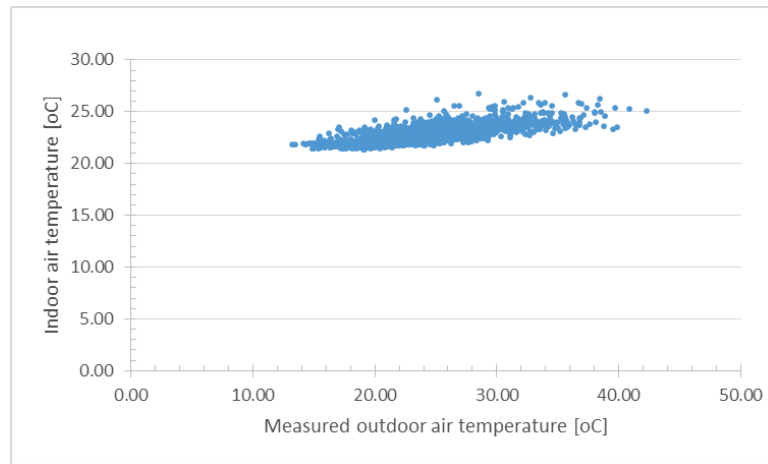


Figure 4.16: Measured hourly indoor air temperature signature for the summer period for zone 2.4 SW

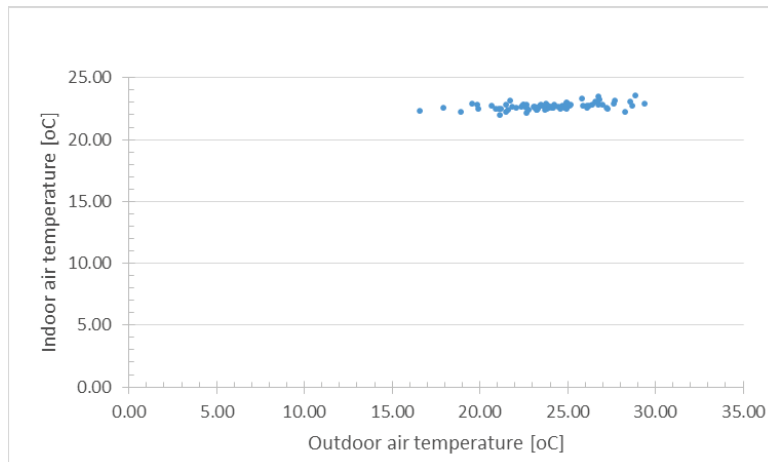


Figure 4.17: Measured daily indoor air temperature signature for the summer period for zone 2.4 SW

The signature of hourly supply air flow rate (Figure 4.18) presents a clear agglomeration of points around 0.5 m³/s for the unoccupied hours and a large variation from about 0.5 to 1.4 m³/s for the occupied hours.

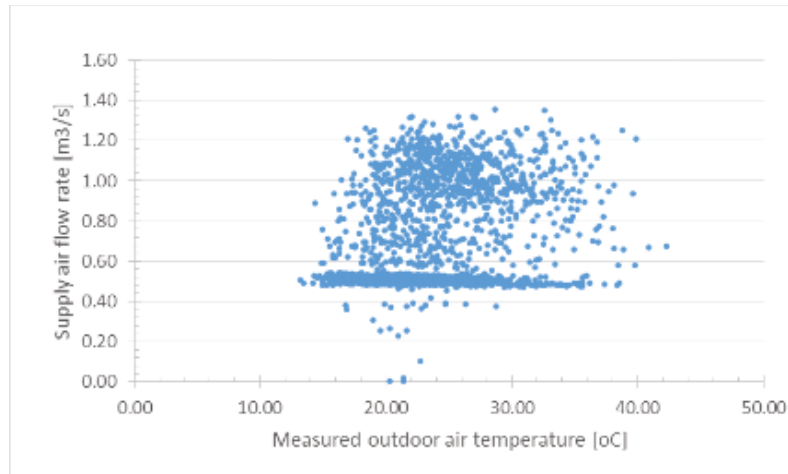


Figure 4.18: Measured hourly supply air flow rate signature for zone 2.4 SW for the summer period

The daily air flow rate signature (Figure 4.19) presents a clear difference between the values for the occupied and unoccupied hours of the daily supply air flow rate. During the occupied hours the values of the supply air flow rate vary from about 0.7 to 0.9 m³/s and during the unoccupied hours the values of the supply air flow rate vary from about 0.5 to 0.6 m³/s.

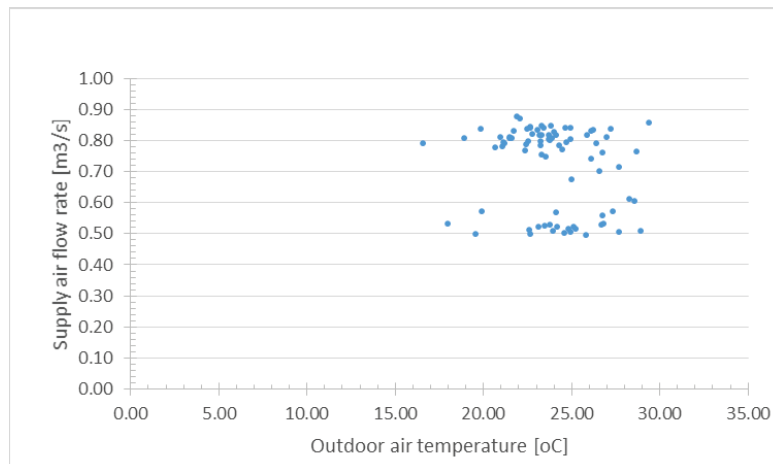


Figure 4.19: Measured daily supply air flow rate signature for zone 2.4 SW for the summer period

4.3.1 Extraction of data for the calibration of thermal zones

Equivalent internal load schedules were developed for each zone, one for the week day and another one for the weekend, based on profiles of cooling loads derived from the three-day measurements of the supply air flow rate, and supply and return air temperature.

Two important inputs are extracted from the hourly data, over the entire summer, for each zone: the design supply air flow rate (selected as the maximum measured), and the minimum air flow ratio, expressed as percentage of the maximum air flow rate (Table 4.6).

An input essential for calculating the cooling/heating load in eQuest, is the thermostat set-point, which is initially found by averaging the return air temperatures over the summer period (Table 4.7).

Table 4.6: Surface area and supply air flow rate for all zones in the building

Zone	Surface area [m ²] (<i>ft</i> ²)	Supply air flow rate [m ³ /s] (<i>cfm</i>)		Minimum flow ratio [%]
		Maximum	Minimum	
1.3 NW	335.75 (3614.01)	0.48 (1017)	0.48 (1017)	100
1.4 SW	100.15 (1078.01)	0.65 (1377)	0.01 (21)	2
1.5 SE	489.41 (5268.01)	0.97 (2055)	0.7 (1483)	72
1.6 NE	226.31 (2436.00)	1.25 (2649)	0.21 (445)	17
2.1 NE	126.16 (1357.99)	1 (2119)	0.33 (699)	33
2.3 NW	96.61 (1039.91)	0.2 (424)	0 (0)	0
2.4 SW	100.15 (1078.01)	1.2 (2543)	0.5 (1060)	42
2.5 SE	489.41 (5268.01)	2.99 (6336)	2.72 (5764)	91
2.6 NE	100.15 (1078.01)	0.78 (1653)	0.48 (1017)	62
3.1 NE	126.16 (1357.99)	0.7 (1483)	0.3 (636)	44
3.2 SW	239.13 (2547.00)	0.5 (1060)	0.3 (636)	60
3.3 NW	96.61 (1039.91)	0.36 (763)	0.07 (148)	19
3.4 SW	100.15 (1078.01)	1 (2119)	0.44 (932)	44
3.5 SE	489.41 (5268.01)	2.46 (5213)	1.64 (3475)	67
3.6 NE	100.15 (1078.01)	0.74 (1568)	0.44 (932)	59

Table 4.7: Average zone air return temperature and standard deviation (SD)

Zone	Return air temperature [oC]					
	June		July		August	
	Average	SD	Average	SD	Average	SD
1.3 NW	21.46	0.21	21.48	0.20	21.48	0.26
1.4 SW	24.81	1.55	25.04	1.48	24.66	1.42
1.5 SE	23.45	0.88	23.58	0.87	23.37	0.76
1.6 NE	24.07	0.67	24.14	0.63	23.71	0.50
2.1 NE	22.60	0.41	22.43	0.38	22.29	0.33
2.3 NW	24.06	0.44	24.15	0.53	24.02	0.82
2.4 SW	22.65	0.87	22.72	0.91	22.74	0.89
2.5 SE	22.83	0.15	22.84	0.11	22.83	0.09
2.6 NE	22.48	0.84	22.89	0.90	22.82	0.90
3.1 NE	23.52	0.60	23.60	0.51	23.50	0.52
3.2 SW	23.36	0.49	23.43	0.46	23.22	0.50
3.3 NW	23.36	0.84	23.70	0.82	23.62	0.80
3.4 SW	22.81	0.87	22.82	0.94	22.91	1.10
3.5 SE	22.91	0.27	22.99	0.21	22.78	0.19
3.6 NE	22.65	0.82	22.94	0.84	22.62	0.79

It should be noted that all values that need to be inserted into eQuest have to be converted to imperial units.

4.3.2 Extraction of data for the calibration of the air handling units

The data that needs to be analyzed in order to extract the right inputs for eQuest consists of outdoor air temperature and enthalpy, supply air flow rate, supply air temperature, cold deck air temperature (the air temperature after the cooling coil) and mixed air temperature.

The outdoor air enthalpy is estimated from measured outdoor air temperature and relative humidity (ASHRAE (2001)):

$$h = 1.006 \times T + w \times (2501 + 1.86 \times T) \quad (4.2)$$

where:

h = moist air specific enthalpy [kJ/kg_{dry air}];

w = humidity ratio [kg/kg dry air];

T = outdoor air temperature [°C];

$$w = 0.621945 \times \frac{P_w}{P - P_w} \quad (4.3)$$

where:

P = atmospheric pressure = 101325 [Pa];

P_w = partial pressure of water vapor [Pa];

$$RH = \frac{P_w}{P_{ws}} \quad (4.4)$$

where:

RH = relative humidity [%];

P_{ws} = saturation pressure [Pa];

$$\ln(P_{ws}) = \frac{C_8}{TK} + C_9 + C_{10} \times TK + C_{11} \times TK^2 + C_{12} \times TK^3 + C_{13} \times \ln(TK) \quad (4.5)$$

where:

$$C_8 = -5.8002006 \times 10^3;$$

$$C_9 = 1.3914993;$$

$$C_{10} = -4.8640239 \times 10^{-2};$$

$$C_{11} = 4.1764768 \times 10^{-5};$$

$$C_{12} = -1.4452093 \times 10^{-8};$$

$$C_{13} = 6.5459673;$$

TK = absolute temperature [K];

Table 4.8 presents the monthly average and standard deviation for the outdoor air temperature and relative humidity, supply air flow rate, supply air temperature, cold deck air temperature and mixed air temperature for the months of June, July and August 2012.

Table 4.8: Monthly average and standard deviation (SD) values of outside air temperature and relative humidity, supply air flow rate and temperature of AHU, cold deck and mixed air temperature for each month of year 2012

	Outdoor air T [°C]		Outdoor air relative humidity [%]		Supply air flow rate [m ³ /s]		Supply air T [°C]		Cold deck air T [°C]		Mixed air T [°C]	
	μ	SD	μ	SD	μ	SD	μ	SD	μ	SD	μ	SD
June	23.6	5.6	35.6	18.6	19.6	2.5	16.7	0.5	14.8	0.5	22.4	3.9
July	24.35	4.6	30.6	16.9	19.6	2.6	16.6	0.4	14.7	0.4	23.4	3.2
August	23.5	4.5	37.8	18.2	20.8	2.9	16.6	0.3	14.8	0.3	22.8	3.1

Figure 4.20 presents the variation of hourly outdoor air temperature measured at Loyola for the three selected months of the summer. The outdoor air temperature varies between about 15°C and 40 °C with higher temperatures during the day and lower temperatures at night.

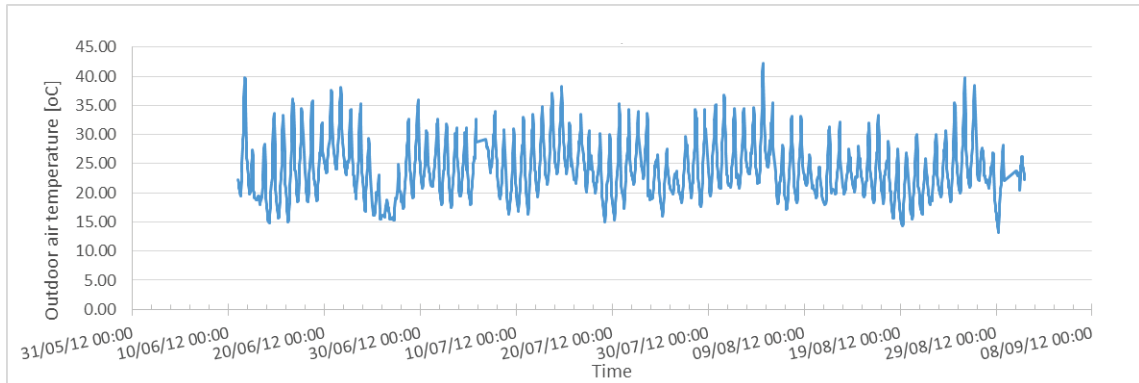


Figure 4.20: Measured hourly outdoor air temperature variation with time for the whole summer period at Loyola

Figure 4.21 presents the daily outdoor air temperature for the three months of summer. It can be observed that the temperature varies between about 15°C and 30 °C, unlike the hourly values which went up to around 40 °C. This is due to the integration effect when averaging hourly temperature values over one day.

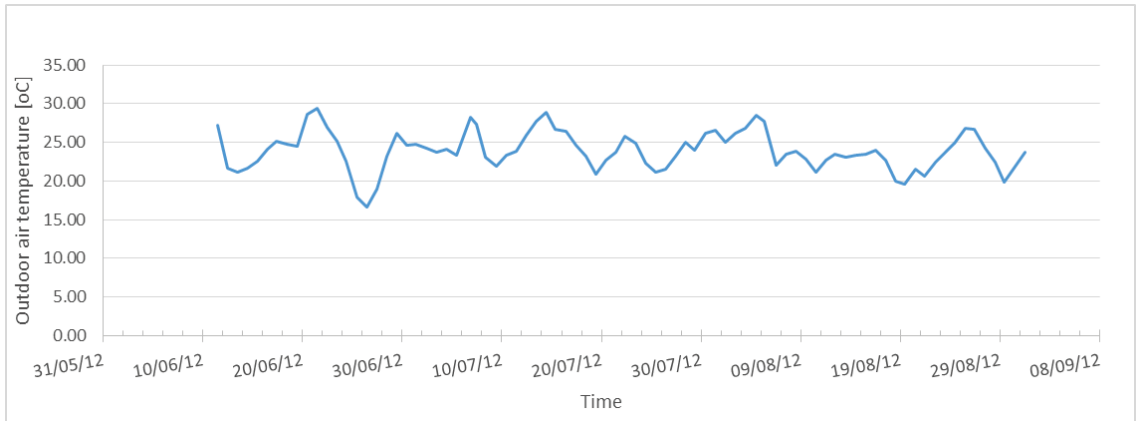


Figure 4.21: Measured daily outdoor air temperature variation with time for the whole summer period

Figure 4.22 presents the measured hourly variation of outdoor air temperature with time over three days in July, namely the period of 18th to the 20th of July. For these particular three days, the outdoor air temperature varies from about 15°C to 35 °C, with lower temperatures being registered at night and higher during the day.

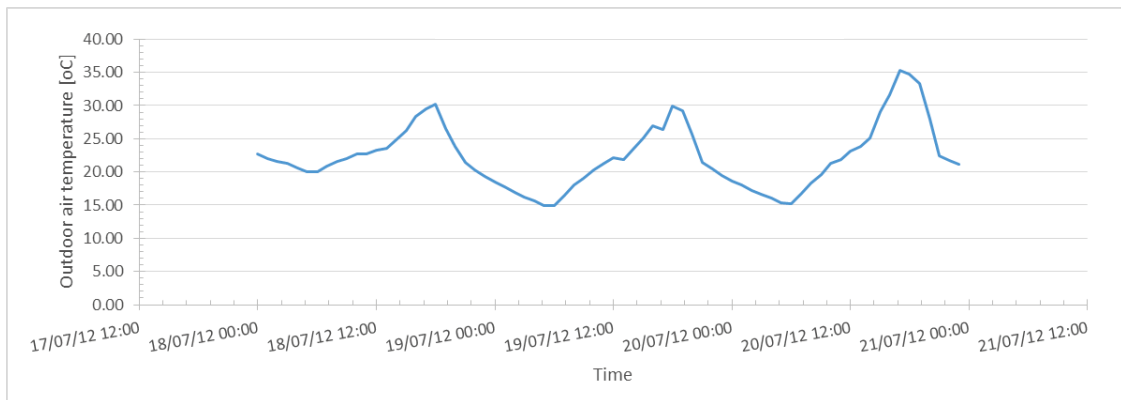


Figure 4.22: Measured hourly outdoor air temperature variation with time from the 18th-20th July

Knowing the conditions of air entering and leaving the cooling coil along with the supply air flow rate, the cooling coil load is calculated with the following formula:

$$Q_{CC} = \dot{m}_{SA} \times (h_{MA} - h_{cd}) \quad (4.6)$$

where:

Q_{cc} = cooling coil load [W];

\dot{m}_{SA} = supply air flow rate [m^3/s];

h_{MA} = mixed air enthalpy [kJ/kg dry air];

h_{cd} = cold deck air enthalpy [kJ/kg dry air].

$$h_{MA} = \alpha \times h_{OA} + (1 - \alpha) \times h_{RA} \quad (4.7)$$

where:

h_{OA} = outdoor air enthalpy [kJ/kg dry air];

h_{RA} = return air enthalpy [kJ/kg dry air];

α = fraction of outdoor air to supply air volumetric flow rate.

$$\alpha = \frac{T_{MA} - T_{RA}}{T_{OA} - T_{RA}} = \frac{\dot{m}_{OA}}{\dot{m}_{SA}} \quad (4.8)$$

where:

T_{MA} = mixed air temperature before entering the cooling coil.

T_{OA} = the average outside air temperature [$^{\circ}C$];

\dot{m}_{OA} is the outside air volumetric flow rate [m^3/s];

When calculating the air handling unit capacity, it was found that α takes values outside of the normal interval [0; 1]. In general, outdoor air is combined with the return air to give the desired mixed air temperature. Investigations revealed that the temperature of the mixed air is sometimes not between the temperatures of outdoor air and return air. This situation could occur because of reading errors by mixing temperature sensors. Because α cannot take values outside of the interval [0; 1], when α is greater than one, it was assumed that $\alpha = 1$ and when α is less than 0, it was assumed that $\alpha = 0$. Also, if supply air temperature is less than two degrees higher than the mixed air temperature, then it was assumed that the increase in temperature is caused by the heat generated by the fan, therefore no mechanical cooling is used.

Three cases have been generated:

Case 1: $\alpha \geq 1$

In this case the temperature of the mixed air is not between the temperatures of outside air and return. Since α cannot be greater than one, it was assumed that $\alpha = 1$, meaning that only outdoor air passes through the air handling unit. Hence, the mixed air temperature is equal to the outdoor air temperature. This case was further divided into two categories, based on the temperature difference between the supply air and mixed air, or in this case outdoor air.

1.a) $0 \leq T_o - T_s \leq 2$

In this case, it was assumed that no mechanical cooling was used, and the increase of air temperature of up to 2 °C difference was due to the losses in the fan operation:

$$Q_{cc} = 0 \tag{4.9}$$

1.b) $T_o - T_s > 2.0$

In this case, the mechanical cooling is employed; the following conditions apply:

$$\dot{m}_{SA} = \dot{m}_{OA} \quad (4.10)$$

$$T_{MA} = T_{OA} \quad (4.11)$$

$$Q_{CC} = \dot{m}_{SA} \times (h_{OA} - h_{cd}) \quad (4.12)$$

Case 2: $\alpha \leq 0$

When $\alpha \leq 0$, no outside air enters the building, therefore only return air temperature contributes to the mixed air temperature. Two categories have been generated, based on the temperature difference between the supply air and mixed air (in this case the return air).

2.a) $0 \leq T_R - T_s \leq 2$

In this case as well, the 2 °C difference is assumed to be caused by air passing through the fan in operation:

$$Q_{CC} = 0 \quad (4.13)$$

2.b) $T_R - T_s > 2.0$

In this case, the mechanical cooling is employed; the following conditions apply:

$$\dot{m}_{SA} = \dot{m}_{RA} \quad (4.14)$$

$$T_{MA} = T_{RA} \quad (4.15)$$

$$Q_{CC} = \dot{m}_{SA} \times (h_{RA} - h_{cd}) \quad (4.16)$$

Case 3: $0 < \alpha < 1$

In this case outside air is mixed with return air to give the mixed air that passes through the cooling coil.

$$Q_{CC} = \dot{m}_{SA} \times (h_{MA} - h_{cd}) \quad (4.17)$$

The measurement errors have been estimated based on the technical specifications of measurement devices, and standard deviation of readings:

- a) $\pm 2\%$ of the mean air flow rate for room and AHU supply and return air flow meters;
- b) $\pm 1^{\circ}\text{C}$ for duct temperature sensor; and
- c) $\pm 0.3^{\circ}\text{C}$ for room temperature sensor.

Chapter 5 Calibration of the eQuest model for supply air flow rates to zones

5.1 Preliminary calibration of supply air flow rate to zones

This section discusses the model calibration of air-side loop of HVAC system, at the zone level applied to the case study building, and using the eQuest energy analysis program. It shows results and limitations of calibration.

To facilitate the development and to find quickly errors in the input file, the first file was developed using the simplified wizard available with eQuest, and based on technical specifications, drawings, measurements from the BAS, and specifications from the ASHRAE standards 90.1 (2007) and 62.1 (2007) and MNECB (1997).

The main drivers of cooling/heating loads in a building are:

- solar radiation
- temperature difference between outdoor and indoor conditions
- thermal mass;
- occupants;
- air infiltration
- lighting loads;
- equipment loads.

eQuest calculates the thermal mass effect on the loads by using Transfer Functions Method. The effects of the lighting, equipment, and occupants were modelled based on specific loads (W/m^2) as input by the user along with schedules of operation. Those loads are split into convective and radiant components, which are accounted for separately, in the space heating and cooling loads using the Transfer Function Method. Then the cooling

load is calculated using the weighting factors that relate the cooling load to the present and previous values of the heat gain and cooling load, as presented in the ASHRAE Fundamentals Handbook (ASHRAE (2001)).

There are a series of assumptions related to this method. Firstly, all processes are linear, therefore the ones that are not linear need to be linearized. Secondly, the system properties are not a function of time; only one set of weighting factors is used for the entire simulation. Then the heat transfer coefficient for the interior of a space is divided into the convective and radiative component and assumed to be constant.

The total cooling load of a space is calculated by simple addition of individual components, while the heat extraction rate and the room air temperature are calculated using the Space Air Transfer Function (ASHRAE (2001)).

Before the eQuest software is used to calculate the thermal loads and energy consumption, a set of data must be assembled beforehand: i) building characteristics, such as location, orientation, building materials, finishing, size and shape, which are usually determined from the drawings and specifications; ii) weather files; iii) indoor conditions; iv) internal heat gains and operating schedules (equipment power density, lighting power density, occupancy schedules, lighting schedules; v) zone typing; and vi) HVAC system configuration, set-points and schedules.

The goal is to try to find these inputs mostly from measured data and if measured data is not available, then technical specifications and drawings would be used. In addition, site visits and interviews with the building operating and commissioning team took place,

for clarification and to obtain any missing information or to better understand the building and its HVAC system.

The building model corresponds to three floors of total floor area of about 3100 m², including the ground floor and the 2nd and 3rd floors. The basement was not included in the model because it has a separate HVAC system. The entire fourth floor is reserved for the mechanical room and it is not conditioned.

Fifteen thermal zones were created by grouping rooms of similar orientations and patterns of occupancy, and using information from architectural drawings to define the walls, floors, roofs and interior partitions. A simple core and perimeter zoning would have been sufficient, since the activity areas are defined as a percentage of the building area and assigned to either core zones or perimeter zones, but because the footprint is not a rectangle, the perimeter and core zones were not adequate.

The construction details were extracted from the architectural plans and input to eQuest. The specification of exterior doors and windows was also very tedious since they are specified by area and Cartesian coordinates for every orientation and for every floor. The curtain walls, covering almost 75% of the exterior walls, were defined as windows. Moreover, each window had side fins which had to be defined individually as well.

The development of input file for footprint shape and thermal zoning was the most time consuming. The building plans are in SI units, while eQuest software uses IP units and as electronic drawing were not available at the beginning of the study, the conversions had to be done manually. Usually, eQuest accepts input from files with the extension .dwg,

but the files with the Autocad drawings were not available, only the paper version of those drawings were available, therefore each zone had to be specified through vertices.

The building was used from 8 am to 11 pm, Monday through Sunday, except for holidays.

It should be noted that the simulation was done for the year 2012. Initially the Montreal weather file for eQuest was downloaded from the DOE website (Department of Energy (DOE) (2013)). Later on, a weather file was acquired from Weather Analytics (2013), which was generated from measurements at the Montreal International Airport.

The eQuest program offers the option to export the hourly values of more than 150 variables. We used this option and exported the hourly values of some variables for the comparison with measurements.

After correcting errors in the input file, we realized that the simplified wizard cannot handle the complexity of the HVAC system installed in this building, and we converted the file to the detailed wizard for the rest of study. Any changes done in the detailed mode would be lost if the user decides to return to the simplified mode.

A few evidences that the input parameters (as presented in the technical specifications) should be changed, are presented below:

a) The initial information indicated that the thermostat set point was constant at 23.2°C in all rooms throughout the entire period. However, the measurements revealed that the indoor air temperature varied from one room to another, and the thermostat set point was increased during weekends and night periods. The change to the thermostat setting for

each zone had a significant impact on the calculation of supply air flow rate, by reducing or eliminating the predicted air flow rates in weekends (Figures 5.1 to 5.4).

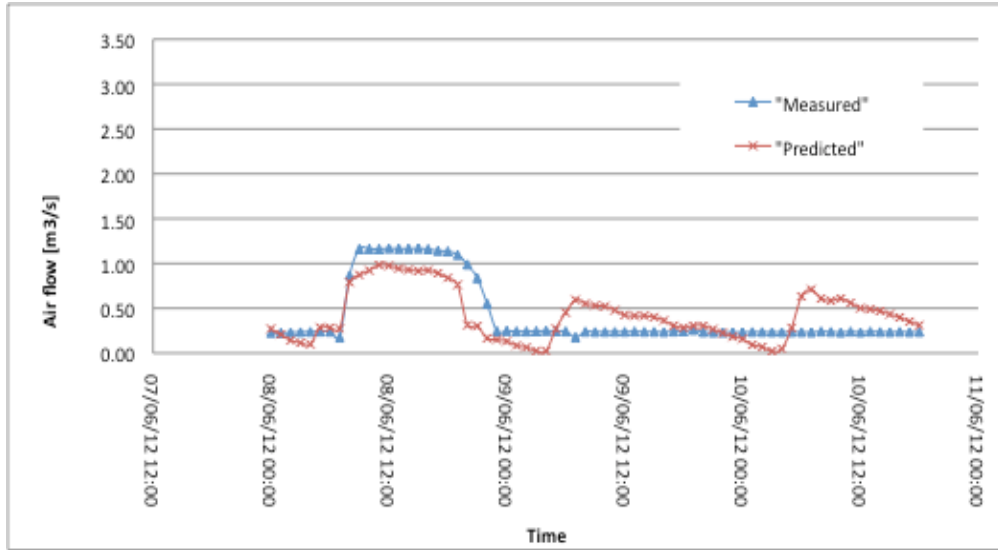


Figure 5.1: Measured vs. predicted hourly supply air flow rate in zone 1.6 NE over three days in June 2012, with constant thermostat set-point

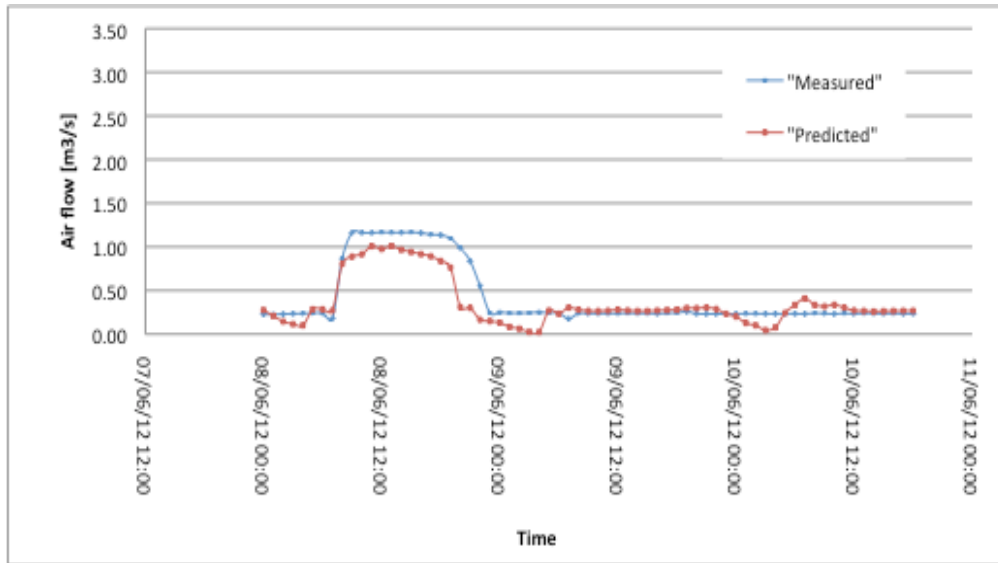


Figure 5.2: Measured vs. predicted hourly supply air flow rate in zone 1.6 NE over three days in June 2012, with thermostat setup during unoccupied hours

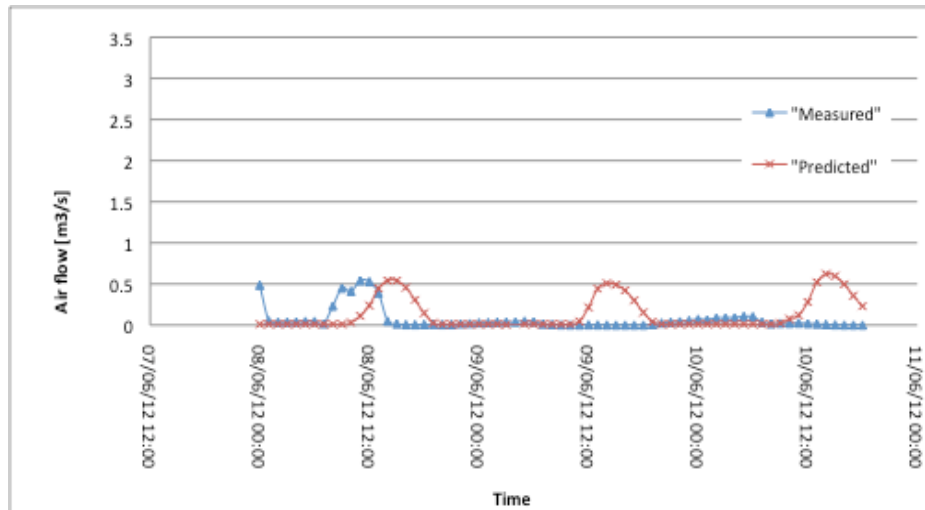


Figure 5.3: Measured vs. predicted hourly supply air flow rate in zone 2.4 SW over three days in June 2012, with constant thermostat set-point temperature

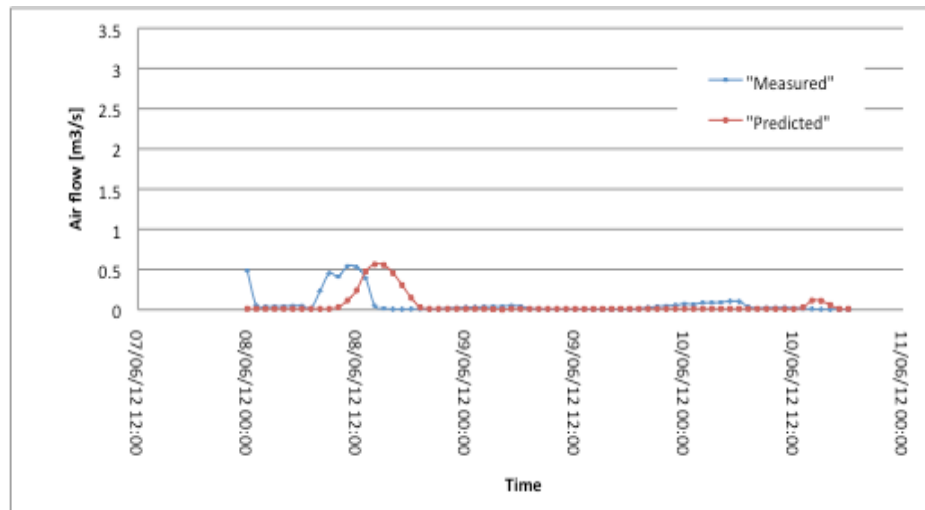


Figure 5.4: Measured vs. predicted hourly supply air flow rate ion zone 2.4 SW over three days in June 2012, with thermostat setup during unoccupied hours

b) In a building with offices and laboratories for research, it is almost impossible to input a regular pattern of usage, as there are random hourly and daily schedules of utilization. Hence, we defined for each room an equivalent rectangular-shape daily schedule. The maximum and minimum values of internal loads from lights were initially input in the software based on installed luminaires data, available in the architectural plans, and corrected based on derived measured loads during the day and at night, respectively.

Figures 5.5 and 5.6 show examples of schedules for zones 1.4 SW and 3.1 NE, for two periods: Monday to Friday and Saturday to Sunday. The blue points represent the hours during the week days, while the red points are the hours during the weekend days.

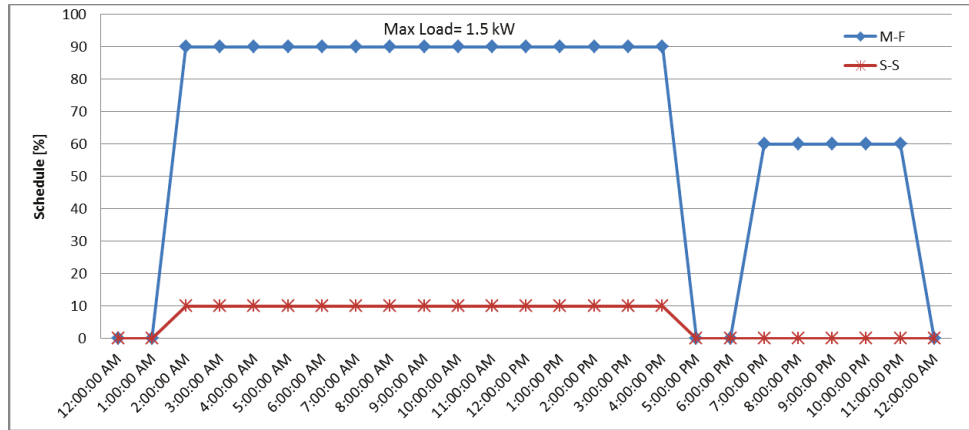


Figure 5.5: Schedule for internal loads in zone 1.4 SW

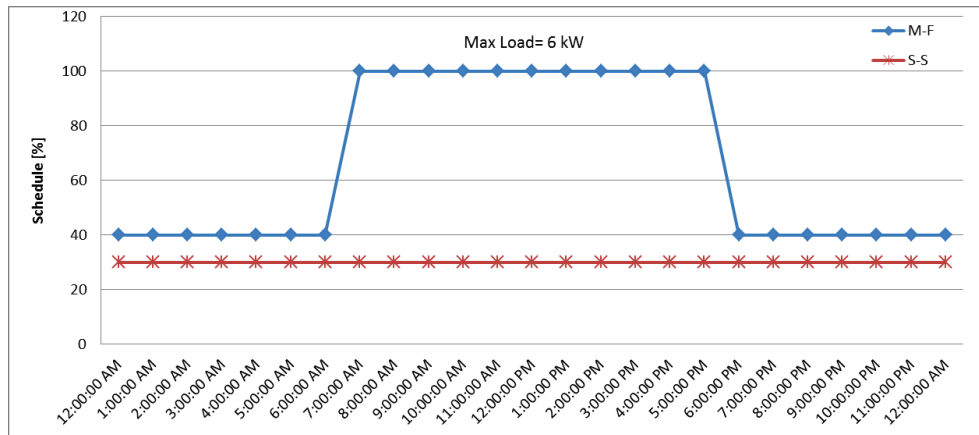


Figure 5.6: Schedule for internal loads in zone 3.1 NE

Table 5.1 summarizes the equivalent rectangular-shape daily schedules. Some zones have the same schedule of operation during week days and weekend days, while others have a different schedule during the weekend. In order to change the shape of the internal load or supply air flow profile, the user must adjust the schedule; to shift the load

higher or lower, the maximum load or “maximum power”, as it is named in eQuest, must be increased or decreased.

For instance, it was observed from the measured data that two zones, 1.4 SW and 2.3 NW, have fluctuations in load schedule during the night time as well, going from 0% to 60% from 6pm to 12 am and 8pm to 2 am respectively. Therefore these fluctuations must be simulated in eQuest, by adjusting the profile of the schedule.

Table 5.1: Schedules of equivalent internal loads

Zone	Schedule [%]						
	Internal Load [KW]	Monday-Friday			Saturday, Sunday		
		Min	Max	Interval	Min	Max	Interval
1.3 NW	3	0.5	0.5	24 h	0.5	0.5	24h
1.4 SW	1.5	0	90	1am-5pm	0	10	1am-5pm
1.5 SE	8	50	100	5am-5pm	50	100	5am-5pm
1.6 NE	13	15	100	7am-11pm	5	5	24h
2.1 NE	8	35	100	6am-6pm	35	45	7am-5pm
2.3 NW	2	0	100	3am-7pm	0	100	3am-7pm
2.4 SW	5	70	100	5am-8pm	70	70	24h
2.5 SE	25	90	100	6am-10pm	90	90	24h
2.6 NE	6	70	100	5am-6pm	70	70	24h
3.1 NE	6	40	100	6am-6pm	30	30	24h
3.2 SW	4.5	15	100	3pm-8am	15	15	24h
3.3 NW	2.25	0	100	6am-8pm	0	100	6am-8pm
3.4 SW	4	100	100	24h	75	75	24h
3.5 SE	20	70	100	6am-7pm	60	60	24h
3.6 NE	5	75	90	6am-10pm	75	75	24h

c) The calibration improved when different schedules were used for day, night and weekend periods (e.g., lights, thermostat setting) for each thermal zone, although it was time consuming

d) The design specifications indicated that during the day the supply air flow rate should correspond to 10 air changes per hour (ACH) during occupied hours, while for unoccupied hours during the day it is limited to 6 ACH, and for unoccupied hours during

the night, the maximum allowed air flow rate is 3 ACH. In this study, the maximum supply air flow rate measured on each thermal zone (as the average of all rooms in the zone) was input as the design flow rate (Table 5.2).

e) Analysis of measurements revealed that the system does not operate as initially specified at 30% minimum supply air flow, when cooling loads are small. Therefore, for each zone and the air-handling unit, respectively, the minimum air flow for the summer period was extracted from measurements and input to eQuest, as the minimum flow ratio.

f) Since at the beginning of September 2012, the actual weather data file for 2012 was not yet available (any energy modeler could face this situation), the CWEC (Canadian Weather file for Energy Calculations) weather file for Montreal, was initially used. Early January 2013, the Montreal 2012 weather file was obtained from Weather Analytics (2013), based on measurements at Montreal International Airport.

For comparison purposes, the outdoor air temperature measured on the campus during the summer of 2012 was on the average higher by 3.6°C than the value from the CWEC weather file; the difference was reduced to 1.5°C when the Montreal 2012 file was used. As a consequence, for example, for zone 1.4 SW, the average air flow rate for three days in July is 0.51 m³/s when CWEC file is used; and 0.36 m³/s when Montreal 2012 file is used (Figure 5.7). The use of Montreal 2012 weather file reduced the peak supply air flow rate by 0.15 m³/s compared with the result from CWEC file. The mean measured air flow rate for these three days is 0.24 m³/s.

g) The exterior shading from nearby buildings or “fixed shade” as it is called in eQuest, reduced the cooling load of zones of North and Northeast orientations. The side fins, which are placed on all the windows, reduced the solar heat gains for all orientations.

The effect of simulating the shades from surrounding buildings, the side fins and the overhangs can be noticed in Figure 5.8.

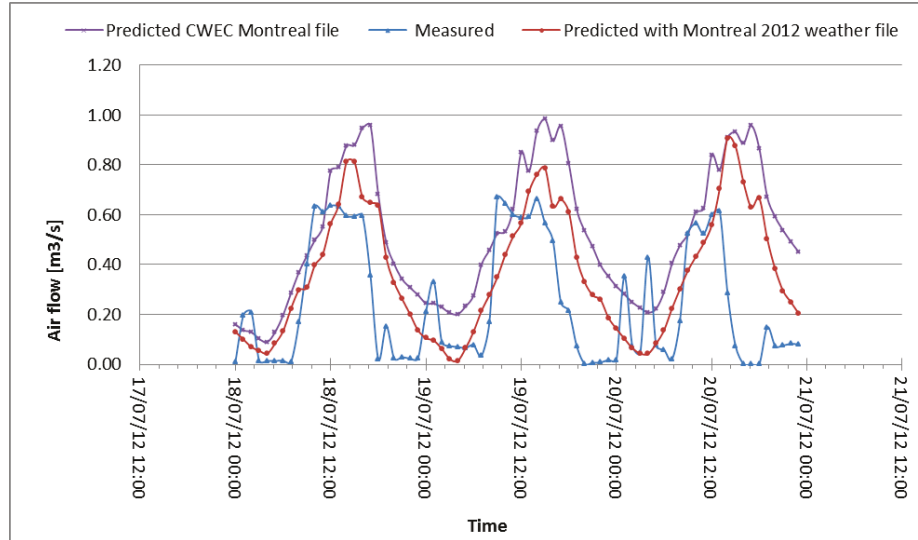


Figure 5.7: Measured vs. predicted air flow rate for zone 1.4 SW with CWEC and Montreal 2012 weather files, for three days in July 2012

Table 5.2: Internal load and supply air flow rate for all the zones

Zone	Internal load [kW]	Supply air flow rate [m ³ /s]		Minimum flow ratio [%]
		MAX	MIN	
1.3 NW	3	0.48	0.48	100
1.4 SW	1.5	0.65	0.01	2
1.5 SE	8	0.97	0.70	72
1.6 NE	13	1.25	0.21	17
2.1 NE	8	1.00	0.33	33
2.3 NW	2	0.20	0.00	0
2.4 SW	5	1.20	0.50	42
2.5 SE	25	2.99	2.72	91
2.6 NE	6	0.78	0.48	62
3.1 NE	6	0.70	0.30	44
3.2 SW	4.5	0.50	0.30	60
3.3 NW	2.25	0.36	0.07	19
3.4 SW	4	1.00	0.44	44
3.5 SE	20	2.46	1.64	67
3.6 NE	5	0.74	0.44	59

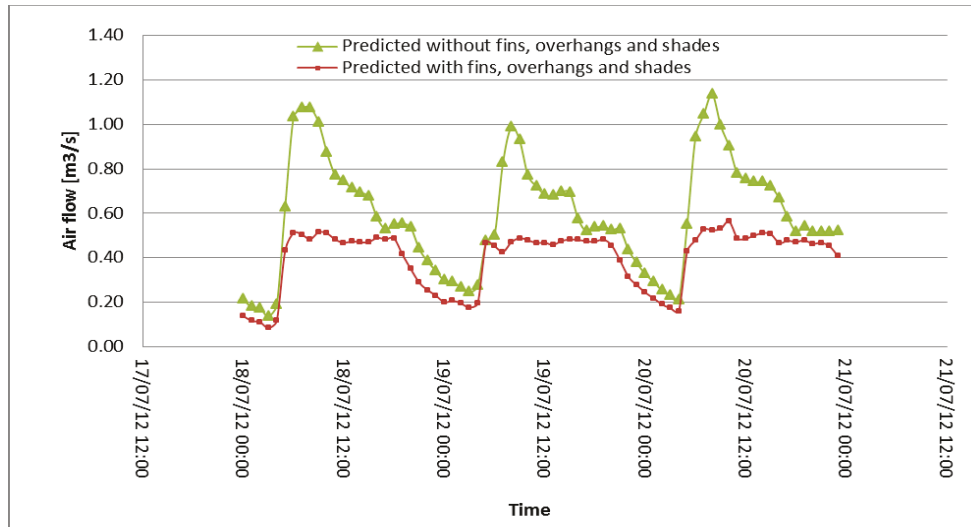


Figure 5.8: Measured vs. predicted air flow rates for zone 1.6 NE, without and with fins, overhangs and building shades, for three days in July 2012.

h) Blinds are used throughout the building and are controlled manually and in a random fashion that cannot be monitored, as seen in Figure 5.9, therefore for the energy model, blinds were assumed to be fixed with blinds schedule at 65% (based on visual assessment).

i) When making changes to the input parameters, we followed Raftery et al. (2011) suggestion to have a hierarchy of sources of information, giving the highest confidence to continuous and short-term measurements, followed by direct observations, information from the building operation and commissioning team, technical specifications and drawings, and finally standards and by-laws.

j) It should be noted that the simulation was performed for the year 2012, which was a leap year. Because eQuest does not have the capabilities to simulate a leap year, all the predictions got shifted by one day. Initially, when the weekend load schedule was allocated to Saturday and Sunday, the results showed three consecutive weekend days: Saturday, Sunday and Monday. In order to fix this problem, the input file was modified to allocate

the weekend schedules to Friday and Saturday instead, but only after February 28th. Before this date, the weekend schedules were assigned to Saturday and Sunday.



Figure 5.9: Research Centre for Structural and Functional Genomics of Concordia University

5.2 Evaluation of the calibration quality

Three methods are proposed for comparing measured the predictions resulting from the energy model simulation with the measurements: graphical representation, statistical indices (RMSE and CV) and hypothesis testing.

5.2.1 Graphical representation

After each change to the input file, the simulation results are compared with measured values in order to establish if more changes are needed and to try to find out which inputs need adjustment. Therefore, a thorough analysis of the comparison is needed.

At the zone level, the measured values are the indoor set-point temperature and the air flow rate to each zone. From these two values along with the supply air temperature from the AHUs, the cooling load is calculated. Hence, the analysis of the comparison is performed for three variables in each zone: indoor air temperature, supply air flow rate to each zone and cooling load. Plots of daily and hourly variables have been developed, for the entire summer period and for ease of viewing the results, for three days with highest outdoor registered temperature for each month. The days with the highest outdoor temperature during the month of June have been removed due to abnormal operation. Supply air flow rate signatures and cooling load signatures have also been analyzed for hourly and daily values.

As an example, Figure 5.10 and 5.11 present the predicted and measured supply air flow rate and cooling load variations with time, for zone 1.6 NE, for three days in July 2012 with the highest outdoor air temperature recorded. It can be concluded that the predictions agree well with the measurements.

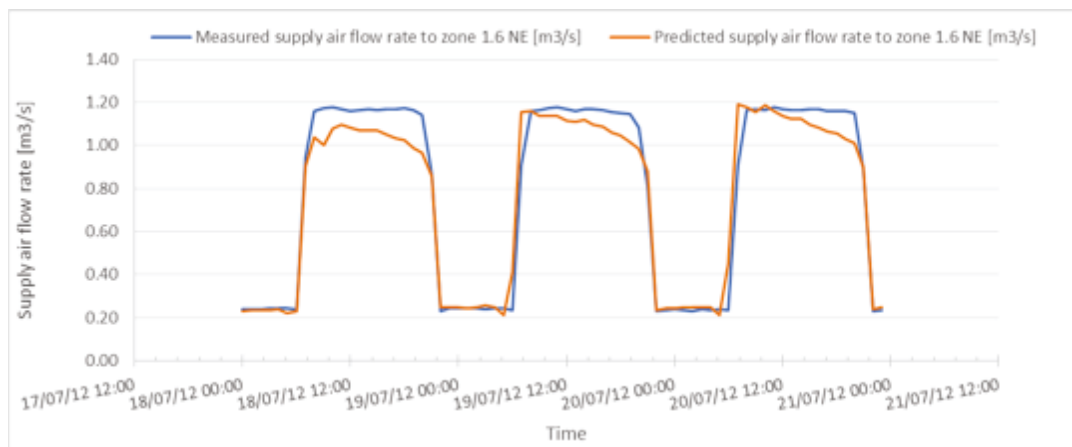


Figure 5.10: Predicted vs. measured hourly supply air flow rate to zone 1.6 NE, 18-20 July 2012

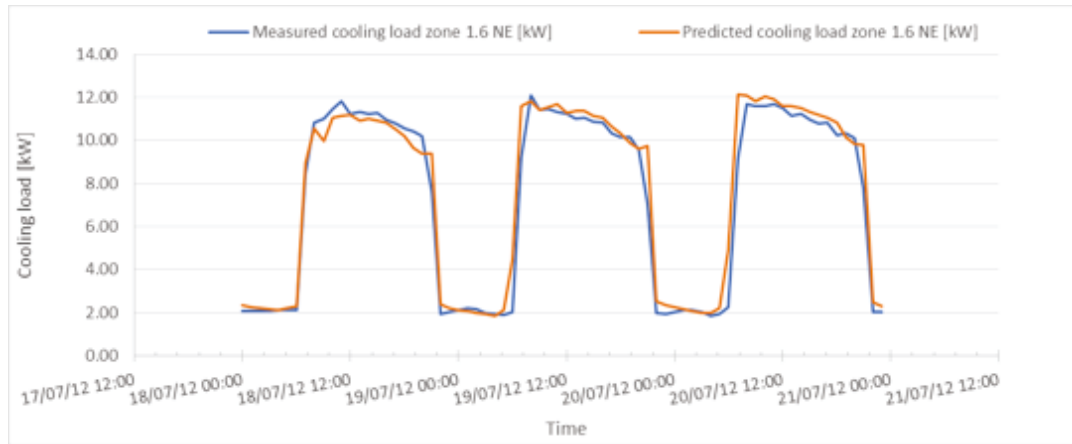


Figure 5.11: Predicted vs. measured hourly cooling load for the zone 1.6 NE, 18-20 July 2012

Figure 5.12 presents as an example, the variation with time of the air flow rate for zone 1.6 NE for the summer period, while Figure 5.13 presents the cooling load variation for the same. Based only on hourly time-series comparison, the predicted values seem to agree well with the measured values, except the weekends, where higher predicted values are noticed.

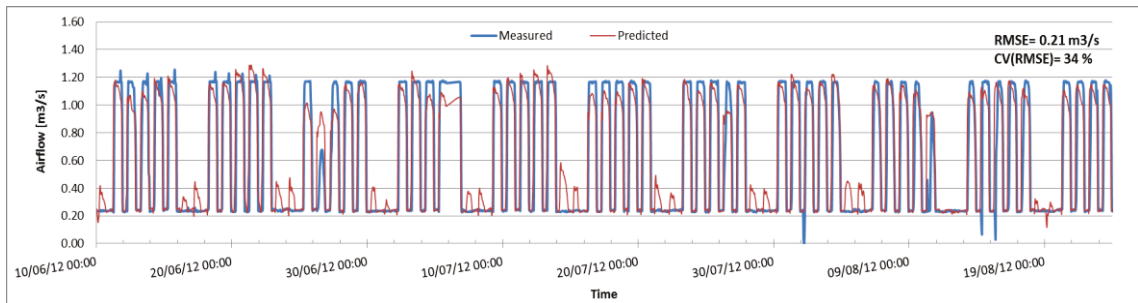


Figure 5.12: Measured vs. predicted air flow rate for zone 1.6 NE

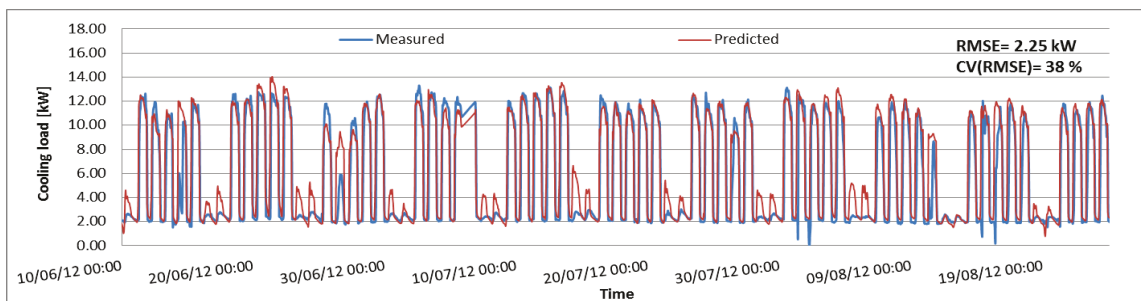


Figure 5.13: Measured vs. predicted cooling load for zone 1.6 NE

Even though the graphical representation might suggest a good agreement, further investigation is normally needed.

The graphical comparison between predictions and measurements is presented in the following sequence, for each zone, in Appendix A: Calibration results at the zone level.

- 1) Hourly values for three days in July 2012, for:
 - a) Indoor air temperature;
 - b) Supply air flow rate;
- 2) Hourly values for the entire summer of 2012, for:
 - a) Indoor air temperature;
 - b) Supply air flow rate;
- 3) Hourly signatures for the entire summer of 2012, for the supply air flow rate;
- 4) Daily signatures for the entire summer of 2012, for the supply air flow rate.

The figures from the Appendix A present a lot of details that can be useful to the modeler to take decisions regarding which input needs to be changed and by how much. It should be noted that the analysis was also performed for hourly values for the month of August, for daily values and for the cooling load in each zone, but due to space limitations the results are presented in Appendix A. However, some conclusions can be drawn from the analysis of the differences between measurements and predictions:

Figures A.1 to A.6 show that the results for zone 1.3 NW are not satisfactory: the indoor air temperature is under predicted on average by 0.06 °C, the supply air flow rate is under predicted by 0.16 m³/s and the cooling load is under predicted by 0.77 kW. The overall uncertainty in the measurement of the supply air flow rate for this zone is 0.009 m³/s, which is lower than the average difference between the predicted and measured

supply air flow rate. The summary of the rest of the figures presented in Appendix A is summed up in Table 5.3.

Table 5.3: Summary of figures presented in Appendix A

Zone	Avg ΔT [°C]	Avg ΔQ [kW]	Avg $\Delta \dot{m}$ [m ³ /s]	Uncertainty in air flow rate [m ³ /s]
1.3 NW	-0.06	-0.77	-0.16	0.01
1.4 SW	0.29	-0.10	-0.04	0.01
1.5 SE	-0.24	0.49	0.02	0.02
1.6 NE	0.05	0.72	0.02	0.02
2.1 NE	0.22	0.40	-0.02	0.01
2.3 NW	0.13	0.05	-0.01	0.01
2.4 SW	-0.05	0.19	-0.03	0.02
2.5 SE	-0.7	1.15	0.23	0.06
2.6 NE	0.22	0.96	0.05	0.01
3.1 NE	-0.46	0.21	0.01	0.01
3.2 SW	-0.17	-0.16	-0.04	0.01
3.3 NW	-0.21	0.26	0.02	0.01
3.4 SW	0.09	0.06	-0.05	0.02
3.5 SE	-0.11	1.26	0.01	0.04
3.6 NE	0.11	0.78	0.04	0.01

The overall uncertainty in the indoor air temperature is around 0.3 °C, the highest variation from the mean being $7.1 \times 10^{(-4)}$. It can be observed from Table 5.3 that the difference between predicted and measured indoor air temperature is less than the uncertainty for all zones, except for zone 3.1 NE; therefore in terms of indoor air temperature, the model could be considered calibrated for all zones, except 3.1 NE.

5.2.2 Statistical indices

Table 5.4 shows for our study, the CV-RMSE [%] of the difference between predicted and measured supply air flow rate for hourly, daily and monthly data over the entire summer of 2012, and over a three-day period using hourly data. The set of three days, July 18 to July 20 2012, were chosen as having the highest outdoor temperature recorded in July 2012.

Following the suggested statistical indices proposed in the literature, even though those indices do not refer to the calibration of air flow rate in rooms, eleven zones out of the fifteen could be considered as being calibrated when hourly values are used since CV-RMSE < 30%; and the same eleven zones are calibrated on a monthly basis since CV-RMSE < 15%. The results of three-day analysis are identical to the hourly data analysis over the whole summer, except zone 1.6 NE, which has a CV-RMSE of 30.3%, which is just above the maximum value. The daily average CV-RMSE [%] is between the hourly and monthly values for each thermal zone. There are no recommendations in the literature for the calibration of daily values.

Table 5.4: CV-RMSE of the difference between predicted and measured air flow rate

CV-RMSE [%]				
Zone	Summer			Hourly over three days
	Hourly	Daily	Monthly	
1.3 NW	38.6	35.7	34.6	41.5
1.4 SW	103.4	40.5	19.0	88.6
1.5 SE	11.6	6.5	3.0	13.4
1.6 NE	20.1	10.8	6.3	30.3
2.1 NE	18.8	9.5	4.2	24.2
2.3 NW	93.5	49.1	23.0	60.9
2.4 SW	28.4	12.7	4.0	29.7
2.5 SE	11.1	8.6	7.7	9.6
2.6 NE	17.1	11.7	8.9	16.5
3.1 NE	19.4	12.1	4.3	21.6
3.2 SW	20.9	14.1	9.5	26.1
3.3 NW	55.1	25.6	16.8	49.8
3.4 SW	26.9	13.6	8.8	24.5
3.5 SE	8.5	4.8	1.2	9.0
3.6 NE	18.6	12.1	7.0	21.5

The coefficient of variation (CV-RMSE) decreases considerably when the daily or monthly values are compared to hourly values, because of the integration effect. The use of hourly average values results in having the highest CV-RMSE values, however variations of each one hour time-scale are calibrated, if needed, since all the fluctuations with time are taken into account.

Table 5.5 presents the normalized mean biased error of the difference between predicted and measured air flow rate for hourly, daily and monthly data over the entire summer and over a three-day period using hourly data. The hourly results show that eleven zones out of fifteen are calibrated, since the NMBE $< 10\%$, while the monthly results suggest that only two zones are calibrated, having an NMBE $< 5\%$. Once again, there are no guidelines for daily values, but it can be observed that the daily values are very similar to the hourly values. Since the calibration of hourly values over a three-day period gives the similar results with the calibration over the whole summer, and to eliminate the impact of randomness of people behavior over longer periods of time, one conclusion of this study is to limit the calibration to only a few days, instead of the whole summer season. However, attention must be paid when choosing the set of three days because the results depend greatly on the thermal response of the building during these days. For this particular study the set of three days are those when the highest outdoor air temperature was recorded.

Table 5.5: NMBE of the difference between predicted and measured air flow rate

NMBE [%]				
Zone	Summer			Hourly over three days
	Hourly	Daily	Monthly	
1.3 NW	34.57	34.91	51.85	37.96
1.4 SW	20.97	21.09	28.36	17.49
1.5 SE	-2.31	-2.26	-1.86	-1.72
1.6 NE	-2.43	-2.17	-6.78	3.81
2.1 NE	3.49	3.85	6.07	9.83
2.3 NW	7.02	7.36	9.66	1.93
2.4 SW	4.11	3.84	5.55	7.34
2.5 SE	-7.52	-7.79	-11.47	-6.29
2.6 NE	-8.47	-8.49	-12.89	-6.19
3.1 NE	-2.93	-3.07	-5.99	2.70
3.2 SW	10.13	10.48	13.41	8.10
3.3 NW	-15.23	-14.46	-22.89	-15.82
3.4 SW	8.89	8.83	13.12	14.44
3.5 SE	0.14	0.13	-0.18	1.43
3.6 NE	-6.96	-6.97	-10.07	-6.58

5.2.3 Hypothesis testing

Another approach proposed in this study uses the statistical hypothesis testing. A paired difference hypothesis test (Reddy (2011)) is performed to assess whether the difference between predicted and measured air flow rates is statistically significant.

The null hypothesis H_0 states that the difference between measured and predicted air flow rate is equal to or smaller than the measurement uncertainty (u), while the alternative hypothesis H_1 states that the difference between measured and predicted values is significantly greater than the uncertainty. The significance level of the test is chosen to be $\alpha = 0.05$.

$$H_0: \mathit{abs}(M - P) \leq u \quad (5.1)$$

$$H_1: \mathit{abs}(M - P) > u \quad (5.2)$$

Equation (5.3) calculates the t-statistic (Reddy (2011)):

$$t = \frac{d-u}{SE} \quad (5.3)$$

where:

d = mean of difference between measured and predicted values [m^3/s];

SE = standard error [m^3/s].

Formulas (5.4) to (5.6) are used to calculate the rest of the parameters (Reddy (2011)):

$$d = \frac{\Sigma(M-P)}{n} \quad (5.4)$$

$$SE = \frac{S_d}{\sqrt{n}} \quad (5.5)$$

$$u = \sqrt{B_x^2 + (t_{critical} \times \frac{S_x}{\sqrt{n}})^2} \quad (5.6)$$

where:

n = sample size;

u = uncertainty in the x value at a specified confidence level [m^3/s];

μ = mean of measured air flow rate [m^3/s];

S_d = standard deviation of the difference between measured and predicted air flow rate [m^3/s];

B_x = bias or fixed component of the sensor uncertainty [m^3/s];

S_x = standard deviation of the random component [m^3/s];

As an example, the calculation of the t statistic is presented for zone 3.6 NE:

$$\mu = 0.54 \frac{m^3}{s} \quad (5.7)$$

$$S_d = 0.094 \frac{m^2}{s} \quad (5.8)$$

$$S_x = 0.096 \frac{m^2}{s} \quad (5.9)$$

$$d = 0.04 \frac{m^3}{s} \quad (5.10)$$

$$SE = \frac{0.094}{\sqrt{1850}} = 0.002 \frac{m^3}{s} \quad (5.11)$$

$$u = \sqrt{(0.02 \times 0.54)^2 + \left(\frac{1.645 \times 0.096}{\sqrt{1850}}\right)^2} = 0.01 \frac{m^3}{s} \quad (5.12)$$

Measurement uncertainty was incorporated into the hypothesis testing. Except for two laboratories (zones 2.5 SE and 3.5 SE), all other zones have the measurement uncertainty ranging from 0.01 to 0.02 m³/s. The two laboratories have the measurement uncertainty of 0.06 m³/s and 0.04 m³/s. This is due to the AIRCUITY system which takes a sample of the indoor air and verifies the chemical composition, then sends a signal to the control system to increase the ventilation rate, if necessary. This system cannot be modeled in eQuest.

The null hypothesis H_0 is true only if the t-value is less than $t_{critical}$; if t-value is greater than the $t_{critical}$, the null hypothesis is rejected and the alternative hypothesis is accepted. The $t_{critical}$ depends on the level of significance and the number of degrees of freedom (df) associated with the sample: $df = n - 1$.

The t-critical value is found from t (Student) distribution (Reddy 2011), based on the desired confidence level and the degrees of freedom. For $\alpha = 0.05$, a confidence level of 95%, and 1820 degrees of freedom, $t_{critical}$ is 1.645 for hourly values. For daily average values, a confidence level of 95% and 90 degrees of freedom, $t_{critical}$ is 1.665. For monthly average values, a confidence level of 95% and 2 degrees of freedom, $t_{critical}$ is 2.920. For the case of 3 day period, using hourly values, $t_{critical}$ is 1.67, corresponding to a 95 % confidence interval and 70 degrees of freedom.

The hypothesis test with t-statistic is based on the assumption that the difference (d) between measured and predicted values is normally distributed or close to normality. Therefore, for each zone, a histogram was plotted to verify that the condition for normality holds. If the sample size is less than 30 (Reddy (2011)), then the condition of normality

must be satisfied, but since in this particular case we are dealing with a large population (>30), a graphical representation is enough to estimate if the distribution is normal or not.

Figures 5.14 and 5.15 show two examples of histograms of the difference (d) between the predicted and measured air flow rates over the whole summer of 2012, which present a fairly normal distribution, therefore the hypothesis testing can be performed. The histograms of the difference between predicted and measured supply air flow rate for other selected zones are presented in Appendix B (Figures B.1 to B.15).

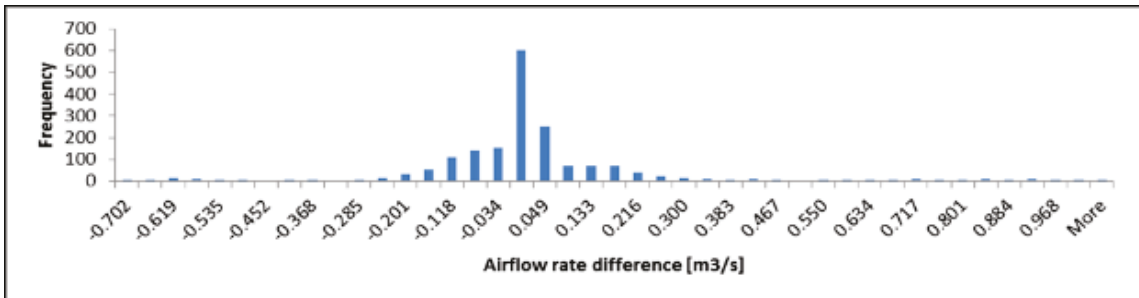


Figure 5.14: Histogram for the difference between hourly predicted and measured air flow rate for zone 1.6 NE

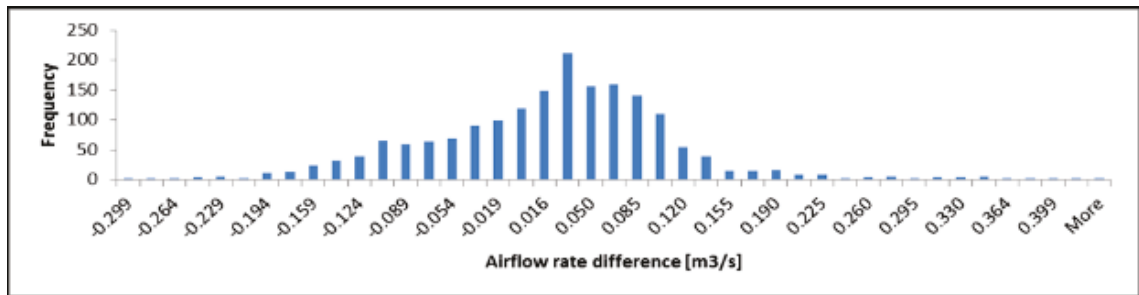


Figure 5.15: Histogram for the difference between hourly predicted and measured air flow rate for zone 3.1 NE

Table 5.6 shows the CV-RMSE based on hourly values for all the zones. According to the t-test, the null hypothesis H_0 is true only for five zones (1.5 SE, 1.6 NE, 2.3 NW, 3.1 NE and 3.5 SE), hence there is no significant difference between hourly predictions and measurements. Therefore the model of these five zones is calibrated. Out of those five calibrated zones, four have CV-RMSE less than 30 %: 11.6 %, 20.1 %, 19.4 % and 8.5 %,

while one zone has a CV-RMSE greater than 30 %: 93.6 %, which would be considered as not calibrated if the CV-RMSE criterion is used.

On the right column there are the zones for which the difference is statistically significant and hence the models are not calibrated according to the t-test. However, there are seven zones in this column with CV-RMSE < 30 %, which would be considered as calibrated if the CV-RMSE criterion is used. For instance, Zone 2.5 SE has a CV-RMSE of 11.1 %, which is much lower than the accepted value of 30%.

Figure 5.16 shows that the air flow for zone 2.5 SE is indeed not calibrated; this zone would wrongly be assumed to be calibrated, if CV-RMSE is used. The hypothesis test proves that the difference between predicted and measured values is statistically significant.

Table 5.6: Hourly coefficient of variation for all the zones in the building for the summer period

CV-RMSE (hourly) [%]		
Zone	$t < t_{critical}$	$t > t_{critical}$
1.3 NW		38.6
1.4 SW		103.4
1.5 SE	11.6	
1.6 NE	20.1	
2.1 NE		18.8
2.3 NW	93.6	
2.4 SW		28.4
2.5 SE		11.1
2.6 NE		17.1
3.1 NE	19.4	
3.2 SW		20.9
3.3 NW		55.1
3.4 SW		26.9
3.5 SE	8.5	
3.6 NE		18.6

Therefore stating that a 30 % maximum CV-RMSE ensures that the model is calibrated appears not to be sufficient; a hypothesis testing should be performed to verify if the differences between predicted values and measurements are significant or not, compared to the measurements uncertainty.

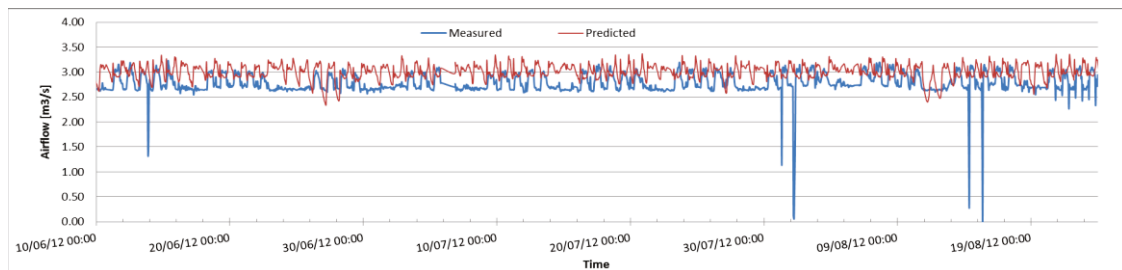


Figure 5.16: Predicted vs. measured air flow rate for zone 2.5 SE, for the entire summer period

Tables 5.7 and 5.8 present more details about the comparison of calibration decision based on the t-test and coefficient of variation (CV-RMSE), based on hourly, daily and monthly mean values. It can be observed that the results vary greatly depending on whether hourly, daily or monthly values are used.

For instance, for zone 2.1 NE, employing hourly values or monthly values over the entire summer results in the model not being calibrated (according to t-test). With the same set of data, using daily average values results in successful calibration, as well as using hourly values over a set of three days. Therefore it is very important to decide whether to do hourly, daily or monthly calibration, and which calibration approach to be used.

Except for zones 2.5 SE and 3.5 SE, which are the two laboratories, all other zones have an uncertainty ranging from 0.01 to 0.02 m³/s. The two laboratories have an uncertainty of 0.06 and 0.04 m³/s, which is due to the AIRCUITY system which takes a sample of the indoor air and verifies the chemical composition of it, then sends a signal to

the control system to bring in more fresh air, if necessary. Modelers should be aware that these kind of systems cannot be modeled in eQuest.

Table 5.7: Hourly, daily and monthly coefficient of variation for zones 1.3 NW to 2.5 SE

CV-RMSE [%]				
Zone	Interval	Time step	t < t _{critical}	t > t _{critical}
1.3 NW	Summer	Hourly		38.6
		Daily		35.8
		Monthly		34.6
	3 days	Hourly		41.5
1.4 SW	Summer	Hourly		103.4
		Daily		40.5
		Monthly		19.0
	3 days	Hourly	88.6	
1.5 SE	Summer	Hourly	11.6	
		Daily	6.5	
		Monthly	3.0	
	3 days	Hourly	13.4	
1.6 NE	Summer	Hourly	20.1	
		Daily	10.8	
		Monthly	6.3	
	3 days	Hourly	30.4	
2.1 NE	Summer	Hourly		18.8
		Daily	9.5	
		Monthly		4.2
	3 days	Hourly	24.2	
2.3 NW	Summer	Hourly	93.6	
		Daily	49.1	
		Monthly	23.0	
	3 days	Hourly	60.9	
2.4 SW	Summer	Hourly		28.4
		Daily	12.8	
		Monthly	4.0	
	3 days	Hourly	29.7	
2.5 SE	Summer	Hourly		11.1
		Daily		8.6
		Monthly		7.7
	3 days	Hourly		9.6

Table 5.8: Hourly, daily and monthly coefficient of variation for zones 2.6 NE to 3.6 NE

CV-RMSE [%]				
Zone	Interval	Time step	t < t _{critical}	t > t _{critical}
2.6 NE	Summer	Hourly		17.1
		Daily		11.7
		Monthly		8.9
	3 days	Hourly	16.6	
3.1 NE	Summer	Hourly	19.5	
		Daily	12.1	
		Monthly	4.3	
	3 days	Hourly	21.7	
3.2 SW	Summer	Hourly		20.9
		Daily		14.1
		Monthly	9.5	
	3 days	Hourly	26.1	
3.3 NW	Summer	Hourly		55.0
		Daily		25.6
		Monthly	16.8	
	3 days	Hourly	49.8	
3.4 SW	Summer	Hourly		27.0
		Daily		13.6
		Monthly		8.8
	3 days	Hourly		24.5
3.5 SE	Summer	Hourly	8.6	
		Daily	4.8	
		Monthly	1.2	
	3 days	Hourly	9.0	
3.6 NE	Summer	Hourly		18.7
		Daily		12.1
		Monthly		7.0
	3 days	Hourly	21.5	

5.3 Improvement of preliminary calibration

Four different techniques were further explored to reduce the difference between measurements and predictions of supply air flow rates. The base case that was previously discussed is called “Run 1” for the ease of understanding. For Runs 2 to 5, the peak value of internal loads is changed, while the schedule is held constant. The different methods of adjusting the load based on air flow rate difference are explained below.

Run 2:

For each zone, two histograms were created: one for measured air flow rate and one for predicted air flow rate; the difference Δm between the most frequent occurring air flow rates (measured vs. predicted) was recorded. From this difference, the correction of the cooling load, ΔQ , was calculated based on equation (4.1); the indoor temperature used in equation (4.1) is the mean indoor temperature for the entire summer. The correction factor of the cooling load was used to adjust the maximum internal load, $Q + \Delta Q$, was input into eQuest.

Run 3:

For each zone, the histogram of the difference between predicted air flow rate and measured air flow rate was created and from this, the most frequent occurring difference in air flow rates (measured vs. predicted) was recorded. From this difference, the correction of the cooling load, ΔQ , was calculated based on equation (4.1); the indoor temperature used in equation (4.1) is the mean indoor temperature for the entire summer. The correction factor of the cooling load was used to adjust the maximum internal load, $Q + \Delta Q$, was input into eQuest.

Run 4:

For each zone the mean indoor temperature, mean predicted and mean measured air flow rates are calculated for the hours of operation only; with these values, the correction of the cooling load, ΔQ , was calculated based on equation (4.1). The correction factor of the cooling load was used to adjust the maximum internal load, $Q + \Delta Q$, was input into eQuest.

Run 5:

For each zone the mean indoor temperature, mean predicted and mean measured air flow rates are calculated for the hours of operation only, but excluding the weekend days (because the indoor temperature set-point is greater during the weekend days); with these values, the correction of the cooling load, ΔQ , was calculated based on equation (4.1). The correction factor of the cooling load was used to adjust the maximum internal load, $Q + \Delta Q$, was input into eQuest.

As an example of Run 2, Figures 5.17 and 5.18 present the histograms of the measured and predicted air flow rate, respectively, for zone 3.1 NE (from the base case or Run1). The indoor temperature for this zone is 23.4 °C and the supply air temperature is 16.5 °C. The measured most frequent air flow rate is 0.298 m³/s while the most frequent predicted air flow rate is 0.347 m³/s, resulting in a correction of mass flow rate $\Delta m = 0.049$ m³/s. This is translated into a correction of the cooling load of 0.42 kW using equation 4.1. Since the predicted air flow rate is higher than the measured one, the corrected cooling load

is obtained by subtracting the correction of 0.47 kW from the initial cooling load of 5.99 kW; the new cooling load for this zone is then 5.57 kW.

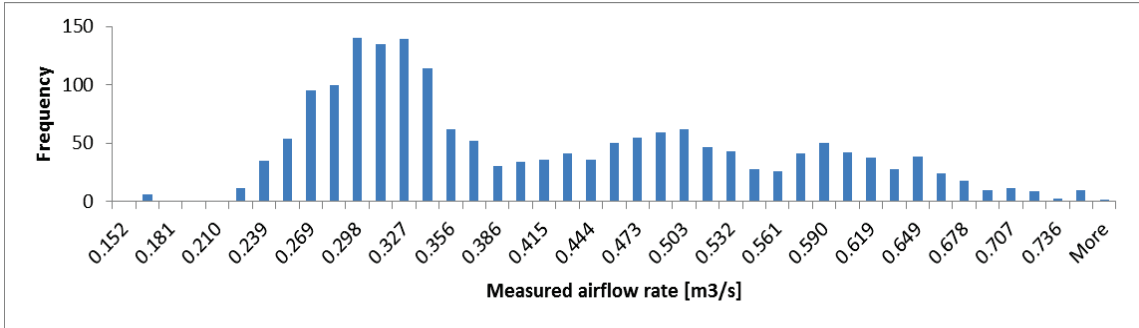


Figure 5.17: Histogram of measured air flow rate for zone 3.1 NE

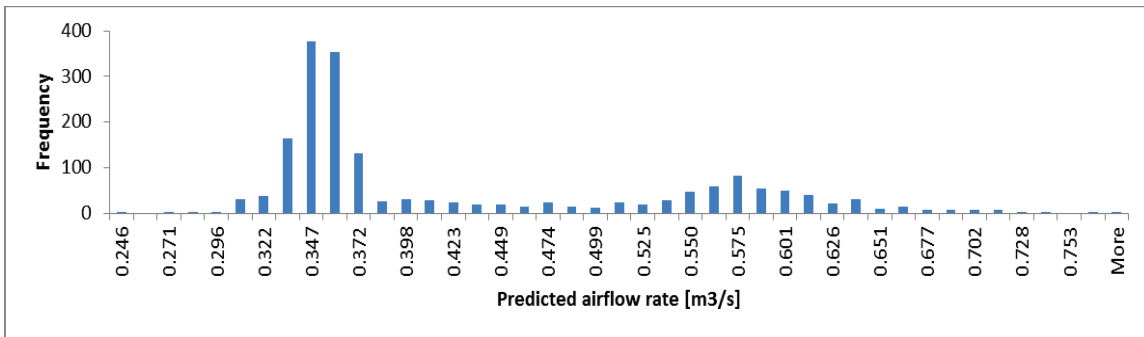


Figure 5.18: Histogram of predicted air flow rate for zone 3.1 NE

As an example of Run 3, Figure 5.19 presents the histogram of the difference between predicted and measured air flow rate for zone 3.1 NE (from the base case / Run1). The indoor temperature for this zone is 23.4 °C and the supply air temperature is 16.5 °C. The most frequent difference in air flow rate is $\Delta m = 0.049 \text{ m}^3/\text{s}$. This is translated into a correction of the cooling load of 0.28 kW. This load difference needs to be subtracted from the previous load condition, since the predicted air flow rate is higher than the measured one, resulting in a new load of 5.71 kW.

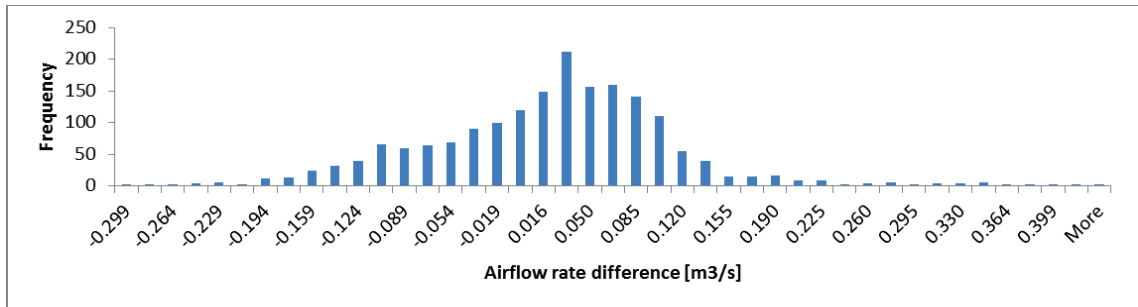


Figure 5.19: Histogram of the difference between predicted and measured air flow rates for zone 3.1 NE

The indoor average set-point temperatures used for Runs 4 and 5 are presented in Table 5.9.

Table 5.9: Mean indoor air temperatures for all zones for the occupied hours for all summer period (Run 4) and for all summer period except weekend days (Run5)

Zone	Run 4	Run 5
	T indoor [°C]	T indoor [°C]
1.3 NW	21.56	21.57
1.4 SW	25.18	24.53
1.5 SE	24.27	24.05
1.6 NE	24.44	24.22
2.1 NE	22.72	22.69
2.3 NW	24.15	24.01
2.4 SW	23.54	23.51
2.5 SE	22.89	22.9
2.6 NE	23.61	23.7
3.1 NE	23.86	23.66
3.2 SW	23.34	23.22
3.3 NW	23.59	23.36
3.4 SW	23.68	23.54
3.5 SE	23.02	23.02
3.6 NE	23.45	23.58

Table 5.10 presents the corrected internal loads for all the runs; Table 5.11 presents the hourly CV values for the entire summer period.

Table 5.10: Corrected internal loads for all zones for all runs

Zone	Run (1)	Run (2)	Run (3)	Run (4)	Run (5)
	Load [kW]				
1.3 NW	3.00	3.91	3.96	3.63	3.70
1.4 SW	1.50	1.57	1.39	1.83	2.10
1.5 SE	8.00	7.94	7.83	7.90	8.00
1.6 NE	13.00	12.92	12.93	13.00	13.00
2.1 NE	8.00	8.17	7.99	8.08	8.08
2.3 NW	2.00	2.05	1.99	1.81	2.00
2.4 SW	5.00	4.52	4.30	5.26	5.61
2.5 SE	25.00	22.69	21.44	24.44	25.40
2.6 NE	6.00	5.41	5.46	5.64	5.64
3.1 NE	6.00	5.58	5.72	6.09	6.00
3.2 SW	4.50	4.81	4.80	4.93	5.00
3.3 NW	2.25	2.24	2.22	1.81	1.65
3.4 SW	4.00	4.14	4.00	4.54	4.88
3.5 SE	20.00	19.14	19.47	20.73	21.14
3.6 NE	5.00	4.58	4.56	4.57	4.56

Table 5.11: Coefficient of variation values for all zones for the entire summer period, based on hourly values

Zone	Run (1)		Run (2)		Run (3)		Run (4)		Run (5)	
	CV-RMSE [%]		CV [%]		CV [%]		CV [%]		CV [%]	
	t<t,cr	t>t,cr	t<t,cr	t>t,cr	t<t,cr	t>t,cr	t<t,cr	t>t,cr	t<t,cr	t>t,cr
1.3 NW		38.00		40.80		41.80		38.00		37.10
1.4 SW		92.00		91.50		92.80		90.40		89.00
1.5 SE	12.00		12.39		12.40		12.40			12.50
1.6 NE	34.00		34.48		34.40		34.00		34.60	
2.1 NE		24.00		24.10		23.90	24.07		24.00	
2.3 NW	89.00			89.62		89.50		89.60	90.00	
2.4 SW		26.00		28.01		28.80	25.50		24.60	
2.5 SE		11.00		8.23	7.83			10.57		11.70
2.6 NE		17.00		17.19		17.15		17.40		17.50
3.1 NE	22.90		23.05		22.90			23.06		23.08
3.2 SW		22.20		22.41		22.50		22.00		21.80
3.3 NW		54.80		52.71		51.65		47.00	45.80	
3.4 SW		24.80		24.71		25.13		23.00		23.50
3.5 SE	9.40		10.00		9.80		9.30		9.40	
3.6 NE		19.00		19.00		19.50		19.50		19.50

It should be noted that for Run 1 and Run 5, zone 1.5 SE has about the same load (8 kW), while the t-statistic values are less than t critical and greater than t critical, respectively. This is due to the fact that the surrounding zones have their loads adjusted as well, but not necessarily in the same manner, therefore one should not expect to obtain the same results, due to heat transfer through the internal walls. The results do not present significant improvement by using these techniques of adjusting the load and therefore the air flow rate.

The hypothesis testing reveals that for Runs 1, 3 and 4 the air flow rate for five zones is calibrated, for run 2 the air flow rate for four zones is calibrated and for run 5 the air flow rate for six zones is calibrated. In order to verify if Run 5 presents indeed better results than the base case, the daily CV values are calculated and presented in Table 5.12.

Table 5.12: CV values for all zones, for the entire summer period, based on daily values

Zone	Run (1)		Run (2)		Run (3)		Run (4)		Run (5)	
	CV-RMSE [%]									
	t<t,cr	t>t,cr								
1.3 NW		41.54		38.22		39.24		35.79		34.25
1.4 SW	88.62			40.45		42.00		38.41	36.55	
1.5 SE	13.42		6.34		6.26		6.47		6.62	
1.6 NE	30.36		10.79		10.77		10.84		10.87	
2.1 NE	24.21		9.63			10.23	9.39		9.21	
2.3 NW	60.94		49.26		50.12		50.60		48.87	
2.4 SW	29.70			14.91		16.06	12.06		11.25	
2.5 SE		9.60		5.05	3.91			8.00		9.36
2.6 NE	16.59			10.32		10.26		10.99		11.15
3.1 NE	21.65		12.37		12.22		12.15		12.18	
3.2 SW	26.12			14.27		14.54		13.21		12.68
3.3 NW	49.77			24.01		23.19	20.31		19.49	
3.4 SW		24.46		13.52		14.17		11.80	10.72	
3.5 SE	9.02		5.37		5.25		4.74		4.95	
3.6 NE	21.47		11.27		11.20		11.41			11.50

The hypothesis test reveals that for Run 1 the air flow rate for twelve zones out of fifteen is calibrated. For Runs 2 and 3, the air flow rate for seven zones is calibrated, which is less than the initial run, therefore these methods are not preferred. For Run 4 the air flow rate for nine zones is calibrated and for Run 5 the air flow rate for ten zones is calibrated.

Therefore, the base case (Run 1) seems to present the best results. It can be observed that indeed the CV value is not sufficient to determine whether a zone is calibrated or not, but should be accompanied by the paired t-statistic hypothesis testing. The air flow for certain zones that have CV's of 90% would be considered uncalibrated, while the hypothesis test reveals that the difference between predicted and measured air flow rates is not significant. The same set of predictions results in less zones being calibrated when using hourly values, than when using daily average values.

Chapter 6 Calibration of the eQuest model of the air handling unit

6.1 Air handling unit model inputs

In order to calibrate the air handling unit model, the following outputs from eQuest are selected for the comparison with measurements: the supply air temperature, the supply air flow rate and the cooling coil load.

Initially the HVAC model was based on the default values offered by eQuest based on standard ASHRAE 90.1. Some inputs to the air handling unit model have been modified in eQuest, based on measurements. The calibration presented in this section is based on measurements available from Building Automation System (BAS) for the summer period of 2012, between June 11th and August 31.

The HVAC system is a Variable Air Volume (VAV) system. The sizing option of the supply air fan was chosen to be COINCIDENT, meaning that every hour the building thermal load is calculated as the sum of coincident thermal loads of all zones.

The maximum allowed relative humidity of return air was set as the average over the summer period of the measured relative humidity in the return air from all zones.

For the supply and return fans in the air handling units, the total static pressure at design flow rate and the overall efficiency of the motor and drive were set from the technical specification of the fan models. Both fans have variable speed drive.

The minimum and maximum fan ratios are the minimum and maximum flows through the supply fan, expressed as a fraction of design flow rate (Table 6.1). The design air flow rate of each AHU is 20 m³/s.

Table 6.1: Mean measured supply air flow rate in the air handling unit from the 11th of June until the 31st of August

	Mean measured supply air flow rate in the AHU
Minimum	17.14 [m ³ /s]
Maximum	24.67 [m ³ /s]
Minimum air flow ratio	69.47 %

The night cycle control was chosen to be CYCLE-ON-ANY, meaning that the fans would be cycled on for the hours when the air temperature of any zone in the system exceeds the upper limit of the throttling range (in the cooling mode).

The minimum outside air ratio was omitted for the HVAC system because the outdoor air flow per person for each zone was input instead. These values were extracted from the standard ASHRAE 62.1 (2007).

The minimum outdoor air control method was selected to be FRACTION OF DESIGN FLOW, which means that the minimum outdoor air flow rate is specified as a required fraction of the design supply air flow rate.

The minimum outdoor air sizing method was chosen to be SUM OF ZONE OA, meaning that the program calculates the system design outdoor air flow fraction based on the sum of the zone requirements divided by the supply air flow rate.

The economizer cycle is based on outdoor temperature, which means that the economizer is enabled whenever the outdoor air temperature falls below the maximum allowed temperature, as specified by the DRYBULB-LIMIT. This maximum outside air temperature is found by plotting the fraction of fresh air entering the building (alpha) against the outside air temperature

The cooling coil design bypass factor is a value used to characterize the operating conditions of a cooling coil and can be found by using Equation (6.1) in terms of the psychrometric process as presented in Figure 6.1.

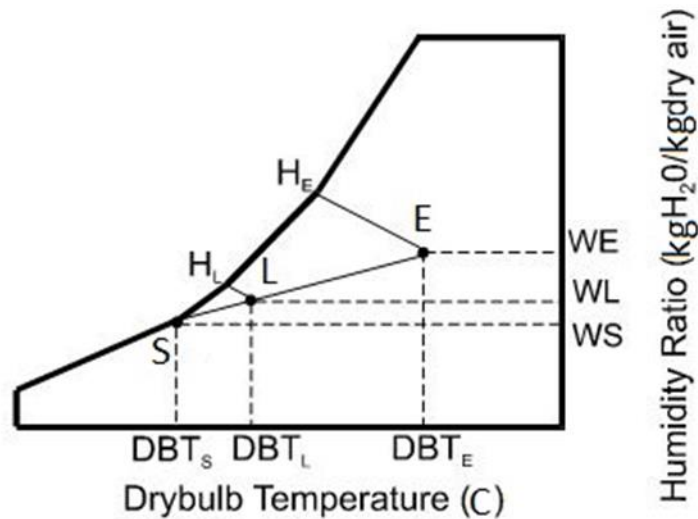


Figure 6.1: Coil bypass conditions that are needed to calculate the coil bypass factor

$$\mathbf{BYPASS\ FACTOR} = \frac{DBT_L - DBT_S}{DBT_E - DBT_S} \quad (6.1)$$

where:

E = coil entering condition

L = coil leaving condition

S = coil surface condition

WE= humidity ratio of air entering the coil

WL= humidity ratio of air leaving the coil

WS= humidity ratio of saturated air on coil's surface

HE= enthalpy of air entering the coil

HL= enthalpy of air leaving the coil

DBT_S = Dry bulb temperature on the surface of the cooling coil

DBT_L = Dry bulb temperature of the air leaving the cooling coil

DBT_E = Dry bulb temperature of the air entering the cooling coil

The dry bulb temperatures of the air leaving and entering the cooling coil were taken from the measurements. The dry bulb temperature of air entering the coil is the mixed air temperature, which is measured by the BAS system. The temperature of the air leaving the cooling coil was calculated by subtracting 1.87 °C (which is the heat gain in the duct released by the supply fan) from the supply air temperature. Then the bypass factor is calculated with equation 6.1 and using the hourly measurements over the summer season and input to eQuest:

$$\mathbf{BYPASS\ FACTOR} = \frac{14.84-11}{22.96-11} = \mathbf{0.32} \quad \mathbf{(6.2)}$$

The minimum temperature of the air delivered to the zones is also taken from the measurements of supply air temperature, as well as the cooling air supply temperature set-point, which is specified in eQuest as the COLD DECK MIN LEAVING TEMP. The cold deck reset schedule is specified as presented in Table 6.2, from the trend line of the measurements (Figure 6.2).

Table 6.2: Measured cold deck reset temperatures

COLD DECK RESET TEMPERATURES	
Outdoor dry bulb high temperature	29.38 °C
Outdoor dry bulb low temperature	14.11 °C
Supply leaving temperature at outdoor low temperature	15.44 °C
Supply leaving temperature at outdoor high temperature	14.50 °C

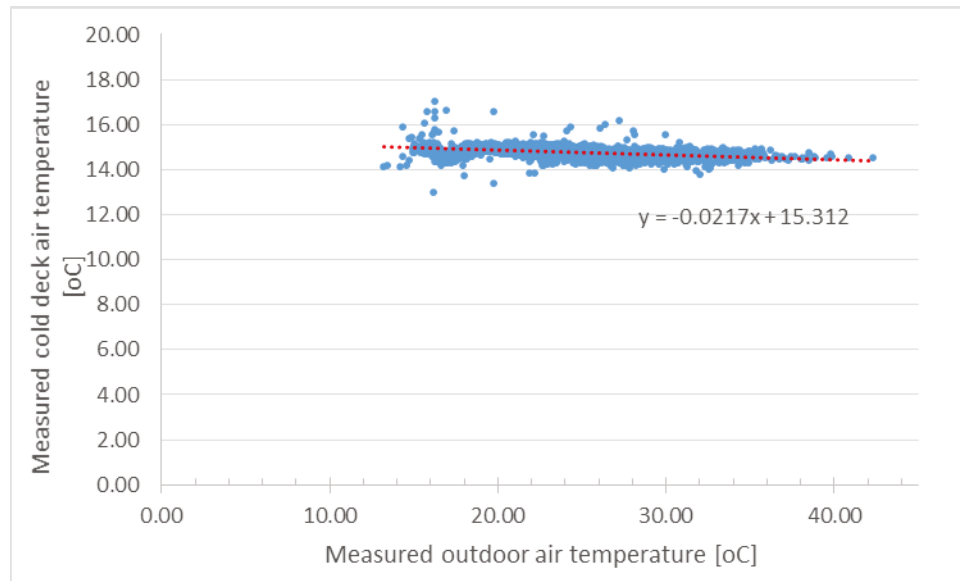


Figure 6.2: Cold deck air temperature vs. outdoor air temperature

The measured supply air flow rate in the AHU is obtained from the measured speed with Elbon device, installed on the supply fan outlet, and the calibration coefficients used in the BAS.

6.2 Analysis of the summation of air flow rates to zones

Before calibrating the air flow rate supplied by the air handling unit, it is good to analyze the summation of the air flow rates that each zone needs to receive. Since not all the air flow rates of the zones are considered calibrated, some discrepancy is expected when comparing the measured and predicted summation of the air flow rates of all the zones.

Figure 6.3 presents the hourly predicted vs. measured summation of supply air flow rates to zones for the summer season. It can be noticed that the predictions are overestimated during the night and weekend periods, where the mean measured air flow rate is about $7.5 \text{ m}^3/\text{s}$, while the mean predicted air flow rate is around $10 \text{ m}^3/\text{s}$. Even though the minimum air flow rate in each zone has been input into eQuest from measured minimum air flow rate from the BAS system, this difference between predictions and measurements still appears, probably because the predicted cooling loads are higher than the corresponding real values.

Figure 6.4 presents the hourly predicted vs. measured air flow rate signatures supplied to zones. Two distinct clouds of points can be observed, one for the occupied periods when the predictions agree well with the measurements, and the second one for the unoccupied periods, such as night and weekend instances, when the simulation results are over predicted.

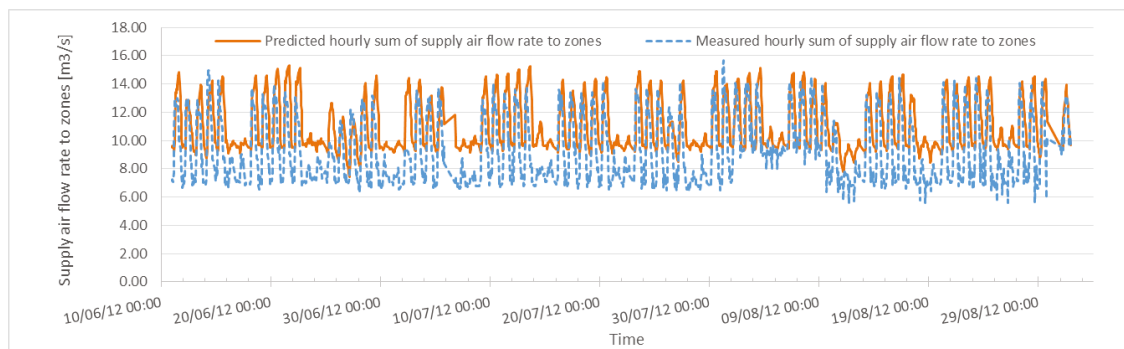


Figure 6.3: Measured vs. predicted hourly summation of air flow rates supplied to zones for the summer period

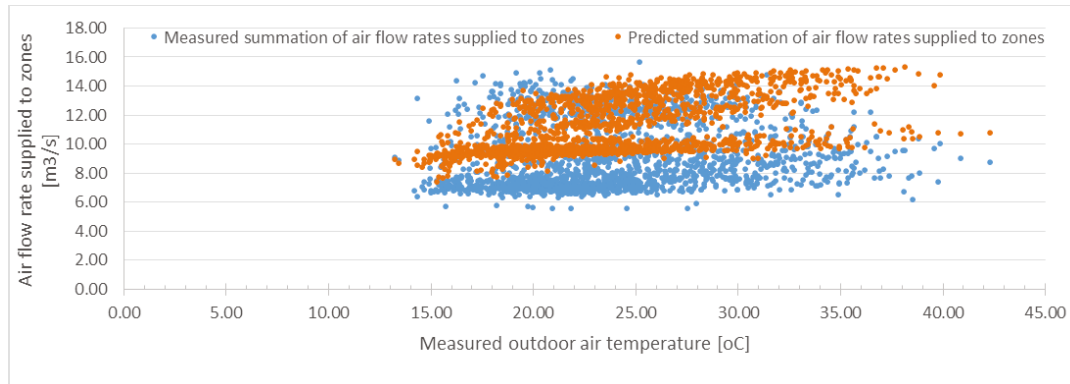


Figure 6.4: Hourly measured and. predicted air flow rates supplied to zones vs. outdoor air temperature

In order to verify if the analysis can be performed for shorter periods of time, due to the large amount of measurements, the measurements and predictions are compared for periods of three days during each month when the highest outdoor temperature was recorded. The first ten days during the month of June were removed due to abnormal operation, therefore the only periods that will be analyzed are (a) 18th - 20th July and (b) 14th - 16th August 2012.

Figure 6.5 presents the hourly measured and predicted summation of airflow rates to zones from the 18th to the 20th of July. The predicted air flow rate is higher than the measured air flow rate at the end of the occupied periods and during unoccupied hours, when the mean measured air flow rate is 9.74 m³/s and the predicted air flow rate is 11.58 m³/s.

Figure 6.6 presents the hourly measured and predicted mean air flow rate to zones signatures from the 18th to the 20th of July. The occupied and unoccupied periods can be noticed as two different clouds of points, which present the same difference of 1.84 m³/s between measurements and simulation results.

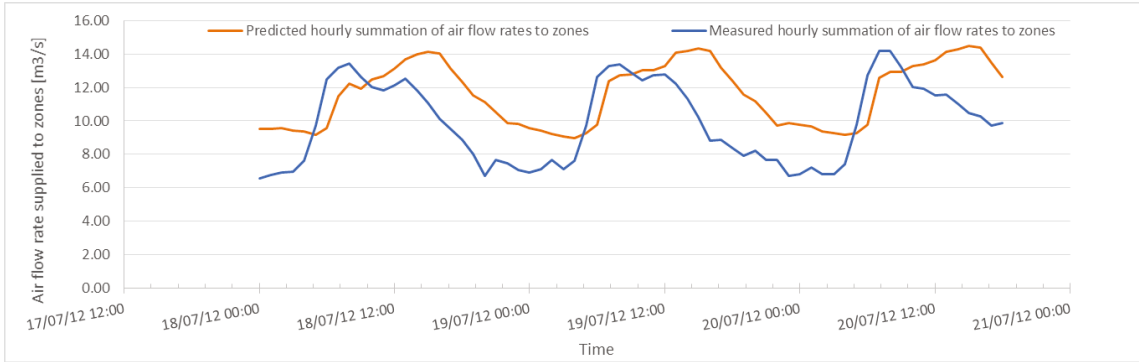


Figure 6.5: Measured vs. predicted hourly summation of air flow rates supplied to zones from July 18th to 20th

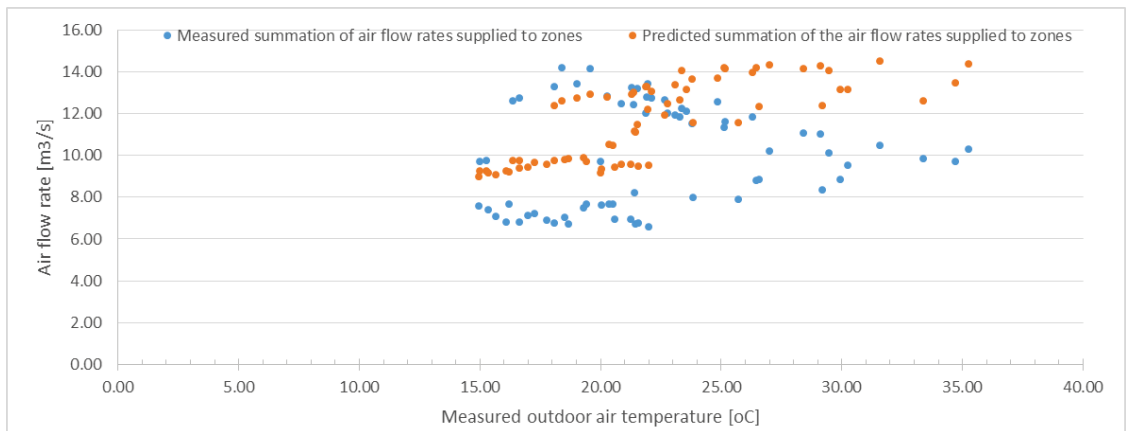


Figure 6.6: Measured vs. predicted air flow rate signatures (supplied to zones) from July 18th to 20th.

Figure 6.7 shows the hourly measured vs. predicted summation of air flow rate supplied to zones from 14th to the 16th of August. During the mean unoccupied hours the measured summation of air flow rates to zones is 9.29 m³/s and the mean predicted value is 11.63 m³/s. It can be observed that the simulated hours of occupancy do not correspond exactly to the measured ones. The real schedule of occupancy of the building will not always be exactly the same as the simulated occupancy, and this could be the case for some zones only, affecting the summation of the air flow rates supplied to the all the zones in the building.

Figure 6.8 presents the signatures of the hourly measured and predicted summation of air flow rates supplied to zones from the 14th to the 16th of August. The same difference of 2.34 m³/s is noticed between the measured and predicted signatures, during the unoccupied periods.

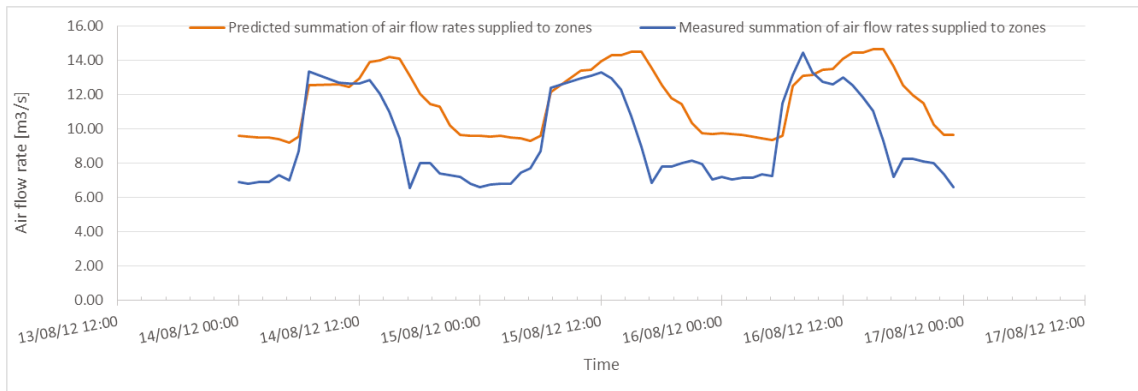


Figure 6.7: Measured vs. predicted hourly summation of air flow rates supplied to zones from August 14th to 16th

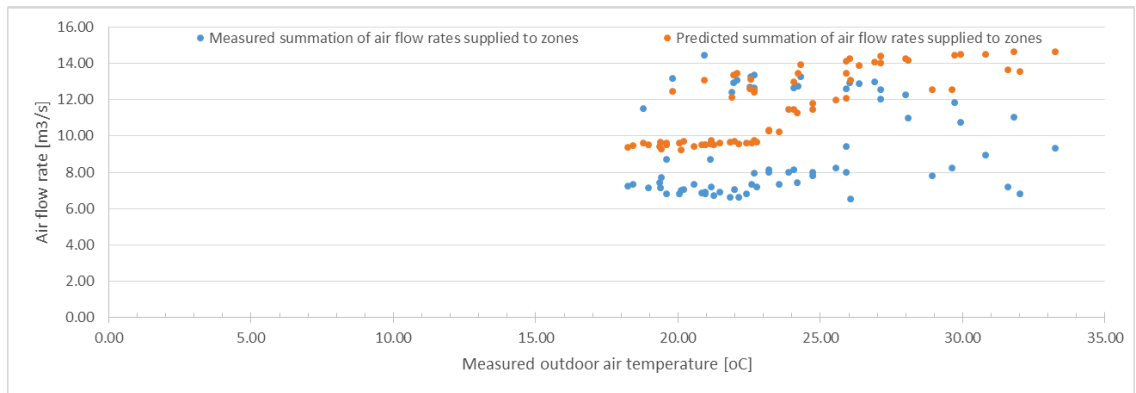


Figure 6.8: Measured vs. predicted air flow rate signatures (supplied to zones) from August 14th to 16th 2012

Figure 6.9 presents the daily averaged measured and predicted summation of air flow rates supplied to the zones. The measured summation of air flow rates supplied to zones during the weekend periods is 9.14 m³/s, while the predicted values are at 11.02 m³/s. Unlike when analyzing hourly values, for daily averaged values, during the week days a difference is observed of 1.88 m³/s between measured and predicted summation of air flow

rates supplied to zones. This is due to the integration effect because the week period is composed of days, or occupied periods and nights, or unoccupied periods, therefore the daily average values will be between the hourly occupied values and hourly unoccupied values.

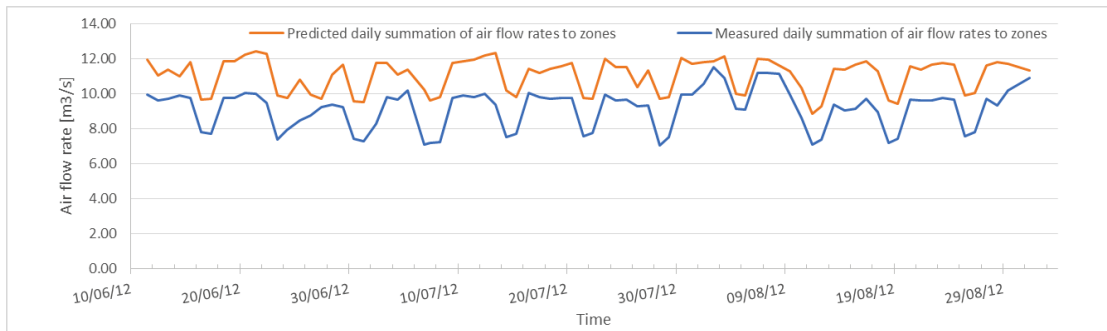


Figure 6.9: Measured vs. predicted daily summation of air flow rates supplied to zones for the summer period.

Figure 6.10 presents the daily measured and predicted signatures of the summation of air flow rates supplied to zones. The two periods of occupation can be noticed, as the measured unoccupied average air flow rate is around $7.5 \text{ m}^3/\text{s}$, while the measured occupied average air flow rate is about $10 \text{ m}^3/\text{s}$. The same is observed for the predicted values: unoccupied daily average air flow rate is $10 \text{ m}^3/\text{s}$, while the daily average air flow rate is $12 \text{ m}^3/\text{s}$. The difference in air flow rate between the measured occupied and unoccupied periods is about $2.5 \text{ m}^3/\text{s}$, while the difference in air flow rate between predicted occupied and unoccupied periods is about $2 \text{ m}^3/\text{s}$.

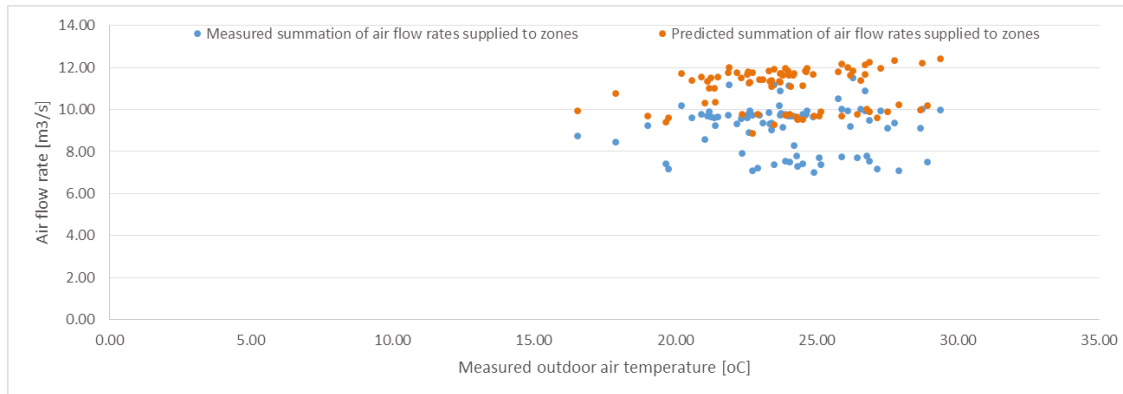


Figure 6.10: Measured vs. predicted daily air flow signatures (supplied to zones) for the summer period

Looking at the statistical indices of the difference between the measured and predicted summation of air flow rates supplied to zones (Table 6.3), on an hourly basis for the whole summer, for three days during July and August and on a daily basis, all the root mean squared errors (RMSE) are much higher than the uncertainty, suggesting that the total air flow rate supplied to zones is not calibrated.

The hourly coefficients of variation for the periods of three days are slightly higher than the accepted limit of 30% (ASHRAE (2002)). The hourly CV-RMSE for the entire summer is 28%, which is less than the 30% limit, thus suggesting that the model is calibrated when the entire period is taken into consideration. The hourly normalized mean biased error is higher than the limit of 10% suggested by ASHRAE Guideline 14, except for the period of 18th to 20th of July. There are no suggested limits in the literature for daily average values.

The hypothesis testing is undertaken for the comparison between the measured and predicted summation of air flow rates supplied to the zones.

Table 6.3: Statistical indices for comparing the measured and predicted summation of air flow rates supplied to zones

Indices	Hourly values (summer)	Hourly values (18-20 July)	Hourly values (14-16 August)	Daily averaged values
u [m ³ /s]	0.31	0.56	0.59	0.37
RMSE [m ³ /s]	2.55	2.66	2.96	1.99
CV-RMSE [%]	28	27	32	22
NMBE [%]	38	16	26	22

The histogram of the difference between measured and predicted summation of air flow rates supplied to the zones is presented in Figure 6.11. The probability distribution is slightly skewed to the right, which was expected since the simulated values are over predicted by approximately 2.5 m³/s.

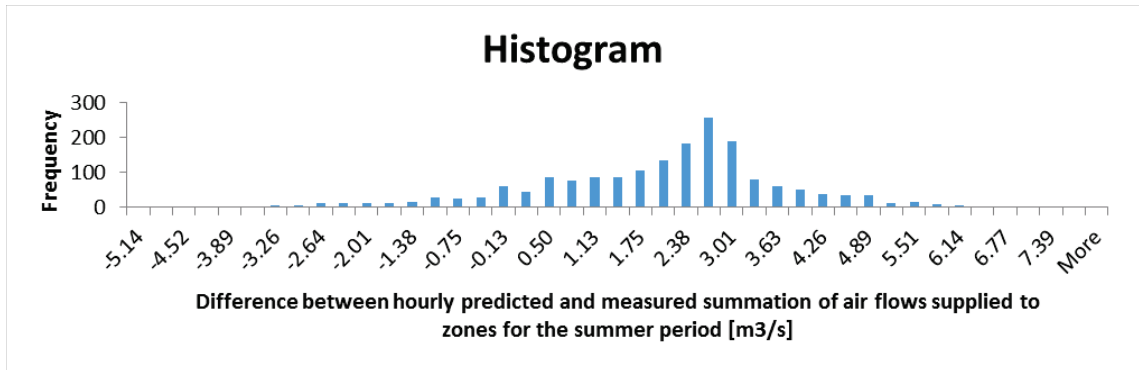


Figure 6.11: Histogram of the difference between predicted and measured summation of air flow rates supplied to the zones for the summer period

The histograms of the difference between measured and predicted summation of air flow rates supplied to zones for hourly averaged values for the three days in July, August and for daily averaged values are presented in Appendix C (Figures C.1 to C.3). All the histograms seem to be a bit skewed to the right, confirming what was already known: that the simulation results are over predicted.

The t-statistic values when using hourly averages for the three days in July, August and for the whole summer period, as well as for daily averaged values are presented in Table 6.4. The hourly and daily t-statistic values are much higher than the critical t values of 1.645 and 1.666 (Reddy (2011)), respectively. Therefore, hypothesis testing suggests that the difference between the measured and predicted summation of air flow rates to zones is indeed significant.

Table 6.4: The t-statistic value for comparing the measured and predicted summation of air flow rates supplied to zones

	Hourly values (summer)	Hourly values (18-20 July)	Hourly values (14-16 August)	Daily average values
t-statistic value	38.46	8.38	8.06	22.35

Figures 6.12 and 6.13 presents the hourly measured supply airflow rate from the air handling unit compared with the summation of measured supply air flow rates for zones, over the whole summer season. Figure 6.14 presents the same comparison between measured supply air flow rate leaving the air handling unit and the summation of air flow rates supplied to the zones, but on a daily basis for the entire summer period. On the average the measured AHU supply air flow rate is about $10 \text{ m}^3/\text{s}$, while the sum of zones is about $20 \text{ m}^3/\text{s}$. The difference of approximately $10 \text{ m}^3/\text{s}$, which is observed between the airflow rate leaving the AHU and the sum of airflow rates reaching the selected zones is due to the omission of the entire basement floor from the simulation. This difference was added to the predicted airflow rate leaving the AHU in order to be able to compare the measured and predicted airflow rate leaving the AHU.

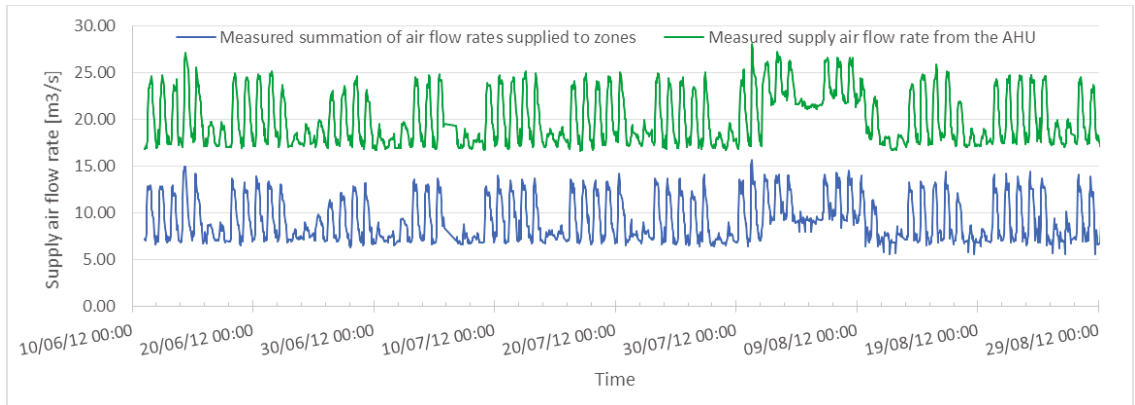


Figure 6.12: Hourly measured supply airflow rate leaving the air handling unit vs. summation of measured airflow rates to zones for the summer period



Figure 6.13: Daily measured supply airflow rate leaving the air handling unit vs. summation of airflow rates to zones for the summer period

Since the summation of air flow rates has been analyzed and the differences between predictions and measurements understood, we can move on to analyzing the air handling unit supply air flow rate. The AHU supply air flow rate calibration results are analyzed by using the three methods previously discussed in section 5.2: graphical representation, statistical indices and hypothesis testing. The results are reported on an hourly and daily basis in order to assess the validity of the results.

6.3. Results of the calibration of the air handling unit supply air flow rate

6.3.1 Graphical representation

The hourly time series for the three day periods show small differences, with slight over predictions (Figure 6.14 and 6.15). The same observation when the hourly and daily time series are presented for the whole summer period (Figure 6.16 and 6.17).

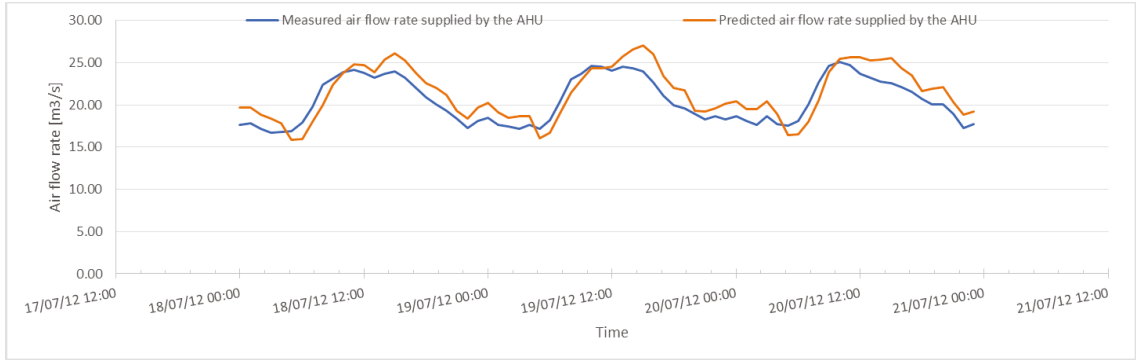


Figure 6.14: Measured vs. predicted air flow rate supplied by the air handling unit from the 18th to the 20th of July

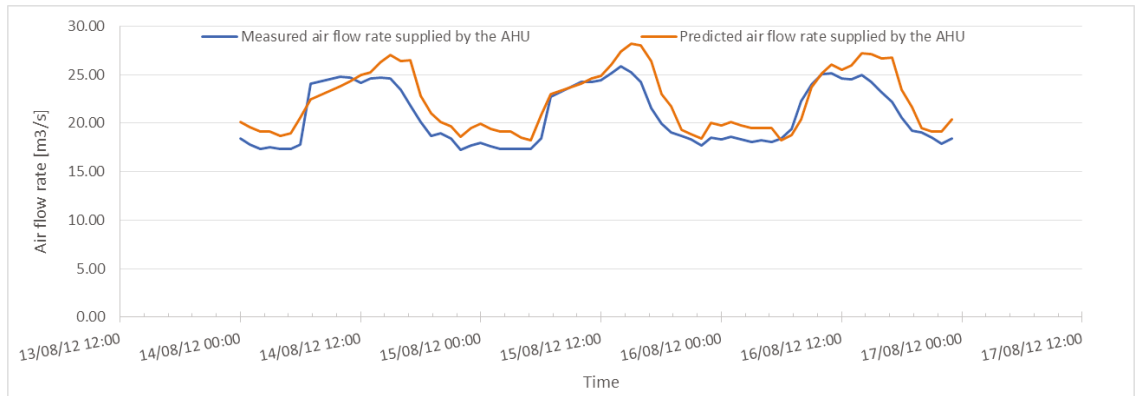


Figure 6.15: Measured vs. predicted air flow rate supplied by the air handling unit from the 14th to the 16th of August

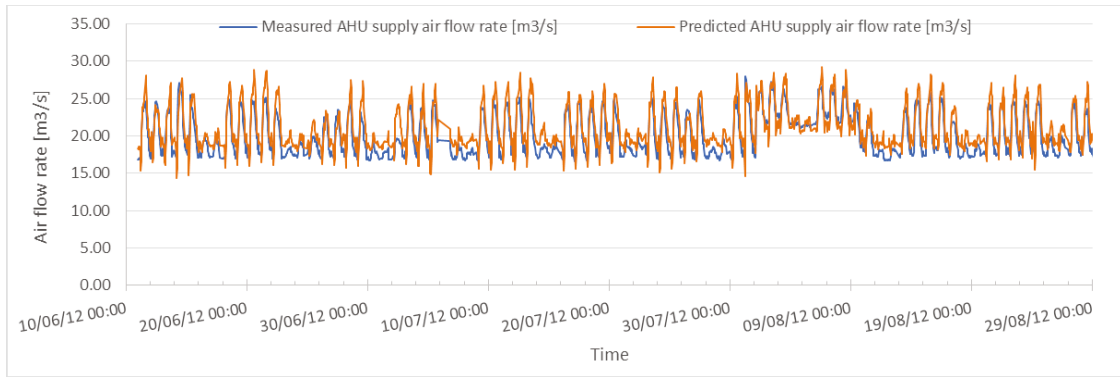


Figure 6.16: Hourly measured vs. predicted airflow rate leaving the AHU for the summer period

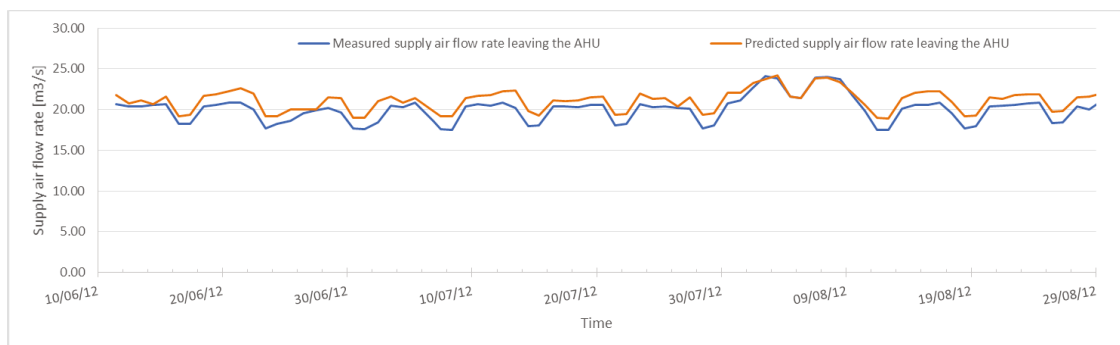


Figure 6.17: Daily measured vs. predicted airflow rate leaving the AHU for the summer period

The daily and hourly airflow rate signatures (Figures 6.18 to 6.21), for the three day periods and for the whole summer, show good agreement between measurements and predictions. The simulation results seem to be slightly over predicted, but the same distribution pattern is followed by the measurements and predictions.

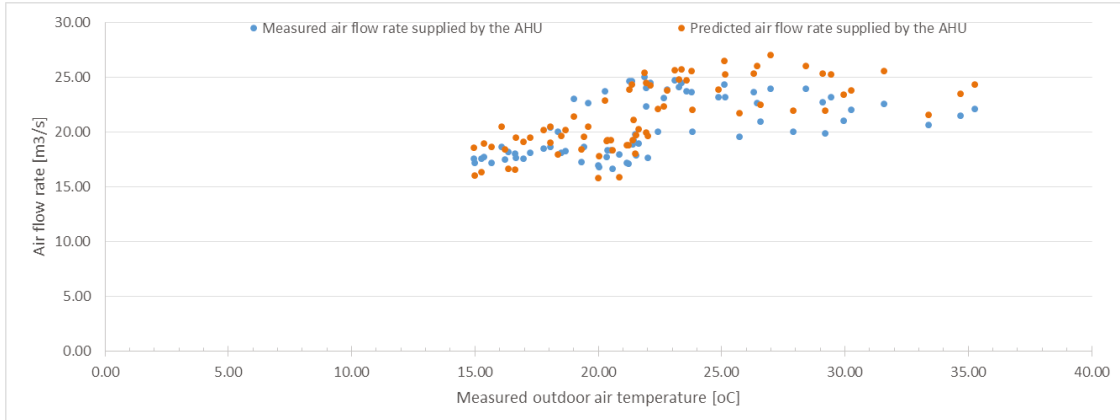


Figure 6.18: Measured vs. predicted air handling unit supply air flow rate signatures from the 18th to the 20th of July

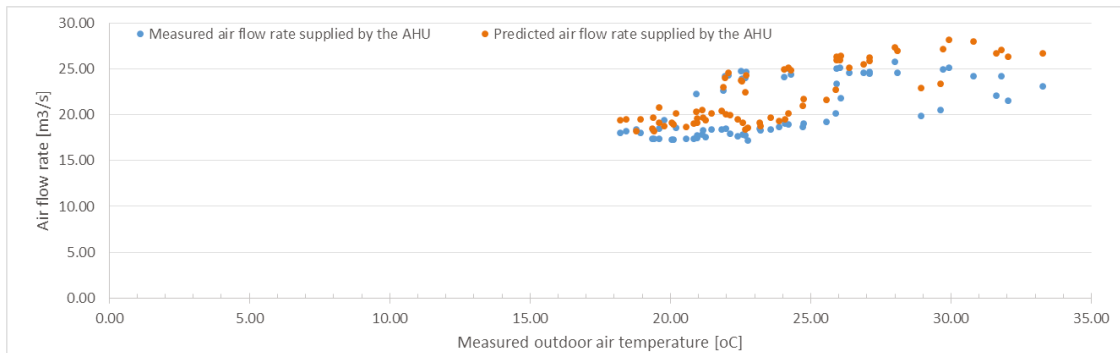


Figure 6.19: Measured vs. predicted air handling unit supply air flow rate signatures from the 14th to the 16th of August

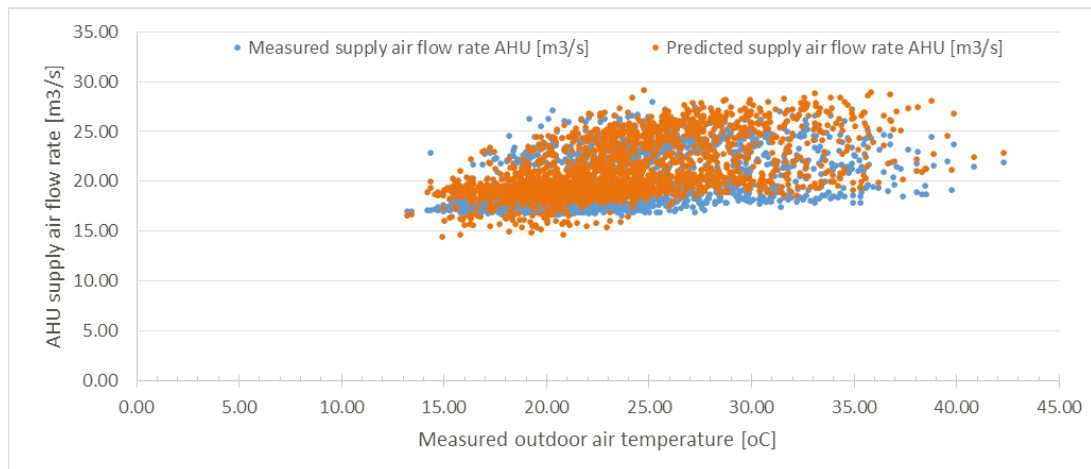


Figure 6.20: Hourly signatures of measured and predicted airflow rate for the summer period

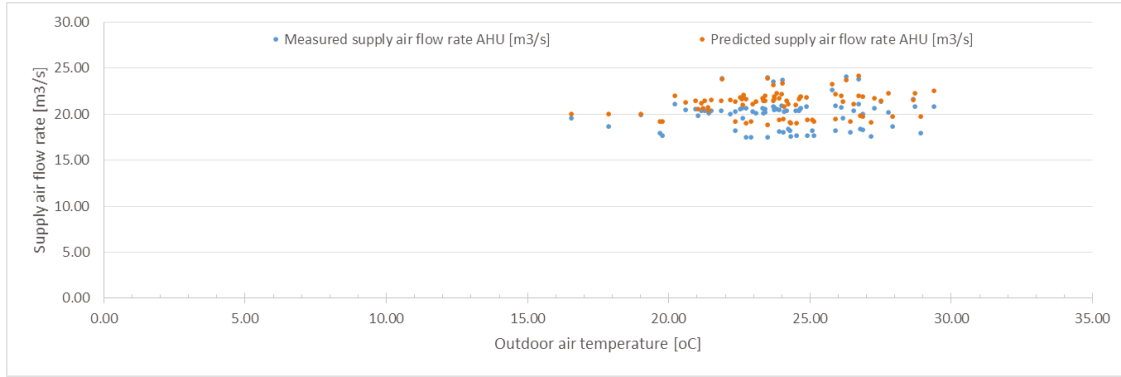


Figure 6.21: Daily signatures of measured and predicted airflow rate for the summer period

Figures 6.22 and 6.23 show good agreement between predictions and measured supply air flow rates. The slope of the linear correlation of hourly values is equal to 0.924 (with $R^2=0.784$) while the slope of the daily values is equal to 0.761 (with $R^2=0.892$).

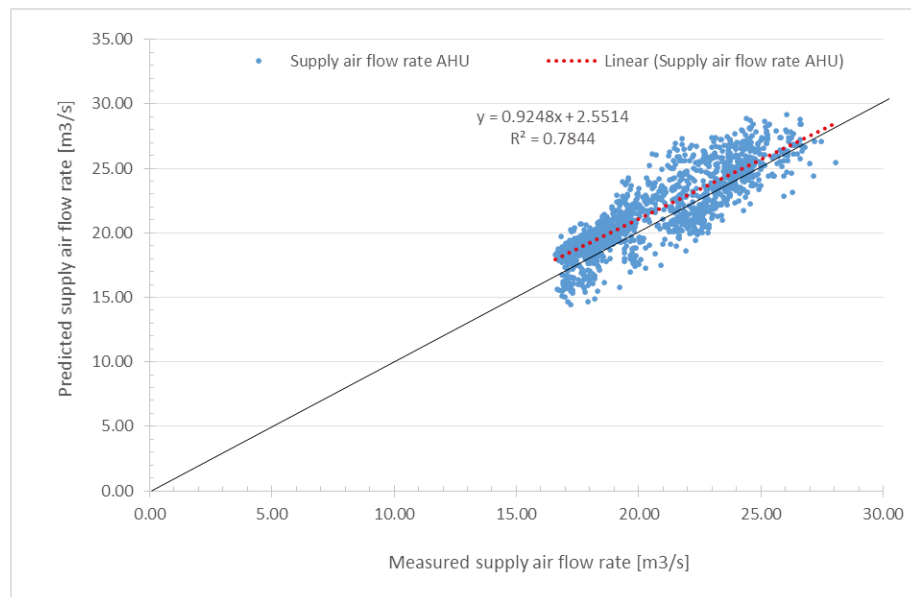


Figure 6.22: Measured vs. predicted hourly supply air flow rate leaving the AHU for the summer period

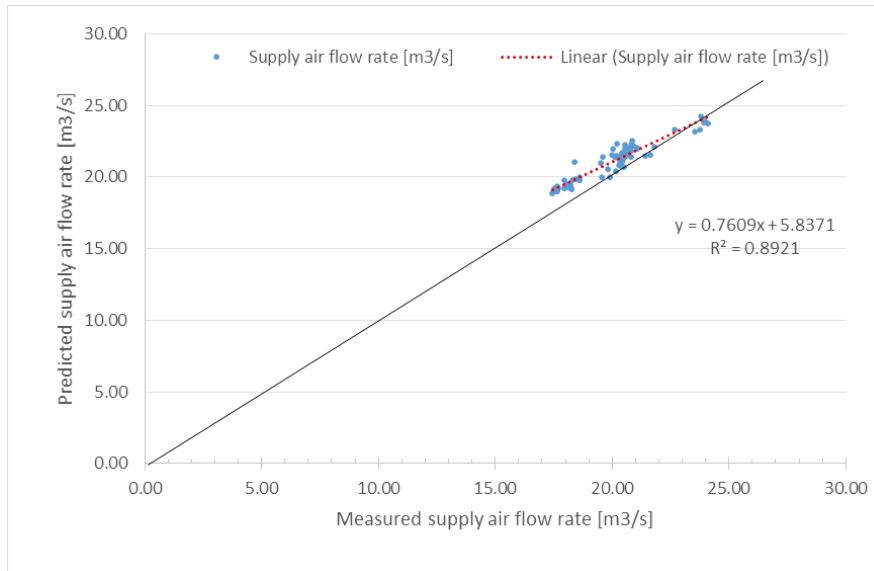


Figure 6.23: Measured vs. predicted daily supply air flow rate leaving the AHU for the summer period

6.3.2 Statistical indices analysis

The difference between the predicted and measured supply air flow rates was analyzed by using the RMSE and CV-RMSE, for both hourly and daily average values (Table 6.5). Since the hourly CV values are less than the accepted values of 30% for hourly data (ASHRAE (2002)), the eQuest model could be considered as being calibrated with respect to the supply air flow rate of the AHU. The normalized mean biased error was also calculated (Table 6.5) and it was found to be less than the suggested hourly value of 10% (ASHRAE (2002)).

Table 6.5: Statistical indices for the difference between the predicted and measured supply air flow rate leaving the air handling unit

Statistical Indices	Hourly values (summer)	Hourly values (July 18-20)	Hourly values (August 14-16)	Daily average values
u [m ³ /s]	0.42	0.67	0.72	0.50
RMSE [m ³ /s]	1.72	1.67	1.98	1.19
CV-RMSE [%]	9.00	8	10	6.00
NMBE [%]	5.17	4.44	7.18	5.26

6.3.3 Hypothesis testing

Figures 6.24 and 6.25 show the distribution of the difference between measured and predicted airflow rate for hourly and daily averaged values, respectively. The graphs show a nearly normal distribution, but a bit skewed to the right. The skewedness is caused by the fact that the simulation results are slightly over predicted. The histograms for the three day periods during the months of July and August show a fairly normal distribution as well (Appendix C: Figures C.1 to C.3)

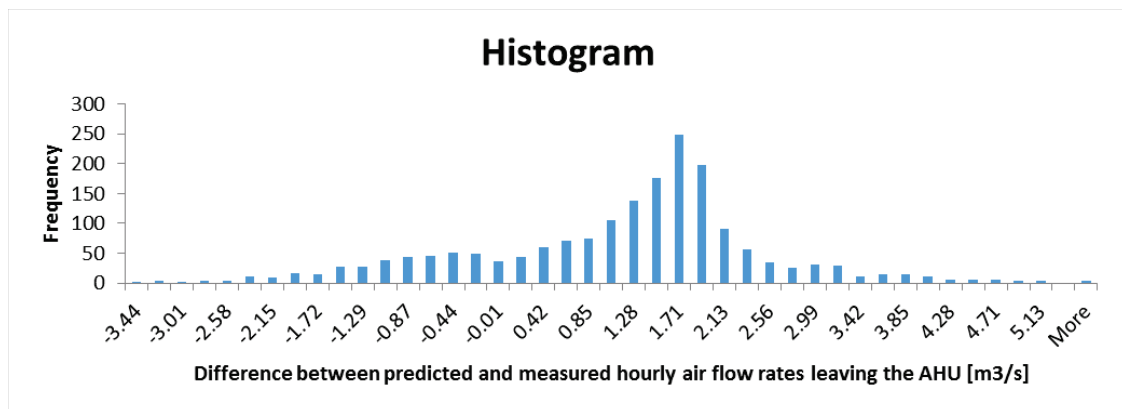


Figure 6.24: Histogram of the difference between predicted and measured hourly airflow rates

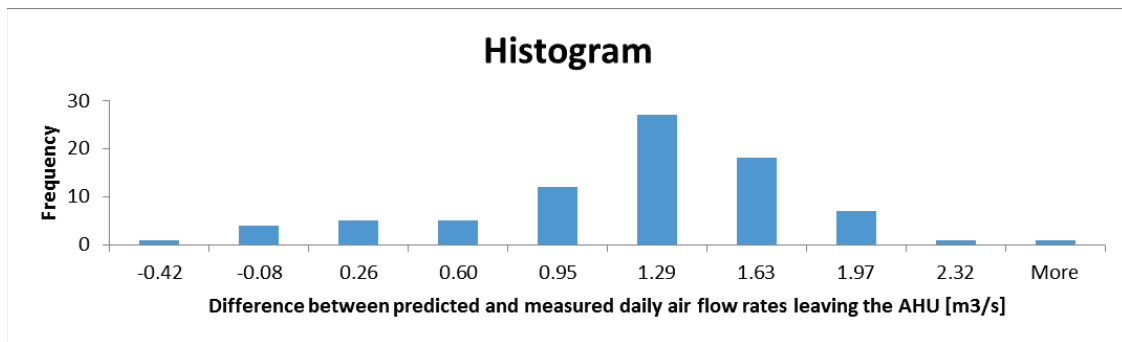


Figure 6.25: Histogram of the difference between predicted and measured daily airflow rates

The t-values were calculated to be 19.61 when using hourly average values, and 8.36 when using daily average values (Table 6.6). These are well above the critical t values

of 1.645 and 1.666 that correspond to a 95% confidence interval for 1846 degrees of freedom on an hourly basis, and 80 degrees of freedom on a daily basis, according to the number of points sampled for the test. Therefore this test suggests that the supply airflow rate is not calibrated indeed, but in fact over predicted, contrary to what was found using the previous method. The results of the hourly calibration over the three day periods are not consistent with each other. During the month of July, the t-statistic values is less than the critical value of 1.666, but the distribution of the points is a bit skewed to the right. The distribution during the month of August is closer to being normal, but the t-statistic is higher than the critical one of 1.666, therefore this result suggests the model is not calibrated for the supply air flow rate.

Table 6.6: The t-statistic for hourly and daily difference between measured and predicted supply air flow rate

Hypothesis test index	Hourly values (summer)	Hourly values (July 18-20)	Hourly values (August 14-16)	Daily average values
t-statistic	19.61	1.39	4.80	8.36

In conclusion, in addition to the graphical time series, both the statistical indices and the hypothesis testing methods should be used to assess whether a model is calibrated or not. In this case the two methods lead to different conclusions: the statistical indices method suggests the model is calibrated, while the hypothesis testing method suggests the model is not calibrated.

6.4 Calibration of the supply air temperature in the air handling unit

This section discusses the results of the calibration of the temperature of the air leaving the air handling unit.

6.4.1 Graphical representation

Figures 6.26 and 6.27 present the hourly measured and predicted supply air temperature from the AHU for the three days periods: July 18-20 and August 14-16, respectively. Figures 6.28 and 6.29 show the same comparison for the whole summer season, on an hourly and daily basis.

From all the graphs it can be noticed that the predictions seem to be slightly underestimated by 0.5 °C, which is around the measurement uncertainty (Table 6.7). The hourly measurements for the whole period present a few abnormal points. Measurements revealed a few instances where the supply air temperature reached values as high as 25 °C. The measured supply air temperature is almost constant, the supply air temperature set-point being kept fixed at 16.5 °C.

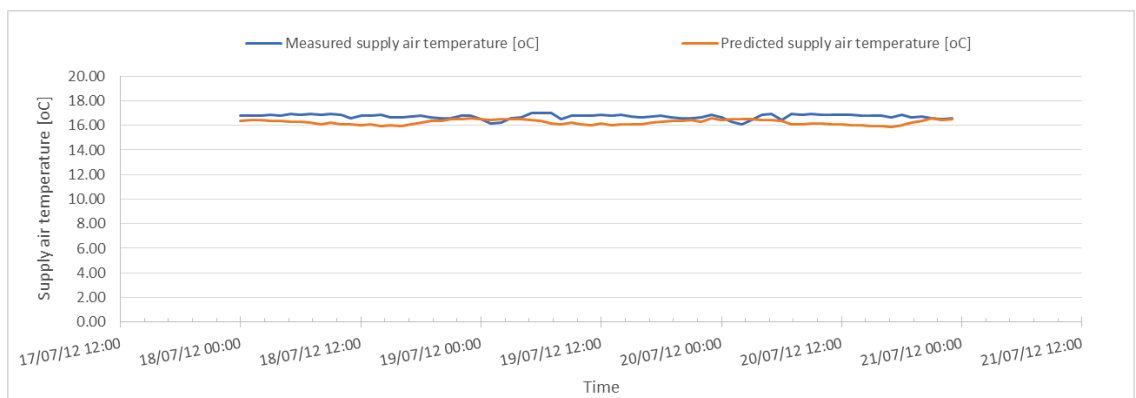


Figure 6.26: Hourly measured vs. predicted supply air temperature from 18-20 July

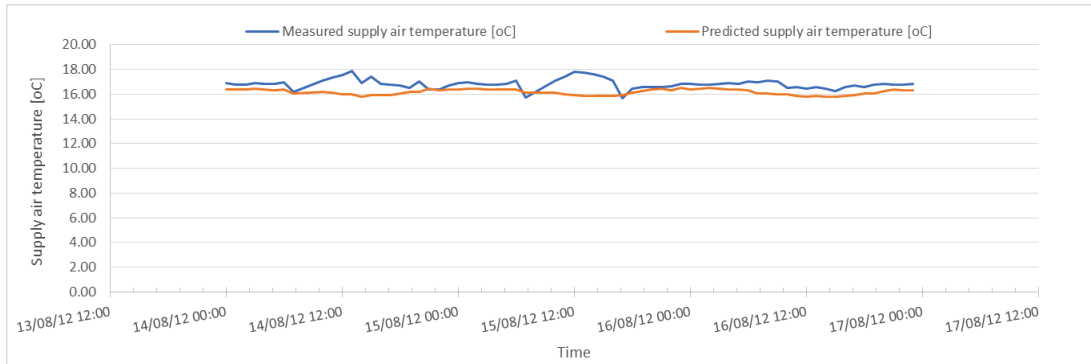


Figure 6.27: Hourly measured vs. predicted supply air temperature from 14-16 August

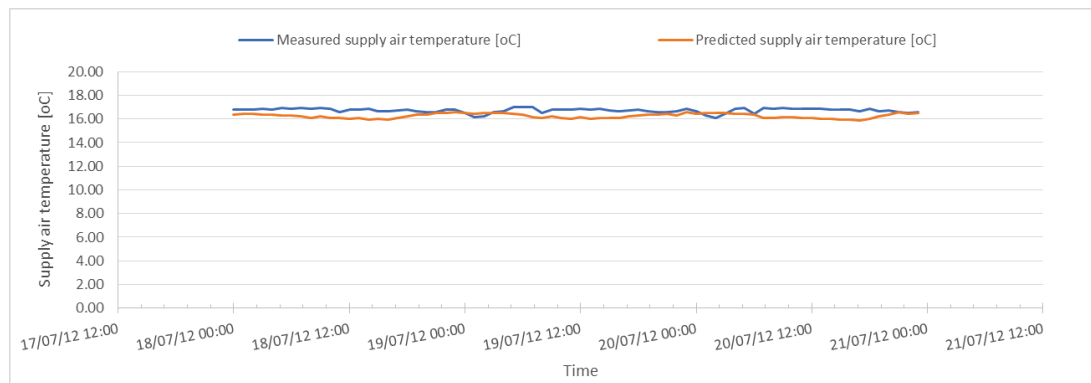


Figure 6.28: Hourly measured vs. predicted supply air temperature from the air handling unit for the summer period

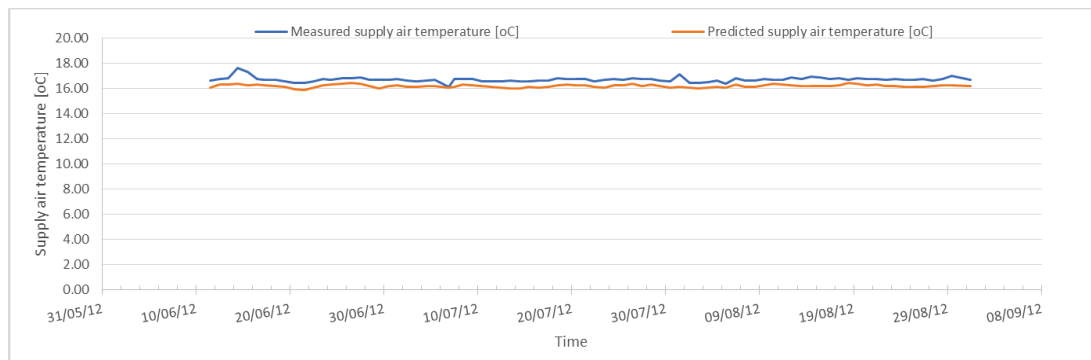


Figure 6.29: Daily measured vs. predicted supply air temperature from the air handling unit

Table 6.7: Measured vs. predicted supply air temperature for three days in July and for the entire summer period

Period	Supply air temperature [°C]		ΔT [°C]
	Measured	Predicted	
July 18-20	16.73	16.26	0.51
June 11-August 31	16.68	16.17	0.47

Figure 6.30 shows good agreement between the hourly measured and predicted supply air temperature signature for the summer period. The average measured hourly and daily temperature is 16.68 °C, while the predicted average temperature is 16.17 °C. The difference of 0.51 °C is smaller than the uncertainty of 1 °C, therefore the temperature of the supply air flow rate seems to be calibrated (Figures 6.30 to 6.33). The supply air temperature signatures show also good agreement for the 3 day interval in July (Figure 6.31) and August (Figure 6.32).

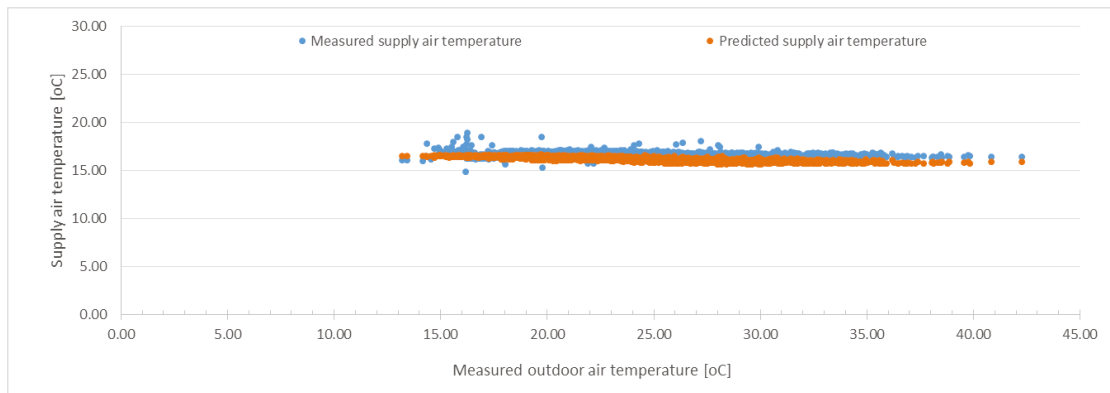


Figure 6.30: Hourly predicted vs. measured supply air temperature signature for the summer period

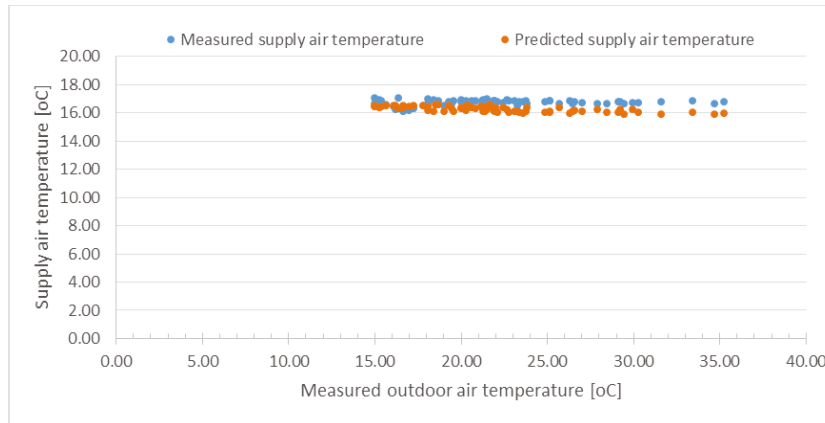


Figure 6.31: Hourly measured and predicted supply air temperature signatures from 18th-20th July 2012

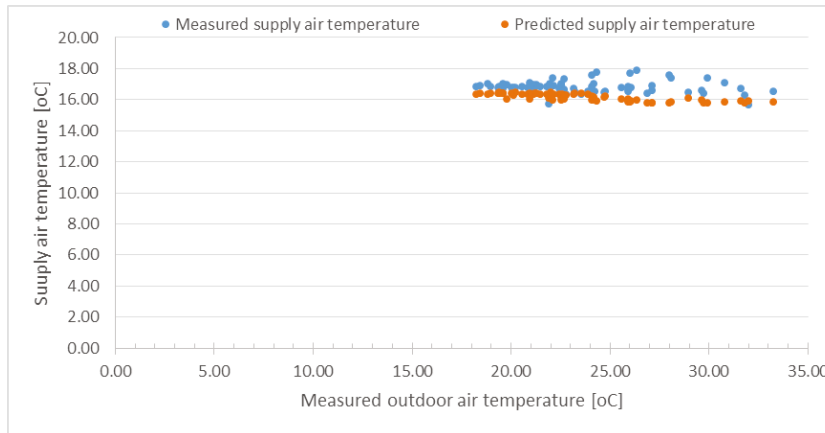


Figure 6.32: Hourly measured and predicted supply air temperature signatures from 14th-16th August 2012

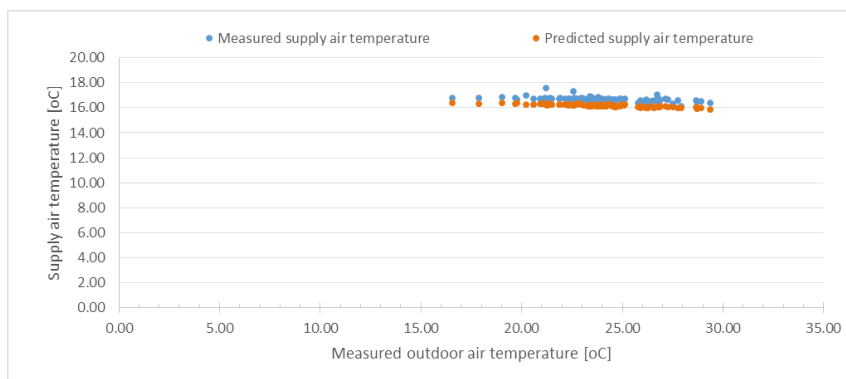


Figure 6.33: Daily predicted vs. measured supply air temperature signature for the summer period 2012

The predictions seem to agree well with the measurements. In order to see if this conclusion is indeed true, some statistical indices are needed to quantify the level of agreement.

6.4.2 Statistical indices analysis

The same indices as previously discussed (section 5.2) were calculated: RMSE, CV-RMSE and NMBE (Table 6.8).

All the RMSE are less than the measurement uncertainty, the hourly CV-RMSE is less than 30%, and the hourly NMBE is lower than 10%. This analysis leads to the conclusion that the model is calibrated for the supply air temperature of the AHU.

Table 6.8: Statistical indices for the difference between predicted and measured supply air temperature

Statistical Indices	Hourly values (summer)	Hourly values (July 18-20)	Hourly values (August 14-16)	Daily average values
u [°C]	1	1	1	1
RMSE [°C]	0.67	0.57	0.8	0.53
CV-RMSE [%]	4	3	5	3
NMBE [%]	3.07	2.81	3.78	3.07

6.4.3 Hypothesis testing

The probability distributions of the hourly and daily difference between predicted and measured supply air temperatures are presented in Figures 6.34 and 6.35, respectively. Both graphs present a normal distribution, slightly skewed to the right.

The hourly t-statistic value is less than the critical t-value of 1.645 and the daily t-value is less than the critical t-value of 1.666 (Table 6.9), suggesting that the model is calibrated for the supply air temperature. The t-values are negative because the root mean squared error is much smaller than the uncertainty.

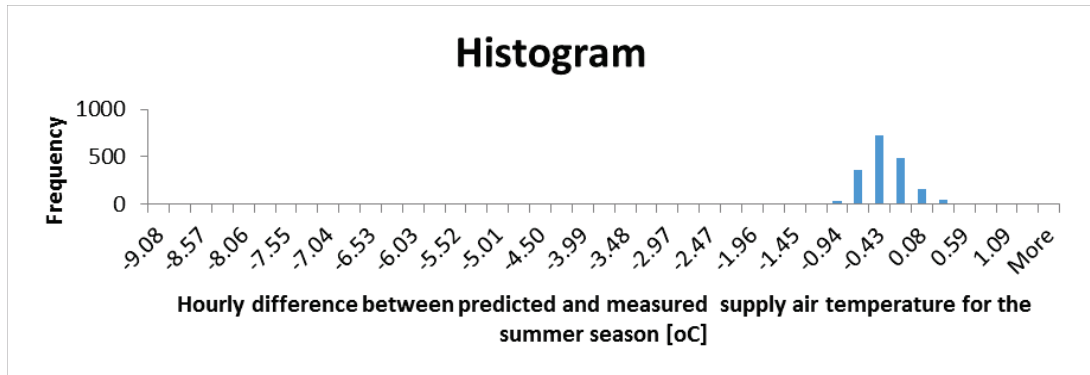


Figure 6.34: Histogram of the hourly difference between the predicted and measured supply air temperature for the summer season

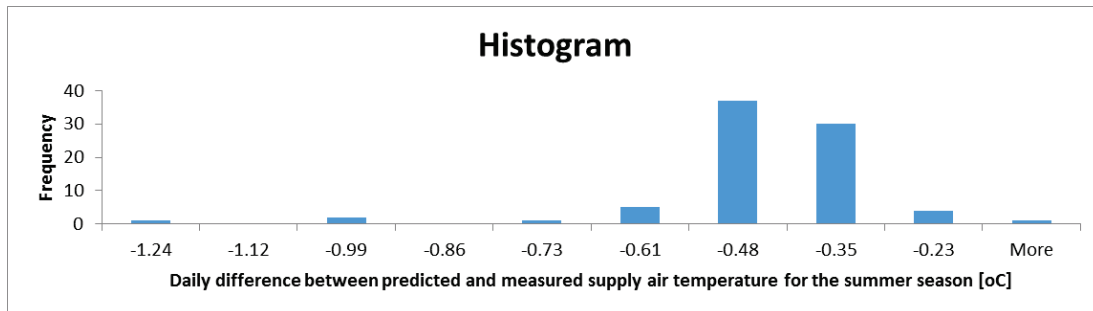


Figure 6.35: Histogram of the daily difference between the predicted and measured supply air temperature for the summer season

Table 6.9: T-statistic value for the difference between predicted and measured supply air temperature

Hypothesis test index	Hourly values (summer)	Hourly values (July 18-20)	Hourly values (August 14-16)	Daily average values
t statistic	-48.55	-14.09	-5.86	-29.21

All the three methods of comparing the measured and predicted supply air temperature lead to the conclusion that the supply air temperature is calibrated.

6.5 Calibration of the cooling coil load in the air handling unit

First, the graphical representation of measured and predicted cooling coil load is plotted and analyzed. Secondly, statistical indices are calculated, and compared with reference values. Thirdly, the hypothesis testing is performed to verify whether the difference between predictions and measurements is significant or not.

6.5.1 Graphical representation

Figures 6.36 and 6.37 present the predicted vs. measured cooling coil load in the AHU over three days in July and August, respectively. It seems that the simulation results are under-predicted.

Figures 6.38 and 6.39 present the variation of measured vs. predicted cooling coil load over the entire summer when using hourly averaged values and daily averaged values, respectively. It is noticed again that the cooling coil load is under-predicted. Further investigation to find out where the problem comes from will be presented in section 6.5.4.

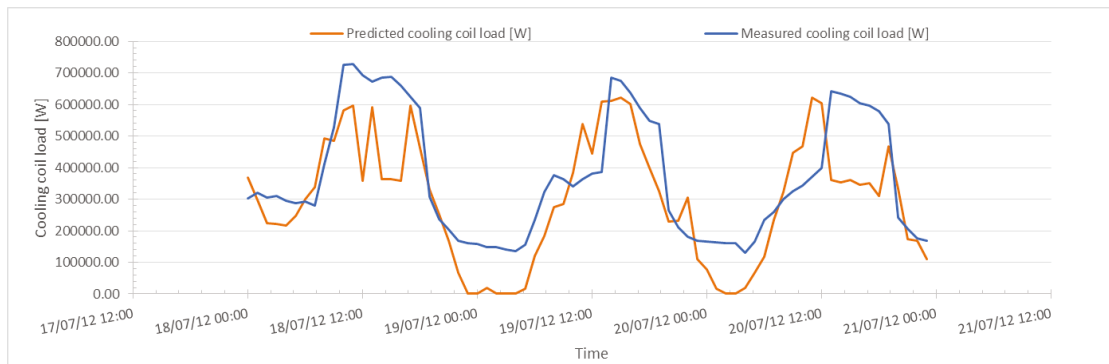


Figure 6.36: Hourly predicted vs. measured cooling coil load in the AHU from 18th-20th July 2012

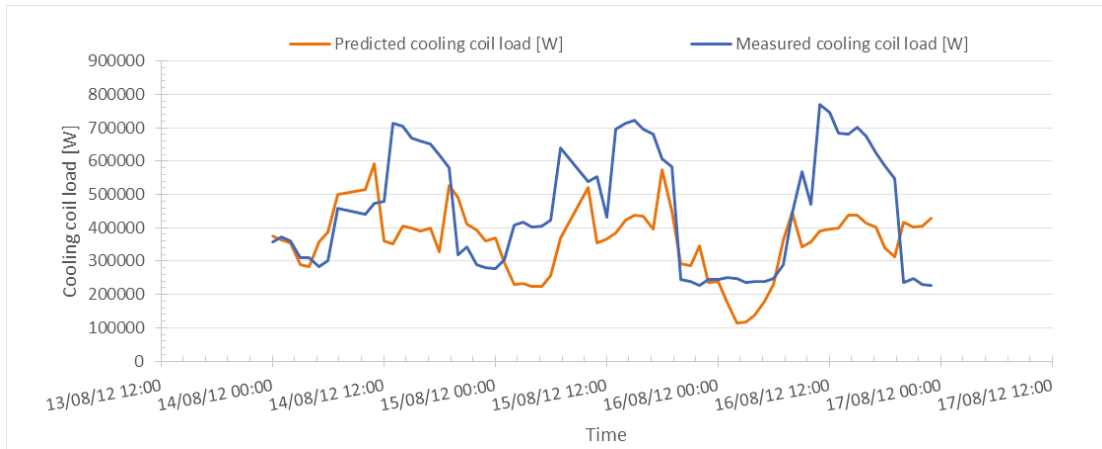


Figure 6.37: Hourly predicted vs. measured cooling coil load in the AHU from 14th-16th August 2012

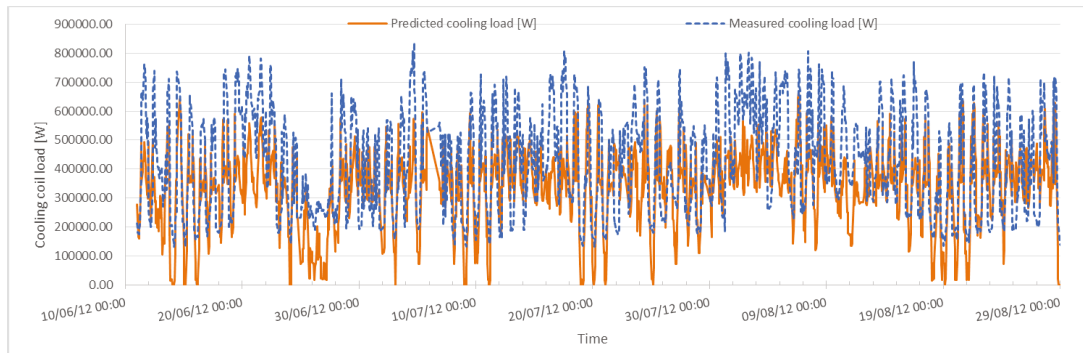


Figure 6.38: Hourly predicted vs. measured cooling coil load in the AHU for the summer period

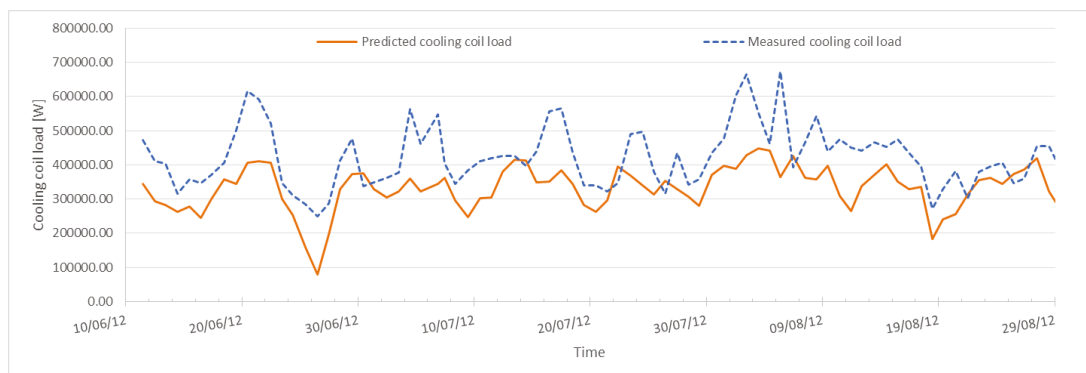


Figure 6.39: Daily predicted vs. measured cooling coil load in the AHU

The cooling coil load signatures are plotted using hourly and daily averaged values (Figures 6.40 to 6.43). Once again, it can be observed that the predicted cooling coil load

is under predicted, being approximately 25% less than the measured cooling coil load, regardless of the outdoor air temperature.

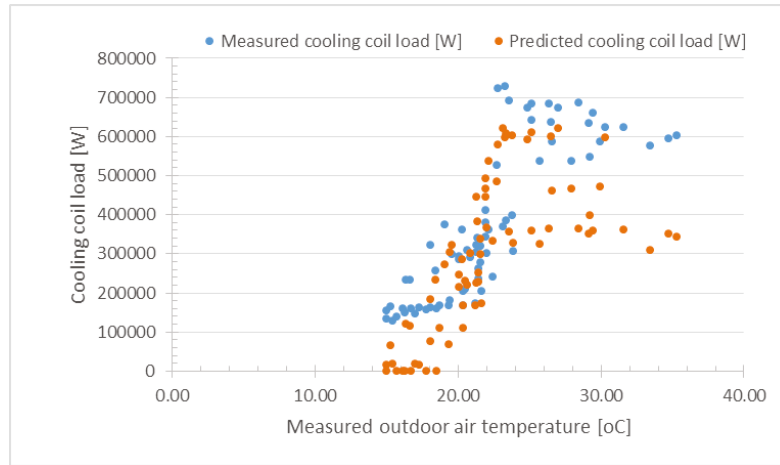


Figure 6.40: Predicted vs. measured hourly cooling coil load signatures from 18-20 July

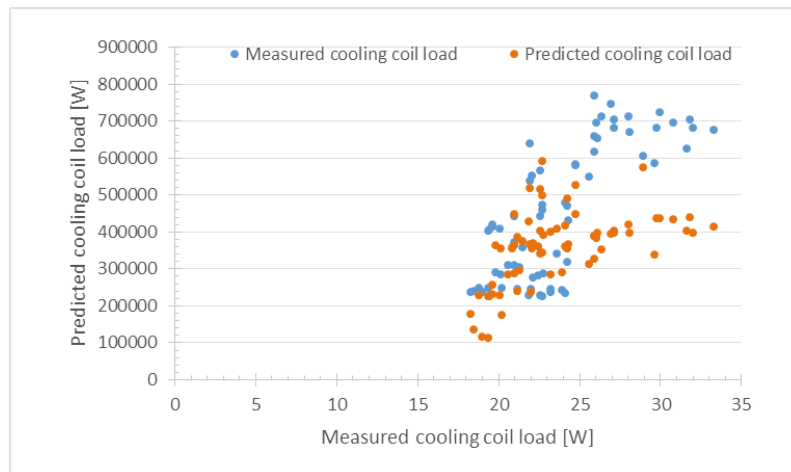


Figure 6.41: Predicted vs. measured hourly cooling coil load signatures from 14-16 August

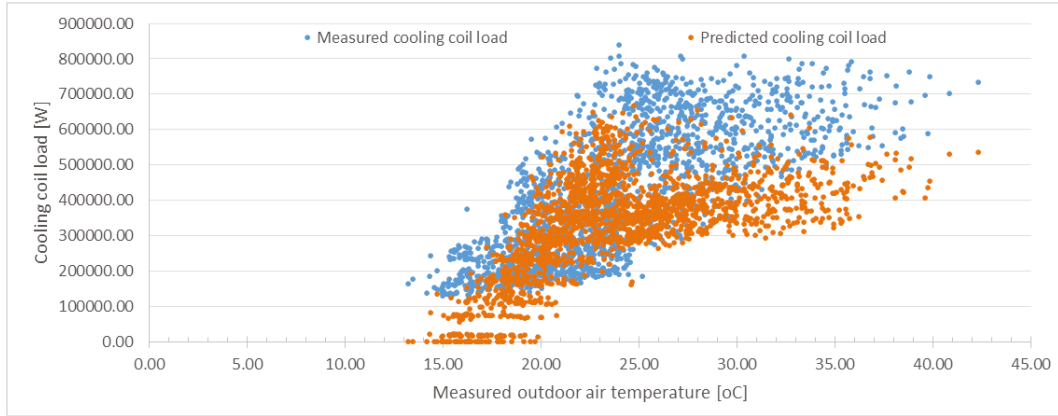


Figure 6.42: Predicted vs. measured hourly cooling coil load signatures for the summer period

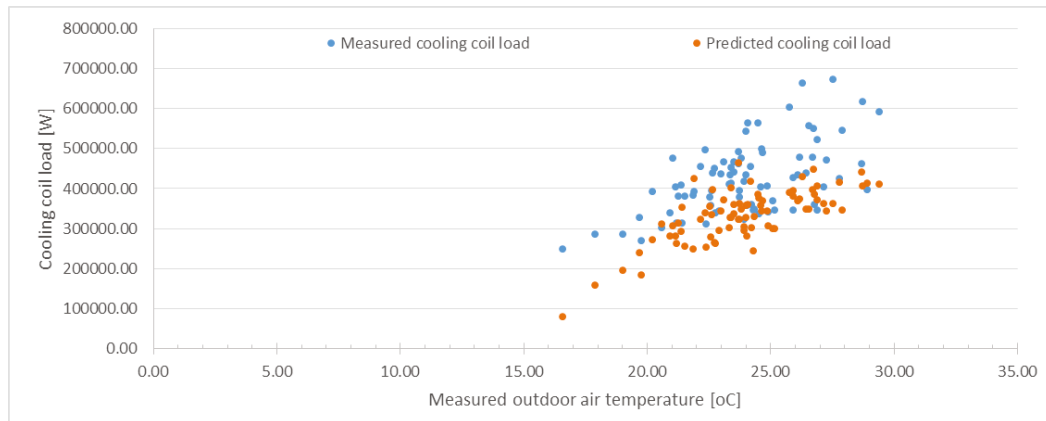


Figure 6.43: Predicted vs. measured daily cooling coil load signatures for the summer period

To better analyze how well the measurements and predictions agree, plots of measured vs. predicted cooling coil load have been also developed (Figures 6.44 and 6.45). We can conclude already that the model is not calibrated, since the slope of linear relationship of predicted vs. measured is only 0.431, that is, for a 1 W variation of measured cooling coil load, the predicted values varies by 0.431 W.

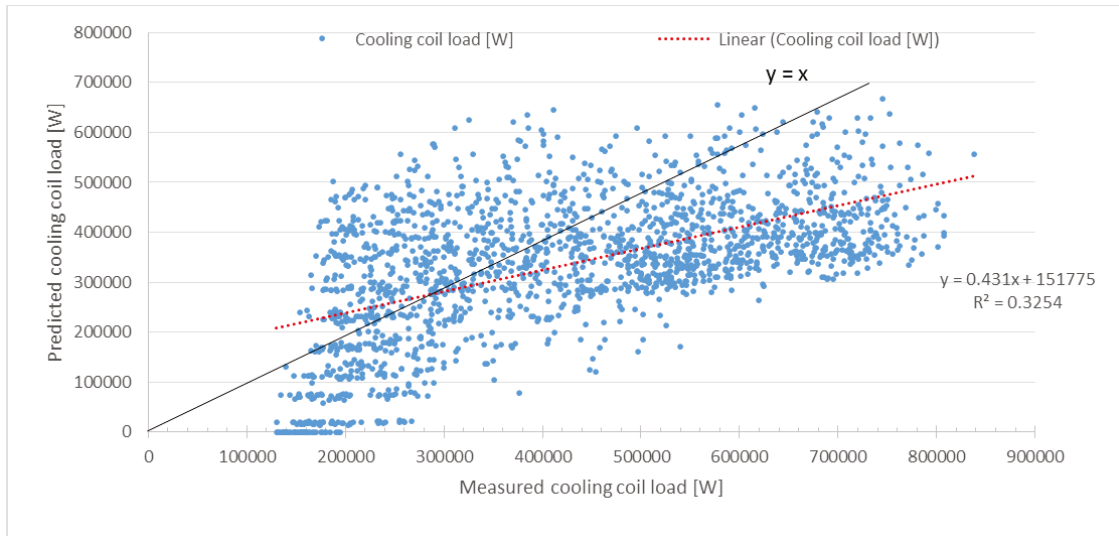


Figure 6.44: Measured vs. predicted hourly cooling coil load for the summer period

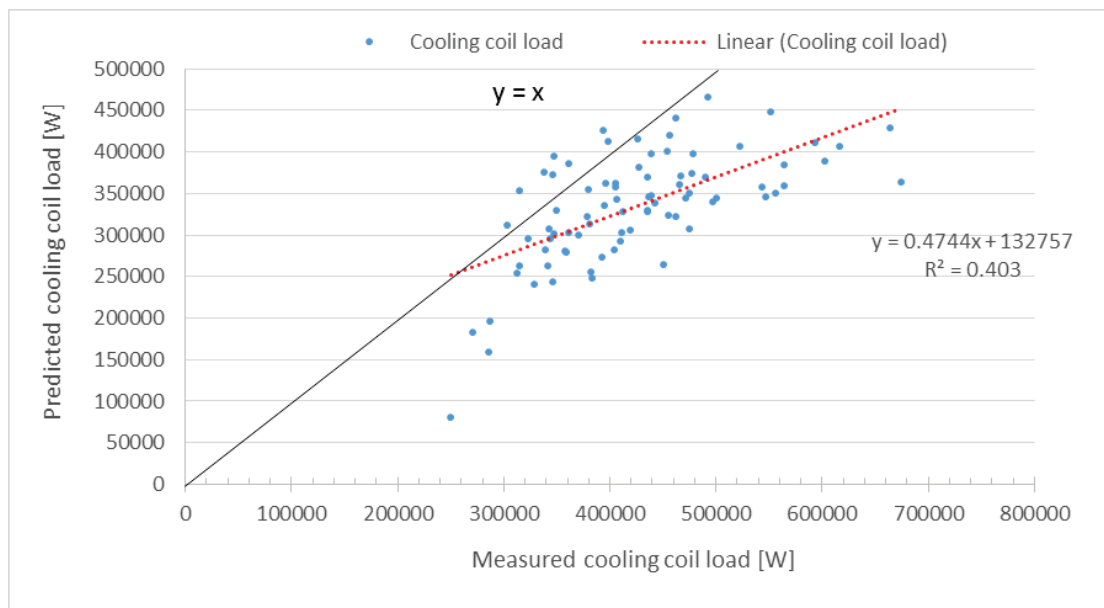


Figure 6.45: Measured vs. predicted cooling coil load for the summer period

Since the predicted and measured supply air flow rates show good agreement, the air enthalpy difference across the cooling coil could be the reason of such a disagreement in the cooling coil loads (this will be discussed in section 6.5.4).

6.5.2 Statistical indices

The hourly and daily values of RMSE, CV-RMSE and NMBE are presented in

Table 6.10:

Table 6.10: Statistical indices for hourly and daily difference between predicted and measured cooling coil load

Statistical Indices	Hourly values (summer)	Hourly values (July 18-20)	Hourly values (August 14-16)	Daily average values
u [W]	16187	40208	39499	21993
RMSE [W]	175860	150532	185899	113511
CV-RMSE [%]	42	40	41	27
NMBE [%]	21.05	20.70	21.20	21.50

The RMSE is much higher than the uncertainty, while the CV-RMSE is well above 30%, for hourly values. The NMBE is higher than 10%; hence, the cooling coil load is not calibrated when using hourly average values. In conclusion, using this method one can estimate that the cooling coil load is not calibrated.

6.5.3 Hypothesis testing

Figures 6.46 and 6.47 show the histograms of the difference between measured and predicted cooling coil load when using hourly and daily average values, respectively. The hourly histogram presents a normal distribution, while the daily histogram is a bit skewed to the right, which also reinstates that the predicted cooling coil load is a bit under predicted. Nevertheless, with a sample size higher than 30, skewedness is expected.

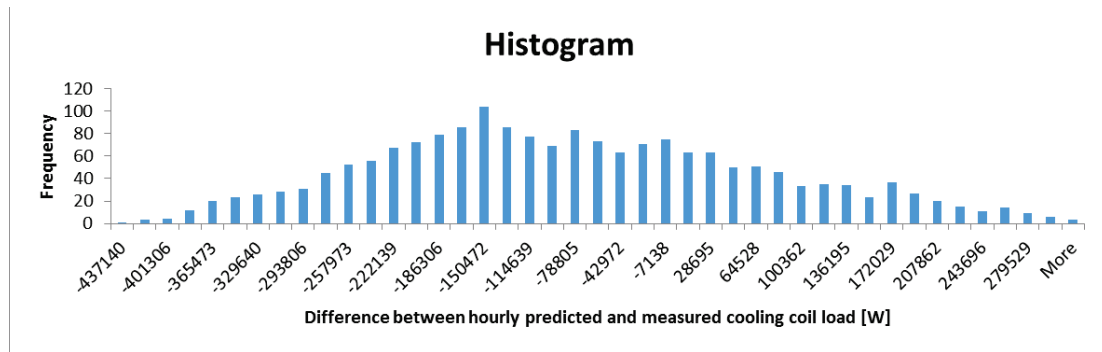


Figure 6.46: Histogram of the difference between predicted and measured hourly cooling coil load

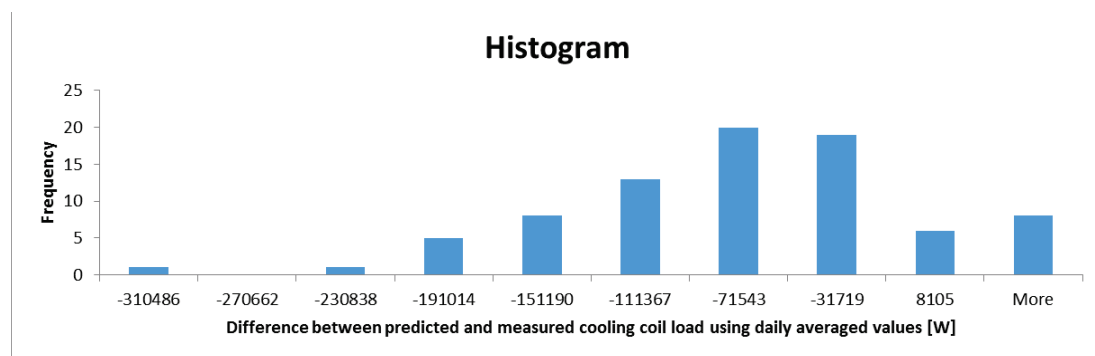


Figure 6.47: Histogram of the difference between predicted and measured daily cooling coil load

The t-statistic values are much higher than the critical t-values of 1.645 (for hourly values) and 1.666 (for daily values) (Table 6.11). The same conclusion is reached using this method: the cooling coil load is not calibrated.

Table 6.11: The t-statistic value using hourly and daily averaged values for the calibration of the cooling coil load

	Hourly values (summer)	Hourly values (July 18-20)	Hourly values (August 14-16)	Daily average values
t-statistic	20.66	2.26	2.86	8.86

6.5.4 Analysis of cooling coil load based on fraction of fresh air entering the building

To better understand why there are differences between measurements and predictions and to improve the calibration, the data is split into three ranges, based on the amount of fresh air that enters the building: Case 1: when 100% return air is used ($\alpha=0$); case 2: when a mix of fresh air and return air enters the cooling coil ($0<\alpha<1$); and case 3: when only fresh air enters the AHU ($\alpha=1$). The value α is calculated with the following equation:

$$\alpha = \left(\frac{T_{Mix} - T_{Return}}{T_{Outdoor} - T_{Return}} \right) \times 100\% \quad (6.3)$$

For ease of understanding, and also using the terms of eQuest program, the condition of the air entering the cooling coil will be called mixed condition, while the condition of air exiting the cooling coil will be called cold deck condition.

Case 1: $\alpha=0$

This case deals with the periods when 100% of the return air enters the AHU. Even though 100% return air is recirculated, it will still be mixed with the outdoor air, because the capacity of the supply air fans is 43 m³/s, while the capacity of the return fans is 33 m³/s. Therefore this difference in air flow rate of 10 m³/s must come from the outside.

Figure 6.48 shows the difference between the outdoor air enthalpy at Loyola campus, calculated based on measured outdoor air temperature and relative humidity, and the predicted outdoor air enthalpy, which is calculated from the weather file Montreal 2012, from Weather Analytics (2013).

The outdoor, mixed and cold deck air enthalpies calculated from measured air temperatures and relative humidity will be called measured values, for ease of

understanding. The measured outdoor air temperature is slightly higher than the predicted one (Figure 6.49), while the measured outdoor air enthalpy, is on average 30 kJ/kg dry air less than the predicted one. The measured mixed air enthalpy is 10 kJ/kg dry air higher than the predicted one (Figure 6.50), while the mean measured cold deck enthalpy is about the same as the predicted cold deck enthalpy, the difference between them being only 2 kJ/kg dry air (Figure 6.51).

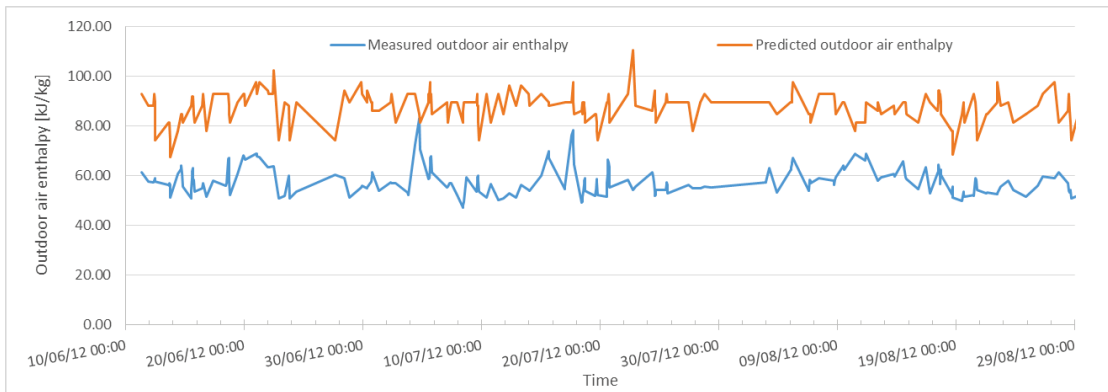


Figure 6.48: Measured vs. predicted outdoor air enthalpy for the periods when 100% return air is used for mixing

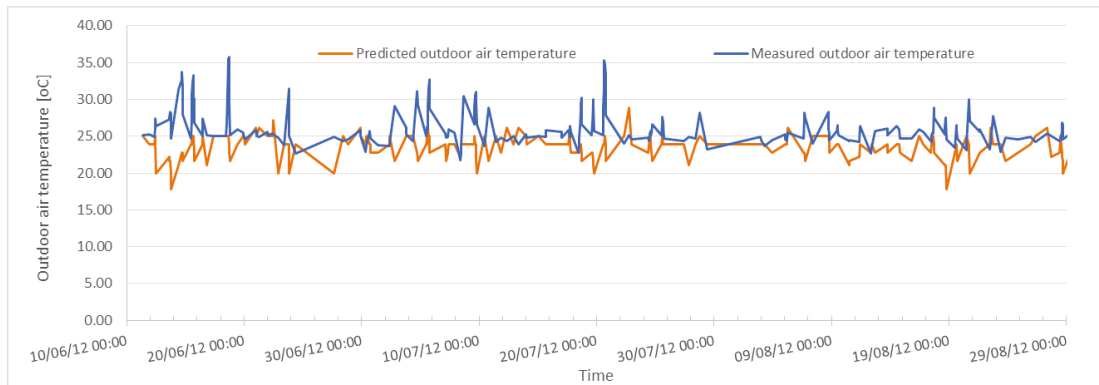


Figure 6.49: Measured vs. predicted outdoor air temperature for the periods when 100% return air is used for mixing

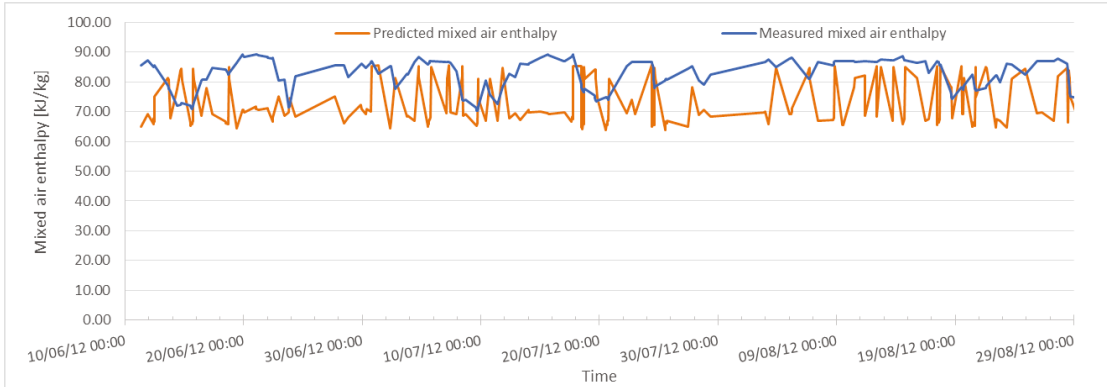


Figure 6.50: Measured vs. predicted mixed air enthalpy for the periods when 100% return air is used for mixing

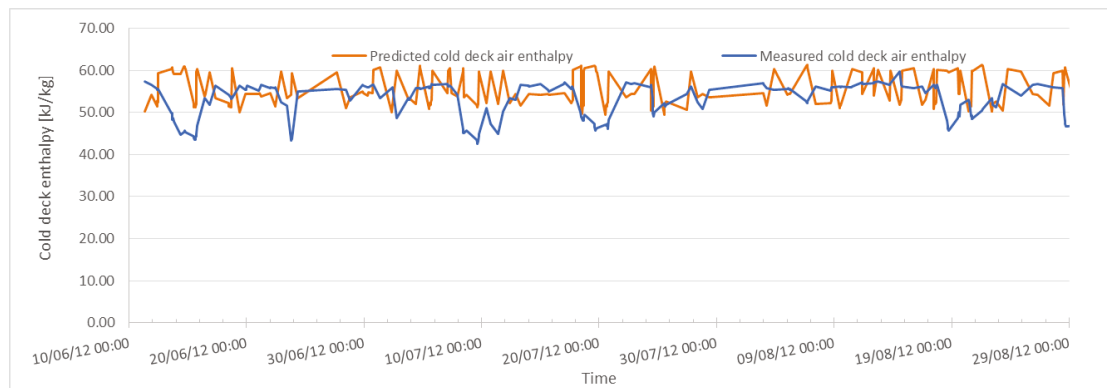


Figure 6.51: Measured vs. predicted cold deck air enthalpy during the periods when 100% outdoor air is used for mixing

The discrepancy in the temperature and enthalpy measured on campus and at Dorval airport (Figure 6.53), contribute to the differences between the measured and predicted cooling coil load. It can be observed (Figures 6.52 and 6.53) that the variation of the predicted cooling coil load follows very closely the variation of the predicted enthalpy difference across the cooling coil. The cooling coil load and the difference in enthalpy across the cooling coil are under predicted, when the measured outdoor condition at the airport are used in calculations, instead of local measurements.

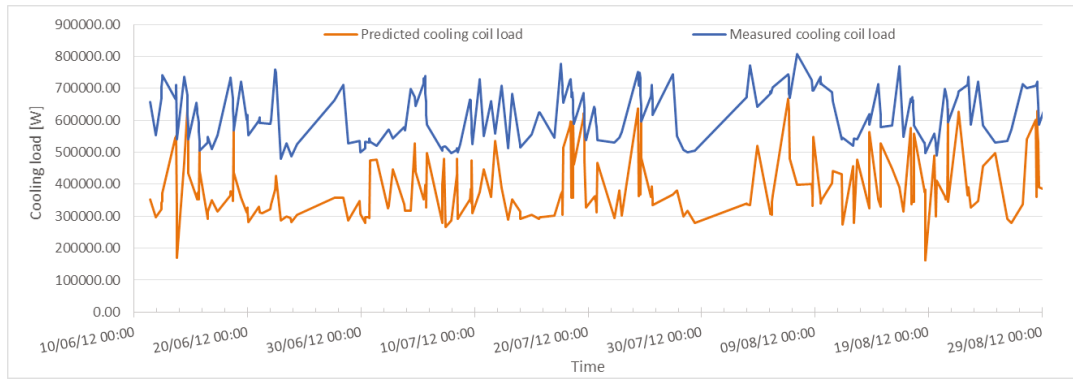


Figure 6.52: Measured vs. predicted cooling coil load for the periods when 100% return air is used for mixing

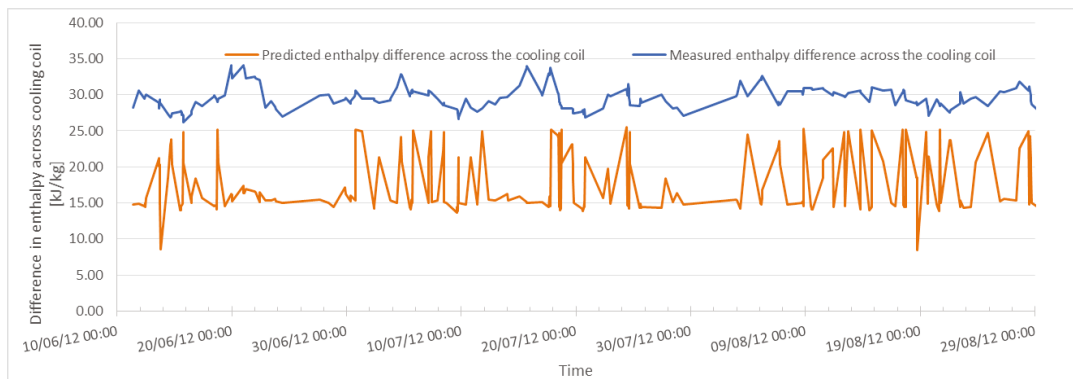


Figure 6.53: Measured vs. predicted enthalpy difference across the cooling coil during the periods when 100% return air is used for mixing

Case 2: $0 < \alpha < 1$

This case represents the instances when there is a mixing between the return and outdoor air streams.

Figures 6.54 to 6.58 present the difference between measured and predicted outdoor air enthalpy, outdoor air temperature, mixed air enthalpy, cold deck air enthalpy and cooling coil load, respectively. Figure 6.59 presents the measured vs. predicted enthalpy across the cooling coil.

The same conclusions as for the previous case can be drawn from these plots:

- Measured outdoor air enthalpy on site is on average 36 kJ/kg dry air lower than the measured outdoor air enthalpy at Dorval airport (Figure 6.54);
- Measured outdoor air temperature on site is slightly higher than the one measured at Dorval airport because the weather data file used by eQuest is based on measurements at Dorval airport (Figure 6.55);
- Mean measured mixed air enthalpy is 7 kJ/kg higher than the predicted mean value (Figure 6.56) with mean measured mixed air enthalpy of 78 kJ/kg and predicted mixed air enthalpy of 71 kJ/kg;
- Mean measured cold deck air enthalpy is lower only by 2 kJ/kg than the mean predicted value (Figure 6.57) with mean measured cold deck air enthalpy of 53 kJ/kg and predicted cold deck air enthalpy of 55 kJ/kg;
- Enthalpy difference across the cooling coil is under predicted by about 36% on average (Figure 6.59); the mean measured enthalpy difference across the coil is 25 kJ/kg, while the mean predicted enthalpy difference across the coil is 16 kJ/kg, the corresponding mean difference being 9 kJ/kg.
- Cooling coil load is under predicted by about 27.4% on average (Figure 6.58); the mean measured cooling coil load is 509 kW, while the mean predicted cooling coil load is 369 kW, resulting in an under prediction of 139kW.
- The variation of the predicted cooling coil load follows very closely the predicted enthalpy difference across the cooling coil (Figures 6.58 and 6.59).

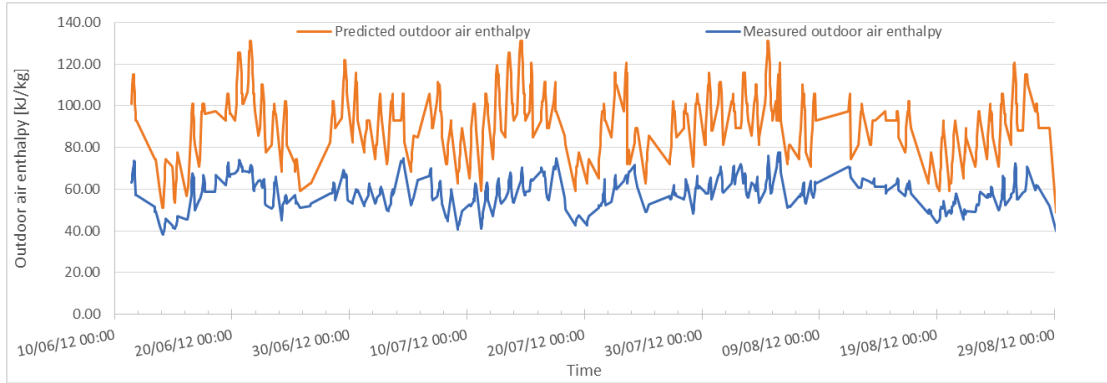


Figure 6.54: Measured vs. predicted outdoor air enthalpy when a portion of return air is mixed with a portion of fresh air to ventilate the building

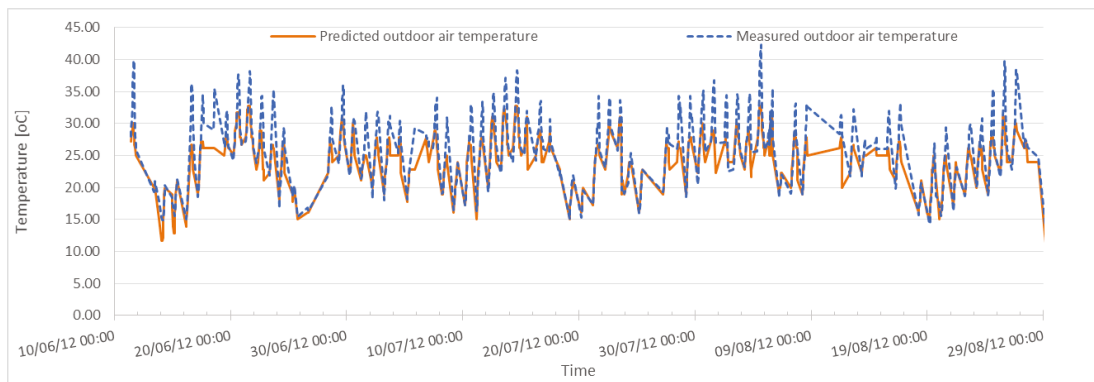


Figure 6.55: Measured vs. predicted outdoor air temperature when a portion of return air is mixed with a portion of fresh air to ventilate the building

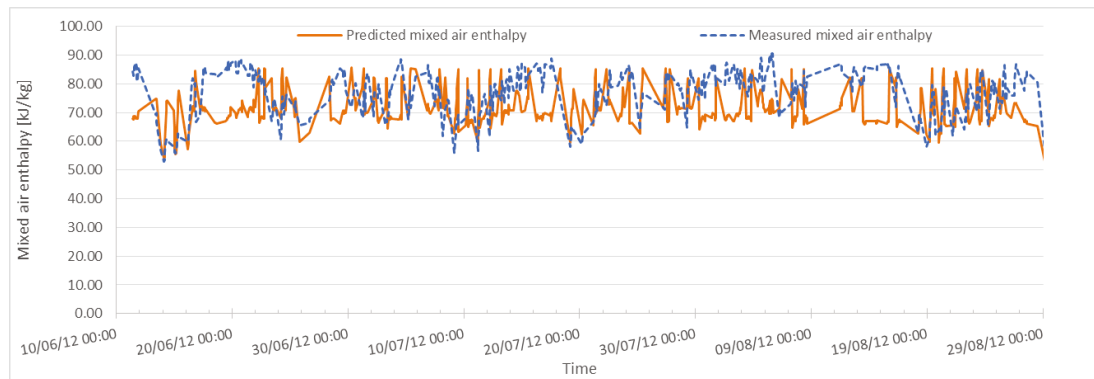


Figure 6.56: Measured vs. predicted mixed air enthalpy when a portion of return air is mixed with a portion of fresh air to ventilate the building

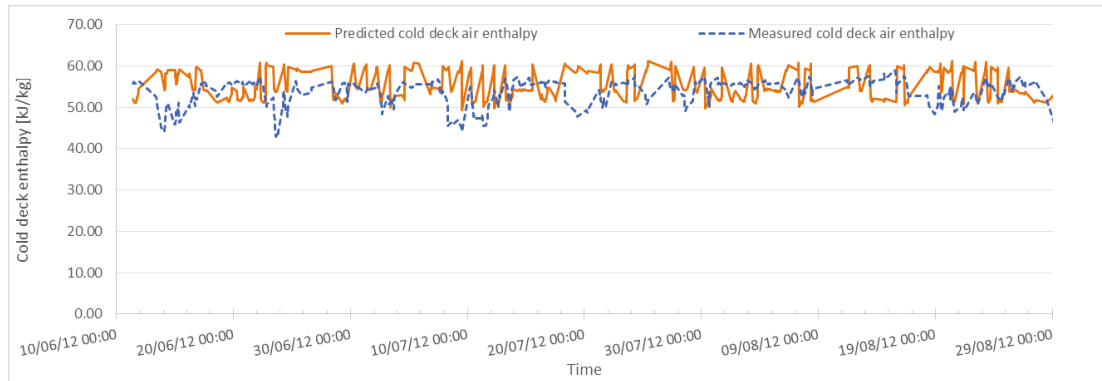


Figure 6.57: Measured vs. predicted cold deck air enthalpy when a portion of return air is mixed with a portion of fresh air to ventilate the building

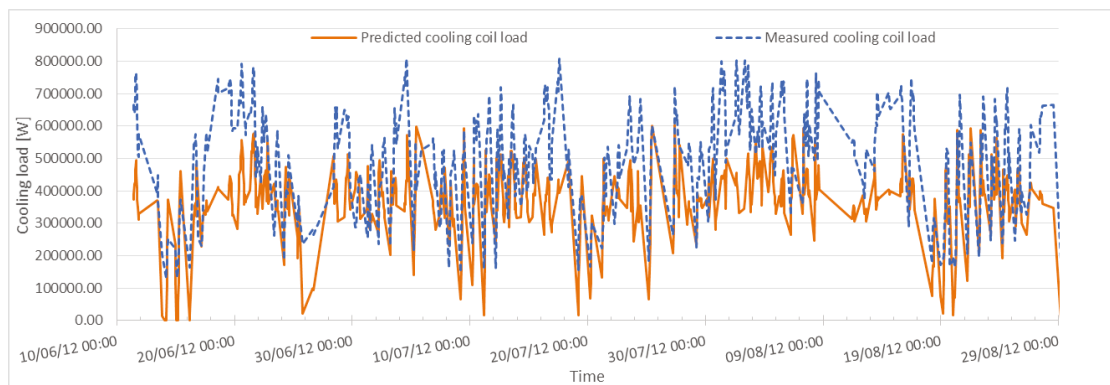


Figure 6.58: Measured vs. predicted cooling coil load when a portion of return air is mixed with a portion of fresh air is used to ventilate the building

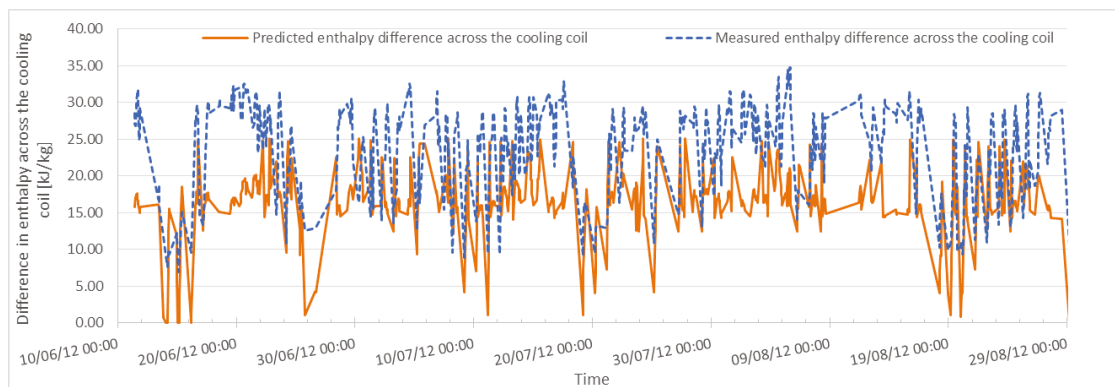


Figure 6.59: Measured vs. predicted enthalpy difference across the cooling coil when a portion of return air is mixed with a portion of fresh air to ventilate the building

It seems that the big discrepancy in cooling coil load is not caused by the difference in cold deck air temperature but by the higher difference in mixed air temperature.

Case 3: $\alpha=1$

This case refers to the instances when 100% outdoor air enters the AHU, meaning that the mixed air temperature is equal to the outdoor air temperature. Figures 6.60 to 6.64 present the difference between measured and predicted outdoor air enthalpy, outdoor air temperature, mixed air enthalpy, cold deck air enthalpy and cooling coil load, respectively.

Some conclusions that can be drawn from these plots are presented below:

- Measured outdoor air enthalpy on site is on average lower by 36% than the measured outdoor air enthalpy at Dorval airport (Figure 6.60); the mean measured outdoor air enthalpy at Loyola is 55.87 kJ/kg, the mean measured outdoor air enthalpy at Dorval is 76.47 kJ/kg and the corresponding difference is 20.6 kJ/kg;
- Measured outdoor air temperature on site is only 4% higher than the one measured at Dorval airport (Figure 6.61); the mean measured outdoor air temperature at Loyola is 21.21 °C , the mean measured outdoor air enthalpy at Dorval is 20.31 °C and the corresponding difference is 0.9 °C;
- Mean measured mixed air enthalpy is 3.7 % lower than the predicted mean value (Figure 6.62). The mean measured mixed air enthalpy is 70.33 kJ/kg, the mean predicted mixed air enthalpy 72.95 kJ/kg and the corresponding difference is only 2.62 kJ/kg;
- Mean measured cold deck air enthalpy is lower by 7.5% than the mean predicted value (Figure 6.63). The mean measured cold deck air enthalpy is 54.40 kJ/kg, the mean predicted mixed air enthalpy 57.49 kJ/kg and the corresponding difference is only 4.09 kJ/kg;

- Enthalpy difference across the cooling coil is under predicted by about 9.2 % on average. Measured enthalpy difference across the cooling coil only 1.5 kJ/kg lower than the predicted cooling coil enthalpy change (Figure 6.65). The mean measured enthalpy difference across the coil is 15.93 kJ/kg, while the mean predicted enthalpy difference across the coil is 14.46 kJ/kg,
- Cooling coil load is under predicted by only 4.8% on average (Figure 6.64); the mean measured cooling coil load is 308 kW, while the mean predicted cooling coil load is 293 kW, resulting in an under prediction of 14.9 kW.
- The variation of the predicted cooling coil load follows very closely the predicted enthalpy difference across the cooling coil (Figure 6.64 and 6.65)

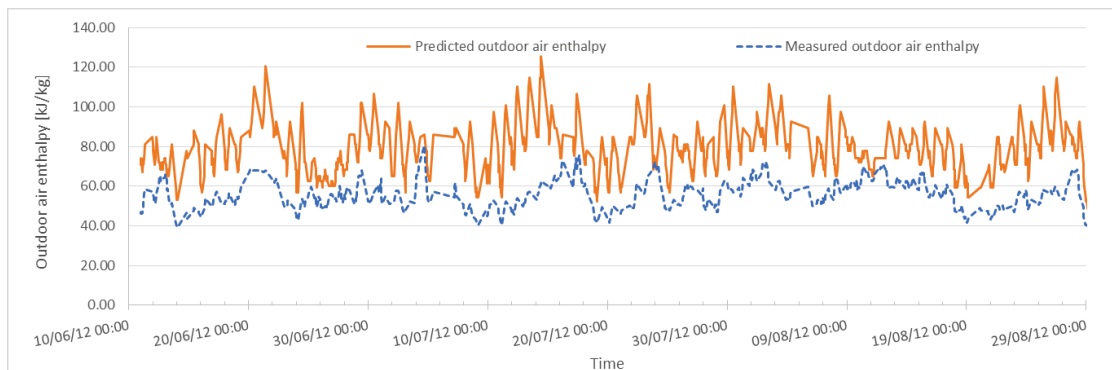


Figure 6.60: Measured vs. predicted outdoor air enthalpy when 100% fresh air is used to ventilate the building

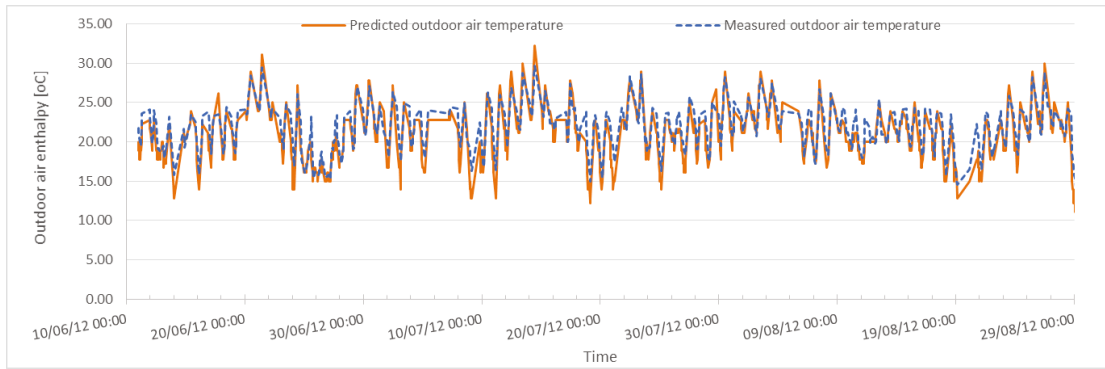


Figure 6.61: Measured vs. predicted outdoor air temperature when 100% fresh air is used to ventilate the building

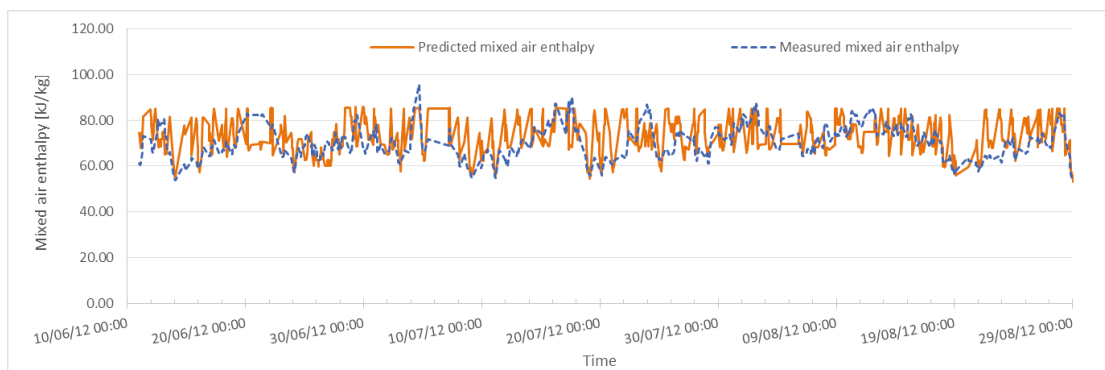


Figure 6.62: Measured vs. predicted mixed air enthalpy when 100% fresh air is used to ventilate the building

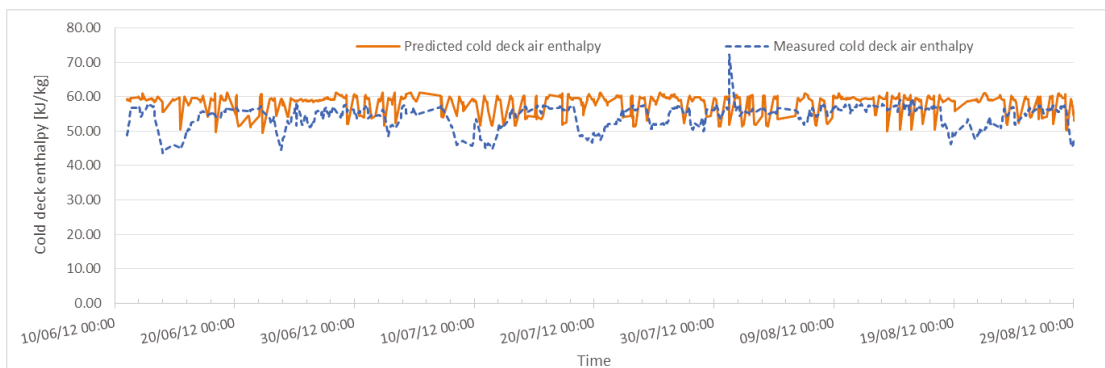


Figure 6.63: Measured vs. predicted cold deck air enthalpy when 100% fresh air is used to ventilate the building

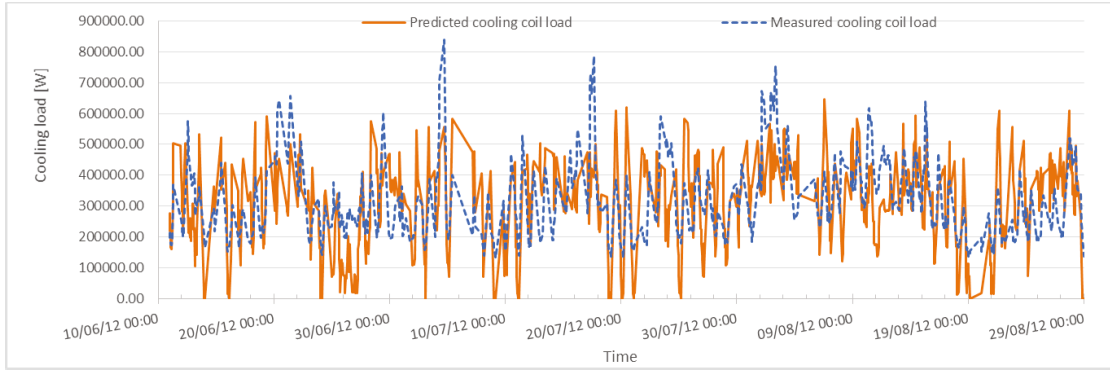


Figure 6.64: Measured vs. predicted cooling coil load when 100% fresh air is used to ventilate the building

Figure 6.68 presents the measured vs. predicted enthalpy change across the cooling coil.

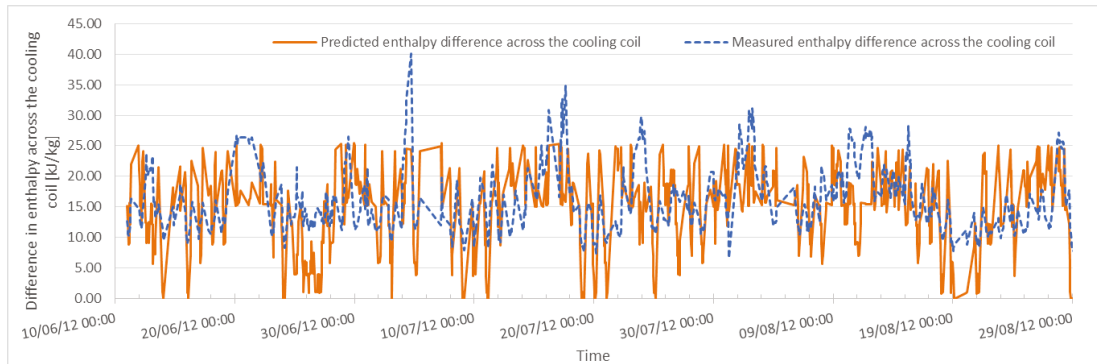


Figure 6.65: Measured vs. predicted enthalpy difference across the cooling coil when 100% fresh air is used to ventilate the building

The statistical indices and t-statistic values are presented in Table 6.12. The RMSE is higher than the uncertainty by 27 kW and 14 kW for the cases of $\alpha=0$ and $\alpha=1$. In the case where $0 < \alpha < 1$, the RMSE is lower than the uncertainty by 19.5 kW. For all cases, the CV-RMSE is higher than the accepted 30% (for energy use though). The NMBE is higher than the 10% limit suggested by ASHRAE Guideline 14 (2002), except for the case where 100% of outdoor air is used to condition the building.

Table 6.12: Statistical indices and t statistic hypothesis testing for the three cases

Statistical indices	$\alpha=0$	$0<\alpha<1$	$\alpha=1$
u [W]	232.1	203	125
RMSE [kW]	259.1	183.5	139
CV-RMSE [%]	41	36	45
NMBE [%]	37.4	27.4	4.8
t	29.67	25.83	0.53

The hypothesis testing requires that the set of data to be analyzed should be normally distributed or close to normality. Since there are many measurement points, the distribution is not expected to be perfectly normal, but could also present some skewedness. For this reason, the histograms are plotted for all three cases and analyzed (Figures 6.66 to 6.68). It can be seen that the distribution is indeed not perfectly normal, but how much this affects the results of the hypothesis testing still needs to be investigated. It is hard to say if the curve presents a distribution close to normality because the closeness itself is a very relative measure that needs to be defined.

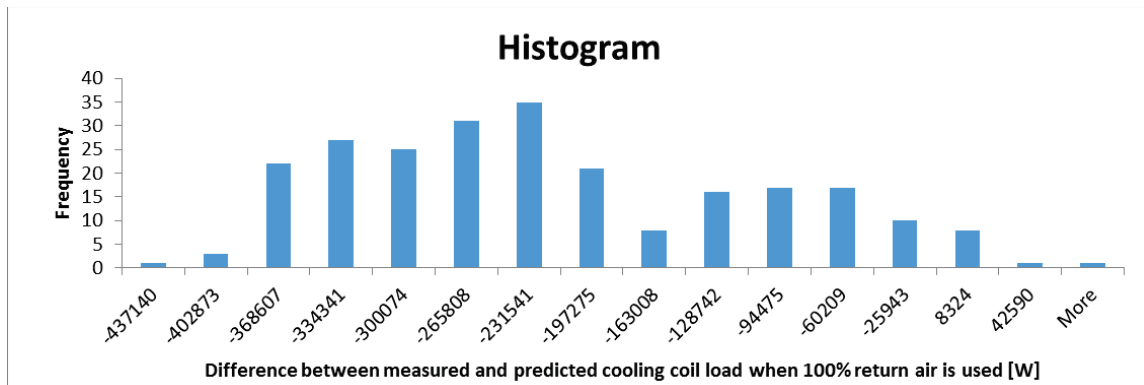


Figure 6.66: Histogram for the difference between measured and predicted cooling coil load when 100% return air is used to ventilate the building

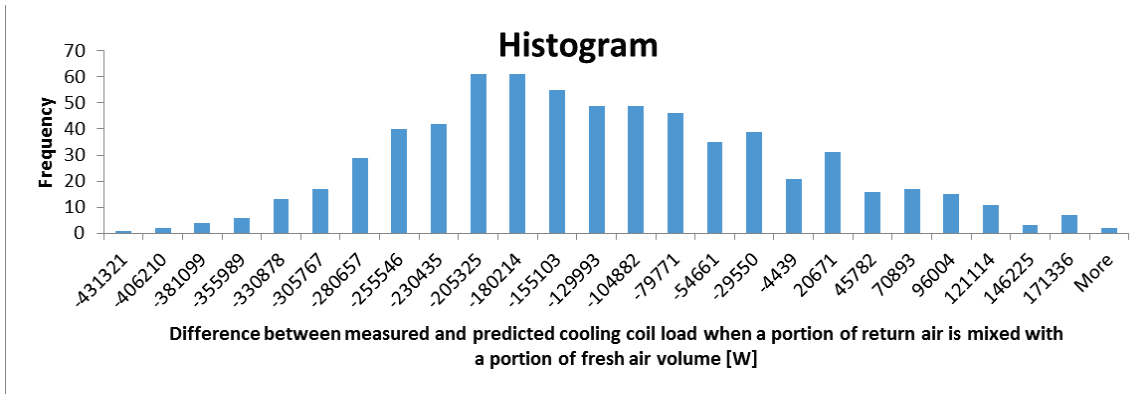


Figure 6.67: Histogram for the difference between measured and predicted cooling coil load when a portion of return air is mixed with a fraction of fresh air to ventilate the building

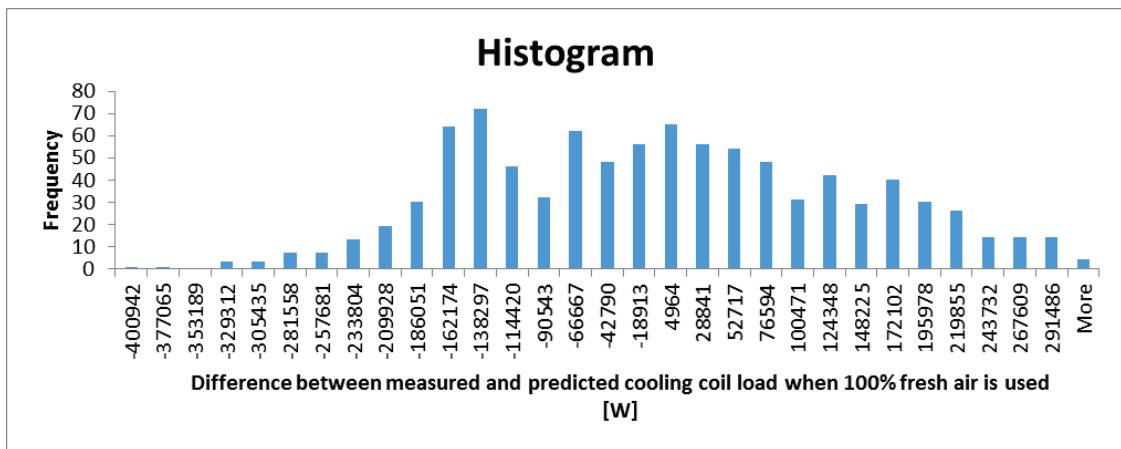


Figure 6.68: Histogram for the difference between measured and predicted cooling coil load when 100% fresh air is used to ventilate the building

For the first case, the distribution is the farthest from being normal, while the second and third case could be interpreted as close to normality. Nevertheless, for the first two cases, the t statistic value is much higher than the critical t value of 1.645. In the case when only fresh air is used to ventilate the building the t statistic is less than the critical value, therefore the cooling coil load is calibrated for those instances.

6.5.5 Cooling coil load based on measured mixed air enthalpy measured on site

In order to reduce the difference between measured and predicted cooling coil load which is due to the difference between the measured and predicted outdoor air enthalpy, the predicted cooling load is calculated based on the mixed air enthalpy that is measured on the site. That is, the outdoor air conditions extracted from eQuest and based on Dorval data, are replaced by the outdoor air conditions measured on site, and used in the calculation of cooling load .

The new calculations show that the predicted cooling coil load is much closer to the measured one and it follows closely the shape of the measured cooling load for both hourly and daily values (Figures 6.69 and 6.70).

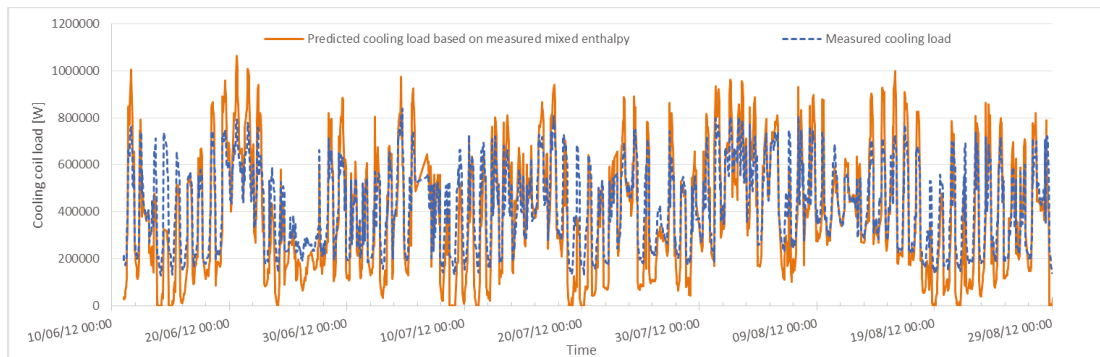


Figure 6.69: Measured vs. predicted hourly cooling coil load based on mixed air enthalpy measured on site

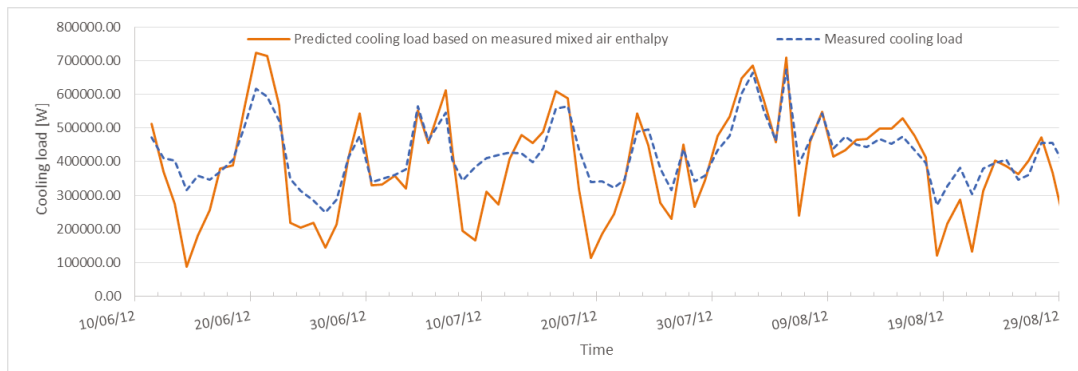


Figure 6.70: Measured vs. predicted daily cooling coil load based on mixed air enthalpy measured on site

The cooling coil load signatures seem to present a better agreement between measurements and predictions for both hourly and daily averaged values (Figures 6.74 and 6.75).

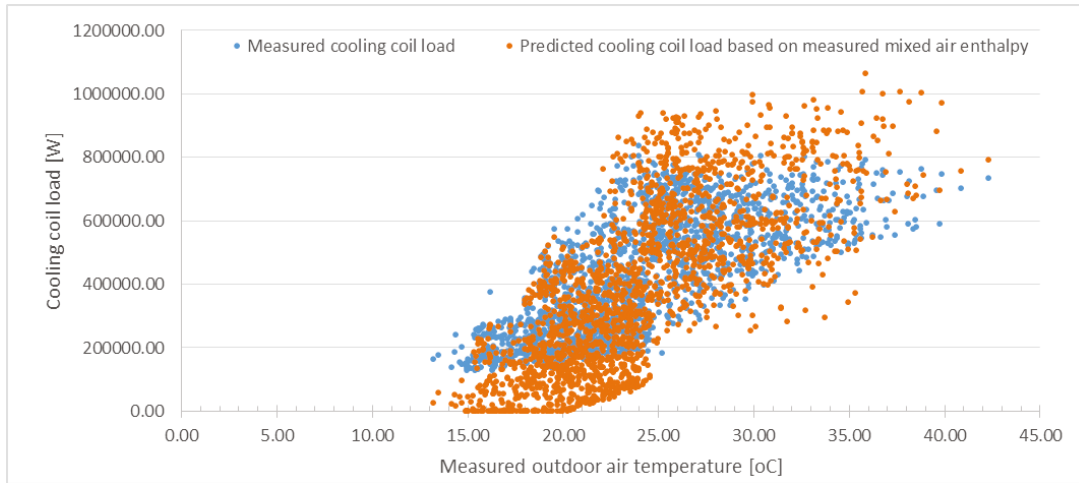


Figure 6.71: Measured vs. predicted hourly cooling coil load signature (based on mixed air enthalpy measured on site)

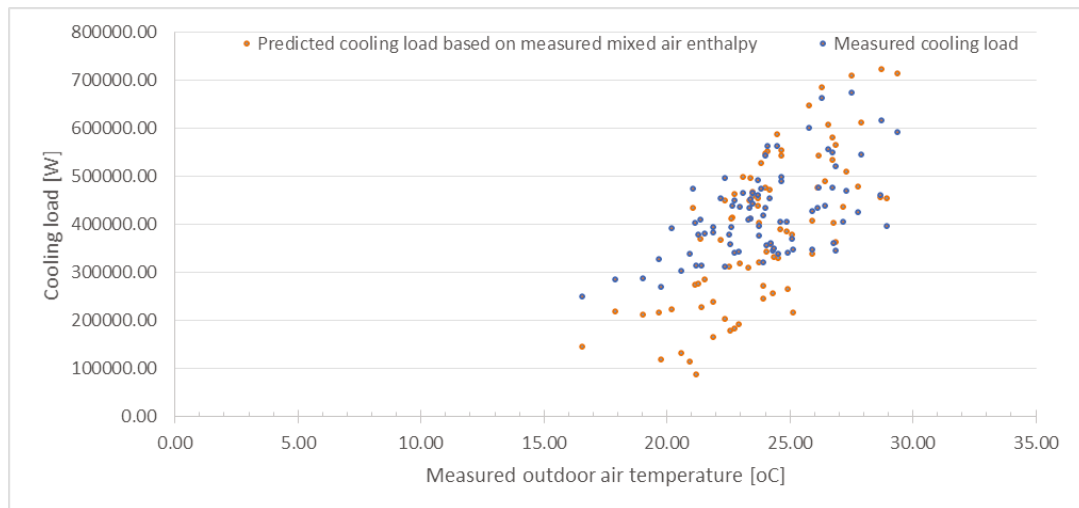


Figure 6.72: Measured vs. predicted daily cooling coil load signature (based on mixed air enthalpy measured on site)

Figures 6.73 and 6.74 show that the model presents a better agreement because the plots of measured vs. predicted cooling coil load present a more linear relationship

than before, the trend line being closer to the line $y=x$ (slope 1.332 vs. 1 for the hourly data).

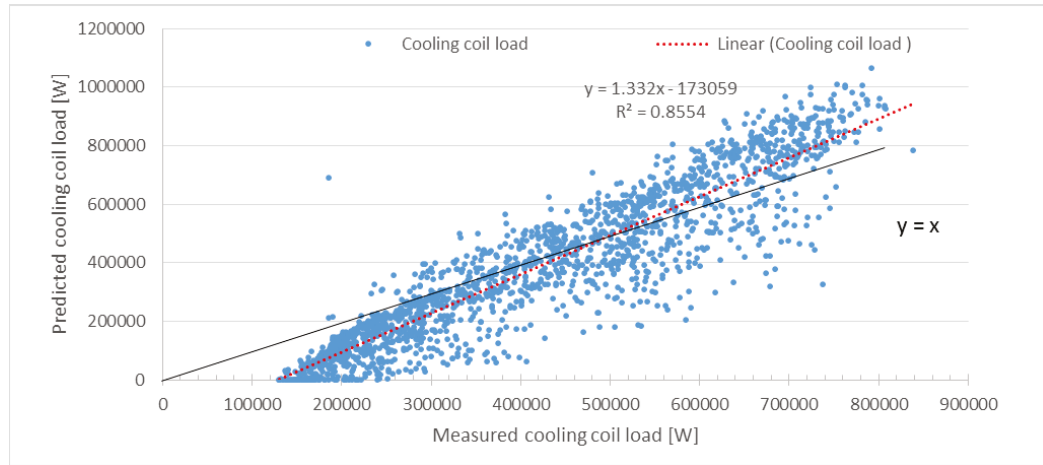


Figure 6.73: Measured vs. predicted hourly cooling coil load (based on mixed air enthalpy measured on site)

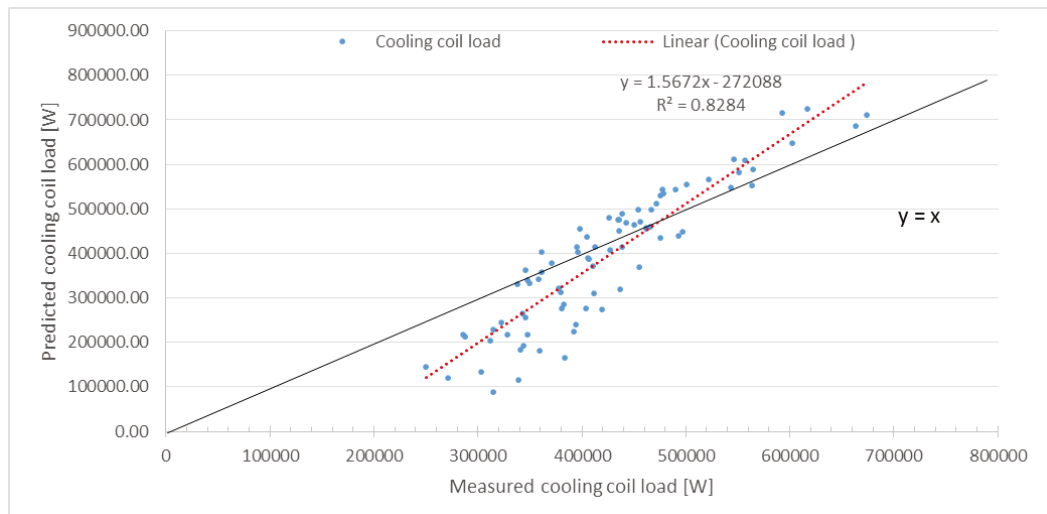


Figure 6.74: Measured vs. predicted daily cooling coil load (based on mixed air enthalpy measured on site)

Table 6.13 presents the statistical indices along with the t-statistic for hourly and daily averaged values. The RMSE is lower than the uncertainty for both hourly and daily averaged values since hourly uncertainty is 161 kW and the daily uncertainty is 219 kW. The hourly CV-RMSE is less than the accepted 30% value, but the daily one is higher than

the 15% limit established by ASHRAE Guideline 14. The hourly NMBE is less than 10% (ASHRAE Guideline 14), but there are no guidelines to follow for calibrating on a daily basis or for calibrating the cooling coil load. Hence, by using the statistical indices approach, we can conclude that the model is now calibrated when hourly values are used, but we cannot conclude anything about daily calibration, since there are no guidelines established.

Table 6.13: Statistical indices for the calibration of the cooling load based on mixed air enthalpy measured on site

Statistical indices	Hourly	Daily
RMSE [kW]	119	86
CV-RMSE [%]	28	20
NMBE [%]	7.69	7.56
t statistic	6.09	1.08

Figures 6.75 and 6.76 present the probability distribution of the difference between measured and predicted hourly and daily cooling coil load. The hourly histogram presents nearly a normal distribution, while the daily histogram shows skewedness to the right. Nevertheless, the t-statistic value of 6.09 is higher than the critical t value of 1.645 when using hourly values, which means that the model is still not calibrated, but compared to the previous results the model greatly improved. The statistical indices method on the contrary, suggests that the model should be considered calibrated.

The t-value of 1.08 is less than the critical value of 1.666 when using daily values, which suggests that the model is calibrated when using daily averaged values, which is the opposite of the result based on the coefficient of variation.

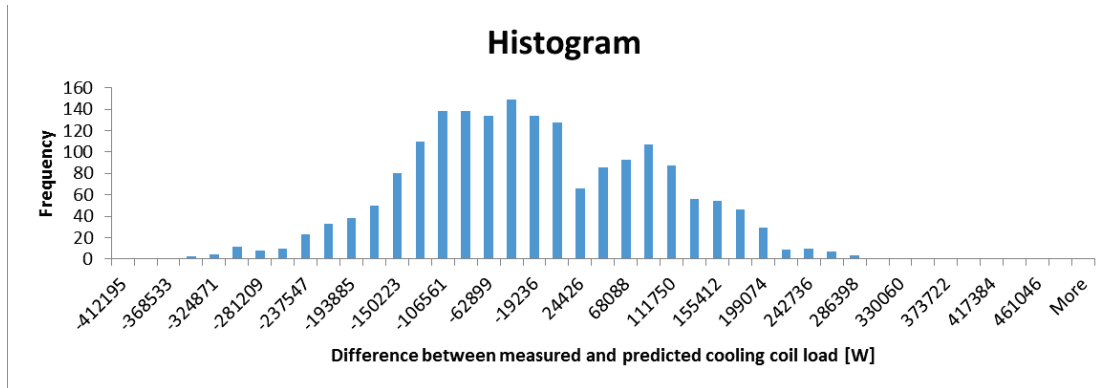


Figure 6.75: Histogram for the difference between measured and predicted hourly cooling coil load (based on mixed air enthalpy measured on site)

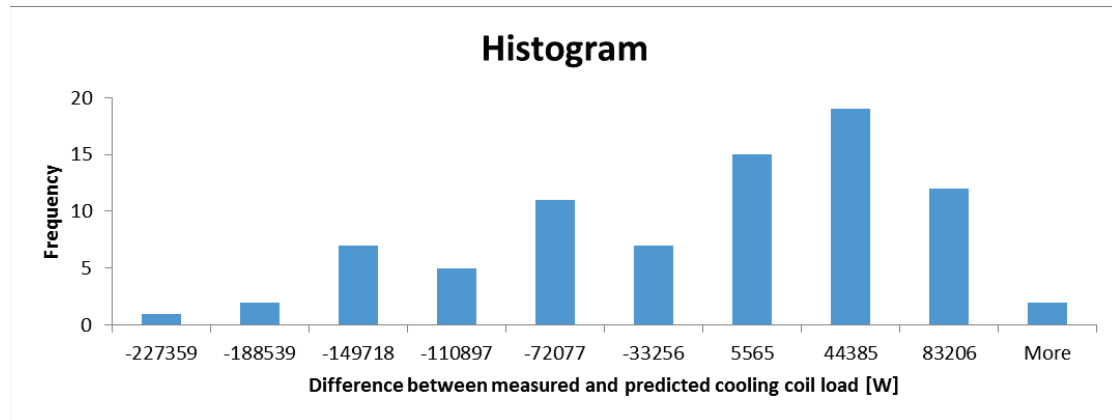


Figure 6.76: Histogram for the difference between measured and predicted daily cooling coil load (based on mixed air enthalpy measured on site)

Further investigation is recommended to determine which method is more accurate and suitable for calibrating a building energy model at the systems or component level.

In conclusion, this section presented the steps to follow in order to calibrate the air handling unit model, based on supply air flow rate, supply air temperature and cooling load. First the inputs changed for the calibration have been discussed.

The calibration of the supply air flow rate starts with the analysis of measured summation of air flow rates supplied to zones vs. the measured air flow rate supplied by

the air handling unit. The difference between the two, due to the omission of the basement floor, is added to the predicted results in order to be able to compare the measurements with the prediction. First, the calibration results are analyzed graphically, and a difference between measurements and predictions is observed only during the night periods. This difference cannot be explained, since the minimum supply air flow rate input to eQuest was taken from the measurements during the unoccupied periods. Second, statistical indices such as RMSE, CV-RMSE and NMBE are calculated for the difference between the measured and predicted air flow rate supplied by the AHU. This method suggests that the model is calibrated, since the hourly coefficient of variation of the root mean squared error is less than the 30% limit suggested by ASHRAE Guideline 14. Third, hypothesis testing is used to verify whether the difference between the measurements and predictions is significant or not, and the result implies that it is indeed statistically significant.

Next the results of the supply air temperature calibration are analyzed with the same three methods: graphical analysis, statistical indices and hypothesis testing. All three method shows good agreement between the measured and predicted supply air temperature, suggesting that the supply air temperature model is calibrated.

The cooling load is analyzed in the same fashion: through graphical analysis, statistical indices and hypothesis testing. Graphical analysis showed discrepancies during the night periods, which was expected, since the cooling load calculation is based on the air flow rate supplied to zones. Also, since the cooling coil load is calculated based on the difference between the mixed and cold deck air enthalpies, and there are big discrepancies in the temperature and enthalpies measured on campus and at Dorval airport, it is expected to have differences in the measured and predicted cooling coil load. It was also observed

that the curve variation of the predicted cooling coil load follows very closely the curve of the predicted enthalpy difference across the cooling coil. The predicted cooling coil load during occupied hours seem to agree well with the measured cooling coil load. The statistical indices suggest that the model is not calibrated for the cooling coil load, and the hypothesis testing confirms this conclusion.

In order to investigate why there are discrepancies between the measured and predicted cooling load, the set of data is split depending on the α , a parameter that represents the fraction of fresh air that enters the building. The hourly coefficient of variation of the root mean squared error is higher than the suggested limit of 30% for all cases while the hypothesis testing suggests that the model is calibrated only for the instance when 100% fresh air enters the building.

A technique that was tried to reduce the difference between measured and predicted cooling coil load which is due to the difference between the outdoor air enthalpy, was to calculate the predicted cooling load based on the mixed air enthalpy that is measured on the site. That is, the outdoor air conditions extracted from eQuest and based on Dorval data, is replaced by the outdoor air conditions measured on site. The results of this change are analyzed in the same manner: graphically, with the aid of statistical indices and with hypothesis testing. The graphs seem to present better agreement between measured and predicted cooling coil load, both for hourly and daily average values. The statistical indices method shows that the hourly coefficient of variation of the root mean squared error is less than the suggested value by the standard ASHRAE Guideline 14, suggesting that the cooling load based on hourly average values is calibrated. On the other hand, the hypothesis testing results in having a t-statistic value higher than the t critical when using hourly

values, implying that the cooling coil load is still not calibrated, while when using daily averaged values, the t statistic value is less than the critical one, meaning that the cooling coil load based on daily averaged values is calibrated.

There are instances when using the statistical indices approach would lead to a different conclusion than when using the hypothesis testing method of evaluating results. It is hard to say whether one method is better than another, since i) there are no standardized limits for the statistical indices when evaluating air flow rate, air temperature or cooling load and ii) the accuracy of the results of the hypothesis testing method depend greatly on the normality of the distribution of the set of data analyzed, in this case, the difference between measured parameters and predictions.

Chapter 7 Sensitivity analysis

Sensitivity analysis is the process of assessing the sensibility of model outputs to a change in the inputs. The sensitivity analysis applies to the final calibrated model (Chapter 5).

In this section, the sensitivity analysis of some selected inputs on selected outputs is presented. The inputs chosen for the analysis are those whose values are uncertain, as they are either estimated or derived from different sources. The outputs that were used in the analysis are those for which the calibration was performed for the air-handling unit: 1) the supply airflow rate leaving the air handling unit, and 2) the cooling coil load.

There are two types of sensitivity analyses: individual sensitivity and total sensitivity analysis. The difference between the two approaches is whether the effect of each input parameter is analyzed independently of changes in other inputs, or the effect of all input parameters is analyzed together. For the purpose of this study, the individual sensitivity analysis is performed.

Two techniques of sensitivity analysis are explored:

- a) Parameter elimination, where the influence of each input is reduced or increased as much as possible, by imposing an extreme value.
- b) Sensitivity coefficients, which relate the changes in outputs due to changes in inputs. They are defined as the ratio of variation of outputs to the variation of inputs (equations 7.1 and 7.2) (Reddy (2011)):

$$SC_1 = \frac{\Delta OP}{\Delta IP} = \frac{OP_1 - OP_{BC}}{IP_1 - IP_{BC}} \quad (7.1)$$

$$SC_2 = \frac{\Delta OP / OP_{BC}}{\Delta IP // IP_{BC}} = \frac{\% \text{ change in output from the base case}}{\% \text{ change in input from the base case}} \quad (7.2)$$

where:

SC_1 = sensitivity coefficient #1 [units of output/units of input];

SC_2 = sensitivity coefficient #2 [dimensionless];

OP_1 , IP_1 = average or maximum values of outputs or inputs, respectively [units of outputs, units of inputs];

OP_{BC} , IP_{BC} = average or maximum base case values of outputs or inputs, respectively [units of outputs, units of inputs];

For comparison purposes, each input was varied one at a time, while keeping all the other inputs constant. The effects of these changes on the selected outputs were recorded and analyzed. Finally the sensitivity coefficients are calculated in order to quantify the sensitivity effects.

Tables 7.1 and 7.2 present the changes introduced to the simulation: cases 1 and 2 correspond to the two extreme cases for parametric elimination; cases 3 and 4 correspond to the decrease/increase of the selected input value, as presented below.

For the U value of the windows, the inputs had to be limited to the available values from the eQuest glass library. Therefore cases 3 and 4 correspond to a single pane and a quadruple pane window type.

The changes in U values for the exterior walls were performed by controlling the insulation thickness. For the walls, the base case scenario corresponds to an insulation

thickness of 0.101 m, while case 1 results from inputting the maximum thickness value allowed by eQuest, which is 1.21 m. The U value from case 2 corresponds to a thickness of 0 m. The last two cases correspond to $\pm 30\%$ change in base case insulation thickness, which corresponds to 0.07 and 0.13 m.

The input that was changed for the blinds model was the multiplier on the solar heat gains through the window. This was varied from 65% to 0 and 100% for the parameter elimination case and $\pm 30\%$ from the base case value for the cases 3 and 4 of the sensitivity analysis part. The same technique was used to vary the infiltration by an increment/decrement of 25%, by varying the multiplier on the infiltration design value.

Table 7.1: Changes to inputs

Input parameter	Base case value	Parameter elimination		Sensitivity analysis	
		Case 1	Case 2	Case 3	Case 4
Windows U value [W/m ² K]	2.72	0	5672	6.30	0.68
Exterior walls U value [W/m ² K]	0.13	0.02	1.12	0.34	0.21
Blinds [%]	65	0	100	85	45
Infiltration [%]	50	0	100	75	25

The changes presented in Table 7.2 come from all the internal loads being increased or decreased by 30% of the base case value. The base case values for the peak loads are the same ones that were used in Chapter 5.

Table 7.2: Changes of internal loads [kW] for all zones

Input parameter: Internal load for zone:	Base case value	Parameter elimination		Sensitivity analysis	
		Case 1	Case 2	Case 3	Case 4
1.3 NW	3	0	99999	3.9	2.1
1.4 SW	1.5	0	99999	1.95	1.05
1.5 SE	8	0	99999	10.4	5.6
1.6 NE	13	0	99999	16.9	9.1
2.1 NE	8	0	99999	10.4	5.6
2.3 NW	2	0	99999	2.6	1.4
2.4 SW	5	0	99999	6.5	3.5
2.5 SE	25	0	99999	32.5	17.5
2.6 NE	6	0	99999	7.8	4.2
3.1 NE	6	0	99999	7.8	4.2
3.2 SW	4.5	0	99999	5.85	3.15
3.3 NW	2.25	0	99999	2.925	1.575
3.4 SW	4	0	99999	5.2	2.8
3.5 SE	20	0	99999	26	14
3.6 NE	5	0	99999	6.5	3.5

Tables 7.3 to 7.7 present the mean values for the supply air flow rate and cooling coil load for the base case and for each of the cases, when changes are performed on the windows U value, walls U value, blinds, infiltration and internal loads.

A sample calculation is presented below for the case 4 of changes done to the internal loads. The sensitivity coefficients are calculated for the output variable “supply air flow rate”:

$$SC_{1(avg)} = \frac{\dot{m}_{base\ case,(avg)} - \dot{m}_{var\ 3,(avg)}}{Q_{base\ case} - Q_{var\ 3}} = \frac{(10.1 - 9.4) \frac{m^3}{s}}{(113.25 - 79.275) kW} = 0.02 \frac{m^3}{kW \times s} \quad (7.3)$$

$$SC_{1(max)} = \frac{\dot{m}_{base\ case,(max)} - \dot{m}_{var\ 3,(max)}}{Q_{base\ case} - Q_{var\ 3}} = \frac{14.5 - 12.9}{113.25 - 79.275} = 0.04 \frac{m^3}{kW \times s} \quad (7.4)$$

$$SC_{2(avg)} = \frac{\frac{\Delta OP_{(avg)}}{OP_{BC\ (avg)}}}{\frac{\Delta IP}{IP_{BC}}} = \frac{\Delta OP_{(avg)}}{\Delta IP} \times \frac{IP_{BC}}{OP_{BC\ (avg)}} = \quad (7.5)$$

$$\begin{aligned}
&= SC_{1(avg)} \times \frac{IP_{BC}}{OP_{BC(avg)}} = 0.02 \frac{m^3}{kW \times s} \times \frac{113.25 kW}{10.1 m^3/s} = 0.24\% \\
SC_{2(max)} &= \frac{\Delta OP_{(max)}/OP_{BC(max)}}{\Delta IP/IP_{BC}} = \frac{\Delta OP_{(max)}}{\Delta IP} \times \frac{IP_{BC}}{OP_{BC(max)}} = \\
&= SC_{1(max)} \times \frac{IP_{BC}}{OP_{BC(max)}} = 0.04 \frac{m^3}{kW \times s} \times \frac{113.25 kW}{14.5 m^3/s} = 0.36\%
\end{aligned} \tag{7.6}$$

Changing the U value of windows and walls does not affect by much the supply air flow rate or the cooling coil load (Tables 7.3 and 7.4):

Table 7.3: Mean output values for each variation in window's U value

	Input value	Supply air flow rate	Cooling coil load
		Mean value [m3/s]	Mean value [kW]
B.C.	2.72	10.1	195.43
Case 1	0	10.54	202.52
Case 2	5672	9.91	186.91
Case 3	6.3	10.24	197.04
Case 4	0.68	9.96	192.77

Table 7.4: Mean output values for each variation in walls' U value

	Input value	Supply air flow rate	Cooling coil load
		Mean value [m3/s]	Mean value [kW]
B.C.	0.13	10.1	195.43
Case 1	0.02	10.08	195.13
Case 2	1.11	10.13	196.19
Case 3	0.34	10.1	195.51
Case 4	0.21	10.16	195.84

Varying the solar heat gain multiplier through the blinds does not have a big impact either on the supply air flow rate or the cooling coil either (Table 7.5).

Table 7.5: Mean output values for each variation in blinds solar heat gain multiplier

	Input value	Supply air flow rate	Cooling coil load
		Mean value [m3/s]	Mean value [kW]
B.C.	0.65	10.1	195.43
Case 1	0	9.18	179.33
Case 2	1	10.71	203.99
Case 3	0.85	10.45	200.41
Case 4	0.45	9.81	190.54

The infiltration rate has a noticeable impact only when it is increased to an extreme value, but when it is varied within reasonable limits, it does not cause a huge impact on the supply air flow rate and cooling coil load (Table 7.6).

Table 7.6: Mean output values for each variation in infiltration rate multiplier

	Input value	Supply air flow rate	Cooling coil load
		Mean value [m ³ /s]	Mean value [kW]
B.C.	0.5	10.1	195.43
Case 1	0	10.1	194.57
Case 2	99	10.36	262.31
Case 3	0.75	10.86	195.84
Case 4	0.25	10.1	195.01

One input that has a big impact on the supply air flow rate and cooling coil load is the internal load of the building (Table 7.7). When increasing the values of the internal loads to extreme values, the supply air flow rate increases from 10.1 m³/s to 15.24 m³/s and the cooling coil load increases from 195.43 kW to 644.89 kW.

Table 7.7: Mean output values for each variation in internal loads

	Input value	Supply air flow rate	Cooling coil load
		Mean value [m ³ /s]	Mean value [kW]
B.C.	113.25	10.1	195.43
Case 1	0	8.71	160.3
Case 2	999999	15.24	644.89
Case 3	147.23	11.14	214.426
Case 4	79.28	9.36	182.4

Tables 7.8 and 7.9 present the sensitivity coefficients based on mean values for the parameter elimination and the sensitivity analysis, for all the selected input parameters. From table 7.8 it can be observed that none of the variations lead to a big variation in outputs. The only variable that causes a big impact is the internal load, because for example for variation 3, a 30 % change in internal loads causes a 32 % change in cooling coil load.

Because the variations with time are sometimes not captured when using average values, maximum values of outputs have been analyzed as well, for consistency purposes. Once again, changing the U value of walls and windows does not have a big impact on the supply air flow rate and cooling coil load (Tables 7.10 and 7.11).

Table 7.8: Sensitivity coefficient SC1 based on average values over the summer

Input	Output	Parameter elimination		Sensitivity analysis		Units
		Case 1	Case 2	Case 3	Case 4	
Windows U value	Supply air flow rate	-0.16	0	0.04	0.07	(m3/s)/(W/m2K)
	Cooling coil load	-2.6	0	0.45	1.29	(kW)/(W/m2K)
Walls U value	Supply air flow rate	0.13	0.03	0.01	0.81	(m3/s)/(W/m2K)
	Cooling coil load	2.88	0.78	0.38	5.29	(kW)/(W/m2K)
Blinds	Supply air flow rate	1.41	1.76	1.77	1.43	(m3/s)/(%)
	Cooling coil load	24.77	24.48	24.92	24.42	(kW)/(%)
Infiltration	Supply air flow rate	0	0	0	0	(m3/s)/(%)
	Cooling coil load	1.71	0.68	1.65	1.69	(kW)/(%)
Interior Loads	Supply air flow rate	0.01	0	0.03	0.02	(m3/s)/(kW)
	Cooling coil load	0.31	0	0.56	0.38	(kW)/(kW)

Table 7.9: Sensitivity coefficient SC2 based on average values over the summer

Input	Output	Parameter elimination		Sensitivity analysis	
		Case 1	Case 2	Case 3	Case 4
Windows U value	Supply air flow rate	-0.0434	0	0.0108	0.0182
	Cooling coil load	-0.0363	0	0.0063	0.0181
Walls U value	Supply air flow rate	0.0016	0.0004	0.0002	0.0106
	Cooling coil load	0.0019	0.0005	0.0003	0.0036
Blinds	Supply air flow rate	0.0909	0.1131	0.1139	0.0918
	Cooling coil load	0.0824	0.0814	0.0829	0.0812
Infiltration	Supply air flow rate	-0.0003	0.0001	-0.0003	-0.0003
	Cooling coil load	0.0044	0.0017	0.0042	0.0043
Interior Loads	Supply air flow rate	0.1373	0.0006	0.3445	0.2431
	Cooling coil load	0.1798	0.0026	0.3239	0.2222

Table 7.10: Maximum values of outputs for each variation in windows' U value

	Input value	Supply air flow rate	Cooling coil load
		Max. value [m ³ /s]	Max. value [kW]
B.C.	2.72	14.56	421.96
Case 1	0	14.96	421.45
Case 2	5672	15.25	432.81
Case 3	6.3	15.04	434.44
Case 4	0.68	13.99	407.84

Table 7.11: Maximum values of outputs for each variation in walls' U value

	Input value	Supply air flow rate	Cooling coil load
		Max. value [m ³ /s]	Max. value [kW]
B.C.	0.13	14.56	421.96
Case 1	0.02	14.5	420.33
Case 2	1.11	14.71	426.49
Case 3	0.34	14.58	422.39
Case 4	0.21	14.89	420.99

The variation of the solar heat gain multiplier on blinds has a minimum impact as well on the outputs (Table 7.12). The only noticeable difference is when the blinds' multiplier is equal to 0, the air flow rate decreases from 14.56 m³/s to 12.17 m³/s and the cooling coil load decreases from 421.96 kW to 368.75 kW.

Table 7.12: Maximum values of outputs for each variation in blinds solar heat gain multiplier

	Input value	Supply air flow rate	Cooling coil load
		Max. value [m ³ /s]	Max. value [kW]
B.C.	0.65	14.56	421.96
Case 1	0	12.17	368.75
Case 2	1	15.24	424.85
Case 3	0.85	15.24	419.34
Case 4	0.45	14.33	416.04

The variations in the infiltration rate do not cause high variations in supply air flow rate and cooling load. Only when an extreme value is imposed as input, then a much higher output is observed (Table 7.13).

The most significant impact on the outputs was caused by the changes in internal loads, when the maximum supply air flow rate decreases from 14.56 m³/s to 10.08 m³/s, corresponding to a decrease of the summation of internal loads maximum power from 113.25 to 0 kW. Similarly, the cooling load decreases from 421.96 to 301.88. When the summation of maximum powers of internal loads is increased to a maximum value, the cooling load increased to 1861.69 kW, while the air flow rate increased to 15.24 m³/s, which is the maximum capacity of the fans.

Table 7.13: Maximum values of outputs for each variation in infiltration rate multiplier

	Input value	Supply air flow rate	Cooling coil load
		Max. value [m ³ /s]	Max. value [kW]
B.C.	0.5	14.56	421.96
Case 1	0	14.49	413.7
Case 2	99	15.24	945.14
Case 3	0.75	15.1	425.98
Case 4	0.25	14.53	417.85

Table 7.14: Maximum values of outputs for each variation in interior loads

	Input value	Supply air flow rate	Cooling coil load
		Max. value [m ³ /s]	Max. value [kW]
B.C.	113.25	14.56	421.96
Case 1	0	10.08	301.88
Case 2	999999	15.24	1861.69
Case 3	147.23	15.24	443.93
Case 4	79.28	12.97	384.01

Tables 7.15 and 7.16 present the sensitivity coefficients of the supply air flow rate and cooling coil load, based on maximum values for the parameter elimination and the

sensitivity analysis, for all the selected input parameters; SC1 is presented in table 7.15 and SC2 is presented in table 7.16. As was the case with the mean values, analyzing maximum values of outputs leads to the same conclusion: no extreme variations in outputs are caused by changes in inputs. The change in internal loads seems to have an impact, since for example for a 30% in inputs, a 36% change is observed in supply air flow rate and a 29% change in cooling coil load (Case 4).

Table 7.15: Sensitivity coefficient SC1 based on maximum values over the summer

Input	Output	Parameter elimination		Sensitivity analysis		Units
		Case1	Case 2	Case 3	Case 4	
Windows U value	Supply air flow rate	-0.15	0	0.13	0.28	(m ³ /s)/(W/m ² K)
	Cooling coil load	0.18	0	3.48	6.91	(kW)/(W/m ² K)
Walls U value	Supply air flow rate	0.6	0.15	0.07	4.29	(m ³ /s)/(W/m ² K)
	Cooling coil load	15.71	4.59	2.11	-12.29	(kW)/(W/m ² K)
Blinds	Supply air flow rate	4.01	1.34	2.34	2.23	(m ³ /s)/(%)
	Cooling coil load	90.41	-7.6	-40.88	57.38	(kW)/(%)
Infiltration	Supply air flow rate	0.13	0	0.12	0.13	(m ³ /s)/(%)
	Cooling coil load	16.49	5.31	16.11	16.41	(kW)/(%)
Interior Loads	Supply air flow rate	0.04	0	0.02	0.04	(m ³ /s)/(kW)
	Cooling coil load	1.06	0.01	0.65	1.11	(kW)/(kW)

Table 7.16: Sensitivity coefficient SC2 based on maximum values over the entire summer

Input	Output	Parameter elimination		Sensitivity analysis	
		Case 1	Case 2	Case 3	Case 4
Windows U value	Supply air flow rate	-0.0276	0	0.0248	0.0525
	Cooling coil load	0.0012	0	0.0225	0.044
Walls U value	Supply air flow rate	0.0055	0.0013	0.0007	0.0389
	Cooling coil load	0.0049	0.0014	0.0007	-0.0038
Blinds	Supply air flow rate	0.1761	0.0589	0.1032	0.0979
	Cooling coil load	0.1374	-0.0115	-0.0622	0.0872
Infiltration	Supply air flow rate	0.0045	0.0002	0.0042	0.0045
	Cooling coil load	0.0195	0.0063	0.0191	0.1945
Interior Loads	Supply air flow rate	0.3077	0	0.1565	0.3635
	Cooling coil load	0.2845	0.0039	0.1736	0.2998

The CV-RMSE was calculated for the difference between measurements and predictions resulting from each variation (Table 7.17). The results of Cases 1 and 2 present some very high values, which was expected, since they are extreme changes that normally do not occur in buildings. Except the internal loads case, all the CV-RMSE from cases 3 and 4 are less than the CV-RMSE of the base case. This indicates that the changes in the envelope of the building do not have a big impact on the selected outputs of the simulation. The only input that significantly affected the supply air flow rate and the cooling coil load, is the internal load of the building. Indeed, the CV of the supply air flow rate in the cases 3 and 4 is slightly higher than the base case coefficient of variation. On the other hand, the CV-RMSE of the cooling coil load is less than the base case coefficient of variation.

Table 7.17: Statistical indices for the supply air flow rate and cooling load sensitivities when various inputs are changed

Input changed	Run	CV-RMSE [%]	
		Supply air flow rate	Cooling coil load
	Base Case	9.00	40.00
Windows U value	Case 1	6.22	5.45
	Case 2	6.91	7.50
	Case 3	2.75	2.87
	Case 4	2.53	3.37
Walls U value	Case 1	0.28	0.32
	Case 2	0.75	0.89
	Case 3	0.07	0.08
	Case 4	1.82	1.78
Blinds	Case 1	14.94	16.11
	Case 2	8.06	7.18
	Case 3	4.52	4.12
	Case 4	4.65	4.61
Infiltration	Case 1	0.26	1.11
	Case 2	14.44	70.49
	Case 3	0.12	0.54
	Case 4	0.13	0.55
Internal loads	Case 1	21.58	30.17
	Case 2	54.14	357.29
	Case 3	12.90	13.16
	Case 4	11.02	11.67

In conclusion, the sensitivity analysis proved that the selection of inputs for the building envelope based on technical specifications, instead of detailed measurements which are not available to the user, do not affect the predictions of supply air flow rate and cooling load.

Chapter 8 Impact of the representation of interior loads on the calibration at the zone level

In the calibration of an energy analysis program for an existing building, it is considered that the representation of internal loads plays an important role but challenging because of limited information available to the modeler about the occupants' energy related loads (e.g., peak loads and schedules of operation for lights and office equipment).

There is a discrepancy between the assumed internal loads used for calibrated models and the real, random interior loads in buildings, which might cause discrepancies between the measured and predicted energy use. Presently, there is not a common accepted method for defining the internal loads' schedules in the calibration studies of building energy models.

There have been many studies conducted on building energy simulations and calibration of building energy models, but only few of them explored how the internal loads have been estimated and even fewer present the methodology used for deriving these internal gains.

Heidell et al. (1985) calibrated a building model by comparison with measured data. They recognized the importance of having a good estimate for the internal loads in large buildings, therefore they compared the measured annual energy consumption with the results of three simulations, using three estimates of internal loads: i) based on power densities calculated from counting the fixtures and equipment and schedules based on building's operators' knowledge; ii) based on same power densities, but with default

schedules from the DOE 2.1 B library and iii) based upon empirical data. The best results were obtained when using internal loads based on measured data (case iii); the difference between the simulated heating energy use and measured data was reduced from 78% to 42%, but the difference between predicted and measured cooling energy increased from 2% to 15%.

Bronson et al. (1992) have developed four different day types as schedules that were input in the simulation software, in order to calibrate the DOE-2 program to non-weather dependent measured loads. The four day types are as follows: i) the default profiles from the DOE-2 library; ii) based on occupancy and electric load factor measurements; iii) based on two-week auditor's data and iv) based on a statistical day-typing routine developed by Katipamula et al. (1991). The use of the default profiles from the DOE-2 library underestimated the energy use during the unoccupied hours, resulting in an annual difference of 25.6%. The second day typing improved the monthly estimates, leading to a total difference of 0.1% between measured and predicted energy use. The third day typing resulted in an increase in the annual difference between measured and predicted total energy use from 0.1% to 3.4%. The fourth day typing provides the best results in the sense that the shape of the hourly estimates fit the measured data better, while the difference in annual energy use is only 0.7%.

Haberl et al. (1998) have analysed different techniques for calibrating hourly simulation models to measured building energy data, however they do not provide an explanation of how the internal loads have been estimated. They do specify that site visits are crucial for developing an energy model, in order to count the lighting fixtures and obtain occupancy information from the building operators.

Pan et al. (2007) calibrated a model of a hotel by adjusting the lighting, plug loads and occupancy loads densities based on hourly measurements; there is no information about the schedules of internal loads. They do acknowledge that the randomness of the operating schedule of the internal loads cannot be reproduced fully and could cause big discrepancies between measurements and simulation results.

Raftery et al. (2009) have developed a methodology to calibrate a building energy model to monitored energy use, in which the adjustment of internal loads was based on measured data from the Energy Management System. A day-typing technique was tried, but due to positioning issues of the measuring devices, the data did not present a daily pattern. Instead, the actual measured values were input on an hourly basis. The occupancy schedules were derived from occupant surveys and interviews with building operators. The same technique is presented in a later study by Raftery et al. (2011).

Love et al. (2013) calibrated a school energy model using hourly monitored data. They have used short-term continuous measurements from micro-loggers to verify the building operator's estimates of lighting use schedules, and spot observations and measurements for luminaires type, office equipment and occupants.

This section compares the simulation results of two different approaches for the representation of hourly internal loads for the calibration of an eQuest energy analysis model of a case study building. The approach A uses the profiles of internal gains from the ASHRAE Research Project 1093-RP "Compilation of diversity factors and schedules for energy and cooling load calculations" (Abushakra et al. (2001)). The approach B uses the simplified step-change profile calculated from the cooling load profile of each thermal

zone. The cooling load profile is derived from measurements of supply air flow rate, room temperature and supply air temperature (Section 4.3).

The estimates of the hourly indoor air temperature and supply air flow rates to zones, obtained from eQuest program under the approaches A and B, are compared with measured data available from the Building Automation System (BAS). Three different methods are used to compare the hourly estimates with measurements: i) graphical representation; ii) statistical indices: root mean squared error (RMSE), the coefficient of variation of the root mean squared error (CV-RMSE) and normalized mean biased error (NMBE); and iii) paired difference statistical hypothesis testing.

Approach A uses the profiles of internal loads from the ASHRAE 1093-RP. This project was intended to compile a library of schedules and diversity factors based on monitored electricity consumption data from 23 office buildings monitored by the Texas A&M Energy Systems Laboratory and information from nine office buildings monitored by the Lawrence Berkeley National Laboratory, with the purpose of being used in energy simulations and to determine peak cooling loads in office buildings. The diversity factors and typical hourly load shapes were developed for weekdays and weekend days.

The buildings analysed were divided into three categories: i) small buildings with a surface area between 93 and 929 m²; ii) medium with an area between 929 and 9290 m²; and iii) large buildings with an area greater than 9290 m².

The Genomic Research Centre of Concordia University, with an area of 3100 m², falls into the medium size buildings category of the project. For this category of buildings,

the diversity factors are presented in Table 8.1. These are the factors used in eQuest for defining the interior loads profiles.

Table 8.1: Combined lights and receptacles profiles for medium buildings for weekdays and weekend days from ASHRAE RP-1093

Combined lights and receptacles profile for medium buildings (from RP-1093)		
Hour	Weekdays	Weekend
	Diversity factor	Diversity factor
1	0.46	0.4
2	0.44	0.39
3	0.44	0.39
4	0.44	0.39
5	0.44	0.39
6	0.46	0.39
7	0.57	0.4
8	0.76	0.46
9	0.87	0.51
10	0.92	0.54
11	0.94	0.55
12	0.93	0.56
13	0.92	0.56
14	0.92	0.55
15	0.92	0.56
16	0.92	0.55
17	0.88	0.53
18	0.73	0.5
19	0.63	0.47
20	0.6	0.46
21	0.59	0.43
22	0.53	0.4
23	0.48	0.39
24	0.46	0.39

The second approach is based on analysis of cooling loads profiles in each zone, therefore resulting in a separate internal loads profile for each zone. The cooling loads were calculated based on measurements of air temperature in each zone, supply air temperature and supply air flow rate to each individual room. A step-change profile was defined for each zone, based on the cooling load profile. The diversity factors and peak internal loads

are presented in Table 5.1. For comparison purposes, the same peak internal load values have been used for both approaches A and B.

For comparison purposes, the diversity factors of approaches A and B have been plotted for zones 1.6 NE (Figure 8.1) and 3.4 SW (Figure 8.2). For instance, in the case of zone 1.6 NE, the diversity factors during unoccupied hours of weekdays of the approach A are 30 to 40% higher than those of the approach B. For the occupied hours (between 10:00 and 18:00) the diversity factors during weekdays of the approach A are close with those of the approach B. It should be noted that for example, the diversity factor at time 7:00, for instance, indicate the value between 7:00 and 8:00.

In the case of the approach A, the same diversity factors are applied to all zones; while those of the approach B have been derived from the measured cooling load profiles in each zone; for example, for zone 3.4 SW, the measured cooling load indicated that a constant profile of 100% during week days and 75% during weekend periods is suitable for this particular zone. Therefore having a different profile for each zone reflects better the internal loads in the existing building.

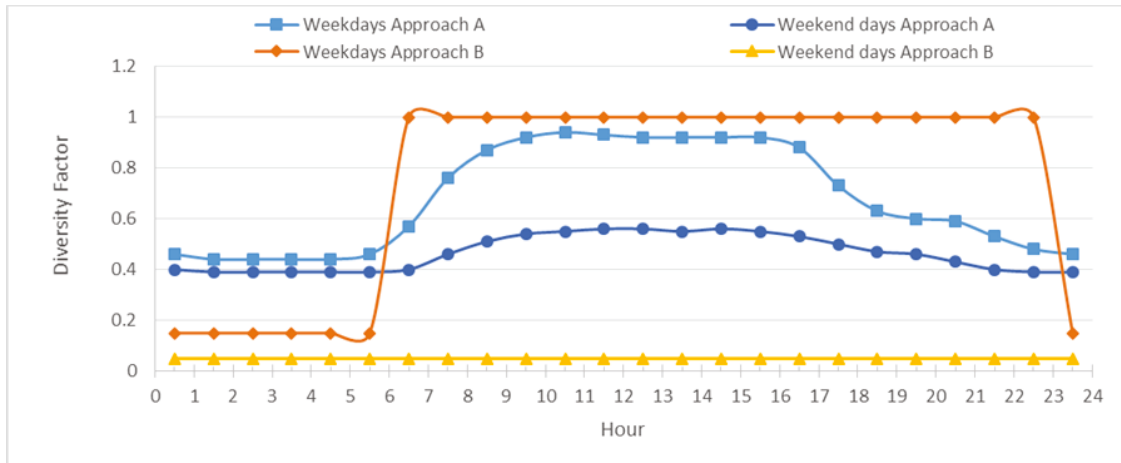


Figure 8.1: Diversity factors for weekdays and weekend days used for simulation of the zone 1.6 NE with approaches A and B

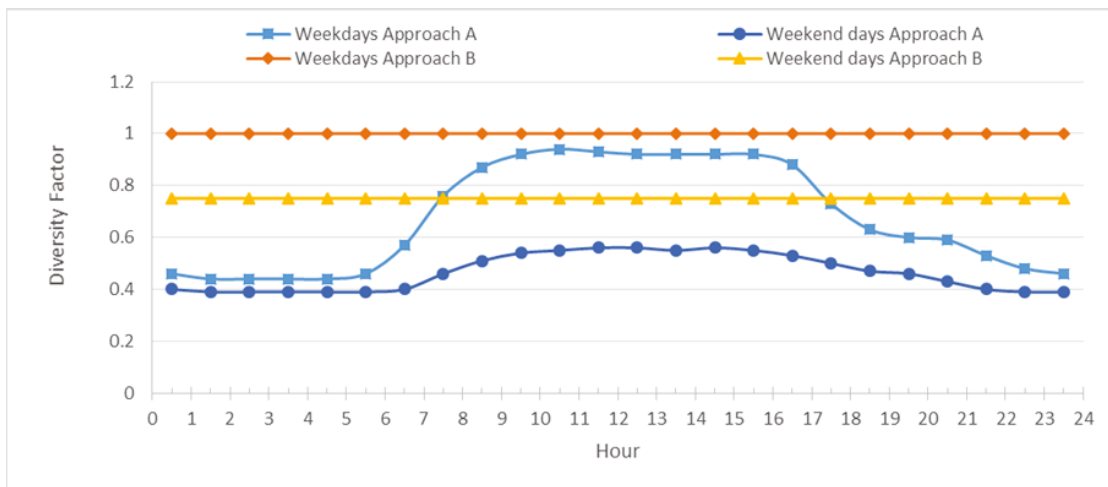


Figure 8.2: Diversity factors for weekdays and weekend days used for simulation of zone 3.4 SW with approaches A and B

8.1 Zone air temperature analysis

The hourly measured indoor air temperature, supply air flow rate and cooling coil loads are compared for each zone with the corresponding values predicted with the equivalent step-change schedule and with the RP-1093 schedule.

8.1.1 Graphical representation

As examples, Figures 8.3 and 8.4 present for the summer period, the measured vs. predicted indoor air temperature in zones 1.6 NE and 3.4 SW when using the equivalent step-change schedule and when using the RP-1093 schedule. The measurements of indoor air temperature seem to agree well with both predictions and this is the case for all zones. The plots for the rest of the zones are presented in the APENDIX D (Figures D.1 to D.45). Nevertheless, the results will be analyzed with the help of some statistical indices.

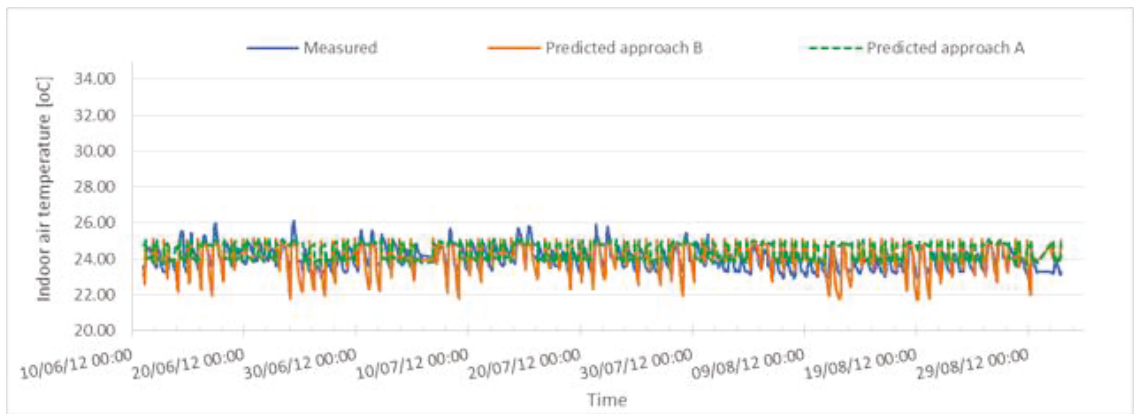


Figure 8.3: Measured vs. predicted indoor air temperature in zone 1.6 NE when using equivalent step-change schedules and when using the RP-1093 schedule, for the entire summer period

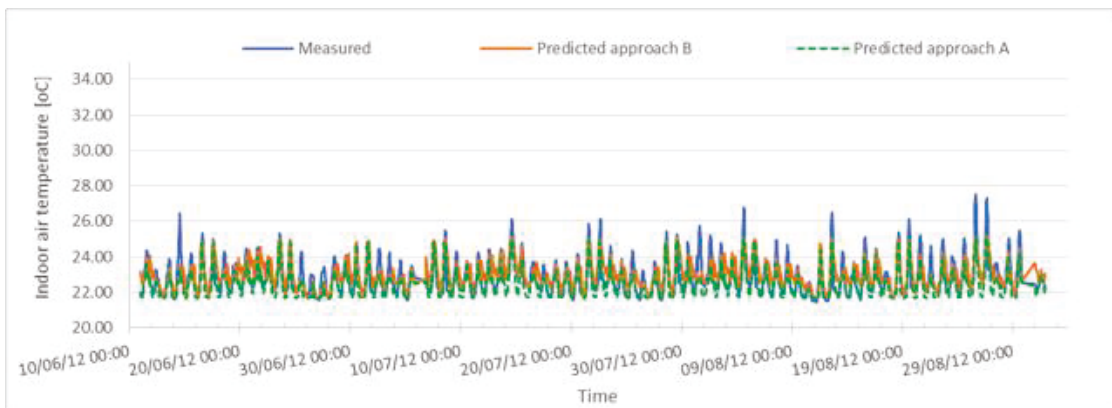


Figure 8.4: Measured vs. predicted indoor air temperature in zone 3.4 SW when using equivalent step-change schedules and when using the RP-1093 schedule, for the entire summer period

8.1.2 Statistical indices

As previously discussed, some statistical indices such as RMSE, CV-RMSE and NMBE are calculated and analyzed for the difference between measured and predicted indoor air temperature in each zone using load shapes from approach A and B.

ASHRAE Guideline 14 suggests having a CV-RMSE less than 30% when using hourly averaged values; it can be seen from Table 8.2 that for all zones, the CV-RMSE is less than this limit. Also, the NMBE should be less than 10% for hourly averaged values; for all the zones this condition is respected when comparing the measured and predicted indoor air temperature. Therefore until now, it seems that both approaches A and B give similar results in terms of simulated versus measured indoor air temperature.

Table 8.2: Hourly RMSE, CV-RMSE and NMBE for temperature differences between measurements and predictions with approaches A and B for the summer period

Zone	RMSE [C]		CV-RMSE [%]		NMBE [C]		Calibrated
	A	B	A	B	A	B	
1.3 NW	0.21	0.21	0.98	0.99	0.28	-0.27	A,B
1.4 SW	1.32	1.26	5.31	5.06	1.69	1.19	A,B
1.5 SE	0.85	0.57	3.64	2.42	-2.87	-1.05	A,B
1.6 NE	0.92	0.69	3.85	2.89	2.06	0.23	A,B
2.1 NE	0.57	0.48	2.54	2.16	1.43	1.01	A,B
2.3 NW	0.61	0.68	2.54	2.82	0.39	0.53	A,B
2.4 SW	0.62	0.64	2.72	2.81	-1.56	-0.23	A,B
2.5 SE	1.02	0.77	4.47	3.37	-4.39	-3.05	A,B
2.6 NE	0.69	0.84	3.04	3.70	-1.10	0.98	A,B
3.1 NE	0.63	0.71	2.66	3.02	-1.85	-1.95	A,B
3.2 SW	0.59	0.54	2.54	2.32	-1.43	-0.72	A,B
3.3 NW	0.66	0.72	2.78	3.06	-0.60	-0.86	A,B
3.4 SW	0.63	0.70	2.74	3.08	-1.69	0.42	A,B
3.5 SE	0.73	0.33	3.21	1.45	-2.66	-0.46	A,B
3.6 NE	0.71	0.83	3.13	3.65	-1.09	0.48	A,B

8.1.3 Hypothesis testing

The hypothesis testing is employed to verify if the difference between measurements and predictions is statistically significant or not. For all zones and both approaches the t-statistic is less than the critical t value, therefore the supply air temperature is considered calibrated (Table 8.3). Moreover, most of the values are negative, which signify that the average difference between measured and predicted indoor air temperature is smaller than the uncertainty in the measurement.

Table 8.3: The t-statistic values for the difference between measured indoor air temperature and predictions using approach A and B for the summer period using hourly values

Zone	t		Calibrated
	Approach A	Approach B	
1.3 NW	-199.24	-199.70	A,B
1.4 SW	-19.95	-24.79	A,B
1.5 SE	-26.75	-63.20	A,B
1.6 NE	-27.91	-58.95	A,B
2.1 NE	-62.09	-77.72	A,B
2.3 NW	-64.52	-56.33	A,B
2.4 SW	-54.98	-64.14	A,B
2.5 SE	0.24	-40.20	A,B
2.6 NE	-50.10	-41.12	A,B
3.1 NE	-54.04	-42.85	A,B
3.2 SW	-58.53	-69.58	A,B
3.3 NW	-57.75	-49.56	A,B
3.4 SW	-53.66	-55.81	A,B
3.5 SE	-40.94	-122.00	A,B
3.6 NE	-48.58	-46.56	A,B

8.2 Analysis of supply air flow rate to each zone

The same three methods are used to compare the measured supply air flow rate with predictions with approach A and approach B: graphical representation, statistical indices and hypothesis testing.

8.2.1 Graphical representation

Because there are fifteen zones in the building, only two zones, 1.6 NE and 3.4 SW, are presented as examples; the results for the other zones are included in APPENDIX D (Figures D.1 to D.45). The plots show that for some zones, the measurements agree more when using approach A while others show that using approach B is better. For zone 1.6 NE, approach B (orange line) seems to fit better with the measurements, while the predictions with approach A (green line) seem to be over predicted during the unoccupied hours (Figure 8.5).

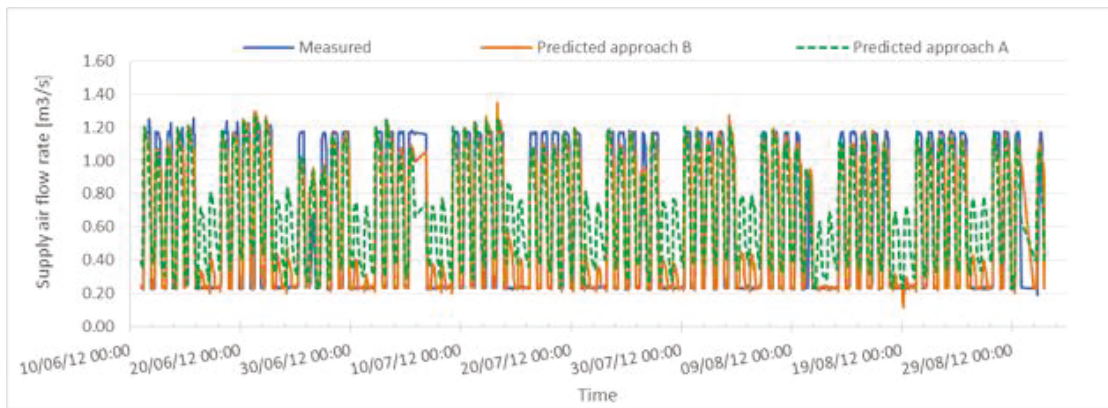


Figure 8.5: Measured hourly supply air flow rate vs. predictions using approach A and B for zone 1.6 NE for the summer period

On the other hand, Figure 8.6 shows that predictions with approach A for zone 3.4 SW are under predicted for the unoccupied hours. Predictions with approach B seem to agree better with the measurements. Similarly, for this particular zone the diversity profiles were under predicted when using approach A against approach B

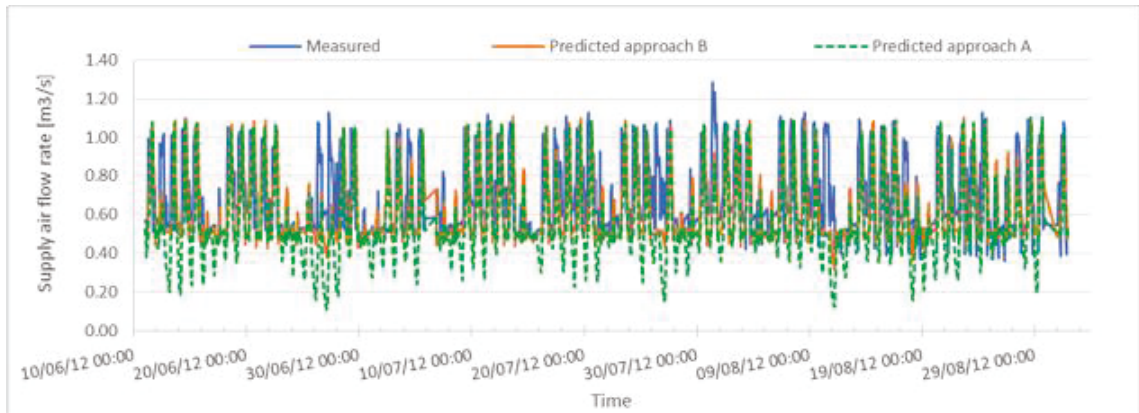


Figure 8.6: Measured hourly supply air flow rate vs. predictions using approach A and B for zone 3.4 SW for the summer period

In order to better visualize the differences between measured supply air flow rate and predictions with approaches A and B, three day plots have been developed for each month. Figures 8.7 and 8.8 show the difference between measured supply air flow rate and predicted ones for the same two zones previously discussed, zone 1.6 NE and 3.4 SW. The same conclusions can be drawn here: for zone 1.6 NE, approach A over predicts the air flow rate during unoccupied periods, while approach B seems to be closer to the measurements (Figure 8.7). For zone 3.4 SW, both approaches predict in the same way the supply air flow rate during the occupied hours, while approach A under predicts the supply air flow rate during the unoccupied hours. In conclusion, the approach B, using a step-change shape of internal loads, which was developed from measurements, give better results than the use of a set of default diversity factors.



Figure 8.7: Measured hourly supply air flow rate vs. prediction using approach A and B for zone 1.6 NE from 18-20 July

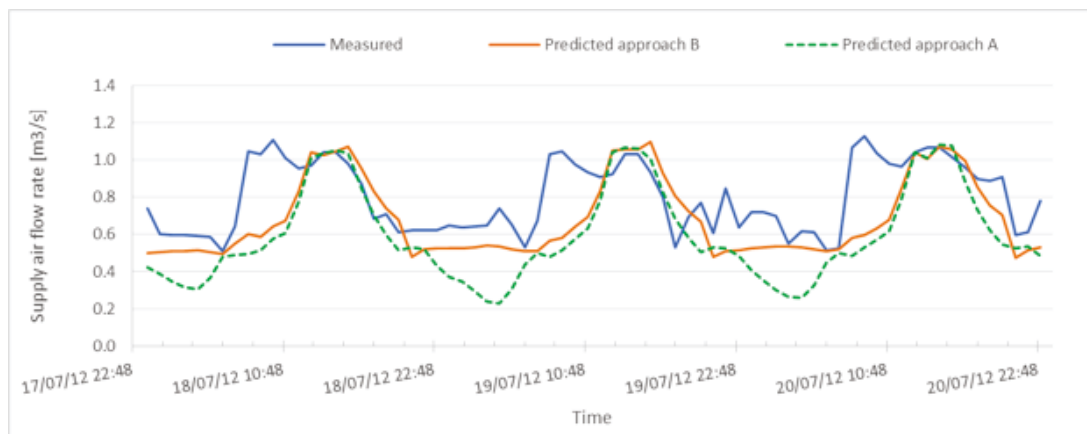


Figure 8.8: Measured hourly supply air flow rate vs. predictions using approach A and B for zone 3.4 SW from 18-20 July

8.2.1 Statistical indices

Table 8.4 presents the three statistical indices: RMSE, CV-RMSE and NMBE for all zones for the summer period, when using hourly values for the difference between measured supply air flow rate and predictions with approach A and B. With approach A, nine out of fifteen zones should be considered calibrated, since the CV-RMSE is less than 30% and the NMBE is less than 10% ASHRAE (2002). With approach B, which is the one used throughout this study, a total of eleven zones should be calibrated according to the

specifications of ASHRAE Guideline 14. Hence, approach B is preferred for estimating the internal loads of the building.

Table 8.4: Hourly statistical indices for the difference between measured and predicted supply air flow rate using approaches A and B for all zones and for the entire summer period

Zone	RMSE [m ³ /s]		CV- RMSE [%]		NMBE [m ³ /s]		Calibrated
	A	B	A	B	A	B	
1.3 NW	0.07	0.18	15.99	38.45	-0.25	-34.46	B
1.4 SW	0.21	0.20	107.73	103.42	-17.19	-20.52	-
1.5 SE	0.10	0.10	11.98	11.77	0.28	2.42	A,B
1.6 NE	0.29	0.13	46.04	20.78	12.16	2.91	B
2.1 NE	0.10	0.11	17.17	18.96	-2.29	-3.37	A,B
2.3 NW	0.07	0.07	95.19	92.97	-25.73	-8.03	-
2.4 SW	0.23	0.21	31.64	28.25	-13.54	-3.82	B
2.5 SE	0.55	0.31	19.71	11.27	-14.02	7.78	A,B
2.6 NE	0.12	0.10	20.34	17.25	-2.79	8.71	A,B
3.1 NE	0.08	0.08	19.25	19.75	0.93	3.19	A,B
3.2 SW	0.09	0.09	21.20	20.96	-8.44	-10.25	A,B
3.3 NW	0.06	0.07	51.26	55.13	10.22	15.56	-
3.4 SW	0.23	0.18	32.97	27.00	-18.57	-8.36	B
3.5 SE	0.28	0.18	13.74	8.97	-7.97	0.23	A,B
3.6 NE	0.13	0.10	23.81	18.89	-4.19	7.27	A,B

The statistical indices have been developed for the shorter periods of three days for each month as well, in order to see if one can reach the same conclusions as when using the hourly values over the entire summer. Table 8.5 presents the statistical indices for the three days with highest outdoor air temperature recorder for the month of July, while Table 8.6 presents the statistical indices for the three days during the month of August. It should be noted that the three days with the highest outdoor air temperature registered for the month of June have been removed since they presented points with abnormal operation, the airflow rate being mostly 0 m³/s. For the three days during the month of July, approach A leads to nine zones being considered calibrated, while approach B suggests that ten zones

are calibrated, which is one zone less than when using hourly values for the entire summer period (Table 8.5). During the month of August, for the three selected zones, using approach A and B, the modeler would conclude that eleven zones are calibrated. Therefore from the 14th to the 16th of August either approaches lead to the same results.

In conclusion, using the periods of three days leads to similar results than when doing the comparison over the entire summer period, when using hourly values, with slight differences. For all cases, approach B seems to be preferred as the difference is diminished between measured supply air flow rate and the predictions using the equivalent time step internal load schedules.

Table 8.5: Hourly statistical indices for the difference between measured supply air flow rate and predictions using approaches A and B for all zones from 18-20 July

Zone	RMSE [m3/s]		CV [%]		NMBE [m3/s]		Calibrated
	A	B	A	B	A	B	
1.3 NW	0.08	0.19	16.49	41.50	1.15	-38.49	A
1.4 SW	0.26	0.25	108.43	104.43	-14.99	-18.02	-
1.5 SE	0.10	0.10	12.51	11.56	-1.19	1.55	A,B
1.6 NE	0.26	0.09	32.38	11.42	-6.96	-3.88	B
2.1 NE	0.12	0.12	17.82	18.15	-9.59	-9.89	A,B
2.3 NW	0.05	0.04	66.18	63.39	-7.98	-0.50	-
2.4 SW	0.29	0.26	35.19	31.61	-18.92	-7.80	-
2.5 SE	0.52	0.27	18.48	9.41	-12.67	6.28	A,B
2.6 NE	0.14	0.10	21.65	15.26	-9.55	6.05	A,B
3.1 NE	0.08	0.08	17.47	16.59	-5.30	-2.67	A,B
3.2 SW	0.11	0.10	25.98	23.55	-5.60	-8.21	A,B
3.3 NW	0.05	0.05	39.04	39.04	15.40	16.89	-
3.4 SW	0.28	0.21	35.29	25.78	-26.17	-14.64	B
3.5 SE	0.29	0.15	13.81	6.95	-10.66	-1.47	A,B
3.6 NE	0.16	0.11	28.06	19.74	-7.13	6.75	A,B

Table 8.6: Hourly statistical indices for the difference between measured supply air flow rate and predictions using approaches A and B for all zones from 14-16 August

Zone	RMSE [m3/s]		CV [%]		NMBE [m3/s]		Calibrated
	A	B	A	B	A	B	
1.3 NW	0.07	0.17	15.69	37.87	2.39	-35.57	A
1.4 SW	0.20	0.19	95.22	89.38	8.81	5.20	-
1.5 SE	0.09	0.09	11.36	11.54	5.52	7.43	A,B
1.6 NE	0.29	0.17	40.34	23.82	0.72	1.99	B
2.1 NE	0.10	0.11	15.03	16.72	-8.38	-8.92	A,B
2.3 NW	0.07	0.06	66.17	55.74	-35.28	-30.52	-
2.4 SW	0.24	0.24	29.79	28.73	-12.22	-3.87	A,B
2.5 SE	0.50	0.28	17.51	9.76	-13.45	5.29	A,B
2.6 NE	0.10	0.08	15.97	12.89	-5.19	6.83	A,B
3.1 NE	0.08	0.08	18.22	17.06	-7.14	-5.07	A,B
3.2 SW	0.07	0.08	16.17	17.61	-12.02	-14.29	A,B
3.3 NW	0.07	0.07	52.58	58.65	22.12	23.96	-
3.4 SW	0.21	0.19	28.54	26.33	-12.77	-4.39	A,B
3.5 SE	0.29	0.20	13.62	9.41	-8.84	-1.43	A,B
3.6 NE	0.11	0.08	18.34	13.65	-7.92	3.16	A,B

8.2.3 Hypothesis testing

The t-statistic values based on hourly values for the summer period are presented in Table 8.7. Using statistical indices to verify if the supply air flow rate is calibrated led to having nine zones calibrated with approach A, and eleven zones with approach B. The statistical hypothesis testing suggests that when using approach A, out of the nine zones, only for five of them the difference between measurements and predictions is not statistically significant (hence five out of nine zones are calibrated). When using approach B, only for six zones the difference is not statistically significant (hence six out of nine zones are calibrated).

The results are quite similar, with a small advantage for the approach B. Hence, the use of the equivalent step-change of interior loads compared favourably with the use of one set of default diversity factors for all zones.

When using hourly values over the set of three days in July, the t-statistic values are less than the critical one ($t_{\text{critical}} = 1.666$) for ten zones, both when using approach A and B (Table 8.8). It should be noted however, that the ten calibrated zones are not the same zones for approaches A and B. Therefore in this case, both methods give the same results.

When using hourly values over three days in August, approach A results in having seven calibrated zones and approach B leads to eight zones to be calibrated, since the t-statistic values are less than the critical value (1.666). It seems that in this case method B is preferred (Table 8.9).

Table 8.7: The hourly t-statistic value for the difference between measured supply air flow rate and predictions using approaches A and B for all zones for the entire summer

Zone	t		Calibrated
	Approach A	Approach B	
1.3 NW	-4.70	81.68	A
1.4 SW	4.97	6.63	-
1.5 SE	-6.37	1.33	A,B
1.6 NE	8.53	-0.91	B
2.1 NE	-0.21	2.31	A
2.3 NW	9.93	1.61	B
2.4 SW	16.73	2.16	-
2.5 SE	37.25	30.43	-
2.6 NE	1.40	18.97	A
3.1 NE	-3.18	1.85	A
3.2 SW	13.99	19.12	-
3.3 NW	6.40	10.43	-
3.4 SW	25.69	10.16	-
3.5 SE	22.63	-8.82	B
3.6 NE	3.82	12.73	-

Table 8.8: The t-statistic values for the difference between measured supply air flow rates and predictions with approach A and B for all zones, using hourly values, from 18-20 July

Zone	t		Calibrated
	Approach A	Approach B	
1.3 NW	-0.45	18.84	A
1.4 SW	-0.40	-0.17	A,B
1.5 SE	-1.47	-1.34	A,B
1.6 NE	-1.12	-5.70	A,B
2.1 NE	1.18	1.33	A,B
2.3 NW	-1.18	-2.21	A,B
2.4 SW	3.60	0.46	B
2.5 SE	6.44	4.76	-
2.6 NE	2.12	0.85	-
3.1 NE	-0.50	-1.85	A,B
3.2 SW	0.60	1.68	A
3.3 NW	1.22	1.60	A,B
3.4 SW	7.36	3.72	-
3.5 SE	7.03	-2.13	B
3.6 NE	1.09	1.42	A,B

In conclusion, using hourly values over a three day period with the highest outdoor air temperature recorded leads to having different results than when using hourly values over the entire summer period.

Since the results of the simulations using approaches A and B lead to almost the same amount of zones being calibrated, but not the same zones are considered calibrated in both cases, then the modeler could replace the schedules of the zones that were found not to be calibrated with approach B with the schedules of the same zones from approach A, if they were found to be calibrated.

Table 8.9: The hourly t-statistic values for the difference between measured supply air flow rates and predictions with approach A and B for all zones, from 14-16 August

Zone	t		Calibrated
	Approach A	Approach B	
1.3 NW	0.11	19.82	A
1.4 SW	-0.99	-1.38	A,B
1.5 SE	2.12	4.13	-
1.6 NE	-2.35	-3.56	A,B
2.1 NE	0.43	0.69	A,B
2.3 NW	2.49	2.16	-
2.4 SW	1.35	-1.09	A,B
2.5 SE	7.94	2.90	-
2.6 NE	0.41	1.78	A
3.1 NE	0.20	-0.83	A,B
3.2 SW	6.50	8.56	-
3.3 NW	2.21	2.24	-
3.4 SW	1.97	-0.68	B
3.5 SE	4.05	-1.94	B
3.6 NE	1.82	-0.63	B

8.3 Analysis of cooling load in each zone

8.3.1 Graphical representation

The measured cooling load is compared against the predicted cooling load when using approach A and B, with the aid of time series plots. The graphs are very similar to the ones presenting the air flow rate therefore the same conclusions can be drawn here: for zone 1.6 NE, the simulation with approach A over-estimates the cooling load at night, while the approach B presents results that agree better with the measurements (Figure 8.9). For zone 3.4 SW, the approach A under-estimates the cooling load for the unoccupied periods, while the results of the simulation using the approach B agrees better with the measurements (Figure 8.10). The plots for the rest of the zones are presented in Appendix D (Figures D.1 to D.45). For some zones, approach A seems to be a better fit, while for others approach B gives better results.

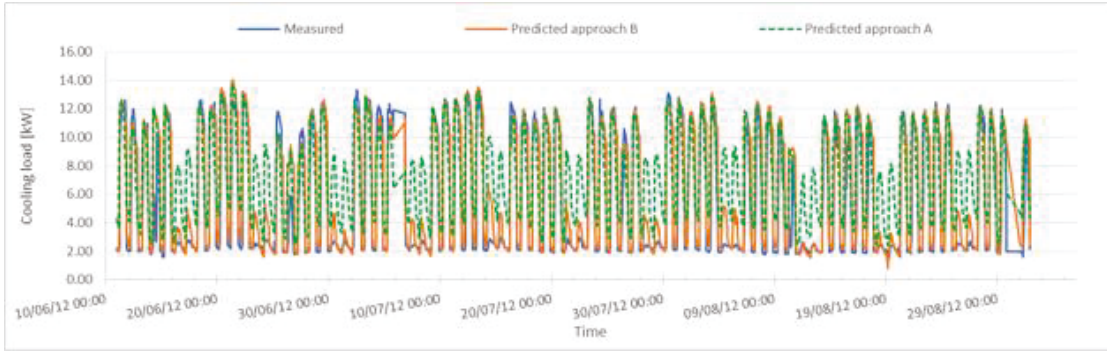


Figure 8.9: Hourly measured cooling load vs. predictions using approach A and B, for zone 1.6 NE, for the entire summer

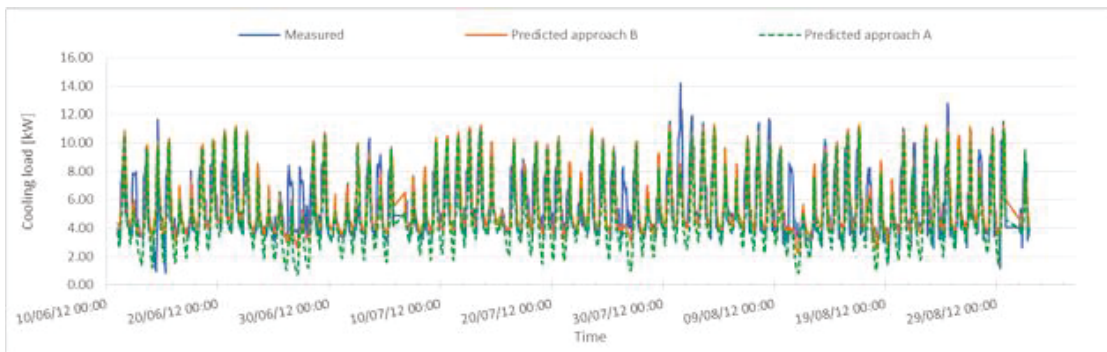


Figure 8.10: Hourly measured cooling load vs. predictions using approach A and B, for zone 3.4 SW, for the entire summer

8.3.2 Statistical indices

Table 8.10 presents the RMSE, CV-RMSE and NMBE based on hourly values, for the entire summer. The CV-RMSE is less than 30% and the NMBE is less than 10% for seven zones when approach A is used and for six zones when approach B is used. In this case the approach A is slightly preferred.

Table 8.10: Statistical indices for the difference between the hourly measured cooling load and predictions using approach A and B for the entire summer

Zone	RMSE [kW]		CV-RMSE [%]		NMBE [kW]		Calibrated
	A	B	A	B	A	B	
1.3 NW	0.72	0.96	25.51	33.98	12.48	-27.68	-
1.4 SW	2.01	1.89	108.80	102.57	-1.38	-5.89	-
1.5 SE	1.01	1.13	14.22	15.86	-1.98	6.38	A,B
1.6 NE	3.20	1.58	54.13	26.70	25.15	11.39	-
2.1 NE	1.04	1.11	23.69	25.35	10.76	8.43	B
2.3 NW	0.64	0.66	92.72	95.52	-15.24	6.80	-
2.4 SW	1.81	1.74	31.24	30.13	-10.58	2.86	-
2.5 SE	5.80	2.48	26.33	11.27	-19.72	4.67	A,B
2.6 NE	1.17	1.39	25.35	30.25	1.96	20.17	A
3.1 NE	0.69	0.78	19.32	21.70	2.97	5.20	A,B
3.2 SW	0.94	0.78	26.47	22.09	-5.09	-5.12	A,B
3.3 NW	0.59	0.65	55.28	60.63	18.00	23.99	-
3.4 SW	1.72	1.50	31.15	27.20	-15.10	0.67	-
3.5 SE	2.61	2.30	16.19	14.31	-8.45	7.29	A,B
3.6 NE	1.19	1.30	27.64	30.22	1.29	17.61	A

8.3.3 Hypothesis testing

Table 8.11 presents the t-statistic values based on hourly average values for the entire summer and for all zones in the building. The results are almost the same as for the statistical indices method, except that different zones that are found to be calibrated. When approaches A or B is used, seven out of the fifteen zones can be considered calibrated.

In conclusion, this chapter explored the impact of using two different methods of defining the internal loads for the calibration of a building energy model of an existing building: i) approach A which uses schedules from the ASHRAE project RP-1093 and ii) approach B which uses an equivalent simplified step-change profile derived from the cooling load which is based on measurements of indoor air temperature in each zone, supply air temperature to each zone and supply air flow rate.

Table 8.11: The hourly t-statistic value for the difference between measured cooling loads and predictions using approaches A and B for the entire summer

Zone	t-statistic		Calibrated
	Approach A	Approach B	
1.3 NW	3.65	37.26	-
1.4 SW	-4.60	-2.99	A,B
1.5 SE	-5.07	8.10	A
1.6 NE	18.77	12.76	-
2.1 NE	8.90	3.68	-
2.3 NW	-9.80	-13.21	A,B
2.4 SW	8.64	-2.60	B
2.5 SE	45.59	14.43	-
2.6 NE	-6.65	27.28	-
3.1 NE	-9.62	-4.16	A,B
3.2 SW	-3.70	-4.41	A,B
3.3 NW	-5.08	-0.15	A,B
3.4 SW	16.09	-6.68	B
3.5 SE	21.06	19.60	-
3.6 NE	-7.75	19.87	A

The findings are not very consistent; for some zones the predictions by using the approach B agree better with the measurements, while for others the approach A gives better agreement with measurements. Overall, approaches B and A lead to about the same number of zones to be calibrated, with a slight advantage for the approach B. The approach B is easier to apply and is based on measurements from BAS, taking into consideration the profiles of different types of zones in the building.

Chapter 9 Conclusions

This study proposed an evidence-based bottom-up approach for calibrating a building energy model by comparing the predictions with measurements. Three techniques are used to compare the predictions and measurements: (i) graphical representation, (ii) comparison of statistical indices such as RMSE, CV-RMSE and NMBE with maximum recommended values, and (iii) the hypothesis testing method, where t statistic is compared with t critical to find if the difference between the predictions and measurements is statistically significant. There are no recommended limits for the statistical indices when calibrating an energy model for other parameters than the energy use (e.g. air temperature, supply air flow rate, cooling load). The results suggest that the graphical representation and the use of statistical indices are not sufficient to determine if a model is calibrated, therefore it should be accompanied by the hypothesis testing as well.

The proposed methodology achieved calibration through an evidence-based technique, meaning that any changes to the input parameters are based on pertinent evidences, such as measured data. This technique is innovative due to its simplicity, since the measured data can be acquired from any BAS system. The bottom-up technique refers to the sequence of the calibration steps; first, the calibration was performed at the zone level, for any available variables, such as indoor air temperature, supply air flow rate to each zone, supply air temperature.; then, the calibration was performed at the air handling unit level, for the supply air flow rate and air temperature.

The hourly results are analyzed for the whole summer period and for periods of three days during each month, with the highest outdoor temperature recorded; daily and monthly results are also analyzed.

Following the suggested statistical indices proposed in the literature, even though those indices do not refer to the calibration of supply air flow rate in rooms, eleven zones out of the fifteen could be considered as being calibrated when hourly values are used since $CV-RMSE < 30\%$; and the same eleven zones are calibrated on a monthly basis since $CV-RMSE < 15\%$. The results of three-day analysis are identical to the hourly data analysis over the whole summer, except zone 1.6 NE, which has a CV-RMSE of 30.3%, which is just above the maximum value. The daily average CV-RMSE is between the hourly and monthly values for each thermal zone. There are no recommendations in the literature for daily calibration.

According to the t-test, the null hypothesis H_0 is true only for five zones (1.5 SE, 1.6 NE, 2.3 NW, 3.1 NE and 3.5 SE), hence there is no significant difference between hourly measurements and predictions for those zones. Therefore the model of these five zones is calibrated. Out of those five calibrated zones, four have CV-RMSE less than 30 %: 11.6 %, 20.1 %, 19.4 % and 8.5 %, while one zone has a CV-RMSE greater than 30 %: 93.6 %, which would be considered as not calibrated if the CV-RMSE criterion is used.

Next, the calibration of the air handling unit model was performed, based on supply air flow rate, supply air temperature and cooling load.

The calibration of the supply air flow rate started with the analysis of measured summation of air flow rates supplied to zones vs. the measured air flow rate supplied by the air handling unit. The calibration results are analyzed graphically, and a difference between measurements and predictions is observed only during the night periods. Second, statistical indices method suggests that the model is calibrated, since the hourly CV-RMSE is less than the 30% limit, which is suggested by ASHRAE Guideline 14. Third, hypothesis

testing was used to verify whether the difference between the measurements and predictions is significant or not, and the result implies that it is indeed statistically significant.

Next the results of the supply air temperature calibration are analyzed with the same three methods. All three methods shows good agreement between the measured and predicted supply air temperatures, suggesting that the supply air temperature model is calibrated.

The cooling load is analyzed in the same fashion: through graphical analysis, statistical indices and hypothesis testing. Graphical analysis showed again discrepancies during the night periods. It was also observed that the variation of the predicted cooling coil load follows very closely the curve of the predicted enthalpy difference across the cooling coil. The statistical indices suggest that the model is not calibrated for the cooling coil load, and the hypothesis testing confirms this conclusion.

In order to investigate why there are discrepancies between the measured and predicted cooling load, the set of data is split depending on the fraction of outdoor air (α) that enters the building. The hourly CV-RMSE is higher than the suggested limit of 30% for all cases while the hypothesis testing suggests that the model is calibrated only for the instance when 100% outdoor air enters the building.

In order to reduce the difference between measured and predicted cooling coil load, the predicted cooling load was re-calculated based on the mixed air enthalpy that is measured on the site. The results of this change are analyzed in the same manner: graphically, with the aid of statistical indices and with hypothesis testing. The graphs seem

to present better agreement between measured and predicted cooling coil load, both for hourly and daily average values. The statistical indices method shows that the hourly CV-RMSE is less than 30% (ASHRAE Guideline 14), suggesting that the cooling load based on hourly average values is calibrated. On the other hand, the t-statistic is greater than the t critical when using hourly values; hence the cooling coil load was still not calibrated. When the analysis was performed using daily averaged values, the t-statistic was less than the critical one; hence the cooling coil load based on daily averaged values is calibrated.

A sensitivity analysis has been performed to determine how sensitive the output parameters are when the input values are changed. Two methods have been used: the parameter elimination technique, where the influence of each parameter is reduced as much as possible, by imposing an extreme value and sensitivity coefficients which relate the input and output parameters' changes to each other. The parameters that have been used for the sensitivity analysis are the U-value of windows, U-values of exterior walls and roof, the blinds percent opening, the infiltration rate, the economizer temperature and the internal load in each zone. The parameter that had the highest impact on the simulation outputs was the change in internal loads, while the changes in the building envelope had a low impact. In conclusion, the simulation model is not sensitive to inputs selected from technical specifications of the exterior envelope. Therefore, for this case study building the user should not spend more resources for detailed measurements of thermal parameters of exterior envelope, for the purpose of calibrating the eQuest model.

Finally, two different approaches for the representation of hourly interior loads were explored. The approach A uses the profiles of internal gains from the ASHRAE Research Project 1093-RP "Compilation of diversity factors and schedules for energy and

cooling load calculations”. The approach B uses a simplified step-change profile calculated from the cooling load profile of each thermal zone, which is derived from measurements of supply air flow rate, room temperature and supply air temperature. The results show that the use of approach B, proposed in this study, gives almost the same predictions as the use of approach A, even better. Approach B has the advantage that it is based on measurements in each thermal zone, and does not use one common schedule for all zones.

There are instances when using the statistical indices approach would lead to a different conclusion than when using the hypothesis testing method of evaluating results. It is hard to say whether one method is better than another, since i) there are no standardized limits for the statistical indices when evaluating air flow rate, air temperature or cooling load and ii) the accuracy of the results of the hypothesis testing method could depend on the normality of the distribution of the set of data analyzed, in this case, the difference between measured parameters and predictions.

Future work would focus on:

- The development of the data mining and automatic export of information to the input file of the software used;
- The calibration of the swing and heating season
- The calibration of water-side loop of HVAC system and energy use
- The whole-building energy use-calibration
- Analysis of a short period of time other than the ones that present the highest outdoor temperature

- Development of standardized limits for the statistical indices for any of the parameters that can be used in calibration, other than the energy use.

References

- Abushakra, B., Sreshthaputra, A., Haberl, J. and Claridge, D. (2001). *Compilation of Diversity Factors and Schedules for Energy and Cooling Load Calculations-Final Report*. submitted to ASHRAE under Research Project 1093-RP. Energy Systems Lab Report No. ESL-TR-01-04.
- ASHRAE (2001). *Fundamentals Handbook*. American Society of Heating, Refrigerating and Air Conditioning Engineers Inc, Atlanta, Georgia.
- ASHRAE (2002). *ASHRAE Guideline 14. Measurement of Energy and Demand Savings*, American Society of Heating, Ventilating, and Air Conditioning Engineers Inc. , Atlanta, Georgia.
- Baumann, O. (2004). *Operation diagnostics-use of operation patterns to verify and optimize building and system operation*. Proceedings of International Conference for Enhanced Building Operations (ICEBO), Paris, France.
- Bazjanac, V. (2005). *Model based cost and energy performance estimation during schematic design*. Proceedings of 22nd Conference on Information Technology in Construction, Dresden, Germany.
- Bertagnolio, S., Masy, G., Andre, P. and Lebrun, J. (2008). *Building and HVAC System simulation with the help of an engineering equation solver*. Proceedings of the 3rd National conference of the International Building Performance Simulation Association (IBPSA), USA, Berkeley, CA.
- Bertagnolio, S., Randaxhe, F. and Lemort, V. (2012). *Evidence-based calibration of a building energy simulation model: Application to an office building in Belgium*. Proceedings of the 12th International Conference for Enhanced Building Operations, Manchester, UK.
- Bordass, B., Leaman, A. and Ruysevelt, P. (2001). *Assessing building performance in use 5: conclusions and implications*. Building Research & Information, vol 29, (2): 144-157.
- Bronson, D. J., Hinchey, S. B., Haberl, J. S. and O'Neal, D. L. (1992). *Procedure for calibrating the DOE-2 simulation program to non-weather-dependent measured loads*. Proceedings of the ASHRAE Winter Meeting, Anaheim, CA, USA, .

- Chou, S. K., Chang, W. L. and Wong, Y. W. (1993). *Effects of multi-parameter changes on energy use of large buildings*. International Journal of Energy Research, vol 17, (9): 885-903.
- Claridge, D. E., Bensouda, N., Lee, S. U., Wei, G., Heinemeier, K. and Liu, M. (2003). *Manual of procedures for calibrating simulations of building systems*, submitted to the California Energy Commission Public Interest Energy Research Program
- Clarke, J. A., Strachan, P. A. and Pernot, C. (1993). *An approach to the calibration of building energy simulation models*. ASHRAE Transactions, vol 99: 917-917.
- Corson, G. (1992). *Input-output sensitivity of building energy simulations*. Proceedings of ASHRAE Winter Meeting, Anaheim, CA, USA
- Department of Energy (DOE) (2006). *eQuest, the QUick Energy Simulation Tool v 3.65*. Retrieved from <http://www.doe2.com/equest/>, February 2014.
- Department of Energy (DOE) (2013). *EnergyPlus v 8.1*, University of Illinois and Ernest Orlando Lawrence Berkley National Laboratory, USA. Retrieved from <http://apps1.eere.energy.gov/buildings/energyplus/>, October 2012.
- Department of Energy (DOE). (2013). *Weather file aquired from* http://doe2.com/index_wth.html. Retrieved 11 November, 2013.
- Diamond, S. C., Cappiello, C. C. and Hunn, B. D. (1986). *DOE-2 Verification project. Phase I. Final report*, Los Alamos National Lab., NM (USA).
- Diamond, S. C., Hunn, B. D. and Cappiello, C. C. (1981). *DOE-2 Verification Project. Phase I. Interim report*, Los Alamos Scientific Lab., NM (USA).
- Diamond, S. C., Hunn, B. D. and Cappiello, C. C. (1985). *Computer modeling: the DOE-2 validation*. ASHRAE journal, vol 27, (11): 25-32.
- DOE (2008). *M&V Guidelines: Measurement and Verification for Federal Energy Projects (FEMP)*. Federal Energy Management Program.
- Eley, C., Goodrich, K., Arent, J., Higa, R. and Rauss, D. (2011). *ML-11-029 Rethinking Percent Savings—The Problem with Percent Savings and zEPI: The New Scale for a Net-Zero Energy Future*. ASHRAE Transactions, vol 117, (2): 787.

- Guiterman, T. and Krarti, M. (2011). *ML-11-C046 Analysis of Measurement and Verification Methods for Energy Retrofits Applied to Residential Buildings*. ASHRAE Transactions, vol 117, (2): 382.
- Haberl, J. S. and Abbas, M. (1998). *Development of graphical indices for viewing building energy data: Part I*. Journal of Solar Energy Engineering - Transactions of The ASME, vol 120, (3): 156-161.
- Haberl, J. S. and Bou-Saada, T. E. (1998). *Procedures for calibrating hourly simulation models to measured building energy and environmental data*. Journal of Solar Energy Engineering, vol 120, (3): 193-204.
- Heidell, J. A. and Taylor, Z. T. (1985). *Comparison of empirically measured end-use metered data with DOE 2. 1 simulation*. Proceedings of the International Building Performance Simulation Association (IBPSA) Conference, Seattle, WA, USA, Pacific Northwest Lab., Richland, WA (USA).
- IPMVP-Committee (2002). *International Performance Measurement & Verification Protocol: Concepts and Options for Determining Energy and Water Savings*.
- Kaplan, M., Caner, P. and Vincent, G. W. (1992). *Guidelines for energy simulation of commercial buildings*. Proceedings from the ACEEE 1992 Summer study on Energy Efficiency in buildings, Pacific Grove, California.
- Kaplan, M. B., McFerran, J., Jansen, J. and Pratt, R. (1990). *Reconciliation of a DOE2.1C model with monitored end-use data for a small office building*. ASHRAE Transactions, vol 96, (1): 981-993.
- Katipamula, S. and Haberl, J. S. (1991). *Methodology to identify diurnal load shapes for non-weather dependent electric end-uses*. Proceedings of the second ASME-JSES-JSME International Solar Energy Conference Reno, Nevada.
- Kelsey, J. and Pearson, D. (2011). *ML-11-C045 Updated Procedures for Commercial Building Energy Audits*. ASHRAE Transactions, vol 117, (2): 374.
- Lam, J. C. and Hui, S. (1996). *Sensitivity analysis of energy performance of office buildings*. Building and Environment, vol 31, (1): 27-39.

- Liu, G. and Liu, M. (2011). *A rapid calibration procedure and case study for simplified simulation models of commonly used HVAC systems*. Building and Environment, vol 46, (2): 409-420.
- Liu, S. and Henze, G. P. (2005). *Calibration of building models for supervisory control of commercial buildings*. Proceedings of the 9th International Building Performance Simulation Association (IBPSA) Conference, Montreal, Canada.
- Love, J. A. and Kandil, A.-E. (2013). *Signature analysis calibration of a school energy model using hourly data* Journal of Building Performance Simulation, vol ahead-of-print: 1-20.
- Lunneberg, T. A. (1999). *Improving simulation accuracy through the use of short-term electrical end-use monitoring*. Proceedings of the International Building Performance Simulation Association (IBPSA) Conference, Kyoto, Japan.
- Mayer, T., Sebold, F., Fields, A., Ramirez, R., Souza, B. and Ciminelli, M. (2003). *DrCEUS: Energy and demand usage from commercial on-site survey data*. Proceedings of the International Energy program Evaluation Conference, Seattle, WA.
- Millette, J., Sansregret, S. and Daoud, A. (2011). *SIMeB: simplified interface to DOE2 and EnergyPlus - a user's perspective - case study of an existing building*. Proceeding of the 12th International Building Performance Simulation Association (IBPSA) Conference, Sydney, Australia.
- Monfet, D., Zmeureanu, R., Charneux, R. and Lemire, N. (2009). *Calibration of a Building Energy Model Using Measured Data*. ASHRAE Transactions, vol 115, (1): 348-359.
- Mottillo, M. (2001). *Better Inputs for Better Outputs-Sensitivity Analysis of Energy Simulation by Building Type*. ASHRAE Transactions, vol 107, (2): 722-732.
- N.R.C. (1997). *Model National Energy Code for Buildings*. Natural Resources Canada, Ottawa, Ontario, Canada.
- N.R.C. (2011). *National Energy Code of Canada for Buildings*. Natural Resources Canada, Ottawa, Ontario, Canada.
- N.R.C. (2013). *CAN-QUEST v 1.5*, Ottawa, Ontario, Canada. Retrieved from.

- Pan, Y., Huang, Z. and Wu, G. (2007). *Calibrated building energy simulation and its application in a high-rise commercial building in Shanghai*. Energy and Buildings, vol 39, (6): 651-657.
- Pedrini, A., Westphal, F. S. and Lamberts, R. (2002). *A methodology for building energy modelling and calibration in warm climates*. Building and Environment, vol 37, (8): 903-912.
- Perez-Lombard, L., Ortiz, J. and Pout, C. (2008). *A review on buildings energy consumption information*. Energy and buildings, vol 40, (3): 394-398.
- Plourde, J. (2011). *Making the Case For Energy Metering*. ASHRAE Journal, vol 53, (4): 20.
- Raftery, P., Keane, M. and Costa, A. (2009). *Calibration of a detailed simulation model to energy monitoring system data: a methodology and case study*. Proceedings of the 11th International Building Performance Simulation Association (IBPSA) Conference, Glasgow, Scotland, UK.
- Raftery, P., Keane, M. and Costa, A. (2011). *Calibrating whole building energy models: Detailed case study using hourly measured data*. Energy and Buildings, vol 43, (12): 3666-3679.
- Raftery, P., Keane, M. and O'Donnell, J. (2011). *Calibrating whole building energy models: An evidence-based methodology*. Energy and Buildings, vol 43, (9): 2356-2364.
- Reddy, T. A. (2006). *Literature review on calibration of building energy simulation programs: uses, problems, procedures, uncertainty, and tools*. ASHRAE Transactions, vol 112, (2): 226-240.
- Reddy, T. A. (2011). *Applied data analysis and modeling for energy engineers and scientists*. Springer, New York, USA.
- Reddy, T. A., Maor, I. and Jian, S. (2006). *Procedures for reconciling computer-calculated results with measured energy data*. ASHRAE Research Project 1051-RP.
- Reddy, T. A., Maor, I. and Panjapornpon, C. (2007). *Calibrating detailed building energy simulation programs with measured data—part II: application to three case study office buildings (RP-1051)*. HVAC & R Research, vol 13, (2): 243-265.

- Sonderegger, R., Avina, J., Kennedy, J. and Bailey, P. (2001). *Deriving loadshapes from utility bills through scaled simulation*. Kansas City, MI.
- Sornay, J. (1985). *Recent developments of building energy simulation tools in Europe*. Proceedings of the International Building Performance Simulation Association (IBPSA) Conference, Seattle, WA.
- Stein, J. (1997). *Calibrated Simulation: An Improved Method for Analyzing Building Energy Use*. Boulder, CO, September.
- Troncoso, R. (1997). *A hybrid monitoring-modeling procedure for analyzing the performance of large central chilling plants*. Proceedings of International Building Performance Simulation Association (IBPSA) Conference, Prague, Czech Republic.
- Waltz, J. P. (2000). *Computerized building energy simulation handbook*. CRC Press, Lilburn, Georgia.
- Weather Analytics (2013). *Weather file acquired from <http://www.weatheranalytics.com>*. Retrieved 15 April, 2013.
- Yoon, J.-H. and Lee, E.-J. (1999). *Calibration procedure of energy performance simulation model for a commercial building*. Proceedings from the International Building Performance Simulation Association (IBPSA) Conference, Kyoto, Japan.

APPENDICES

Appendix A: Calibration results at the zone level

This section presents the calibration results at the zone level, for each zone in the building.

The comparison between measurements and predictions is presented for each zone:

Zone 1.3 NW

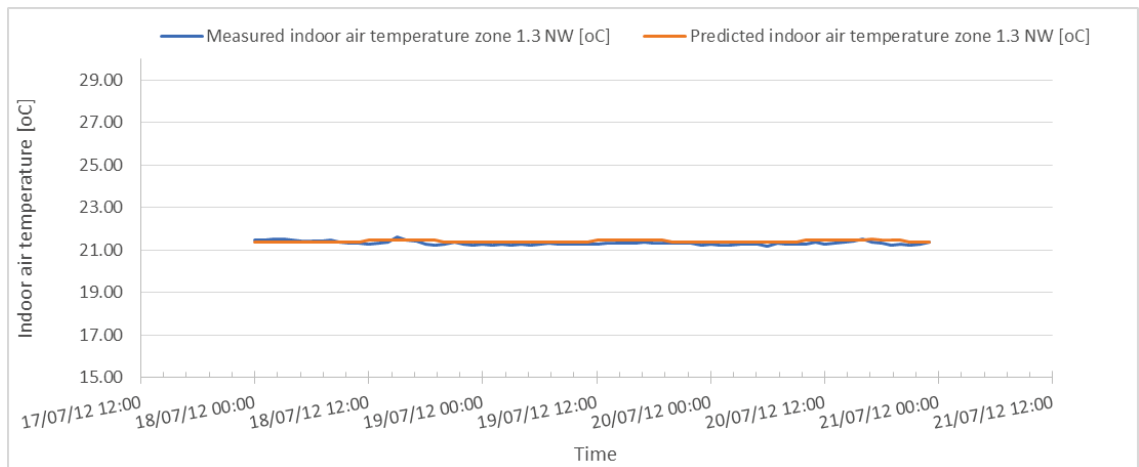


Figure A. 1: Predicted vs. measured hourly indoor air temperature for zone 1.3 NW from 18-20 July 2012

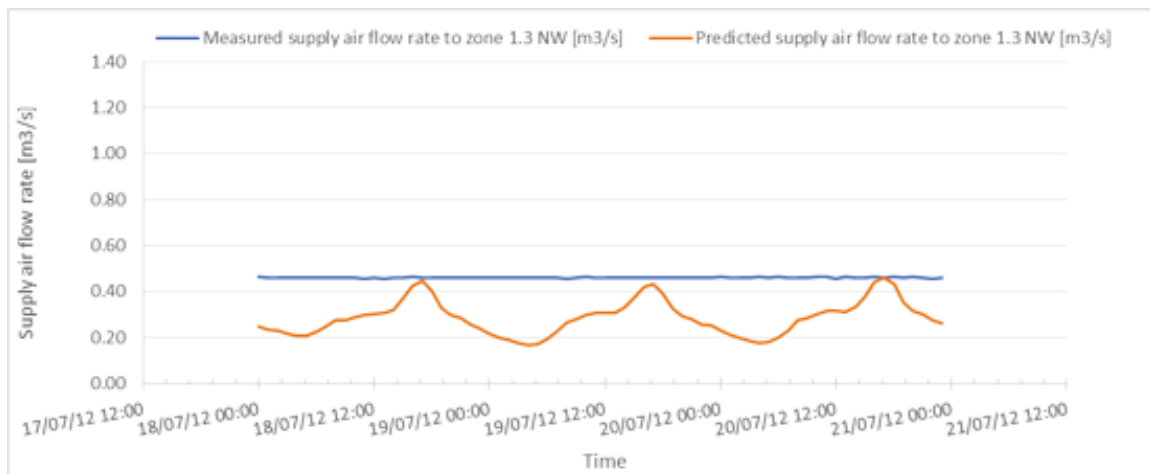


Figure A. 2: Predicted vs. measured hourly supply air flow rate to zone 1.3 NW from 18-20 July 2012

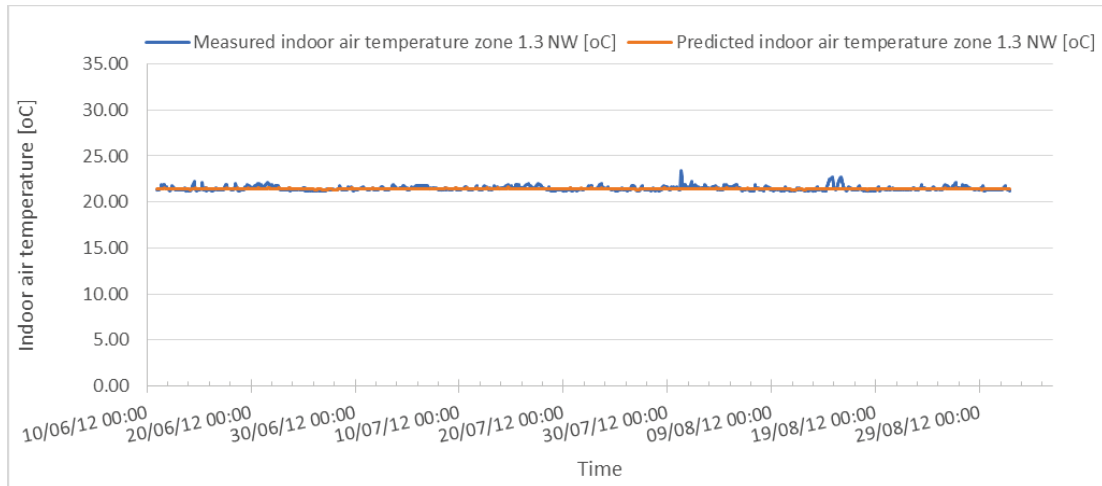


Figure A. 3: Predicted vs. measured hourly indoor air temperature for zone 1.3 NW, for the summer 2012

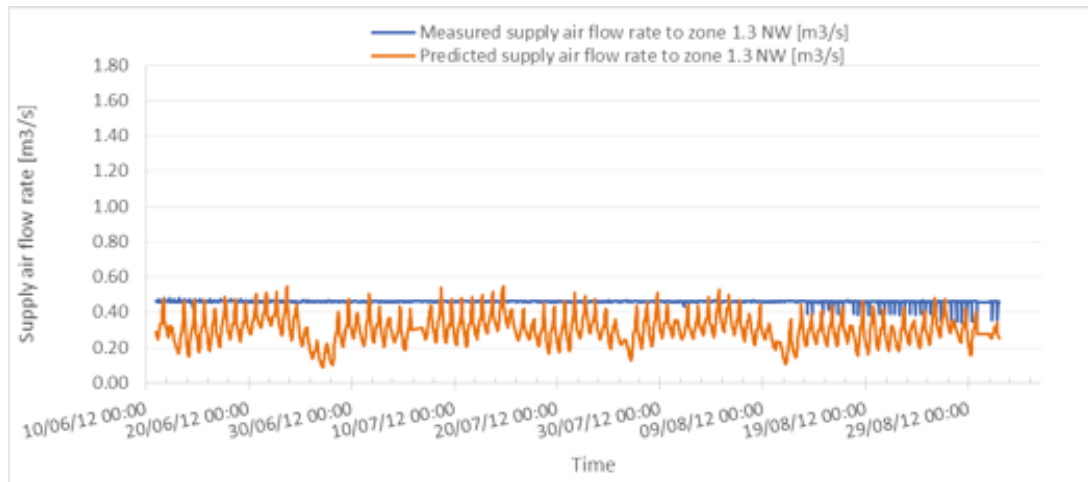


Figure A. 4: Predicted vs. measured hourly supply air flow rate to zone 1.3 NW, for the summer 2012

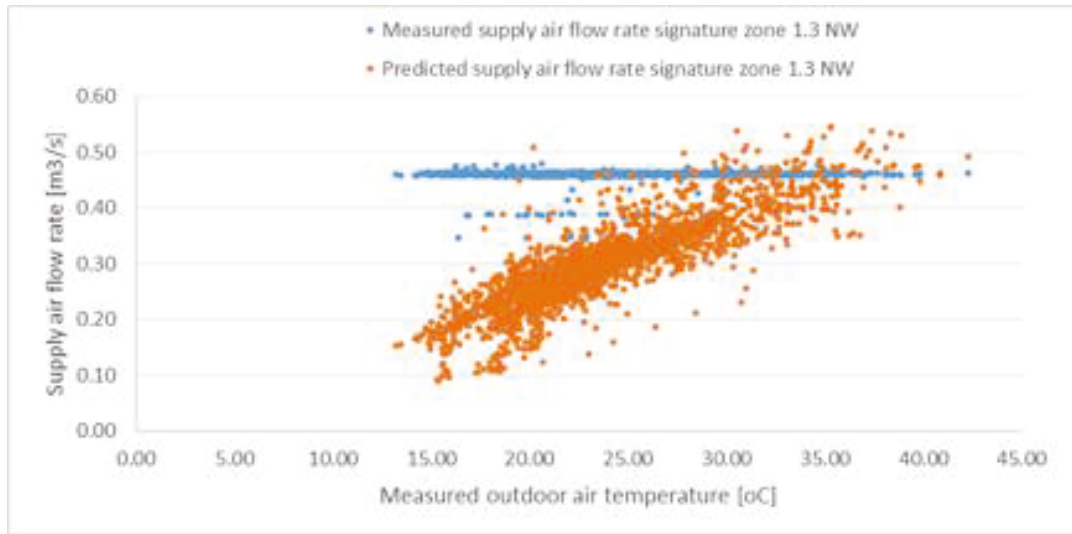


Figure A. 5: Predicted vs. measured hourly supply air flow rate signature for zone 1.3 NW for summer 2012

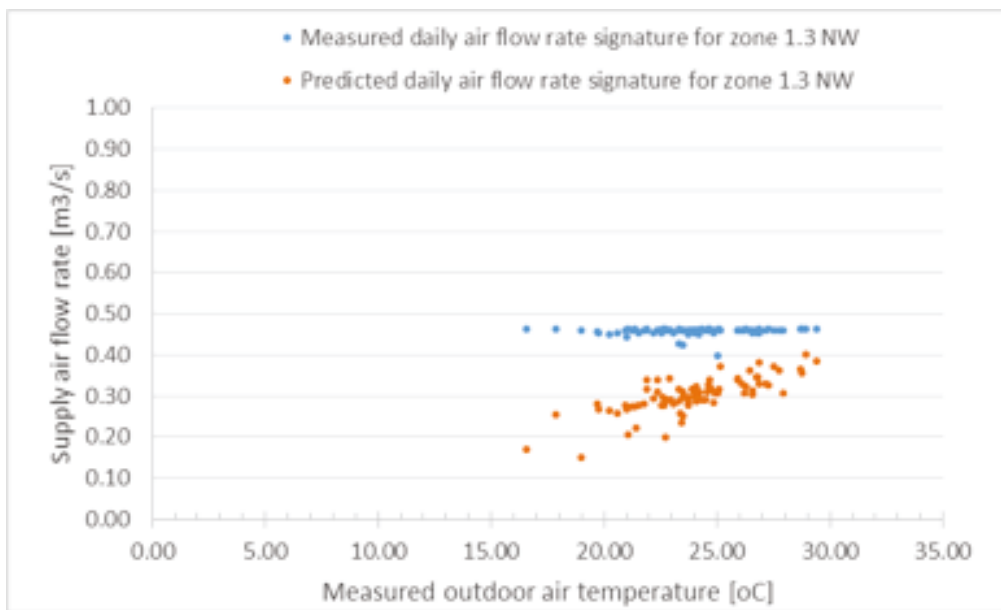


Figure A. 6: Predicted vs. measured daily supply air flow rate signature for zone 1.3 NW for summer 2012

Zone 1.4 SW

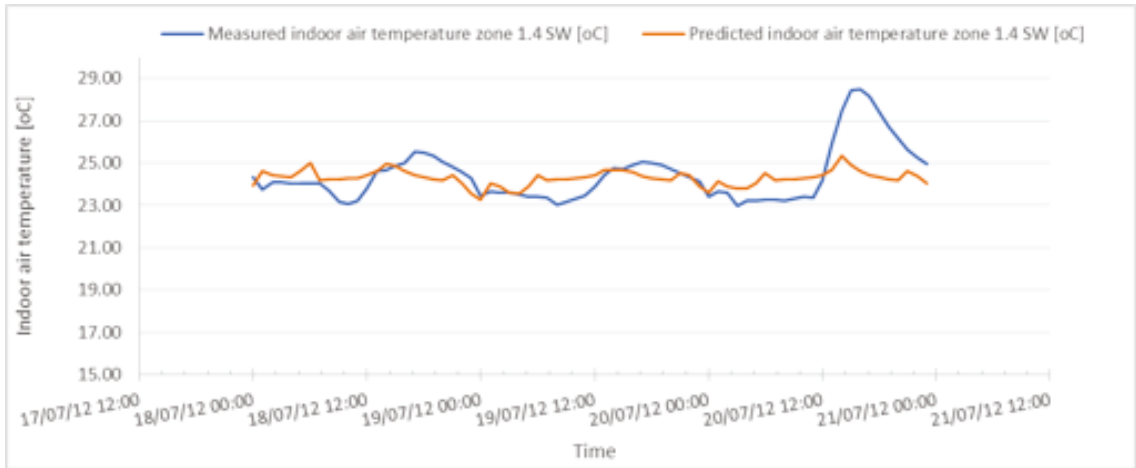


Figure A. 7: Predicted vs. measured hourly indoor air temperature for zone 1.4 SW, from 18-20 July 2012

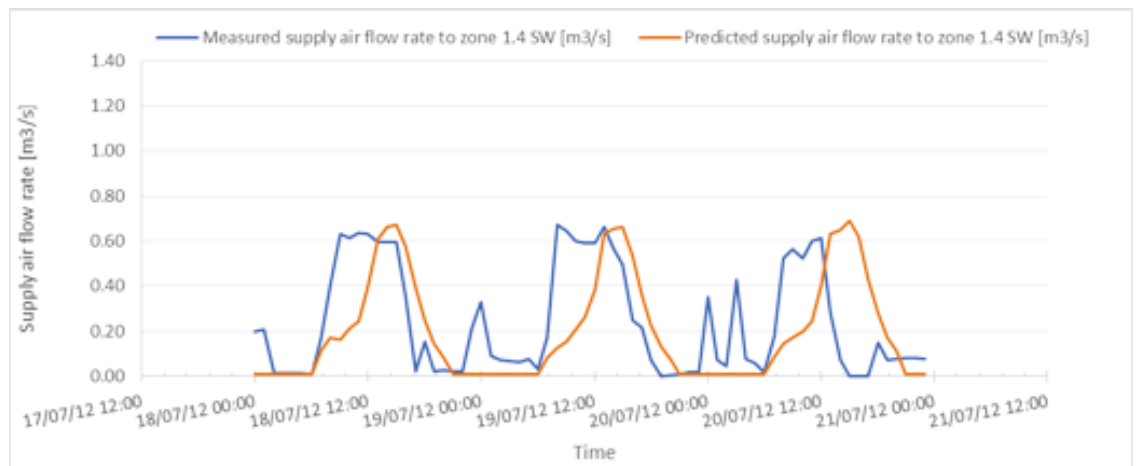


Figure A. 8: Predicted vs. measured hourly supply air temperature to zone 1.4 SW, from 18-20 July 2012

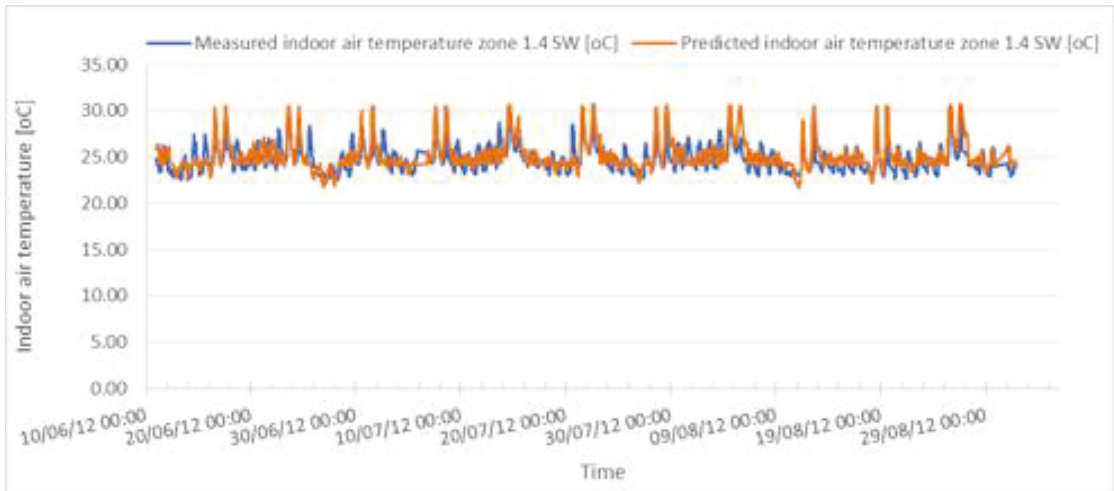


Figure A. 9: Predicted vs. measured hourly indoor air temperature for zone 1.4 SW, for summer 2012

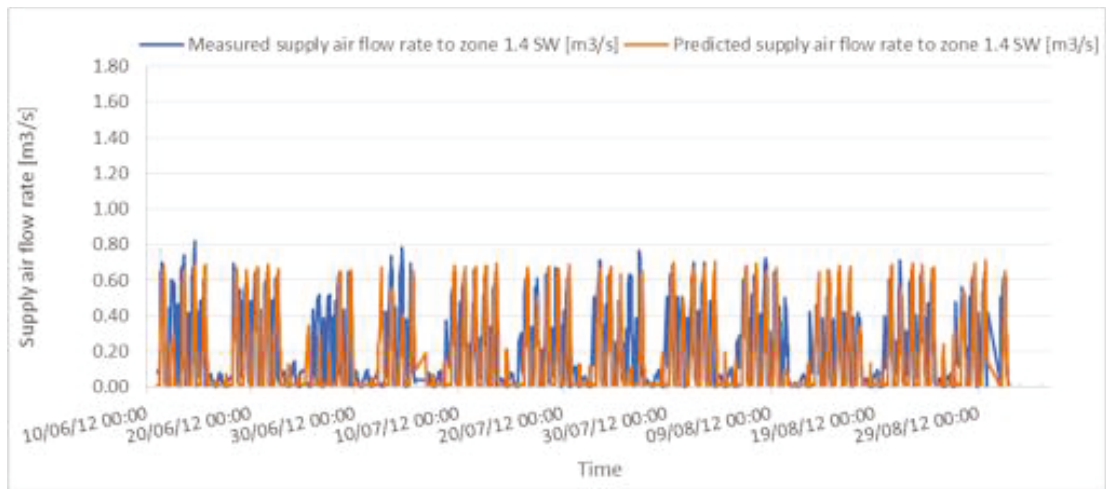


Figure A. 10: Predicted vs. measured hourly supply air flow rate to zone 1.4 SW, for summer 2012

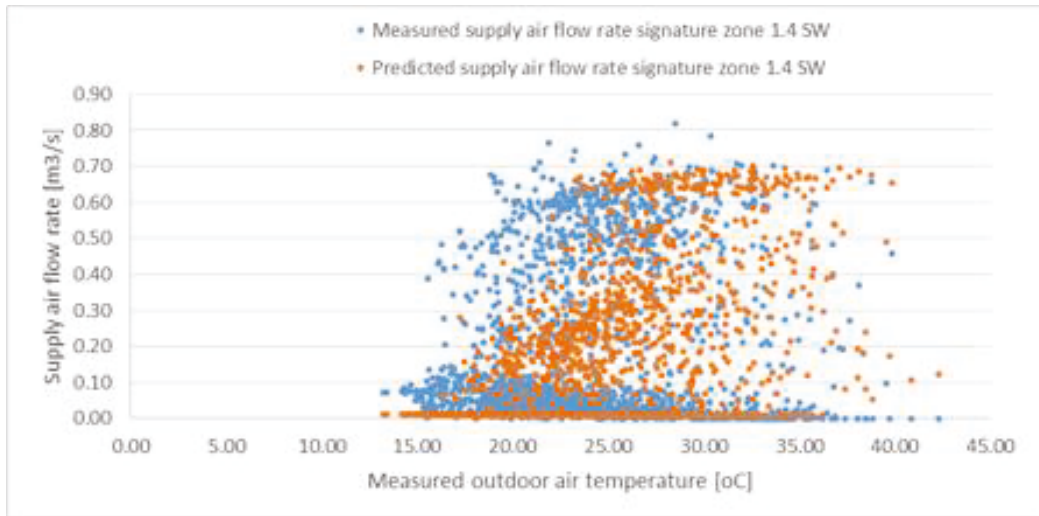


Figure A. 11: Predicted vs. measured hourly supply air flow rate signature for summer 2012

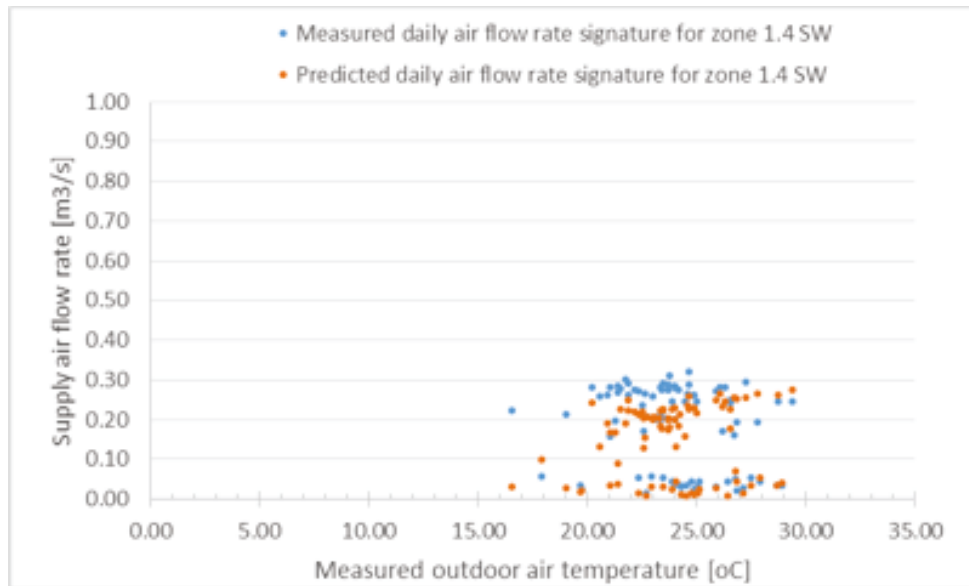


Figure A. 12: Predicted vs. measured daily air flow rate signature for summer 2012

Zone 1.5 SE

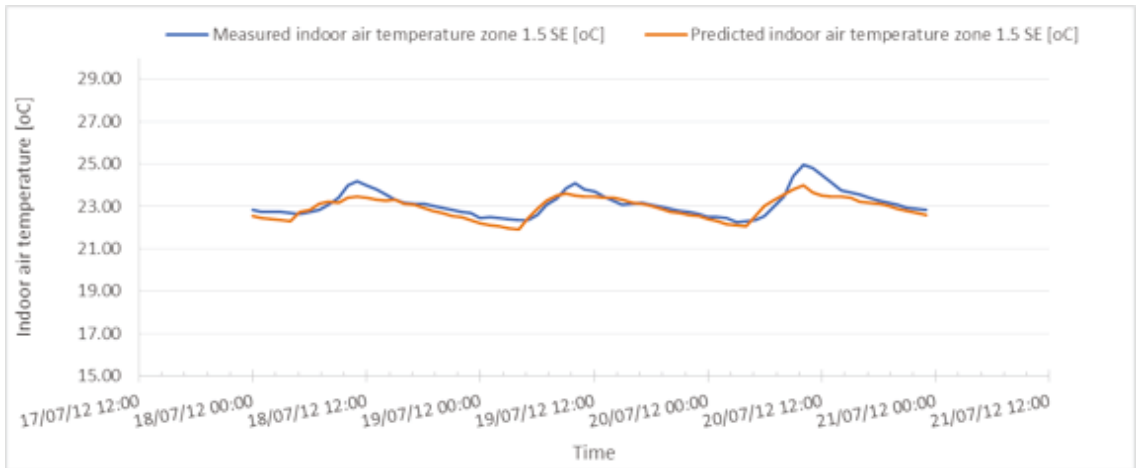


Figure A. 13: Predicted vs. measured hourly indoor air temperature for zone 1.5 SE, from 18-20 July 2012

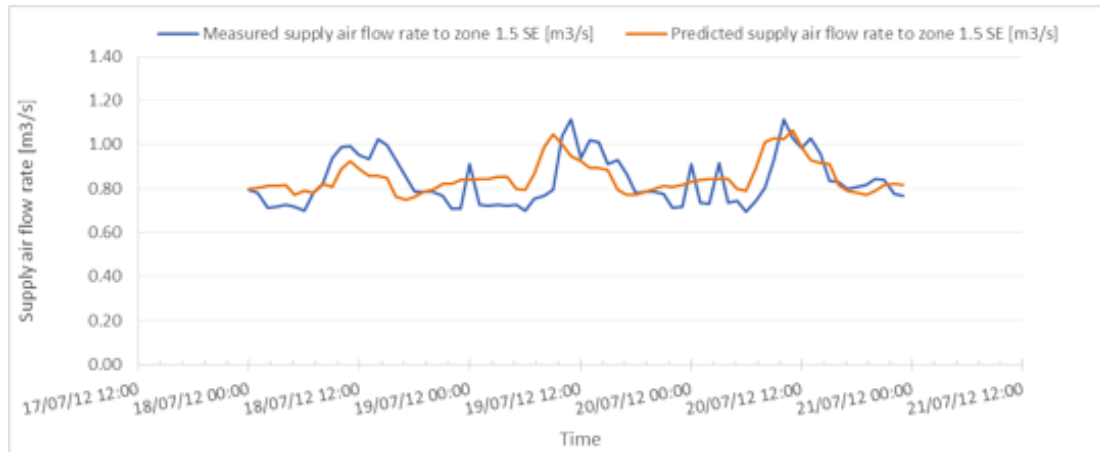


Figure A. 14: Predicted vs. measured hourly supply air flow rate to zone 1.5 SE, from 18-20 July 2012

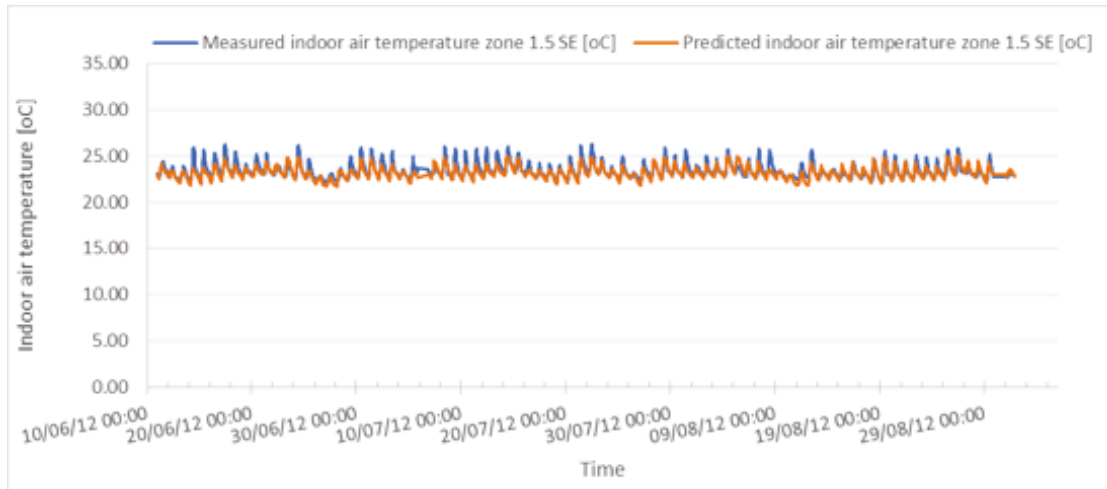


Figure A. 15: Predicted vs. measured hourly indoor air temperature for zone 1.5 SE, for summer 2012

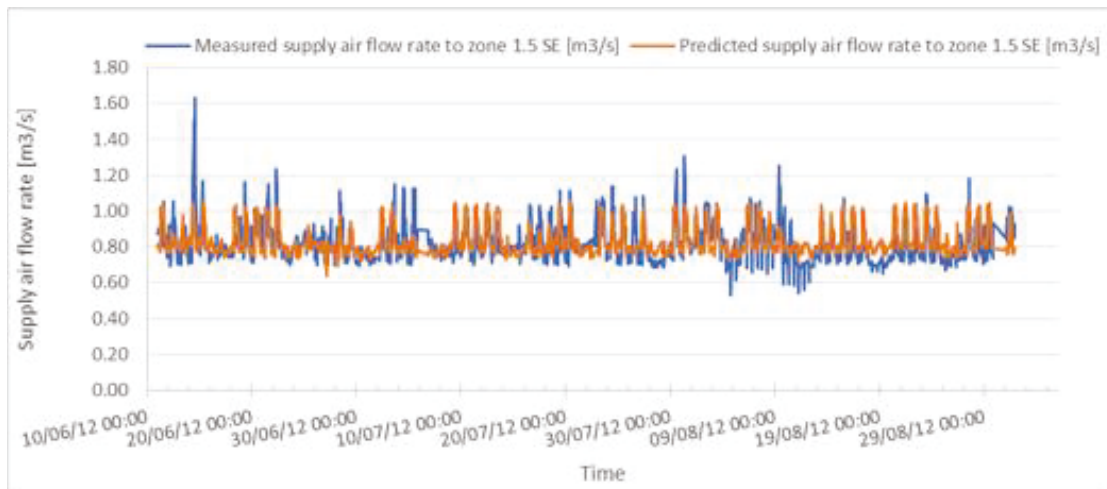


Figure A. 16: Predicted vs. measured hourly supply air flow rate to zone 1.5 SE, for summer 2012

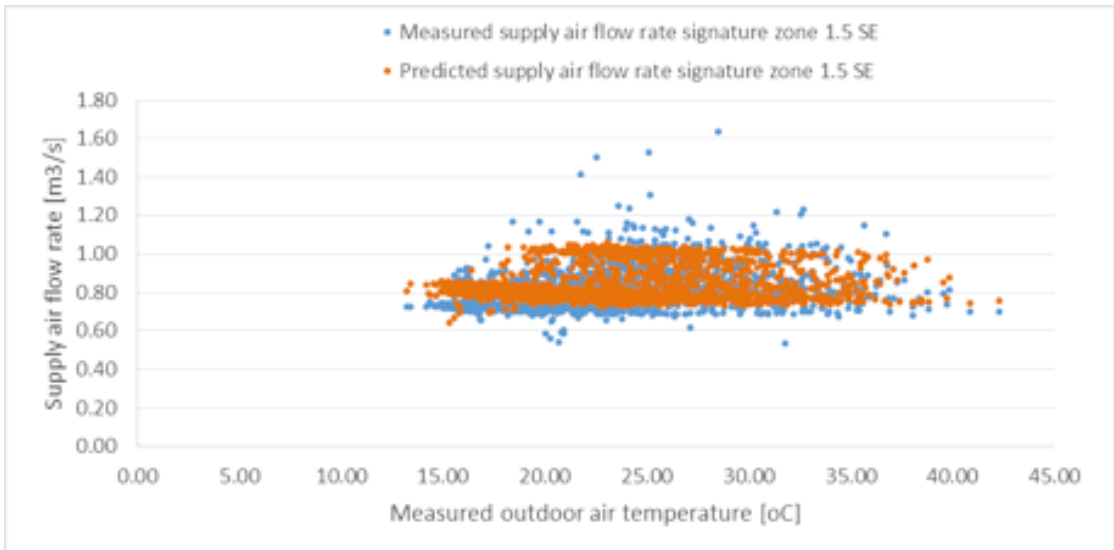


Figure A. 17: Predicted vs. measured hourly supply air flow rate signature for zone 1.5 SE, for summer 2012

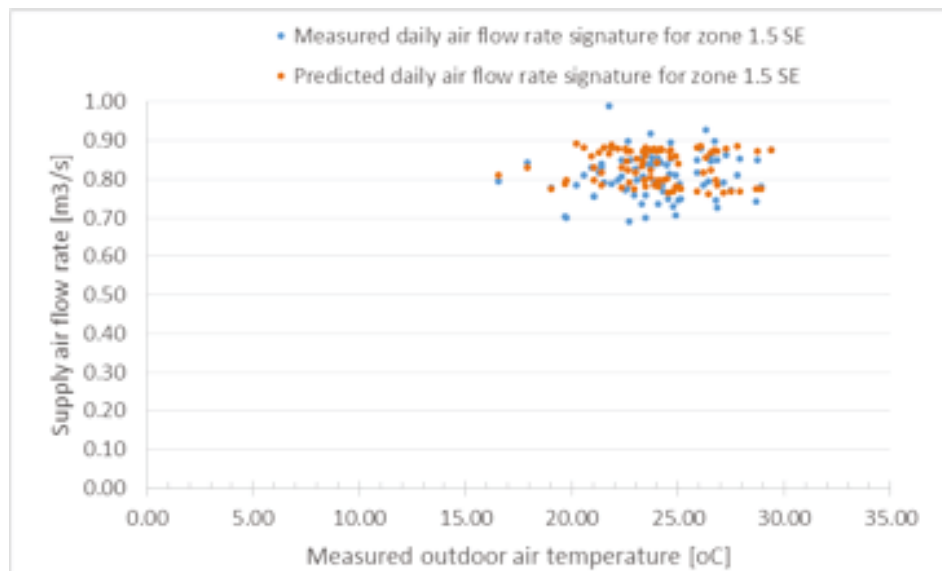


Figure A. 18: Predicted vs. measured daily supply air flow rate signature for zone 1.5 SE, for summer 2012

Zone 1.6 NE

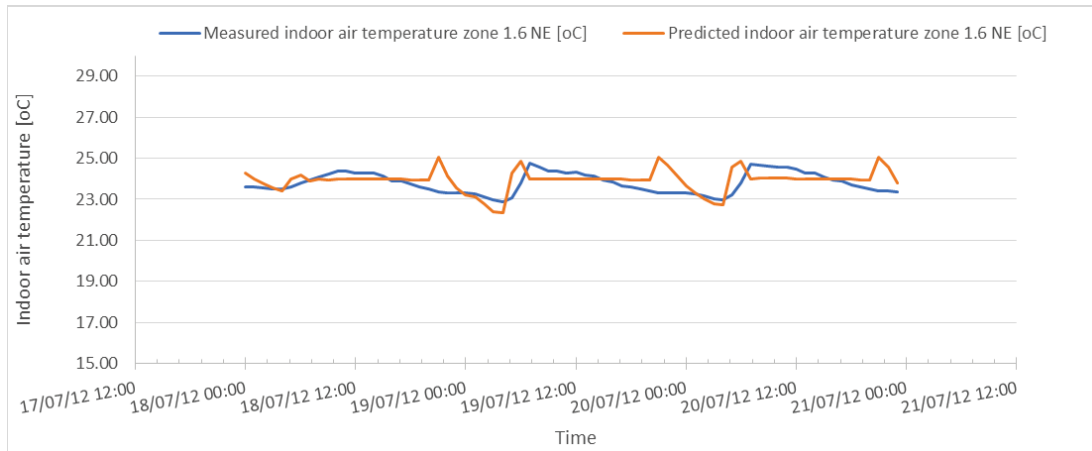


Figure A. 19: Predicted vs. measured hourly indoor air temperature for zone 1.6 NE, from 18-20 July 2012



Figure A. 20: Predicted vs. measured hourly supply air flow rate to zone 1.6 NE, from 18-20 July 2012

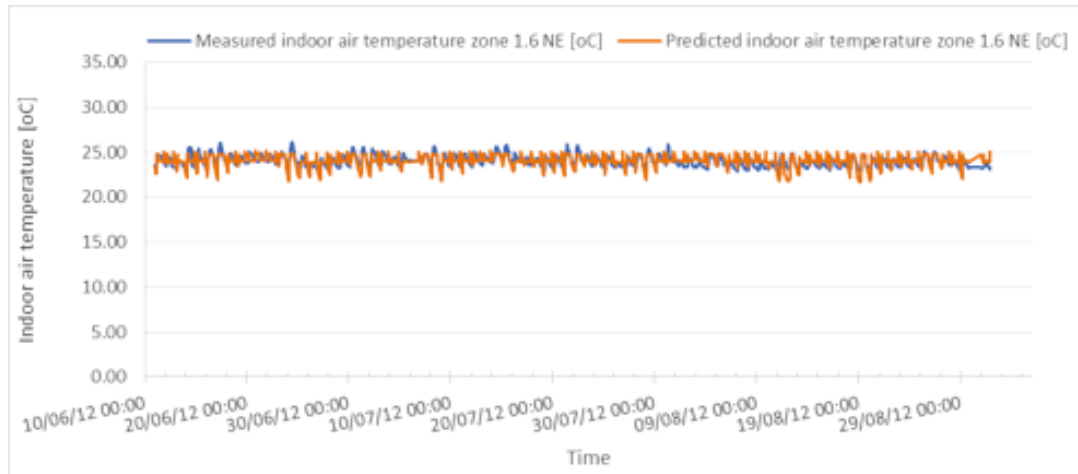


Figure A. 21: Predicted vs. measured hourly indoor air temperature for zone 1.6 NE, for summer 2012

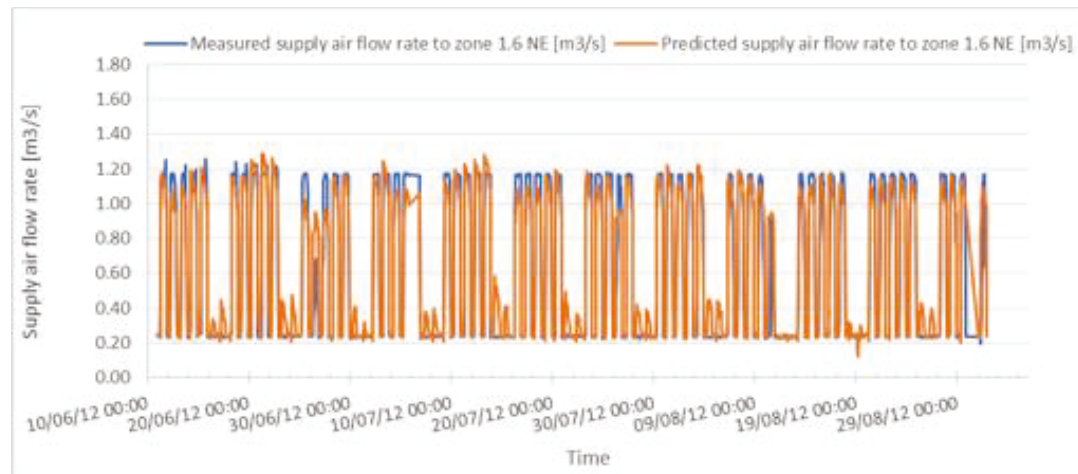


Figure A. 22: Predicted vs. measured hourly supply air flow rate to zone 1.6 NE, for summer 2012

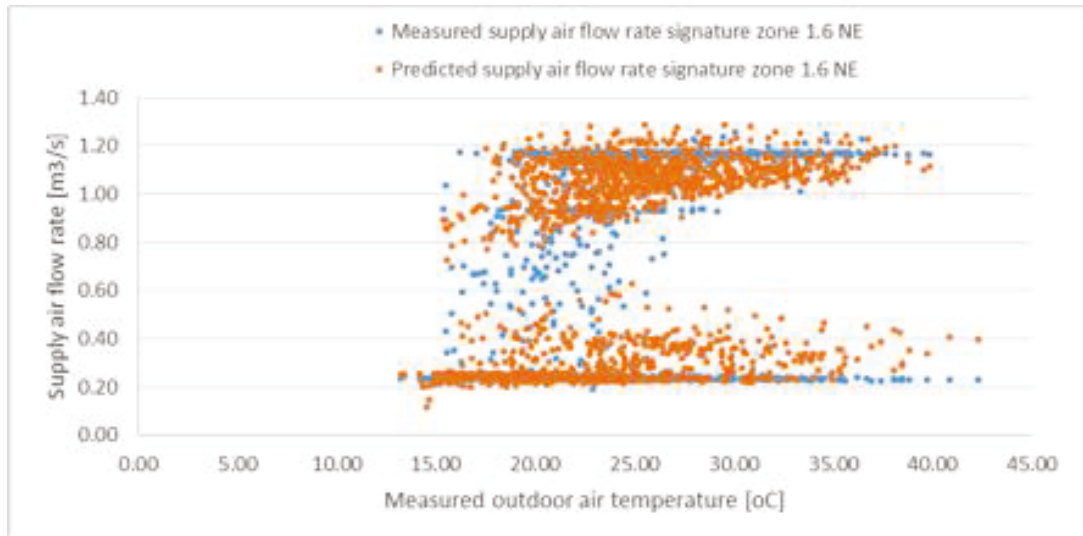


Figure A. 23: Predicted vs. measured hourly supply air flow rate signature for zone 1.6 NE, for summer 2012

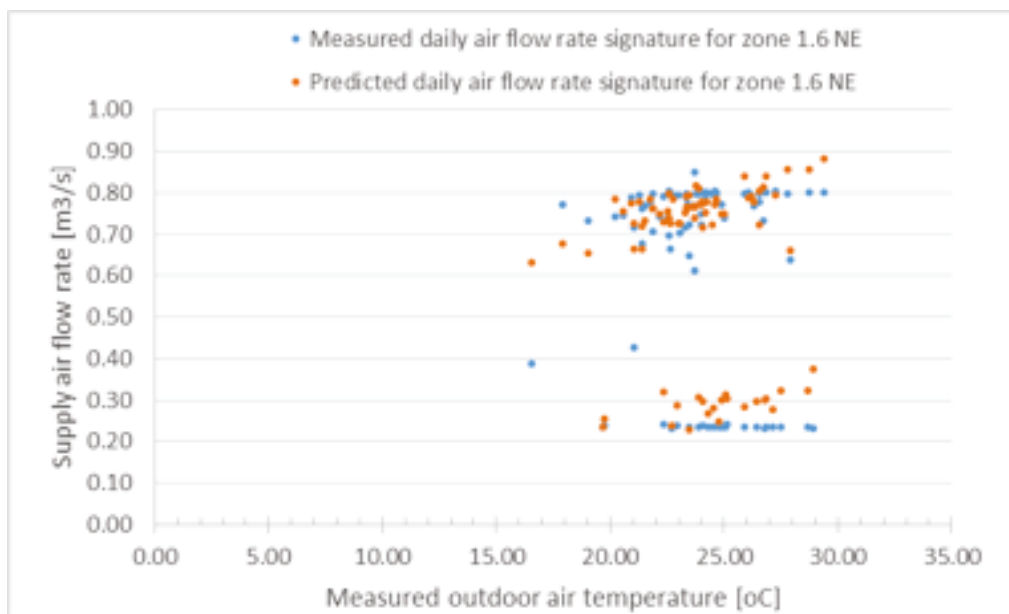


Figure A. 24: Predicted vs. measured daily supply air flow rate signature for zone 1.6 NE, for summer 2012

Zone 2.1 NE

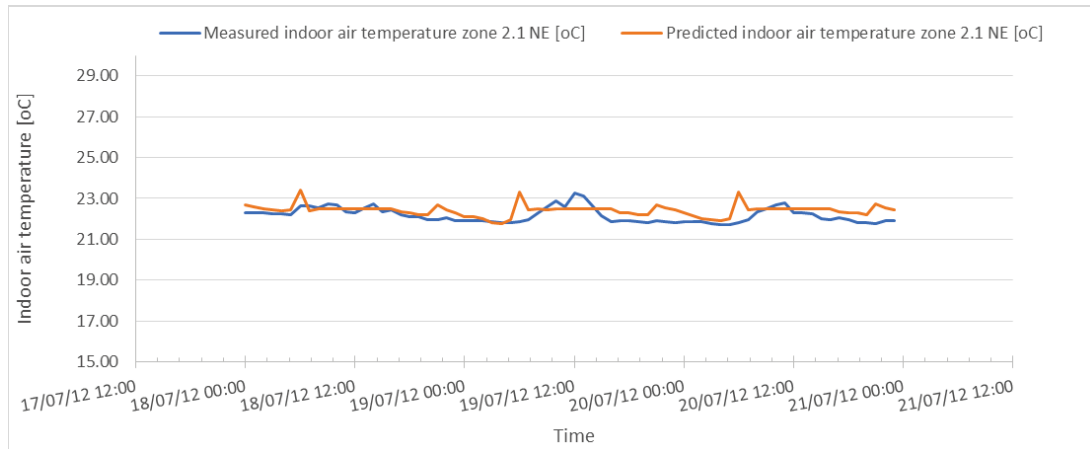


Figure A. 25: Predicted vs. measured hourly indoor air temperature for zone 2.1 NE, from 18-20 July 2012

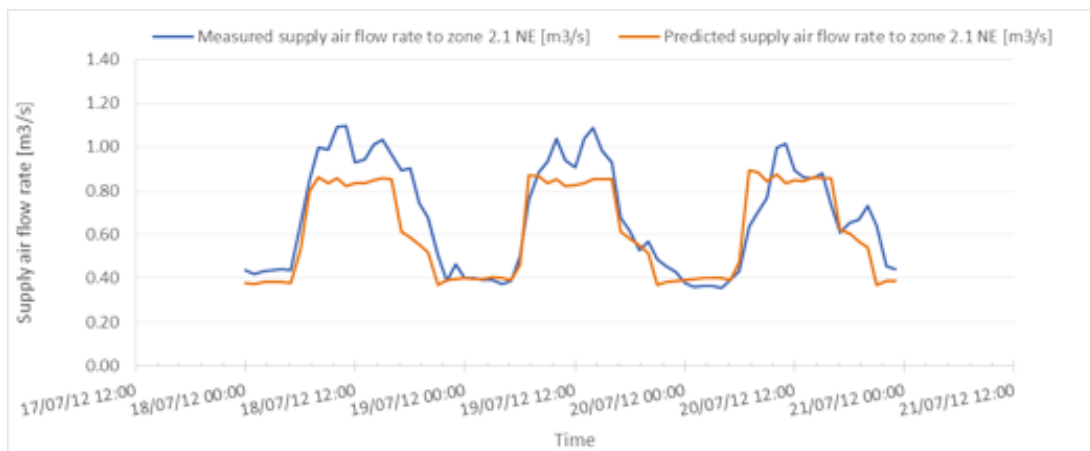


Figure A. 26: Predicted vs. measured hourly supply air flow rate for zone 2.1 NE, from 18-20 July 2012

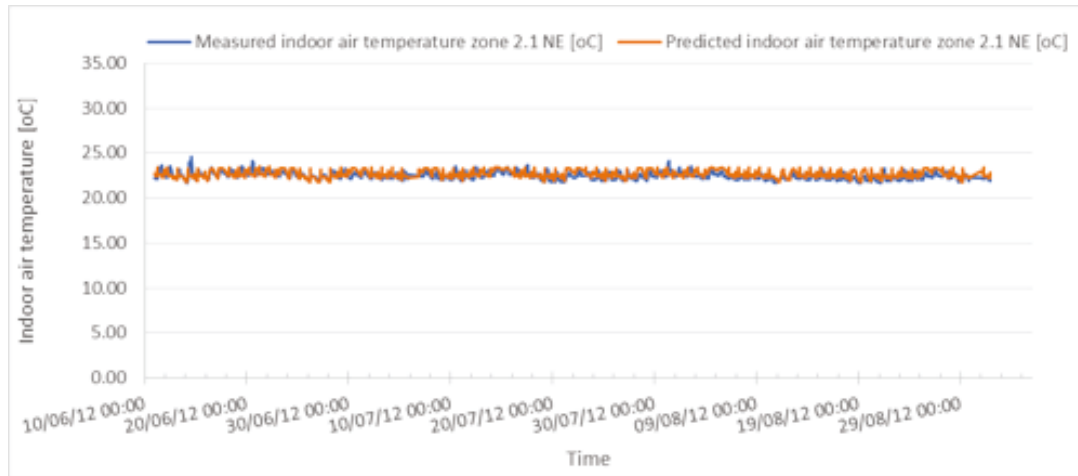


Figure A. 27: Predicted vs. measured hourly indoor air temperature for zone 2.1 NE, for summer 2012



Figure A. 28: Predicted vs. measured hourly supply air flow rate to zone 2.1 NE, for summer 2012

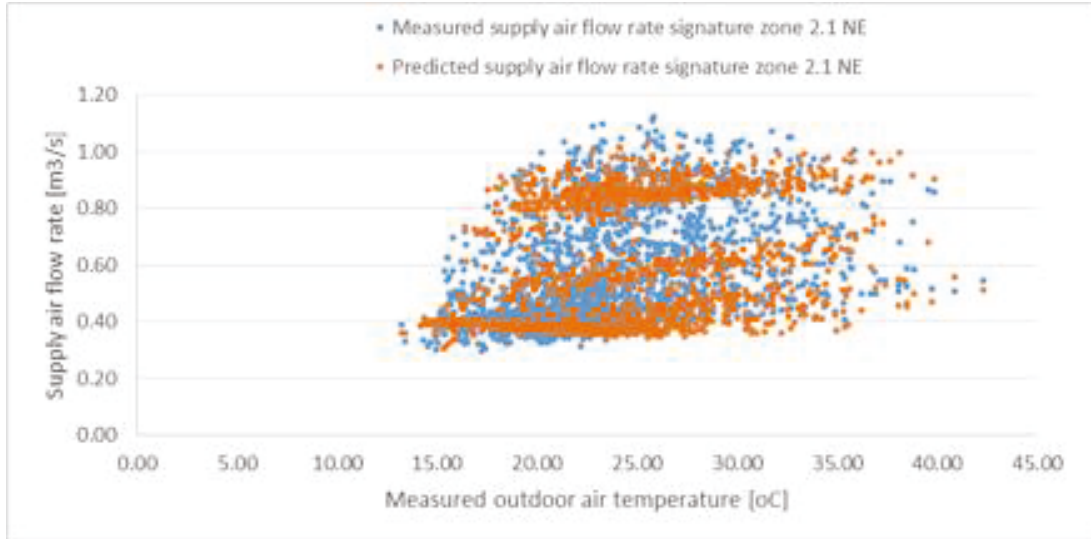


Figure A. 29: Predicted vs. measured hourly supply air flow rate signature for zone 2.1 NE, for summer 2012

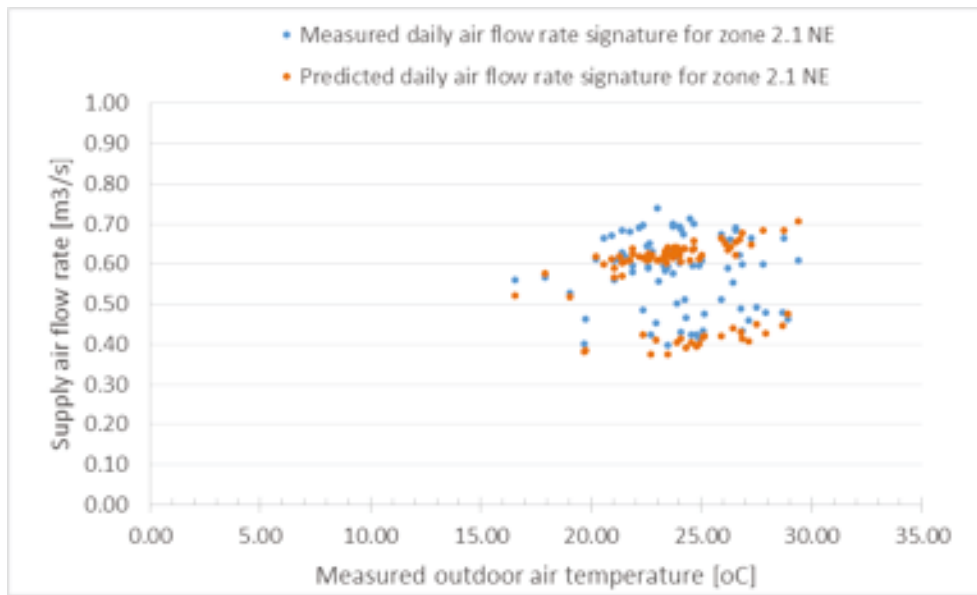


Figure A. 30: Predicted vs. measured daily supply air flow rate signature for zone 2.1 NE, for summer 2012

Zone 2.3 NW

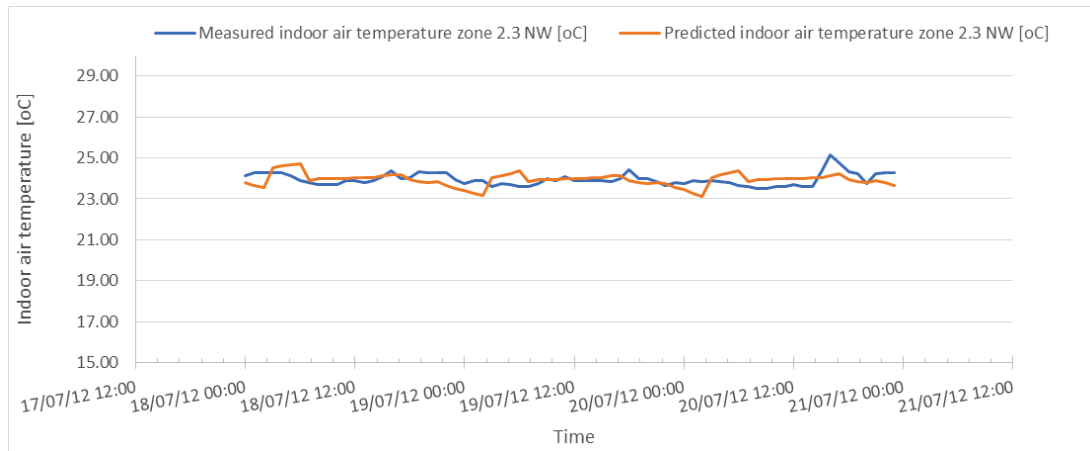


Figure A. 31: Predicted vs. measured hourly indoor air temperature for zone 2.3 NW, from 18-20 July 2012

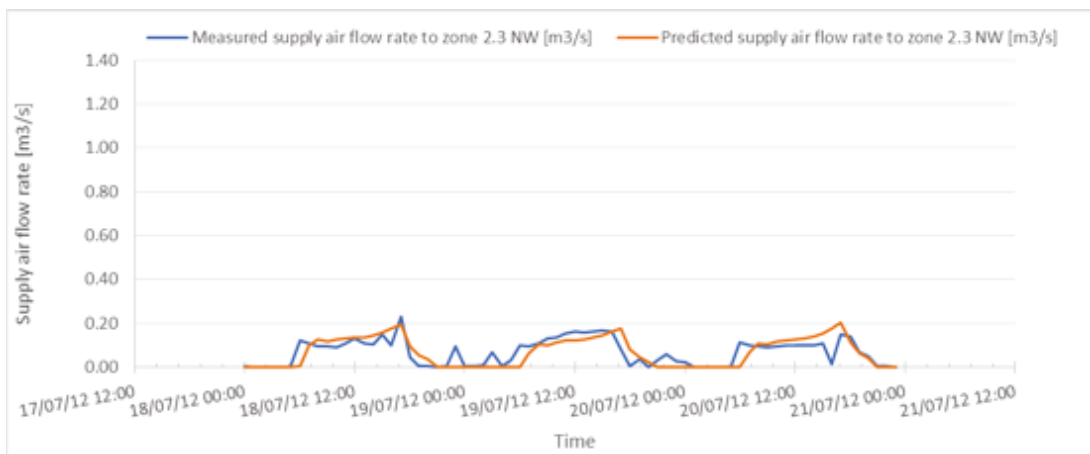


Figure A. 32: Predicted vs. measured hourly supply air flow rate to zone 2.3 NW, from 18-20 July 2012

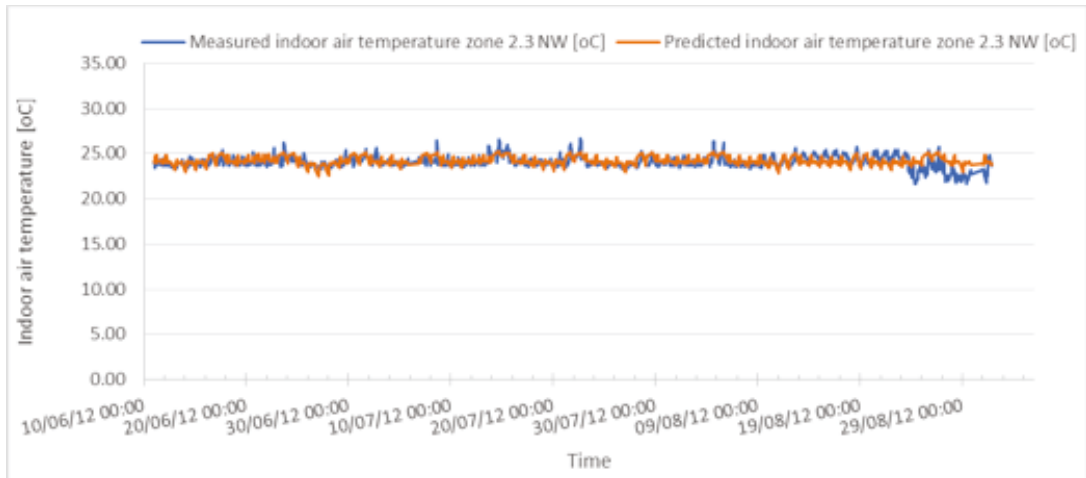


Figure A. 33: Predicted vs. measured hourly indoor air temperature for zone 2.3 NW, for summer 2012

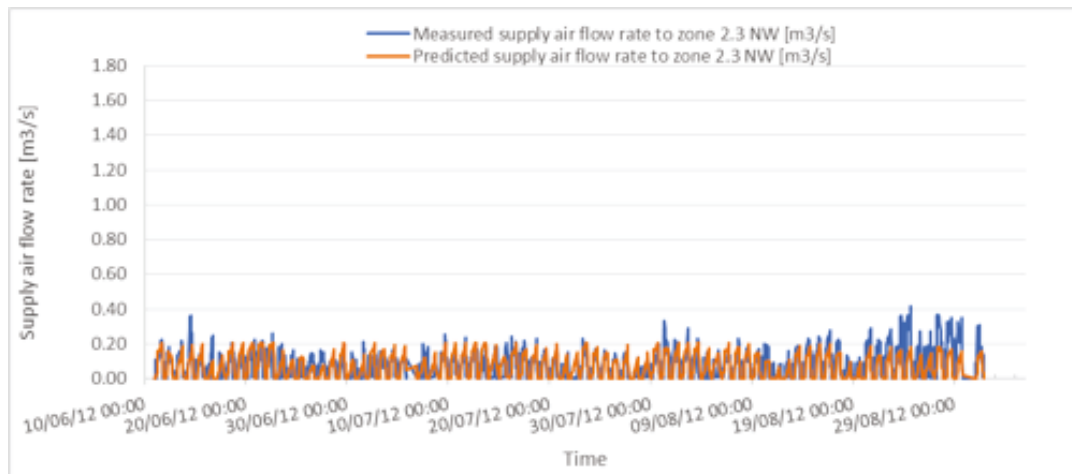


Figure A. 34: Predicted vs. measured hourly indoor supply air flow rate for zone 2.3 NW, for summer 2012

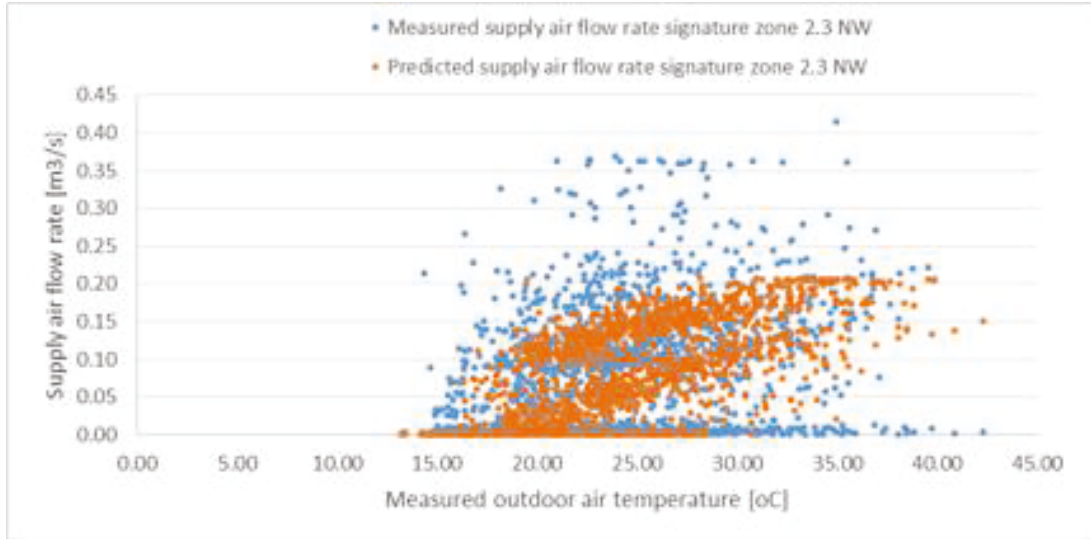


Figure A. 35: Predicted vs. measured hourly supply air flow rate signature for zone 2.3 NW, for summer 2012

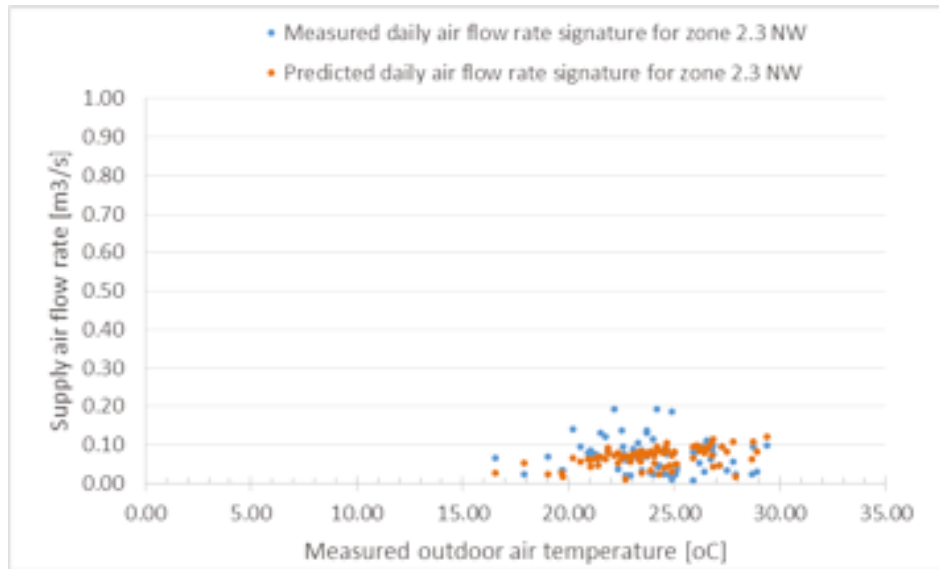


Figure A. 36: Predicted vs. measured daily supply air flow rate signature for zone 2.3 NW, for summer 2012

Zone 2.4 SW

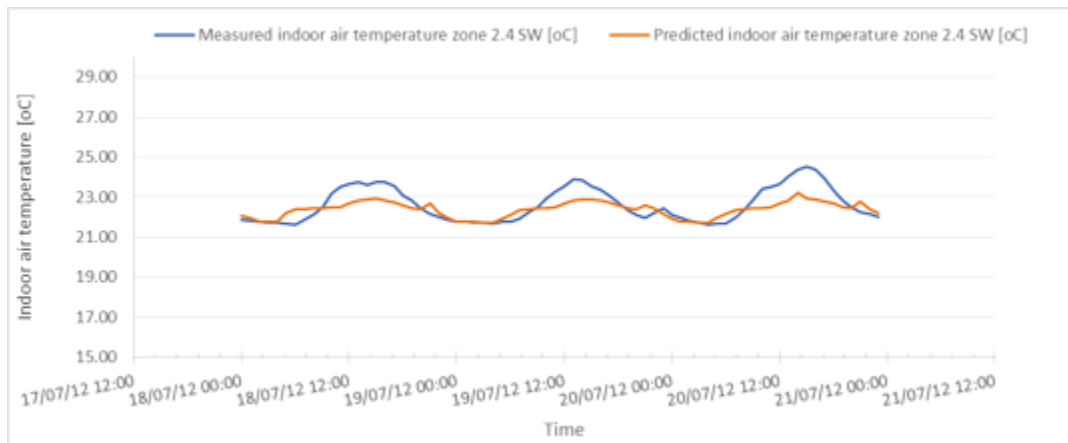


Figure A. 37: Predicted vs. measured hourly indoor air temperature for zone 2.4 SW, from 18-20 July 2012

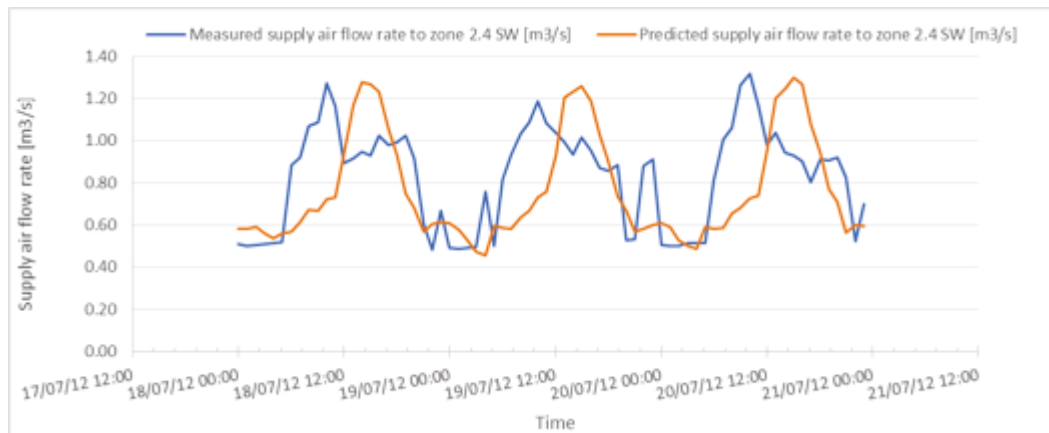


Figure A. 38: Predicted vs. measured hourly supply air flow rate to zone 2.4 SW, from 18-20 July 2012

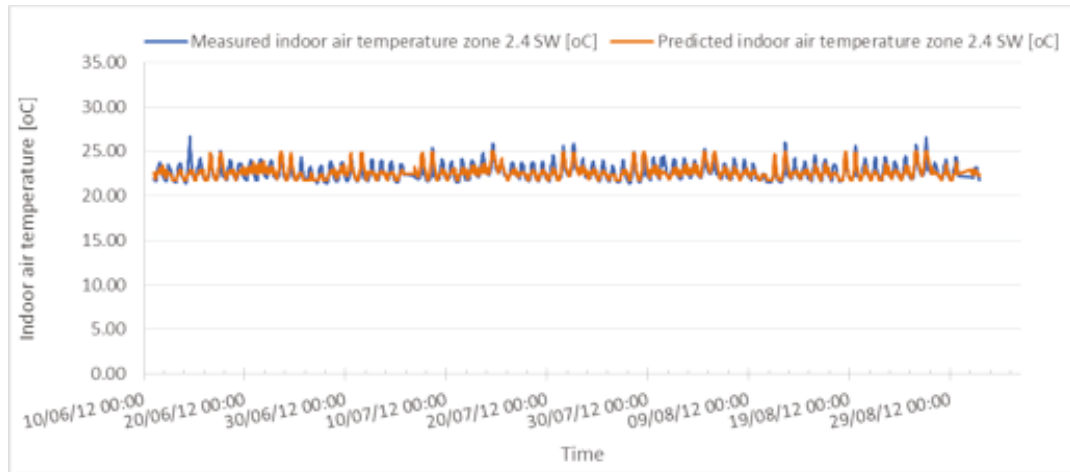


Figure A. 39: Predicted vs. measured hourly indoor air temperature for zone 2.4 SW, for summer 2012



Figure A. 40: Predicted vs. measured hourly supply air flow rate to zone 2.4 SW, for summer 2012

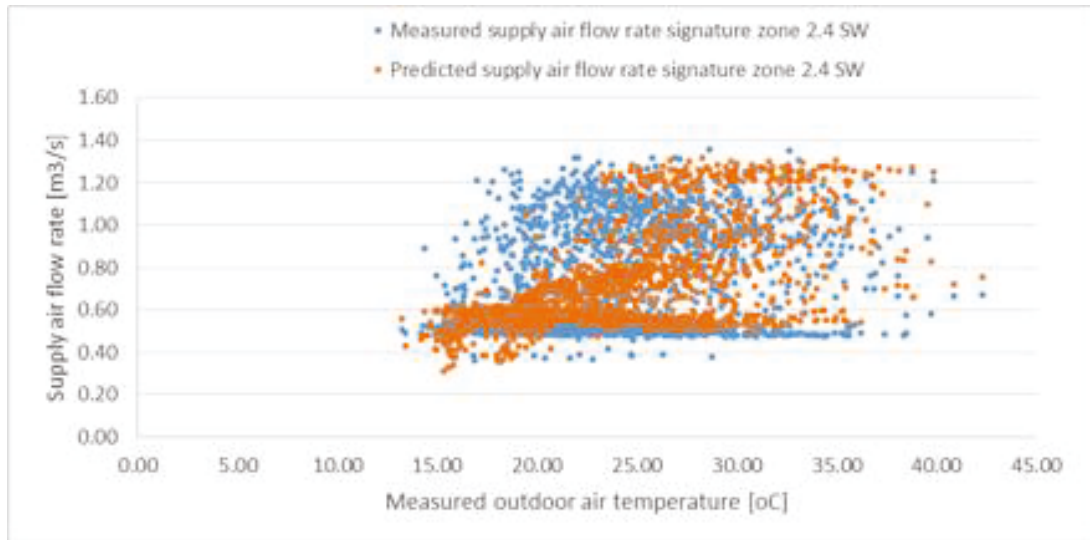


Figure A. 41: Predicted vs. measured hourly supply air flow rate signature for zone 2.4 SW, for summer 2012

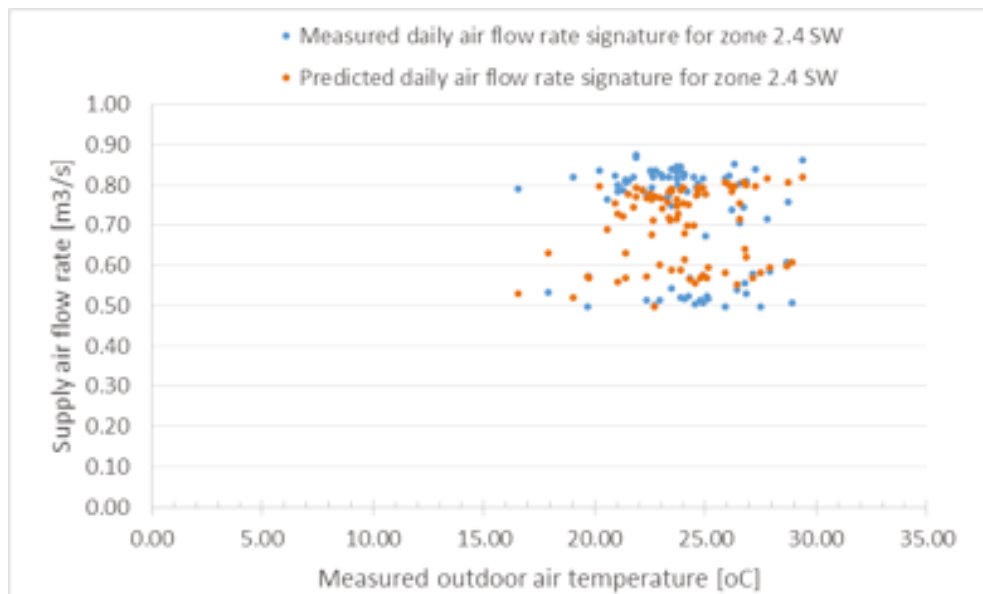


Figure A. 42: Predicted vs. measured daily supply air flow rate signature for zone 2.4 SW, for summer 2012

Zone 2.5 SE

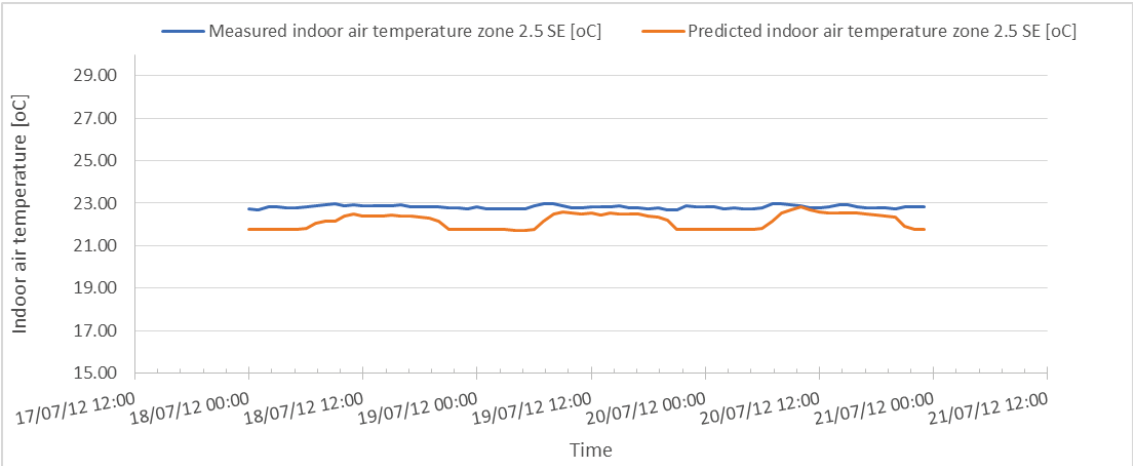


Figure A. 43: Predicted vs. measured hourly indoor air temperature for zone 2.5 SE, from 18-20 July 2012

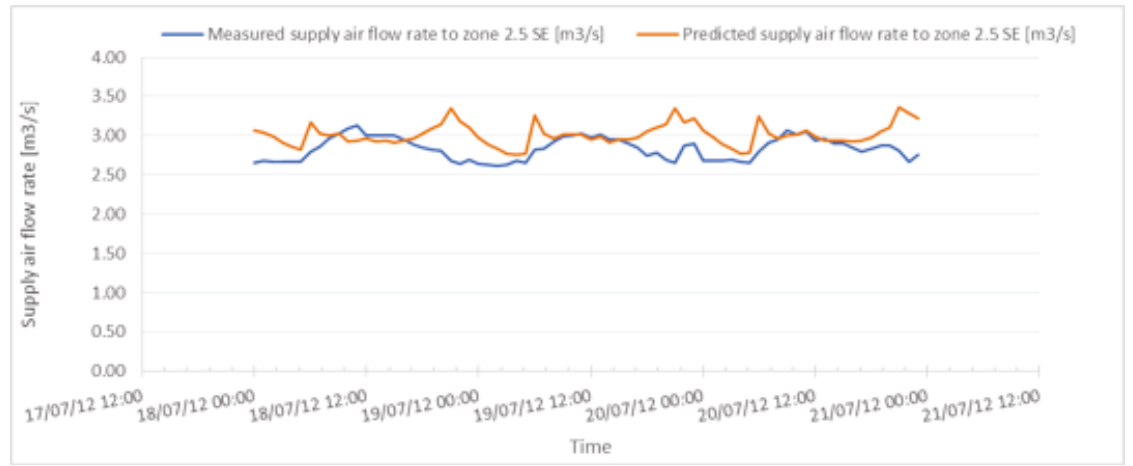


Figure A. 44: Predicted vs. measured hourly supply air flow rate to zone 2.5 SE, from 18-20 July 2012

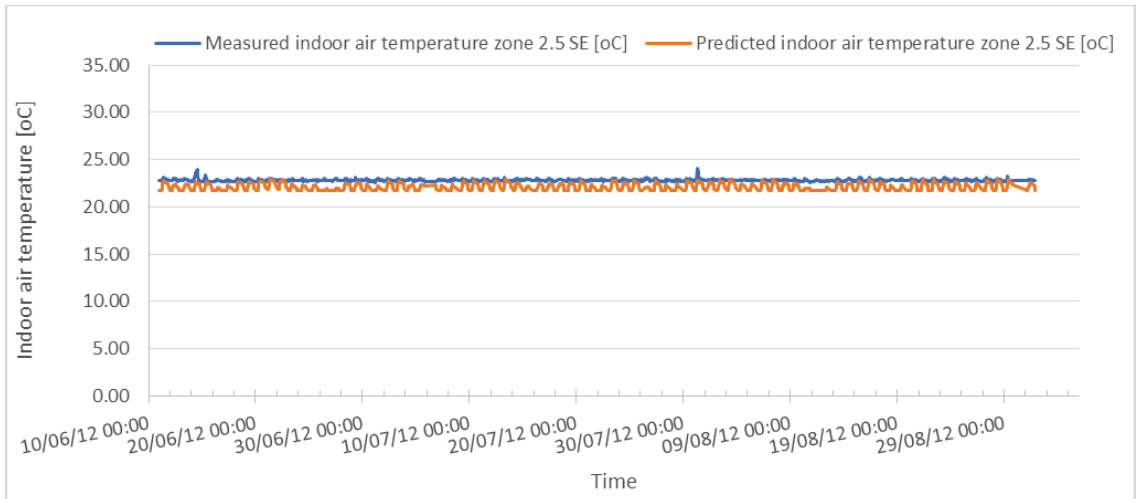


Figure A. 45: Predicted vs. measured hourly indoor air temperature for zone 2.5 SE, for summer 2012

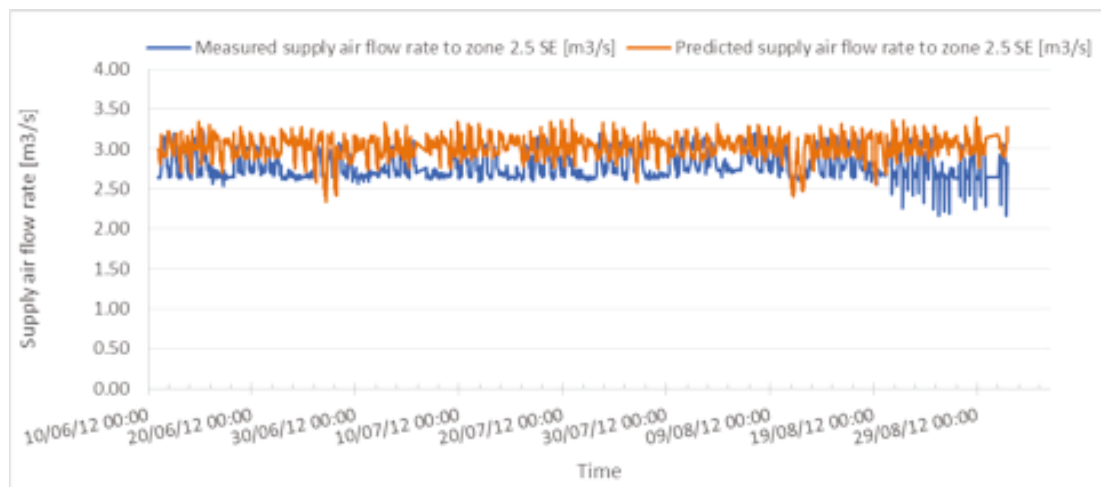


Figure A. 46: Predicted vs. measured hourly supply air flow rate to zone 2.5 SE, for summer 2012

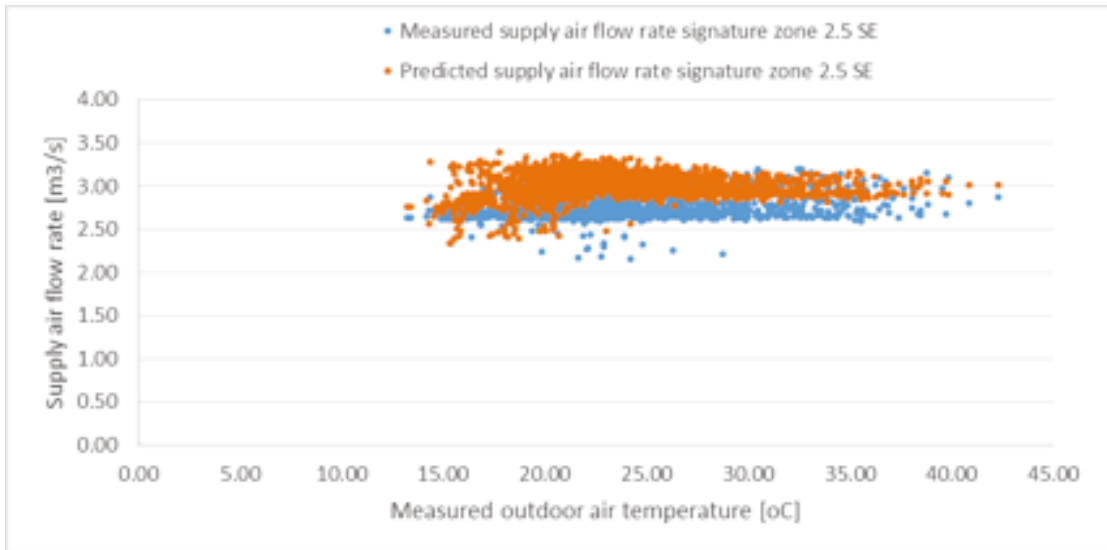


Figure A. 47: Predicted vs. measured hourly supply air flow rate signature for zone 2.5 SE, for summer 2012

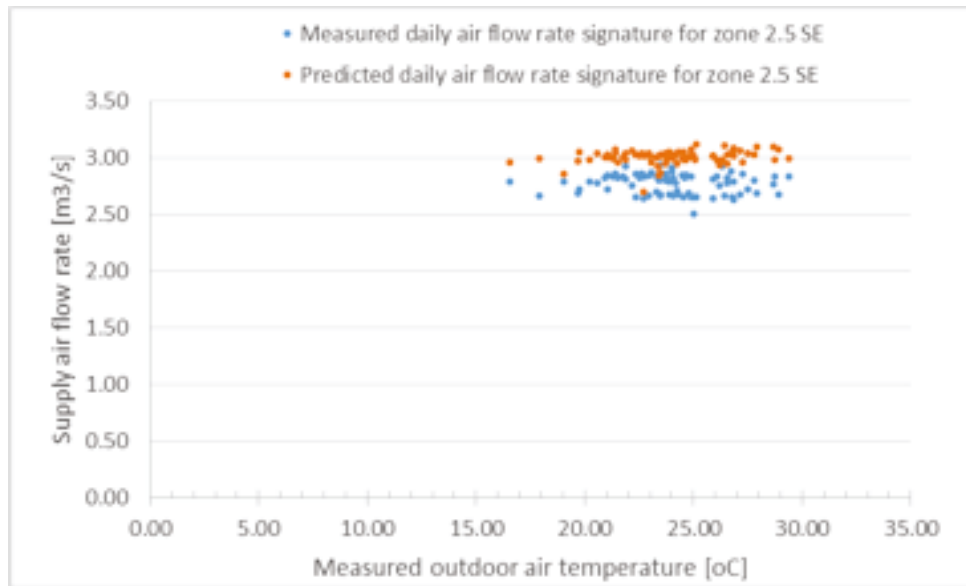


Figure A. 48: Predicted vs. measured daily supply air flow rate signature to zone 2.5 SE, for summer 2012

Zone 2.6 NE

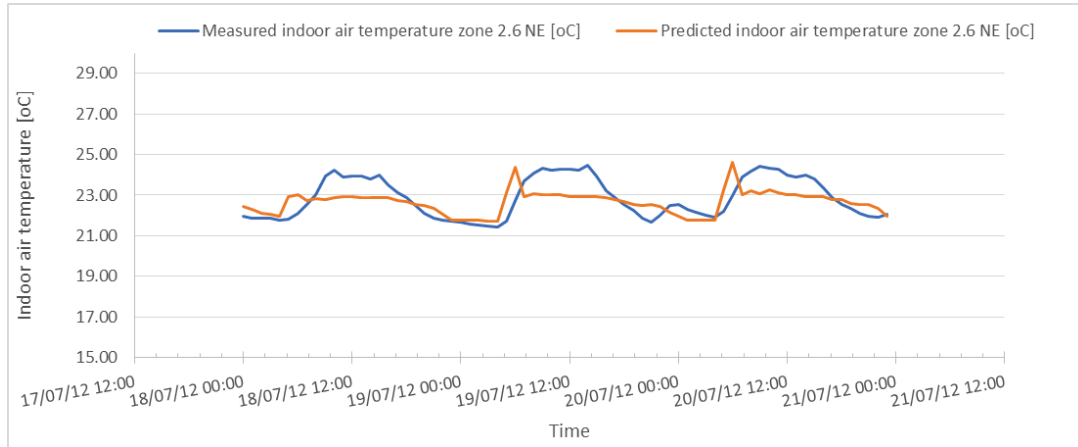


Figure A. 49: Predicted vs. measured hourly indoor air temperature for zone 2.6 NE, from 18-20 July 2012

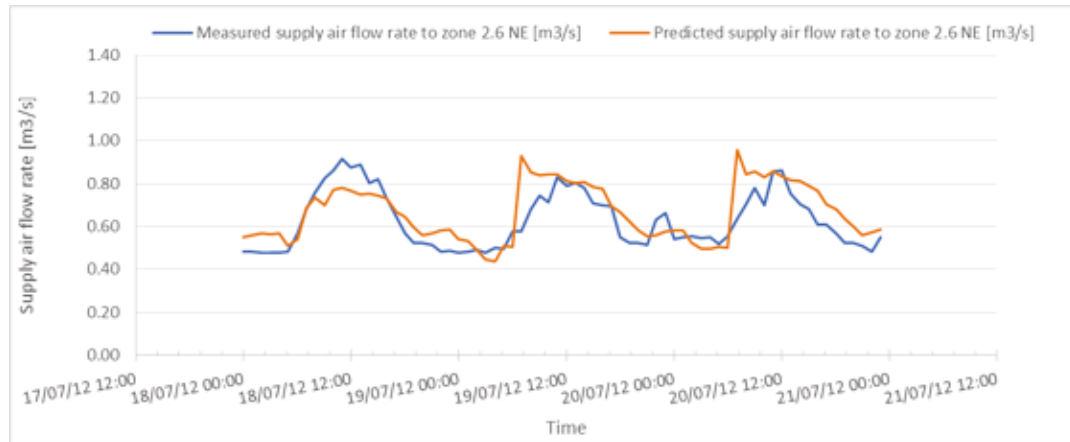


Figure A. 50: Predicted vs. measured hourly supply air flow rate to zone 2.6 NE, from 18-20 July 2012

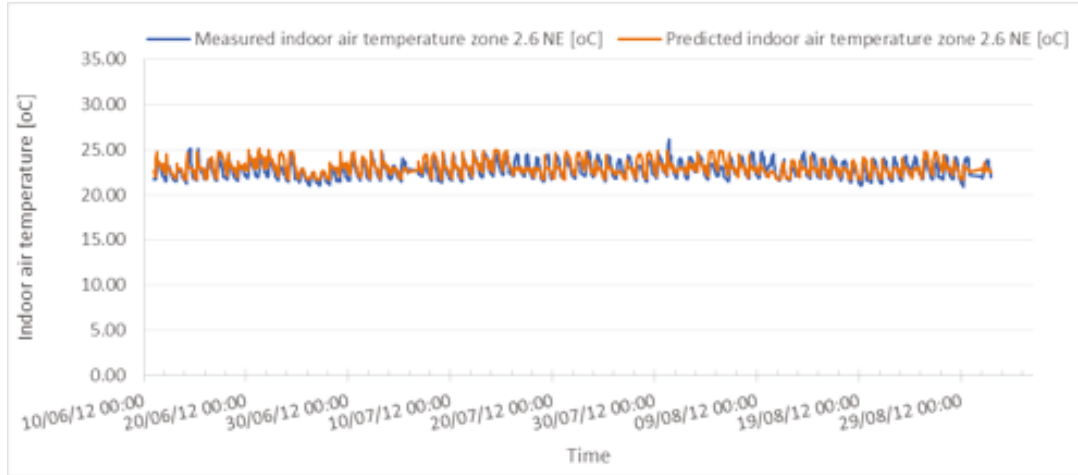


Figure A. 51: Predicted vs. measured hourly indoor air temperature for zone 2.6 NE, for summer 2012

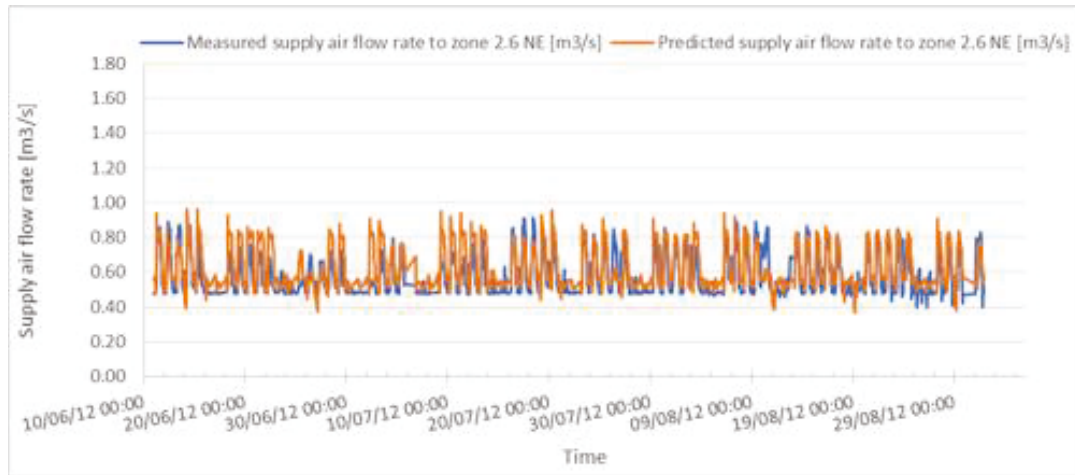


Figure A. 52: Predicted vs. measured hourly supply air flow rate to zone 2.6 NE, for summer 2012

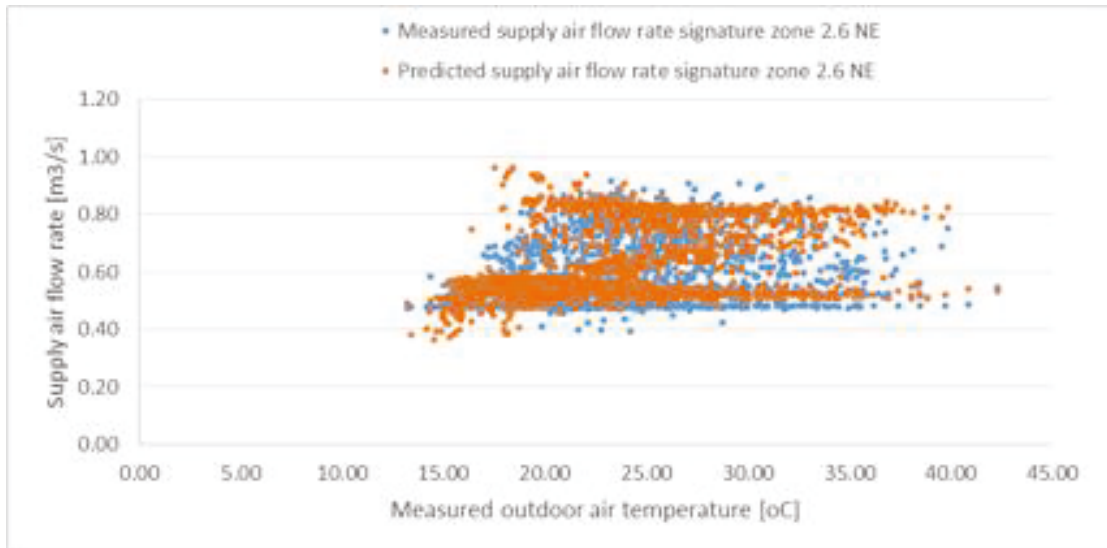


Figure A. 53: Predicted vs. measured hourly supply air flow rate signature for zone 2.6 NE, for summer 2012

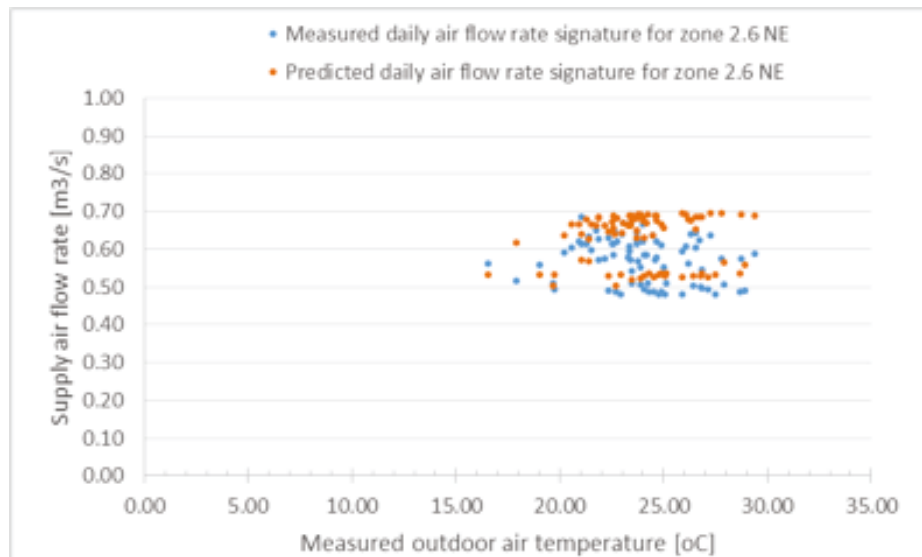


Figure A. 54: Predicted vs. measured daily supply air flow rate signature for zone 2.6 NE, for summer 2012

Zone 3.1 NE

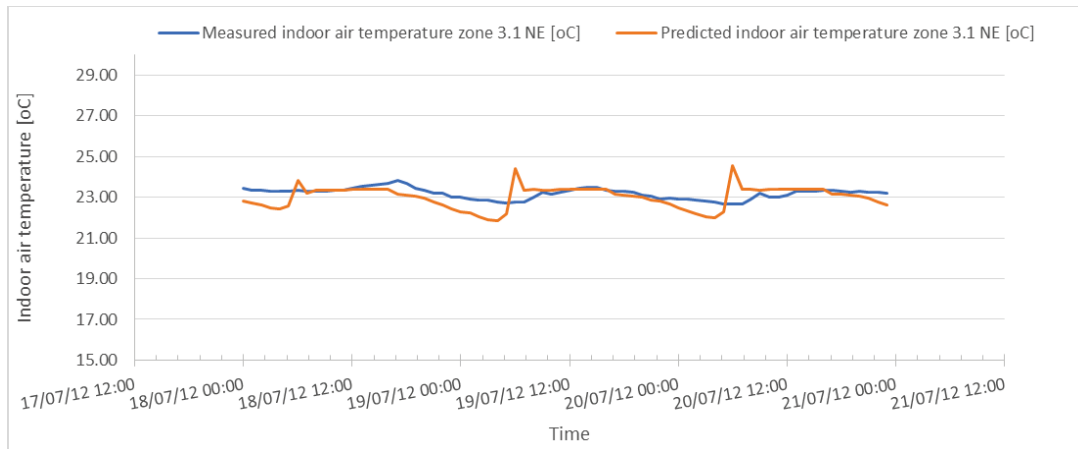


Figure A. 55: Predicted vs. measured hourly indoor air temperature for zone 3.1 NE, from 18-20 July 2012

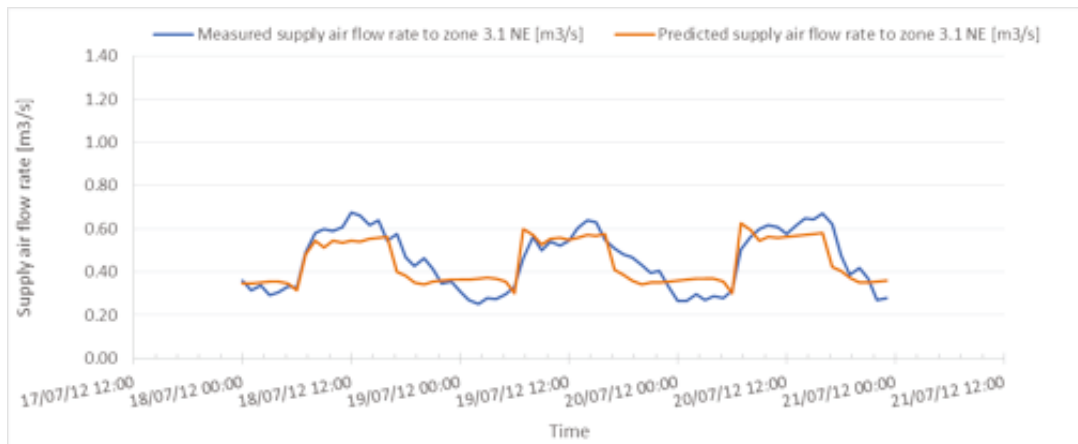


Figure A. 56: Predicted vs. measured hourly supply air flow rate for zone 3.1 NE, from 18-20 July 2012

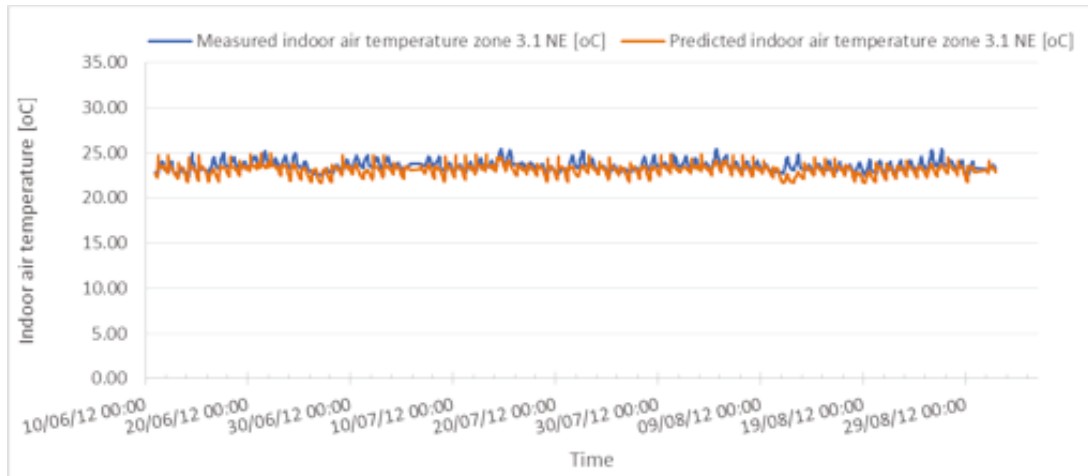


Figure A. 57: Predicted vs. measured hourly indoor air temperature for zone 3.1 NE, for summer 2012

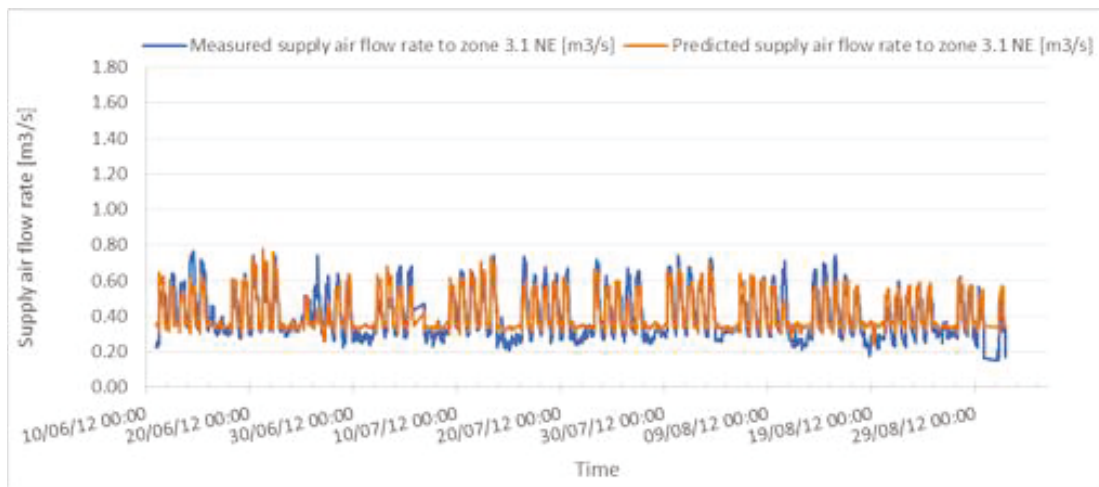


Figure A. 58: Predicted vs. measured hourly supply air flow rate to zone 3.1 NE, for summer 2012

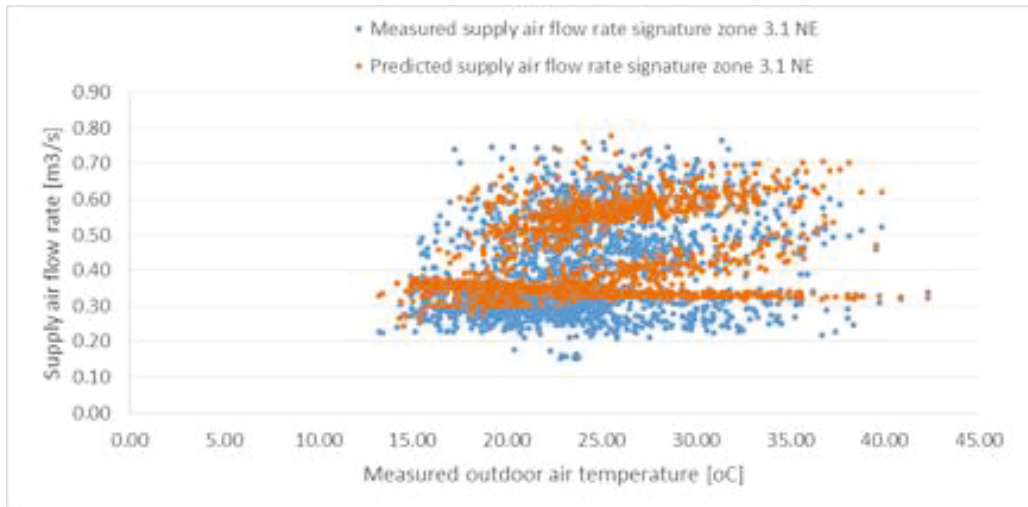


Figure A. 59: Predicted vs. measured hourly supply air flow rate signature for zone 3.1 NE, for summer 2012

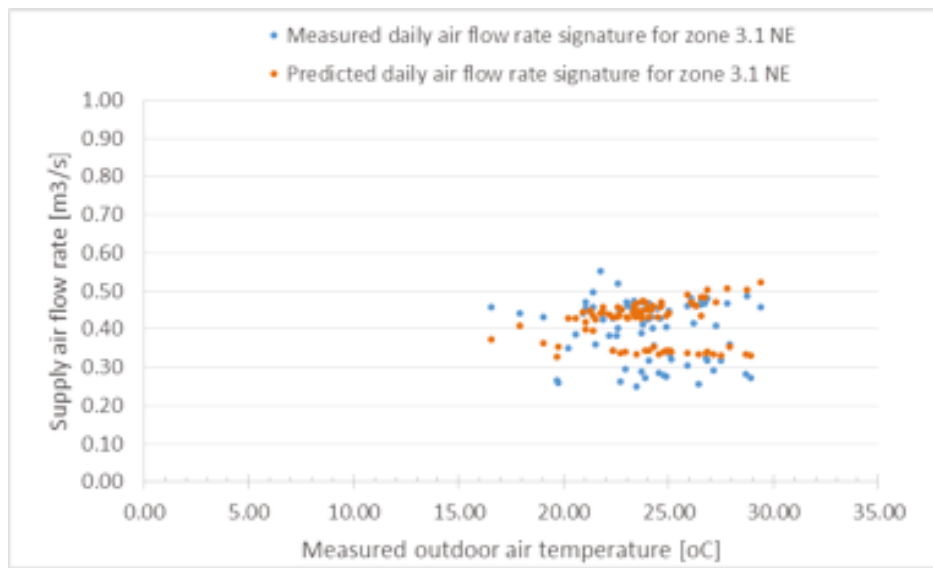


Figure A. 60: Predicted vs. measured daily supply air flow rate signature for zone 3.1 NE, for summer 2012

Zone 3.2 SW

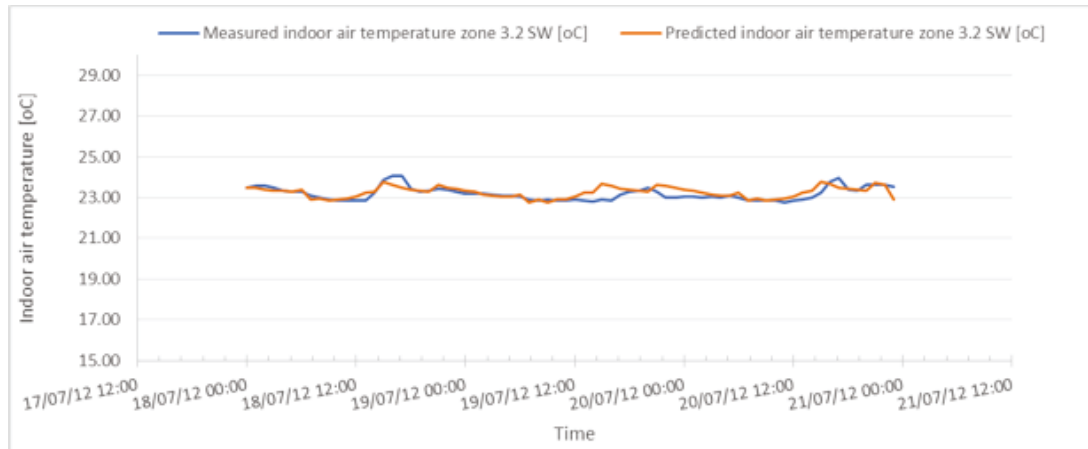


Figure A. 61: Predicted vs. measured hourly indoor air temperature for zone 3.2 SW, from 18-20 July 2012

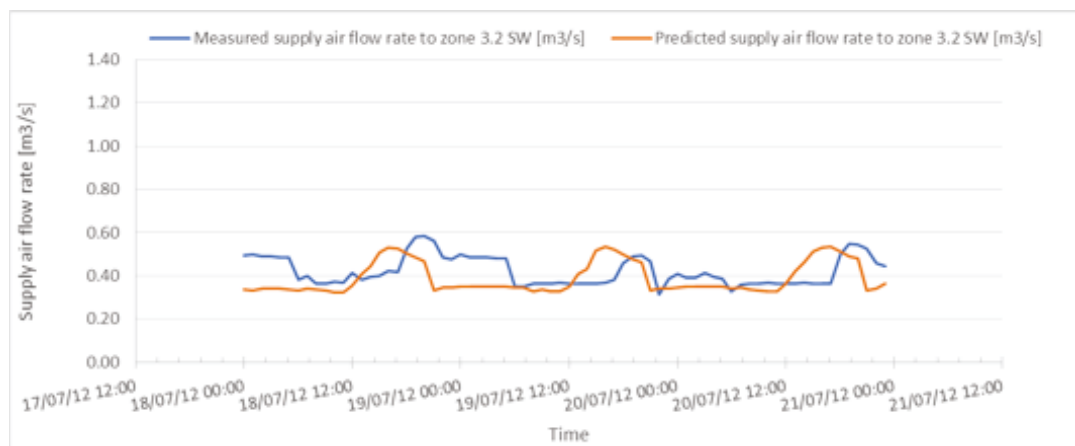


Figure A. 62: Predicted vs. measured hourly supply air flow rate to zone 3.2 SW, from 18-20 July 2012

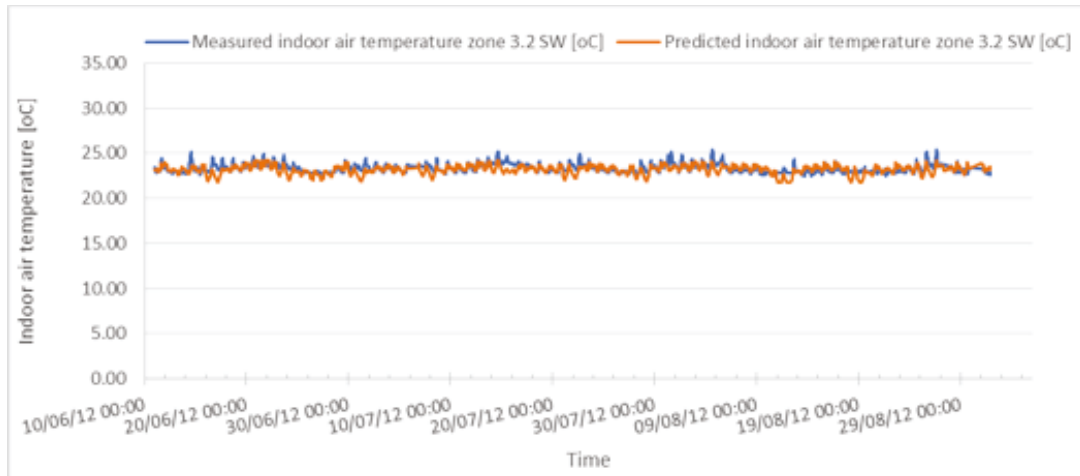


Figure A. 63: Predicted vs. measured hourly indoor air temperature for zone 3.2 SW, for summer 2012

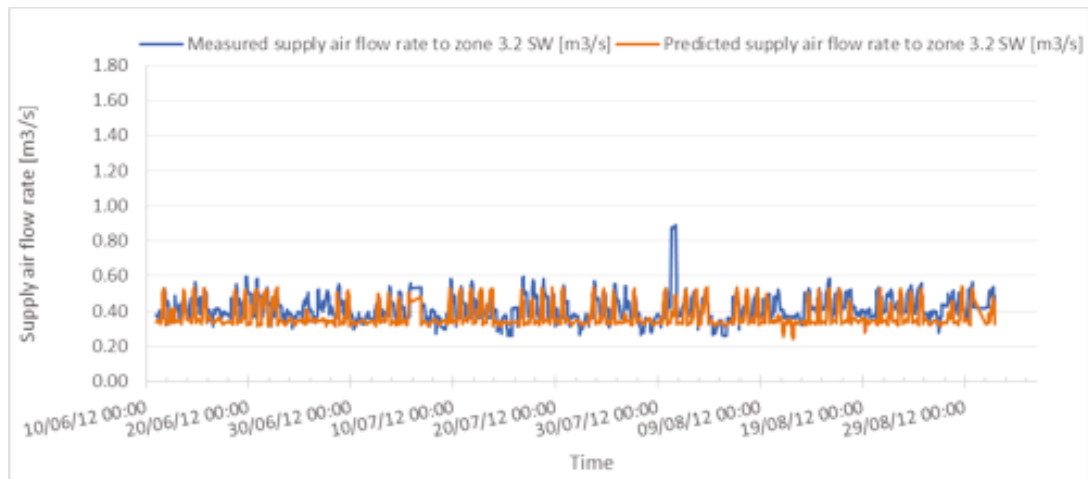


Figure A. 64: Predicted vs. measured hourly supply air flow rate to zone 3.2 SW, for summer 2012

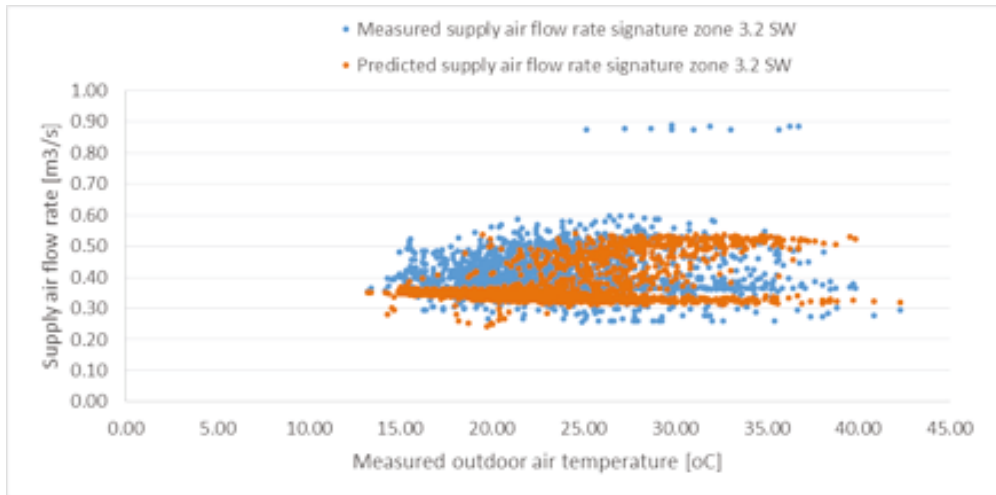


Figure A. 65: Predicted vs. measured hourly supply air flow rate signature for zone 3.2 SW, for summer 2012

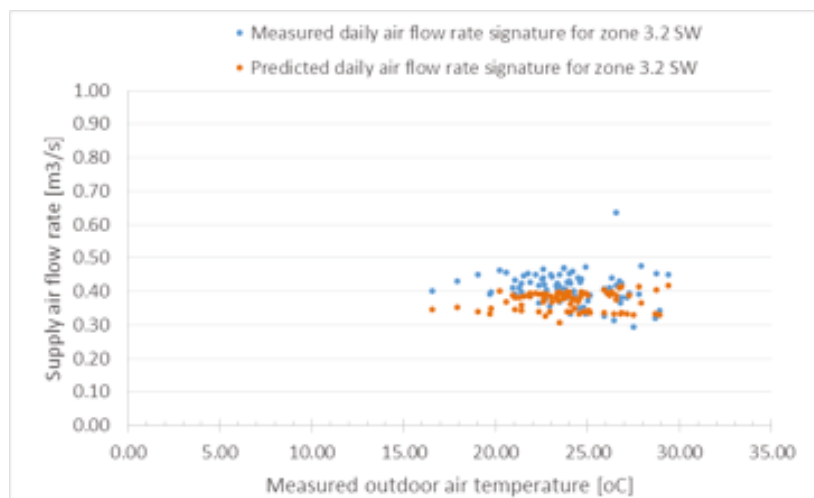


Figure A. 66: Predicted vs. measured daily supply air flow rate signature for zone 3.2 SW, for summer 2012

Zone 3.3 NW

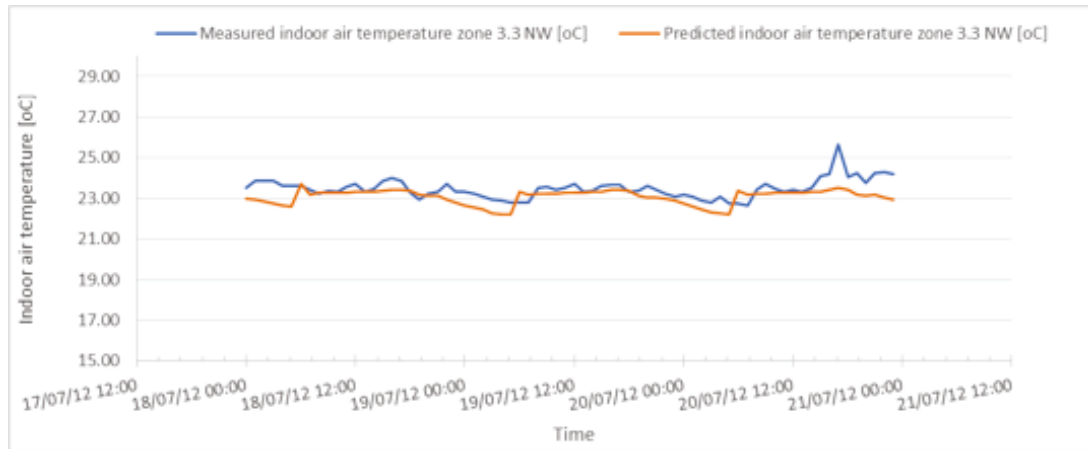


Figure A. 67: Predicted vs. measured hourly indoor air temperature for zone 3.3 NW, from 18-20 July 2012

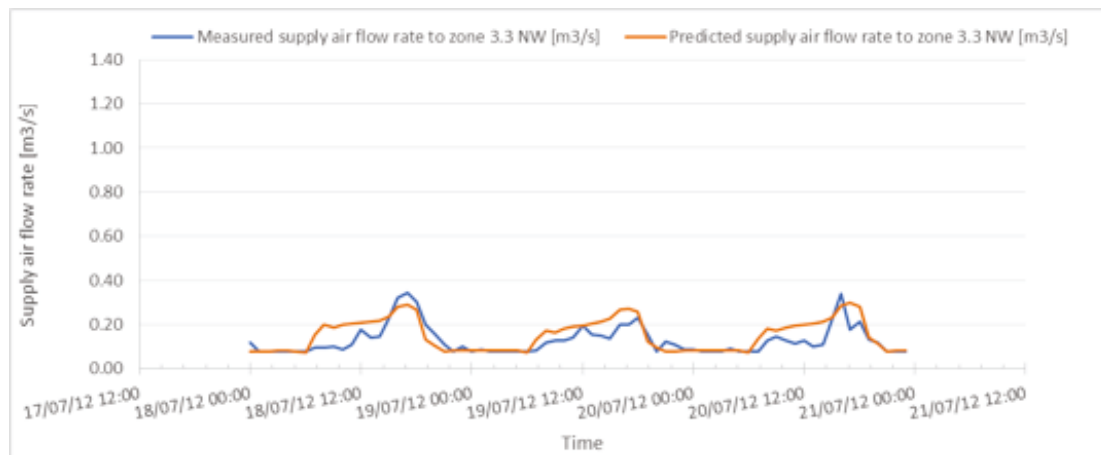


Figure A. 68: Predicted vs. measured hourly supply air flow rate to zone 3.3 NW, from 18-20 July 2012

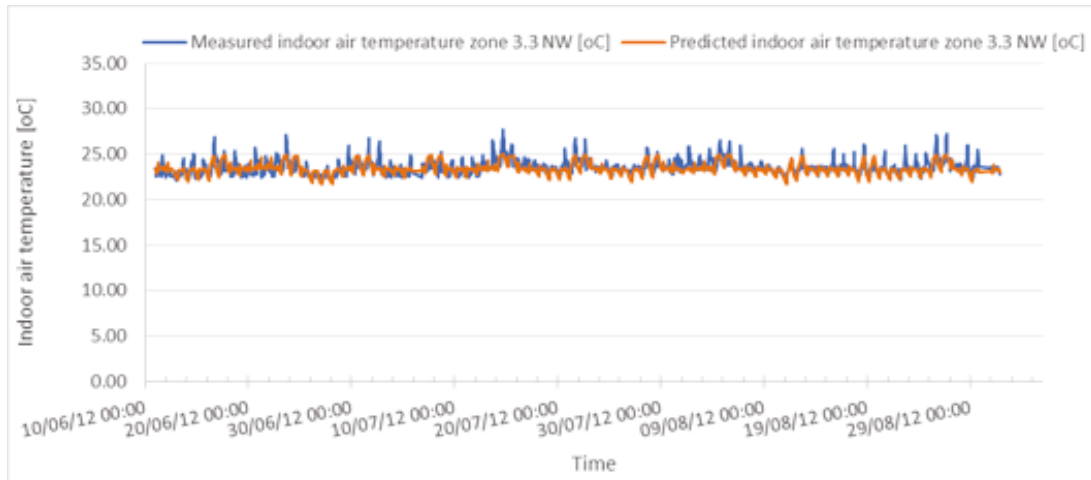


Figure A. 69: Predicted vs. measured hourly indoor air temperature for zone 3.3 NW, for summer 2012

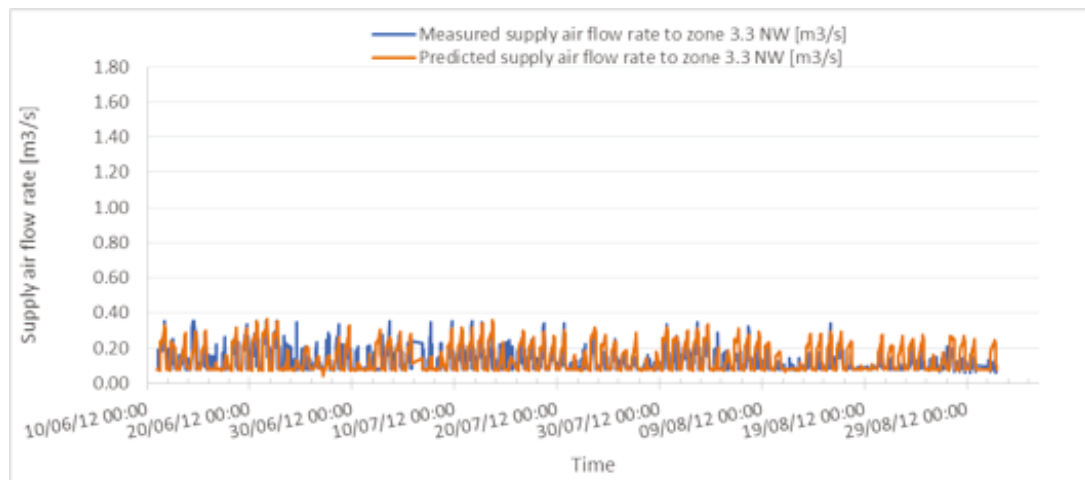


Figure A. 70: Predicted vs. measured hourly supply air flow rate for zone 3.3 NW, for summer 2012

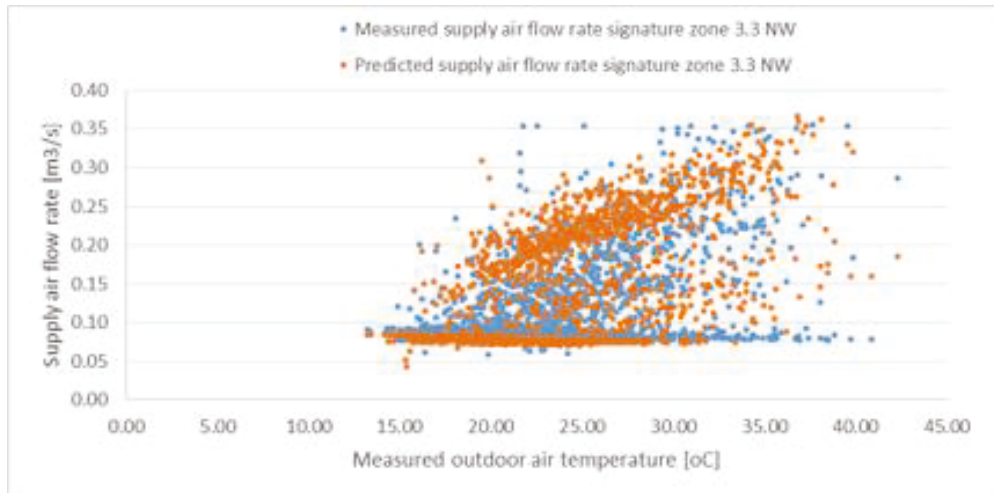


Figure A. 71: Predicted vs. measured hourly supply air flow rate signature for zone 3.3 NW, for summer 2012

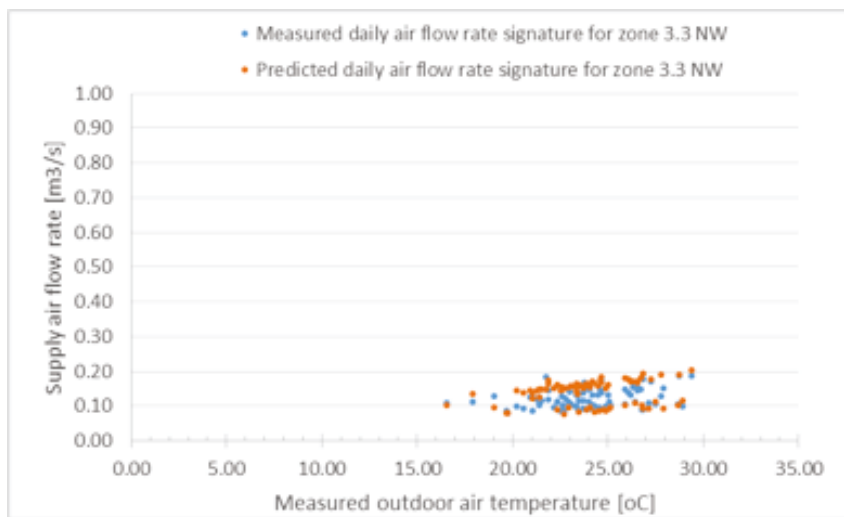


Figure A. 72: Predicted vs. measured daily supply air flow rate signature for zone 3.3 NW, for summer 2012

Zone 3.4 SW

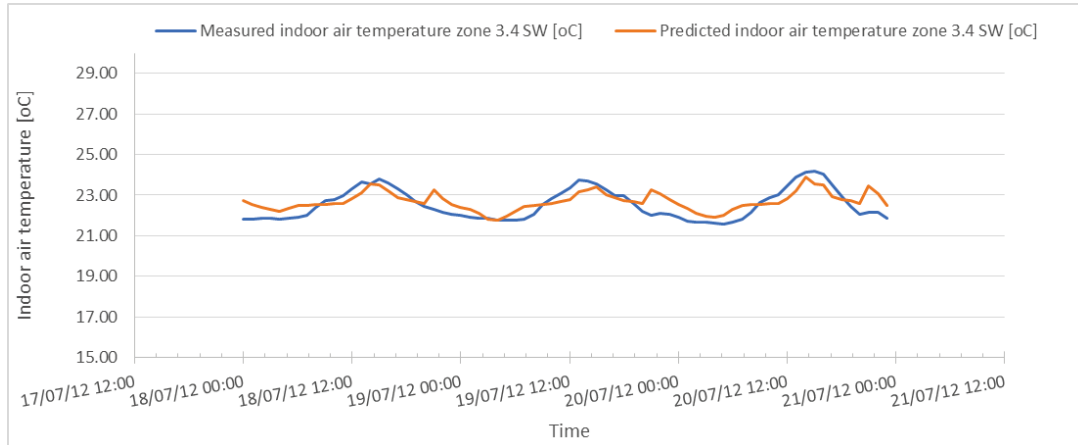


Figure A. 73: Predicted vs. measured hourly indoor air temperature for zone 3.4 SW, from 18-20 July 2012

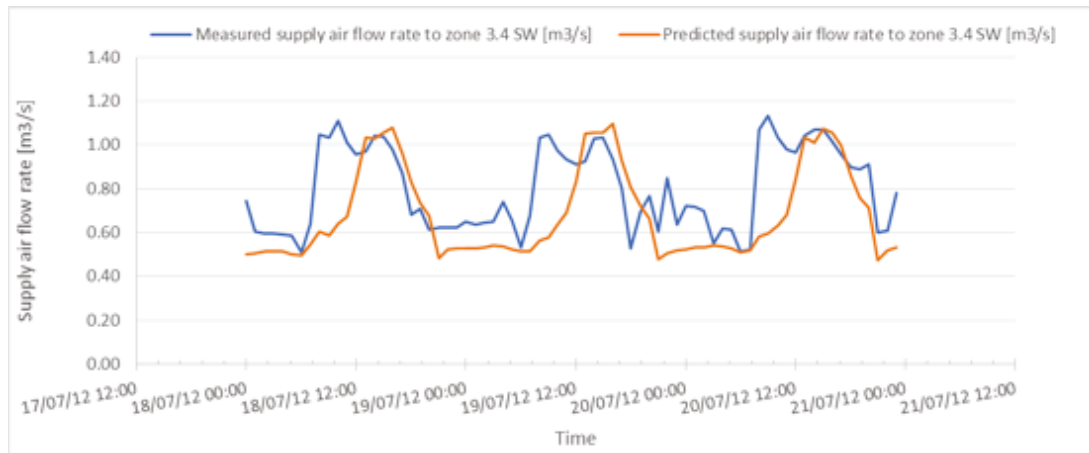


Figure A. 74: Predicted vs. measured hourly supply air flow rate for zone 3.4 SW, from 18-20 July 2012

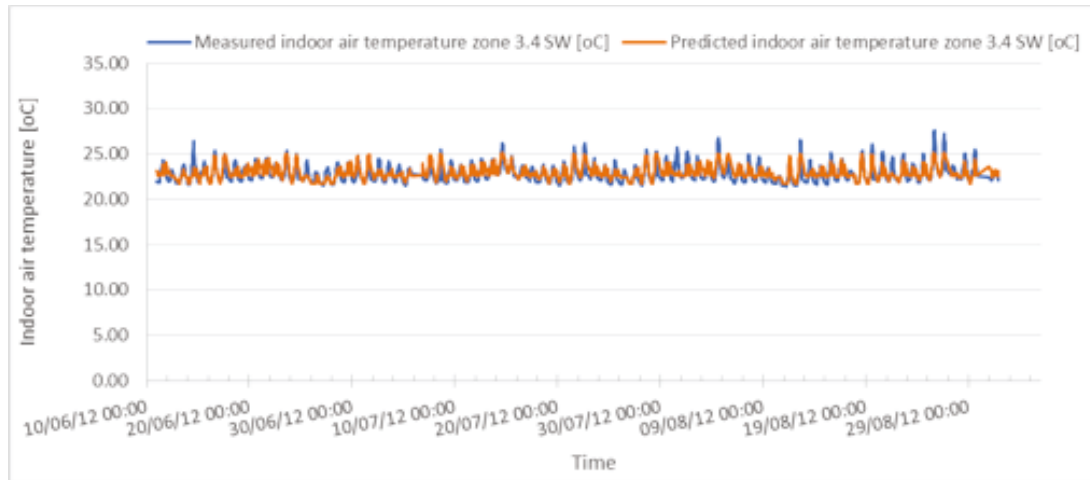


Figure A. 75: Predicted vs. measured hourly indoor air temperature for zone 3.4 SW, for summer 2012

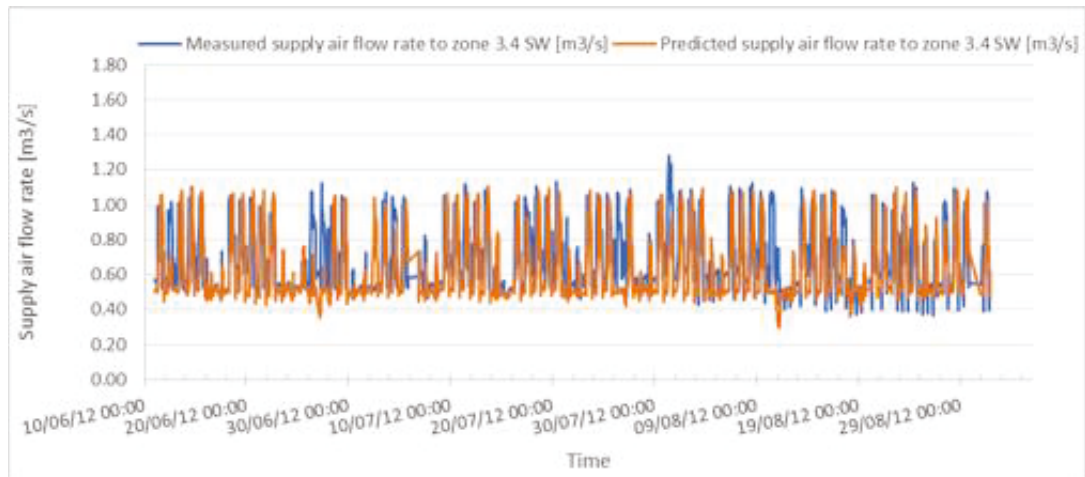


Figure A. 76: Predicted vs. measured hourly supply air flow rate for zone 3.4 SW, for summer 2012

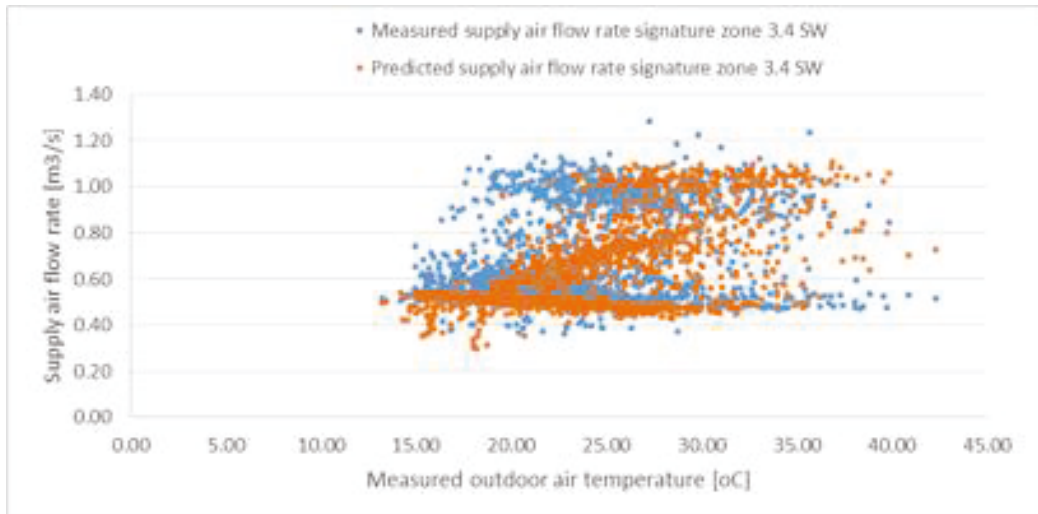


Figure A. 77: Predicted vs. measured hourly supply air flow rate signature for zone 3.4 SW, for summer 2012

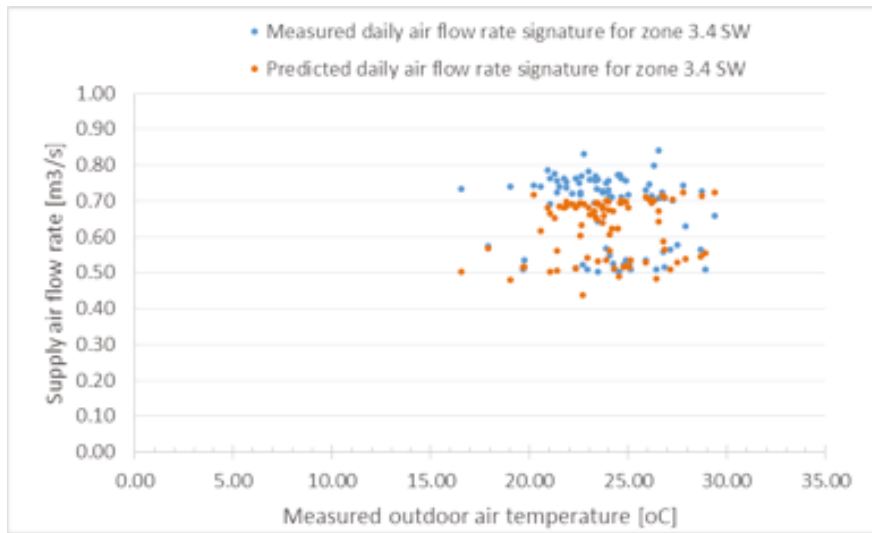


Figure A. 78: Predicted vs. measured daily supply air flow rate signature for zone 3.4 SW, for summer 2012

Zone 3.5 SE

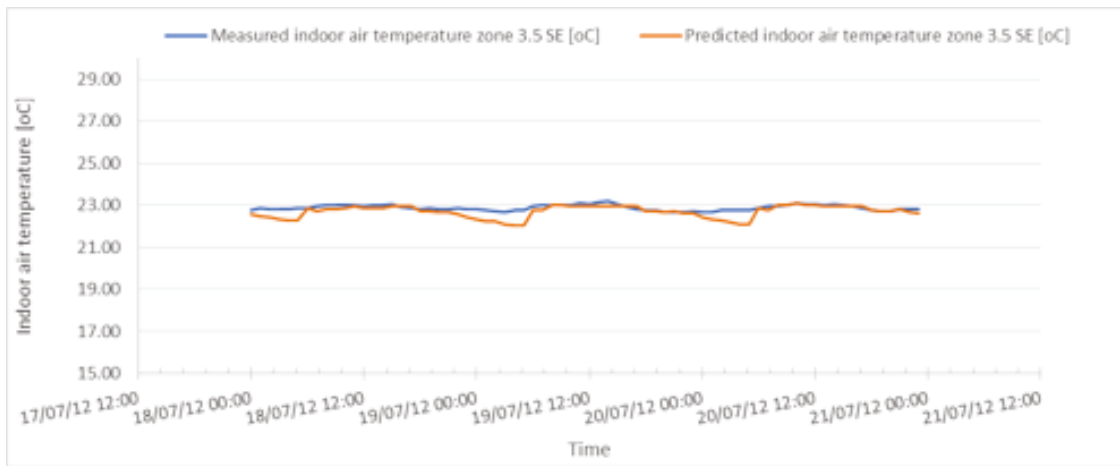


Figure A. 79: Predicted vs. measured hourly indoor air temperature for zone 3.5 SE, from 18-20 July 2012

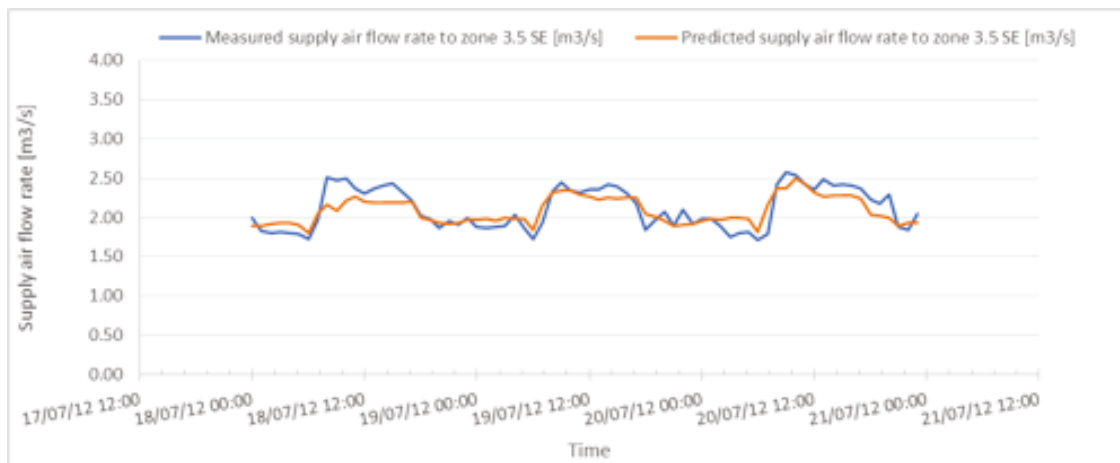


Figure A. 80: Predicted vs. measured hourly supply air flow rate to zone 3.5 SE, from 18-20 July 2012

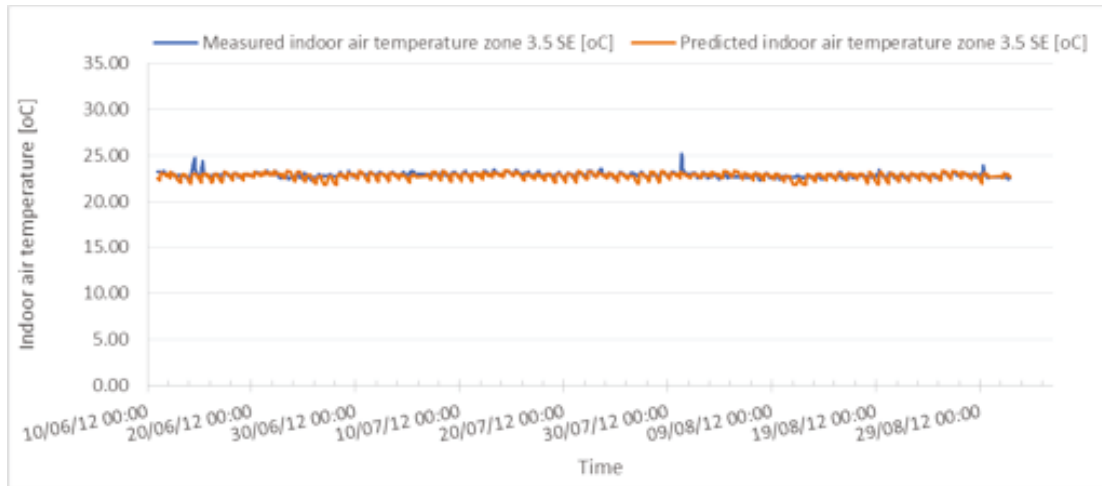


Figure A. 81: Predicted vs. measured hourly indoor air temperature for zone 3.5 SE, for summer 2012

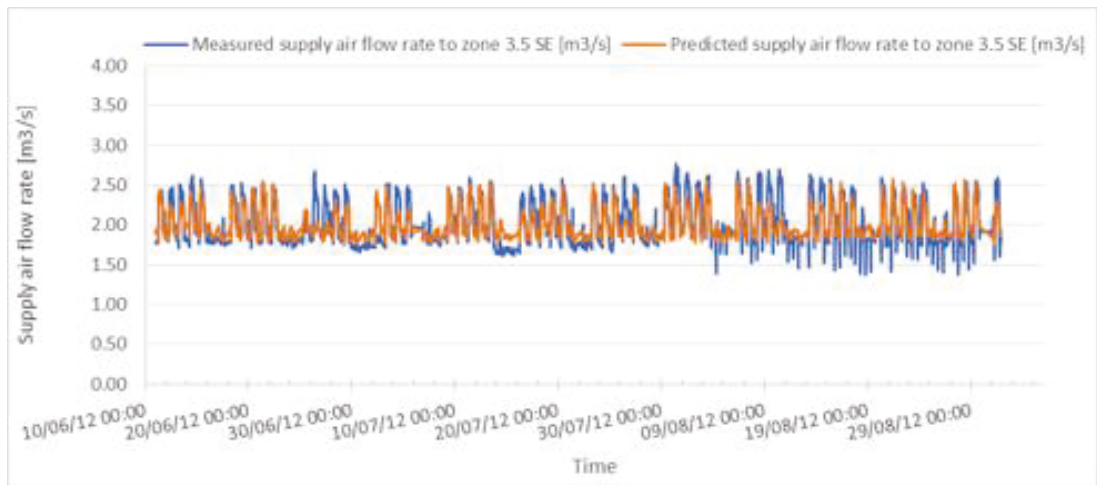


Figure A. 82: Predicted vs. measured hourly supply air flow rate to zone 3.5 SE, for summer 2012

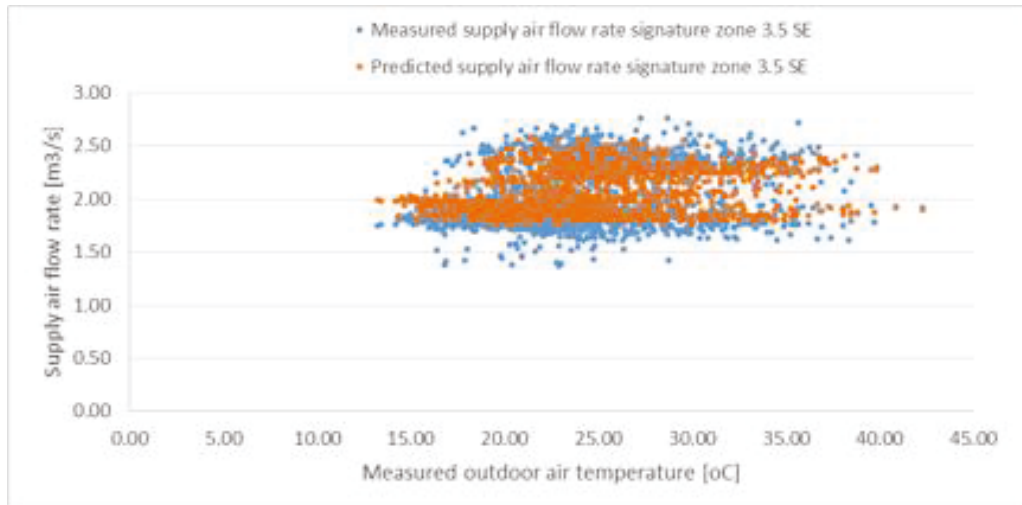


Figure A. 83: Predicted vs. measured hourly supply air flow rate signature for zone 3.5 SE, for summer 2012

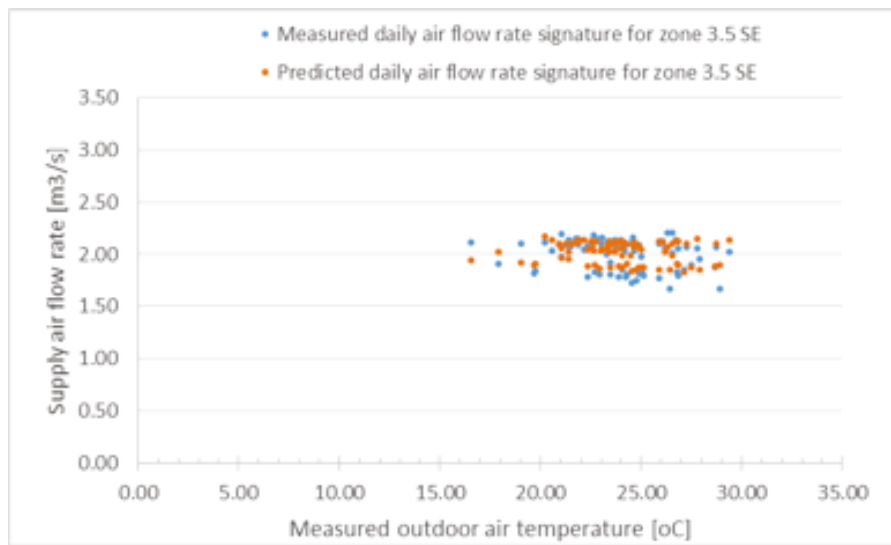


Figure A. 84: Predicted vs. measured daily supply air flow rate signature for zone 3.5 SE, for summer 2012

Zone 3.6 NE

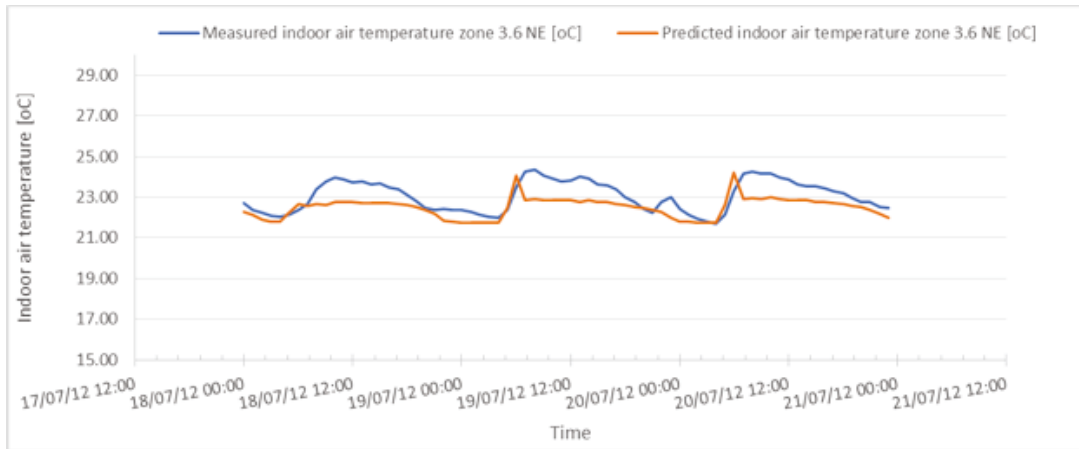


Figure A. 85: Predicted vs. measured hourly indoor air temperature for zone 3.6 NE, from 18-20 July 2012

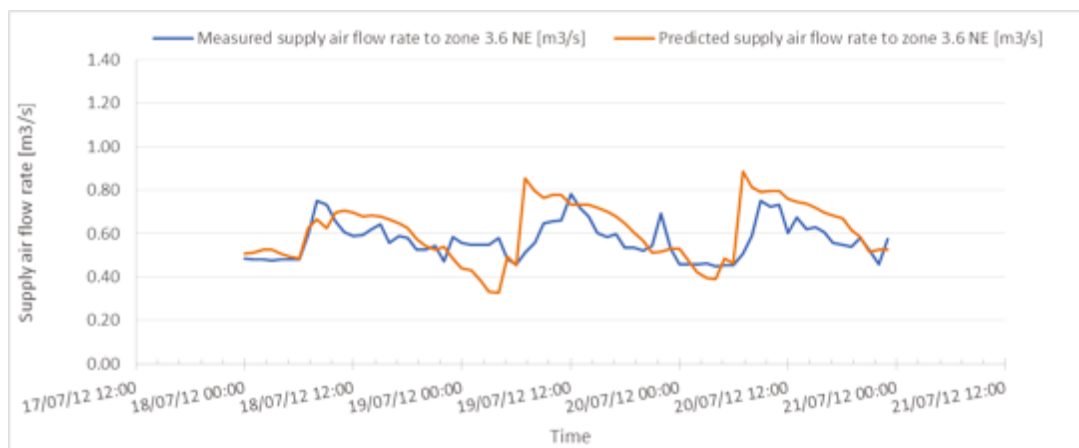


Figure A. 86: Predicted vs. measured hourly supply air flow rate to zone 3.6 NE, from 18-20 July 2012

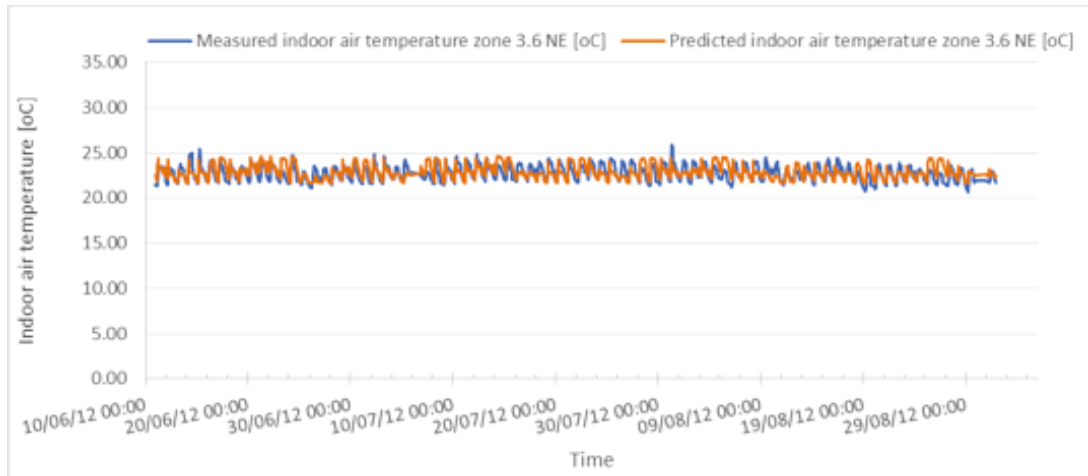


Figure A. 87: Predicted vs. measured hourly indoor air temperature for zone 3.6 NE, for summer 2012

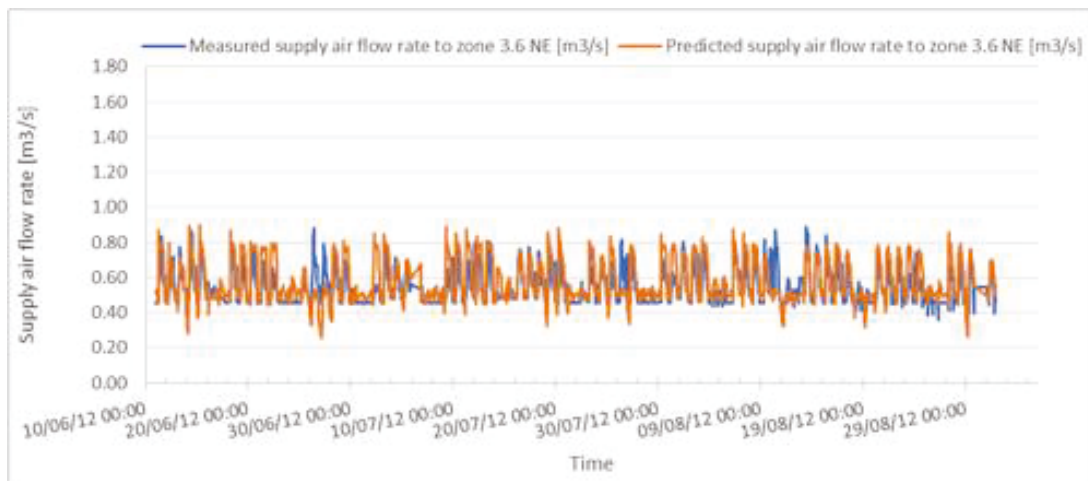


Figure A. 88: Predicted vs. measured hourly supply air flow rate to zone 3.6 NE, for summer 2012

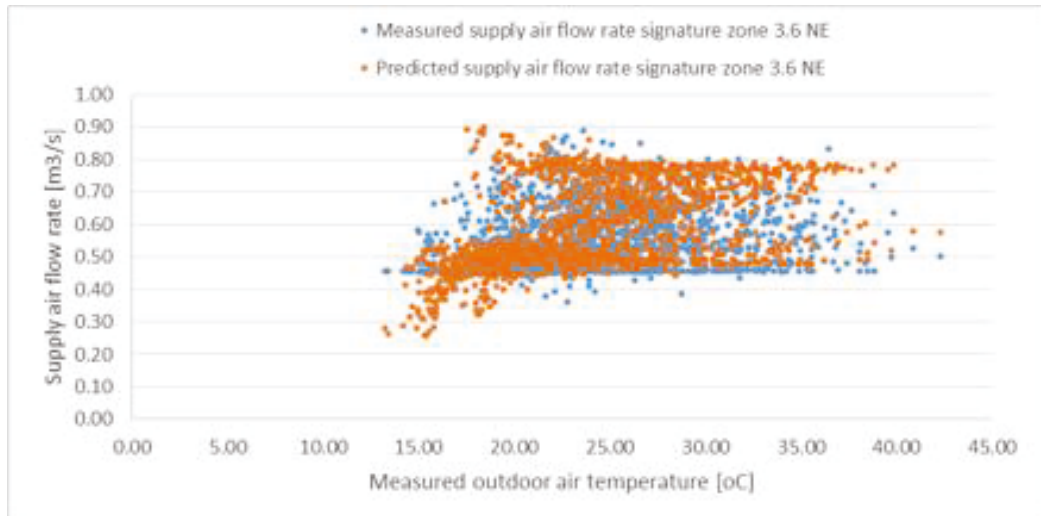


Figure A. 89: Predicted vs. measured hourly supply air flow rate signature for zone 3.6 NE, for summer 2012

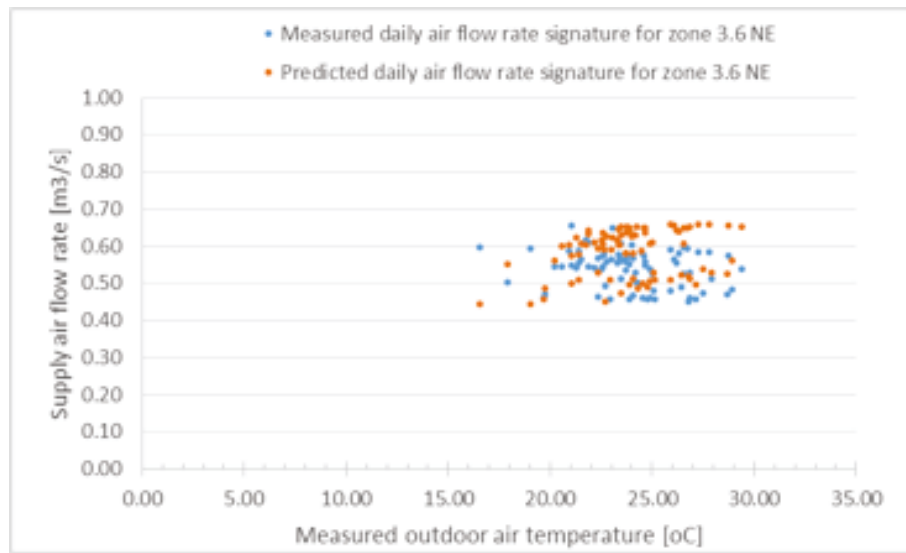


Figure A. 90: Predicted vs. measured daily supply air flow rate signature for zone 3.6 NE, for summer 2012

Appendix B: Histograms of the difference between predicted and measured supply air flow rate to each zone

This section presents for each zone, the histogram of the difference between predicted and measured supply air flow rate to each zone. The hypothesis testing requires that the distribution of the values analyzed, in this case the difference between predictions and measurements, to present a normal distribution or to be close to a normal distribution.

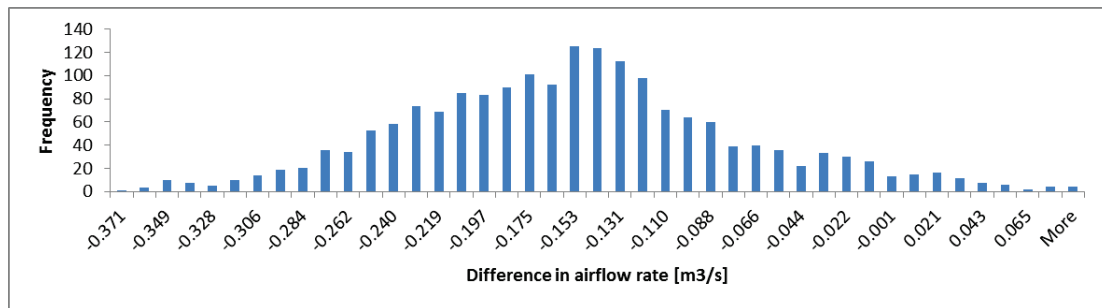


Figure B. 1: Histogram for the difference between hourly predicted and measured supply air flow rate to zone 1.3 NW for the summer period

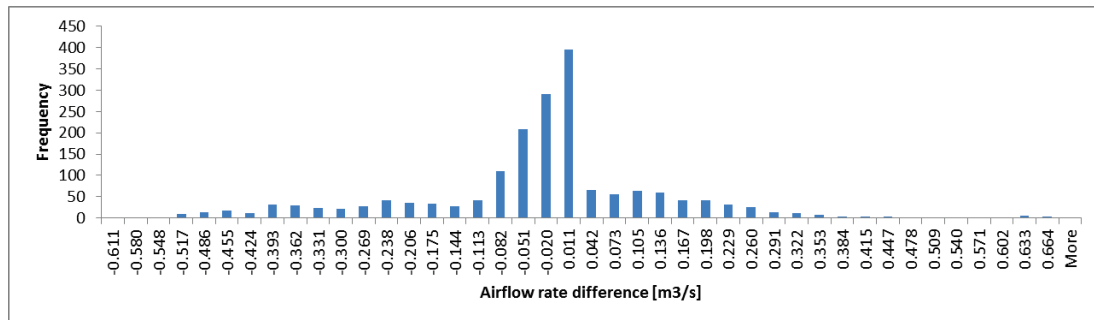


Figure B. 2: Histogram for the difference between hourly predicted and measured supply air flow rate to zone 1.4 SW for the summer period

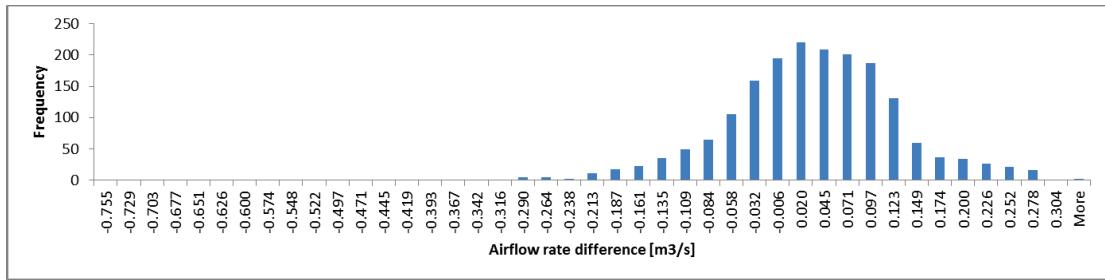


Figure B. 3: Histogram for the difference between hourly predicted and measured supply air flow rate to zone 1.5 SE for the summer period

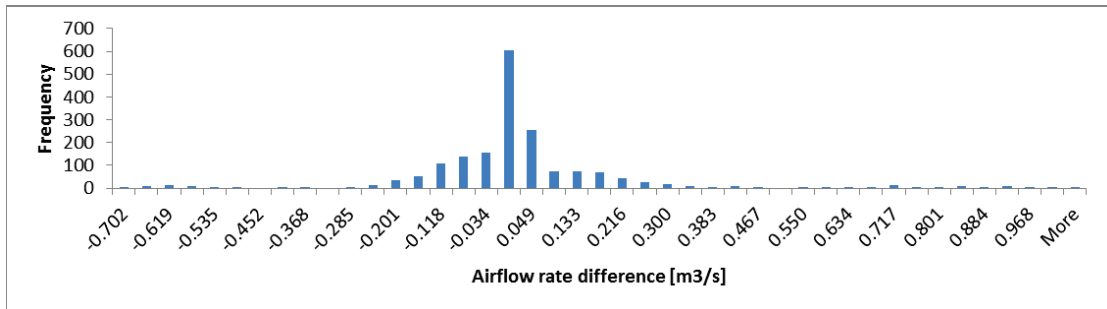


Figure B. 4: Histogram for the difference between hourly predicted and measured supply air flow rate to zone 1.6 NE for the summer period

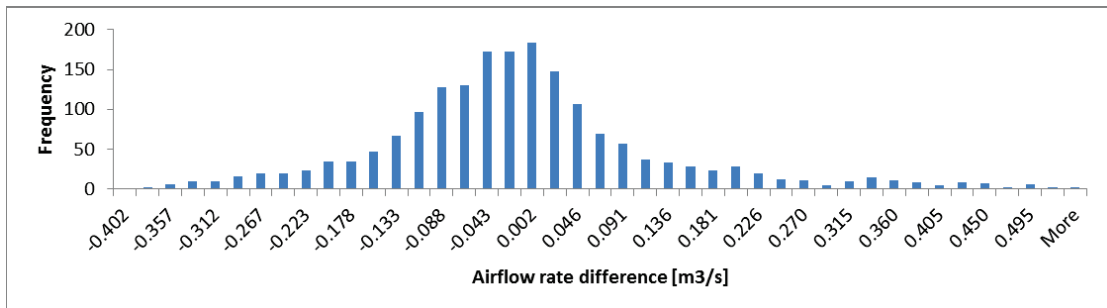


Figure B. 5: Histogram for the difference between hourly predicted and measured supply air flow rate to zone 2.1 NE for the summer period

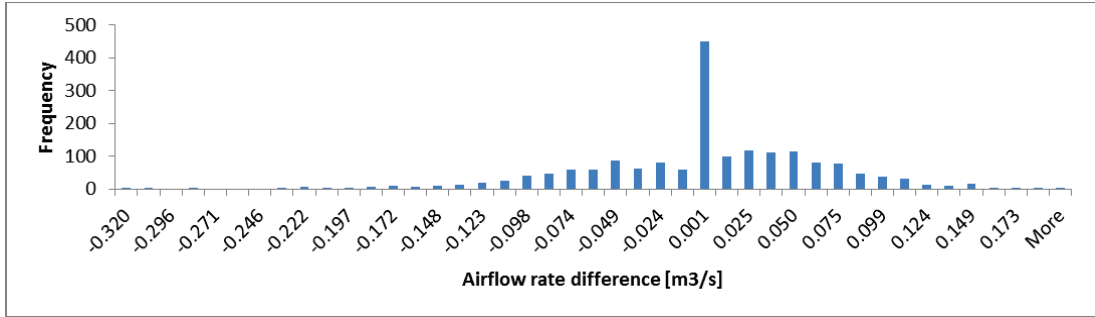


Figure B. 6: Histogram for the difference between hourly predicted and measured supply air flow rate to zone 2.3 NW for the summer period

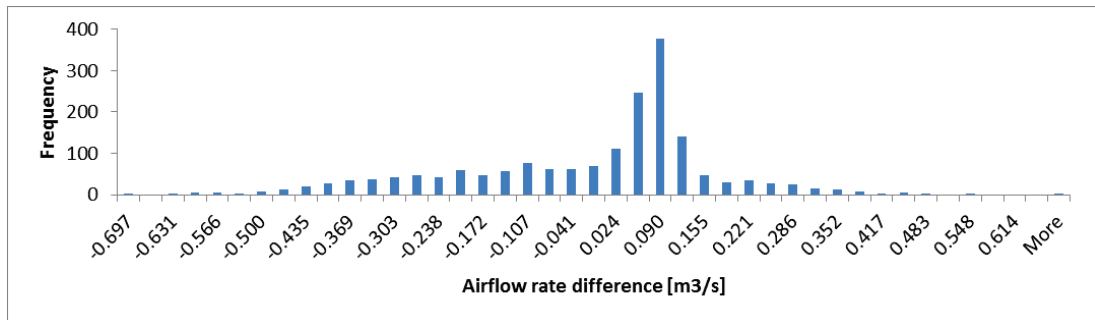


Figure B. 7: Histogram for the difference between hourly predicted and measured supply air flow rate to zone 2.4 SW for the summer period

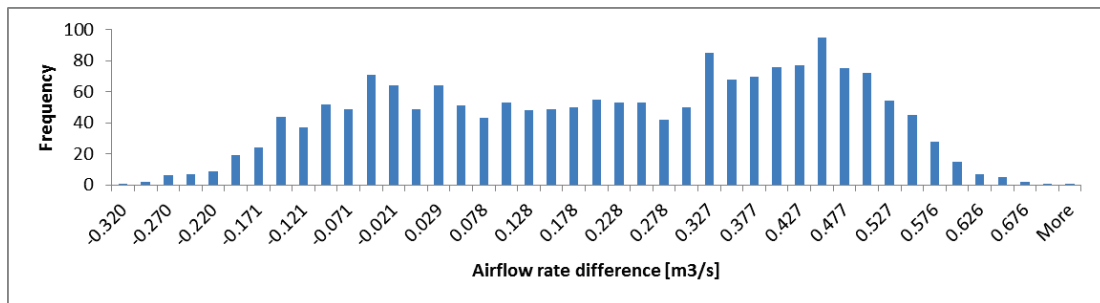


Figure B. 8: Histogram for the difference between hourly predicted and measured supply air flow rate to zone 2.5 SE for the summer period

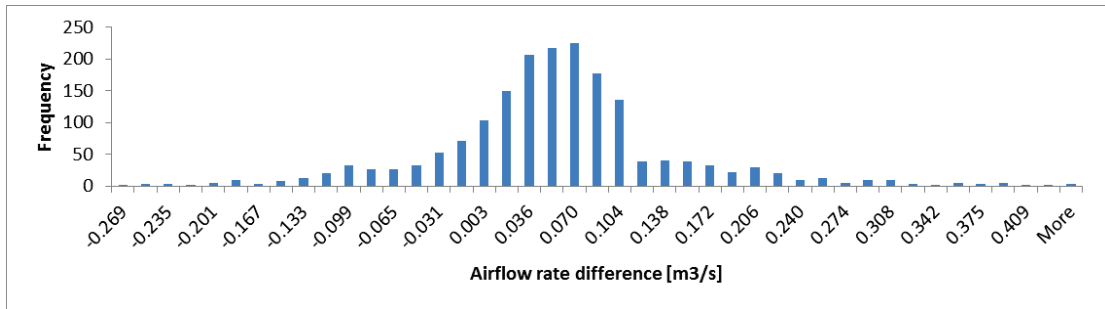


Figure B. 9: Histogram for the difference between hourly predicted and measured supply air flow rate to zone 2.6 NE for the summer period

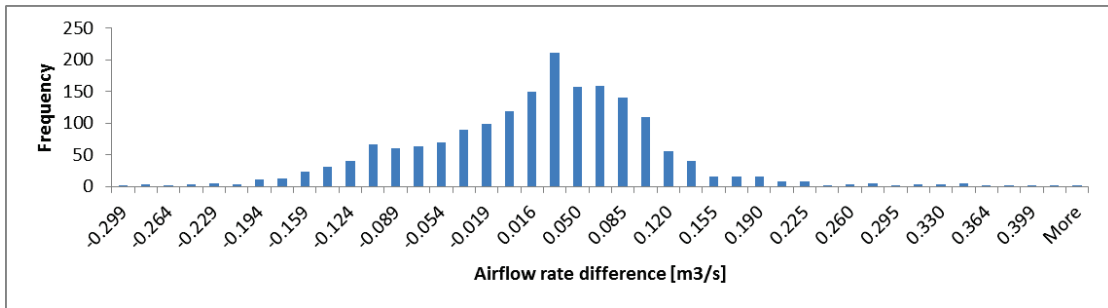


Figure B. 10: Histogram for the difference between hourly predicted and measured supply air flow rate to zone 3.1 NE for the summer period

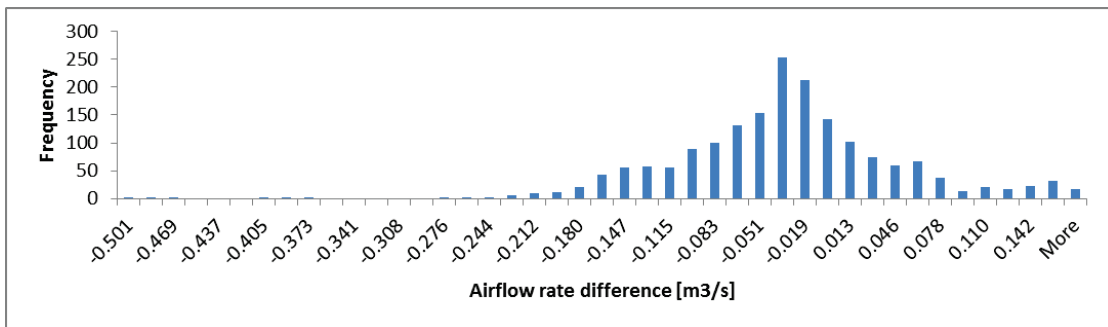


Figure B. 11: Histogram for the difference between hourly predicted and measured supply air flow rate to zone 3.2 SW for the summer period

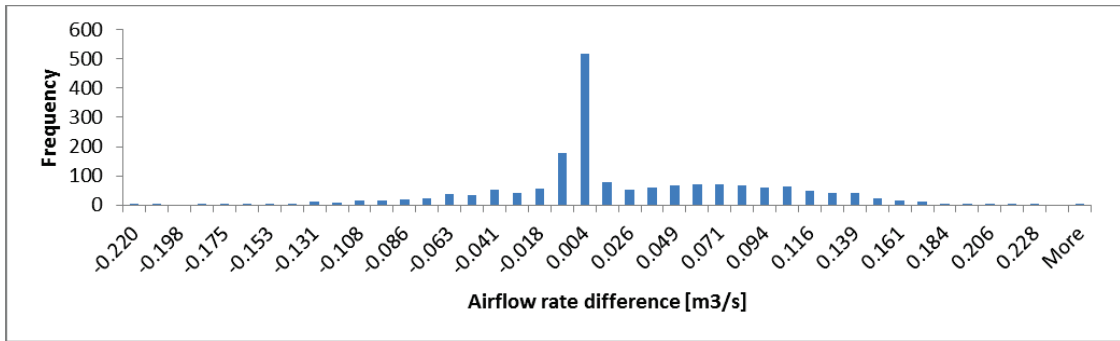


Figure B. 12: Histogram for the difference between hourly predicted and measured supply air flow rate to zone 3.3 NW for the summer period

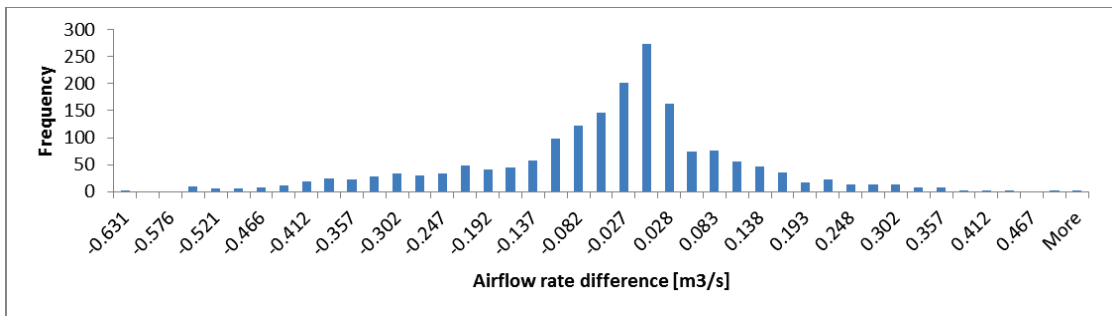


Figure B. 13: Histogram for the difference between hourly predicted and measured supply air flow rate to zone 3.4 SW for the summer period

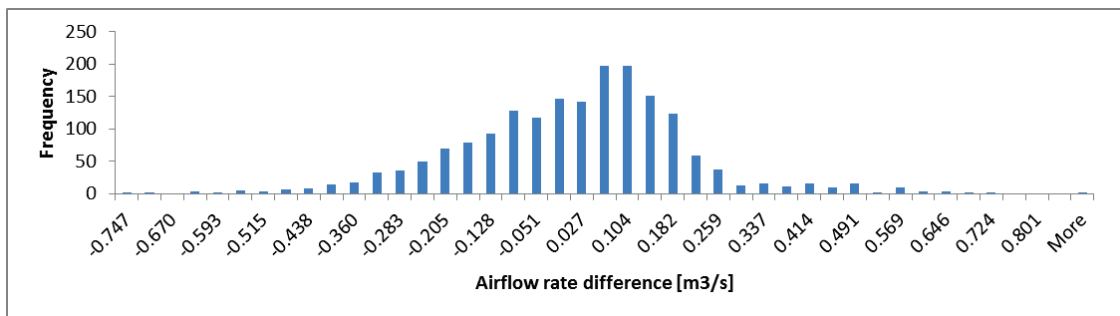


Figure B. 14: Histogram for the difference between hourly predicted and measured supply air flow rate to zone 3.5 SE for the summer period

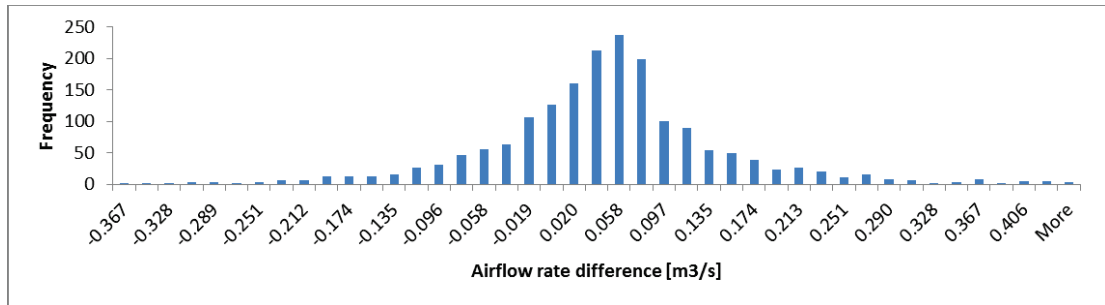


Figure B. 15: Figure B. 14: Histogram for the difference between hourly predicted and measured supply air flow rate to zone 3.6 NE for the summer period

Appendix C: Histograms for the difference between the predicted and measured summation of air flow rates supplied to zones

This section presents histograms for the difference between predicted and measured summation of air flow rates supplied to the building for hourly and daily values.

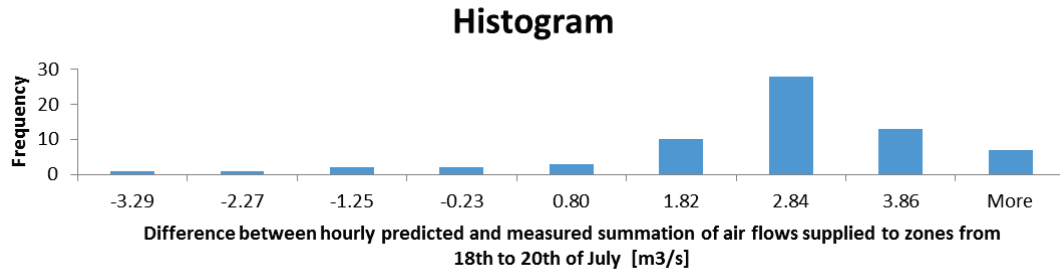


Figure C. 1: Histogram of the difference between hourly predicted and measured summation of air flow rates supplied to zones from 18-20 July

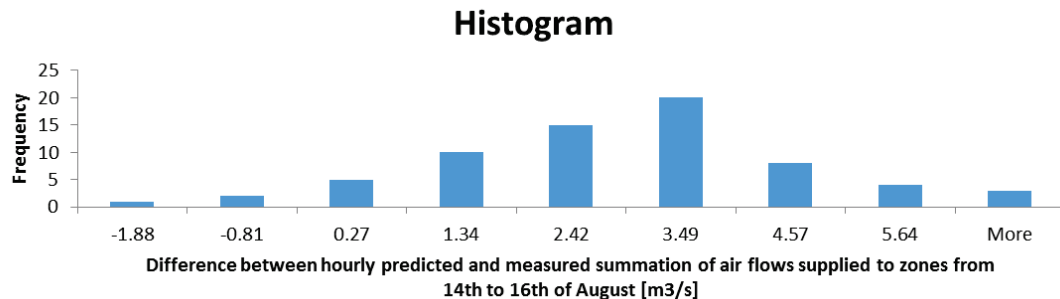


Figure C. 2: Histogram of the difference between hourly predicted and measured summation of air flow rates supplied to zones from 14-16 August

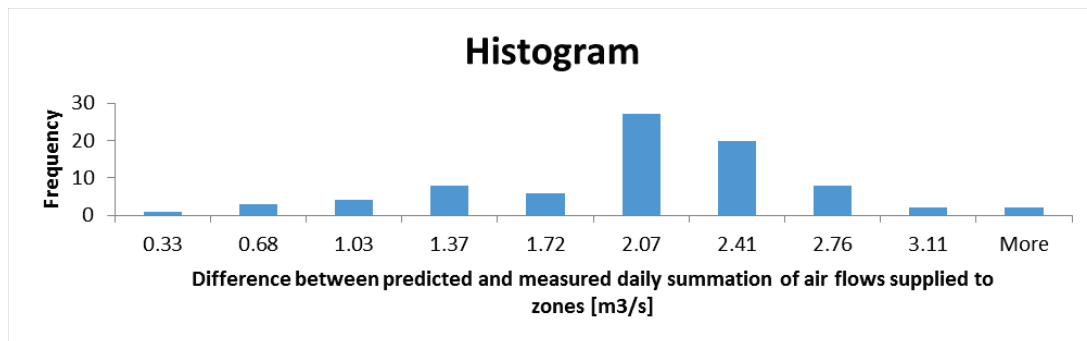


Figure C. 3: Histogram of the difference between predicted and measured daily summation of air flow rates to zones for summer period

Appendix D: Results of predictions for each zone with approach A and B from 18th to 20th July 2012

Zone 1.3 NW

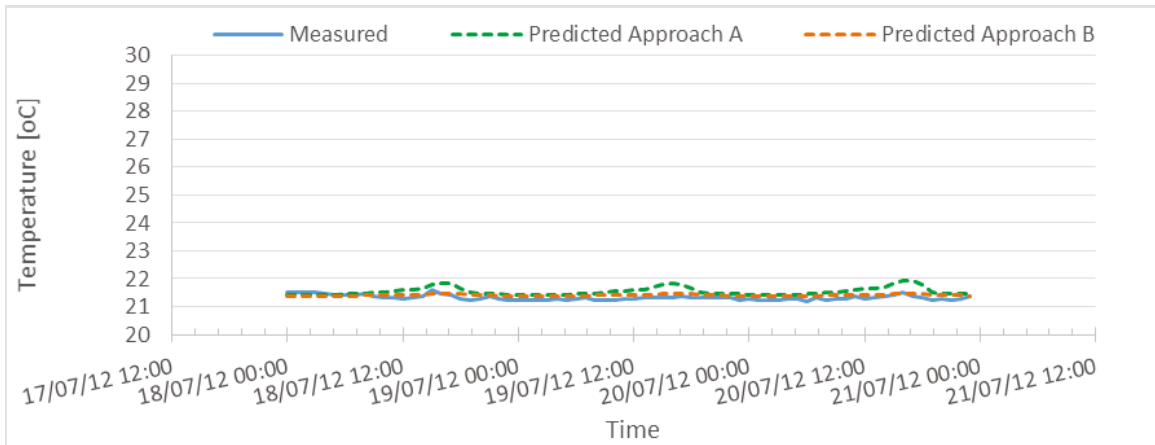


Figure D. 1: Measured vs. predicted indoor air temperature in zone 1.3 NW when using equivalent step-change schedules and when using the RP-1093 schedule, from 18th to 20th of July 2012

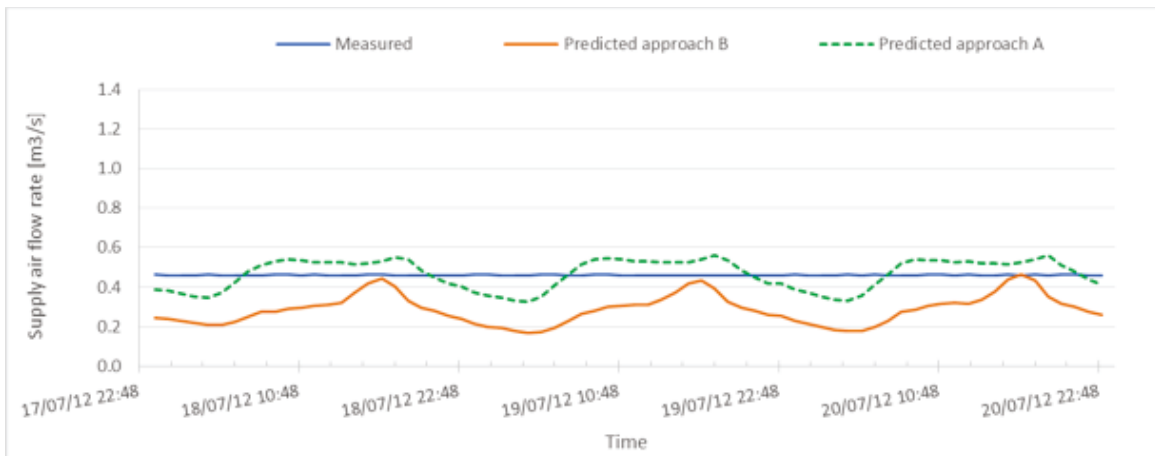


Figure D. 2: Measured vs. predicted supply air flow rate in zone 1.3 NW when using equivalent step-change schedules and when using the RP-1093 schedule, from 18th to 20th of July 2012

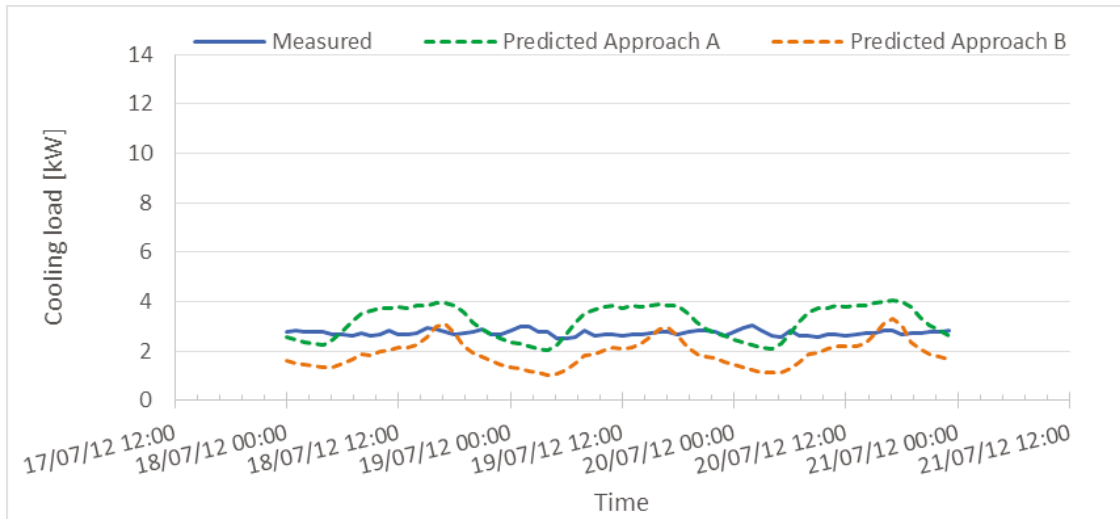


Figure D. 3: Measured vs. predicted cooling load in zone 1.3 NW when using equivalent step-change schedules and when using the RP-1093 schedule, from 18th to 20th of July 2012

Zone 1.4 NW

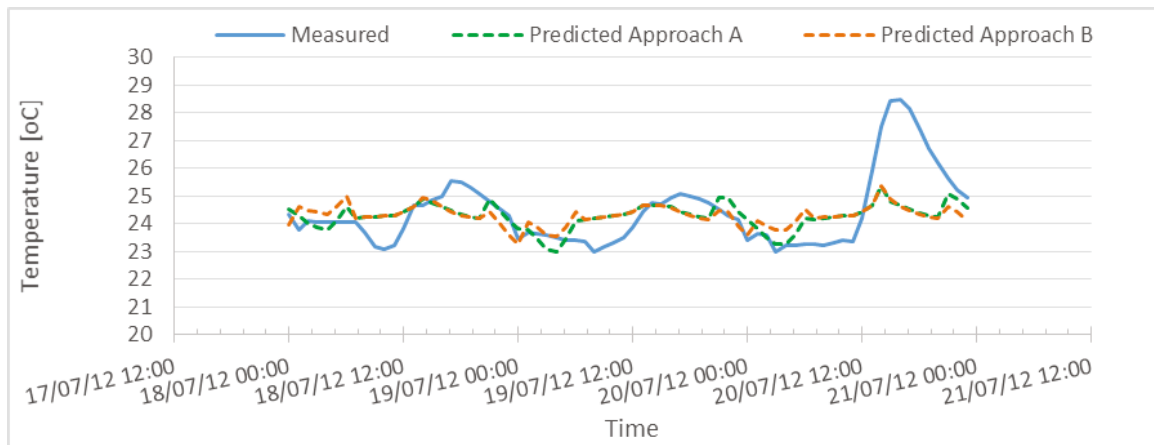


Figure D. 4: Measured vs. indoor air temperature in zone 1.4 SW when using equivalent step-change schedules and when using the RP-1093 schedule, from 18th to 20th of July 2012

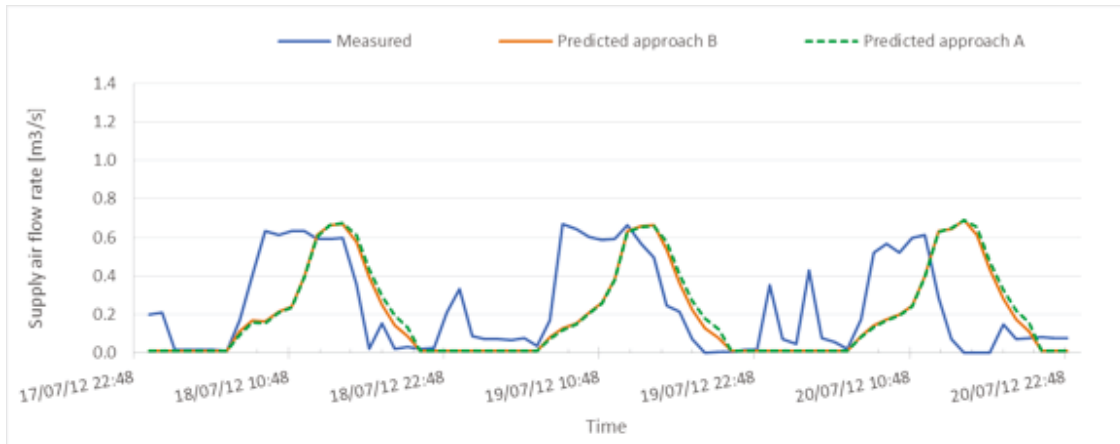


Figure D. 5: Measured vs. predicted supply air flow rate in zone 1.4 SW when using equivalent step-change schedules and when using the RP-1093 schedule, from 18th to 20th of July 2012

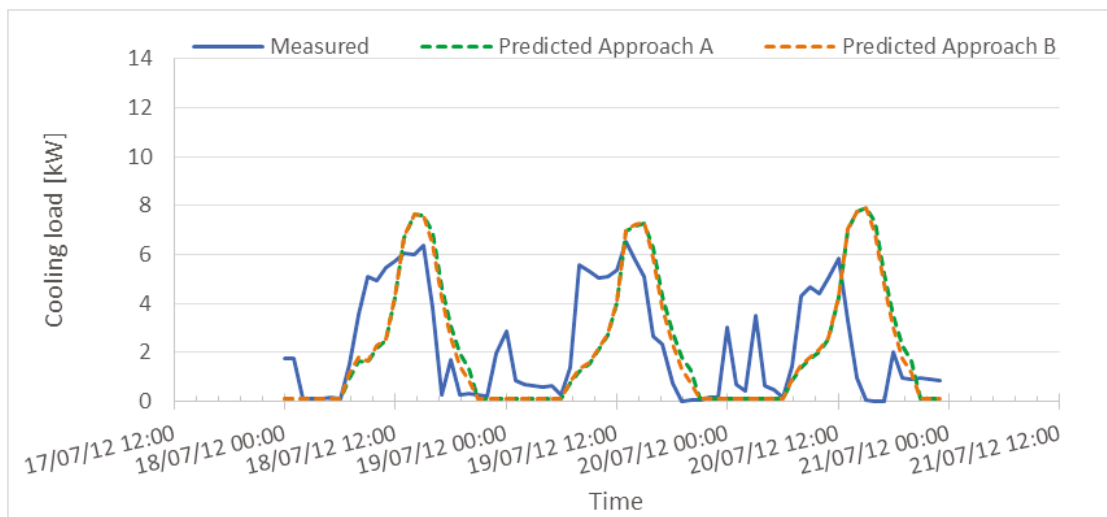


Figure D. 6: Measured vs. predicted cooling load in zone 1.4 SW when using equivalent step-change schedules and when using the RP-1093 schedule, from 18th to 20th of July 2012

Zone 1.5 SE

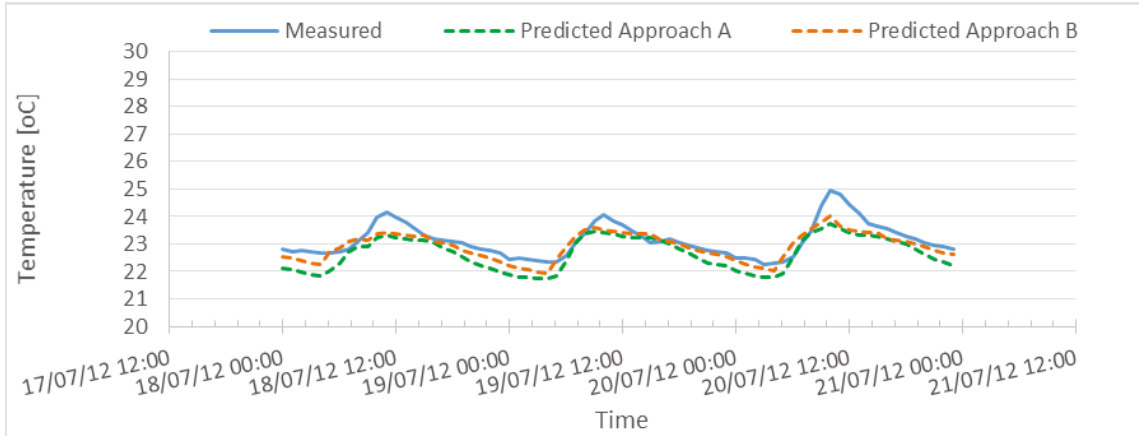


Figure D. 7: Measured vs. predicted indoor air temperature in zone 1.5 SE when using equivalent step-change schedules and when using the RP-1093 schedule, from 18th to 20th of July 2012

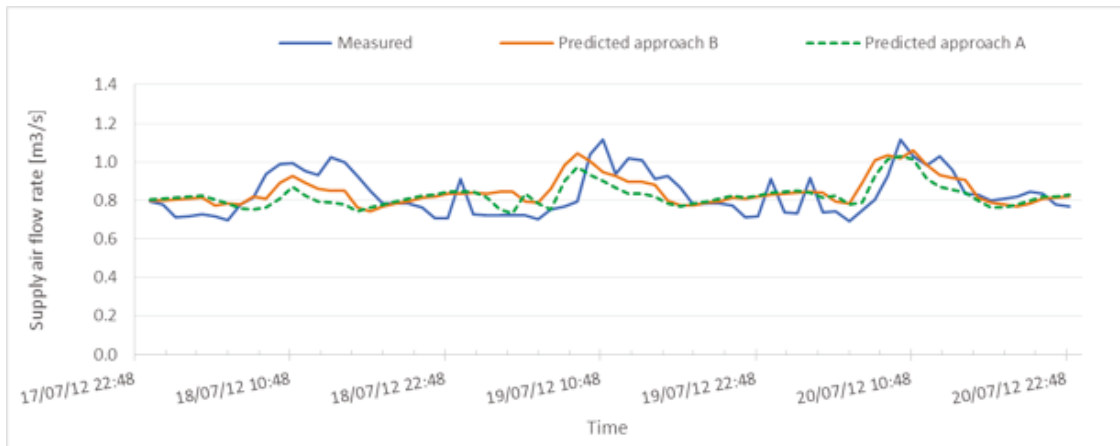


Figure D. 8: Measured vs. predicted supply air flow rate to zone 1.5 SE when using equivalent step-change schedules and when using the RP-1093 schedule, from 18th to 20th of July 2012

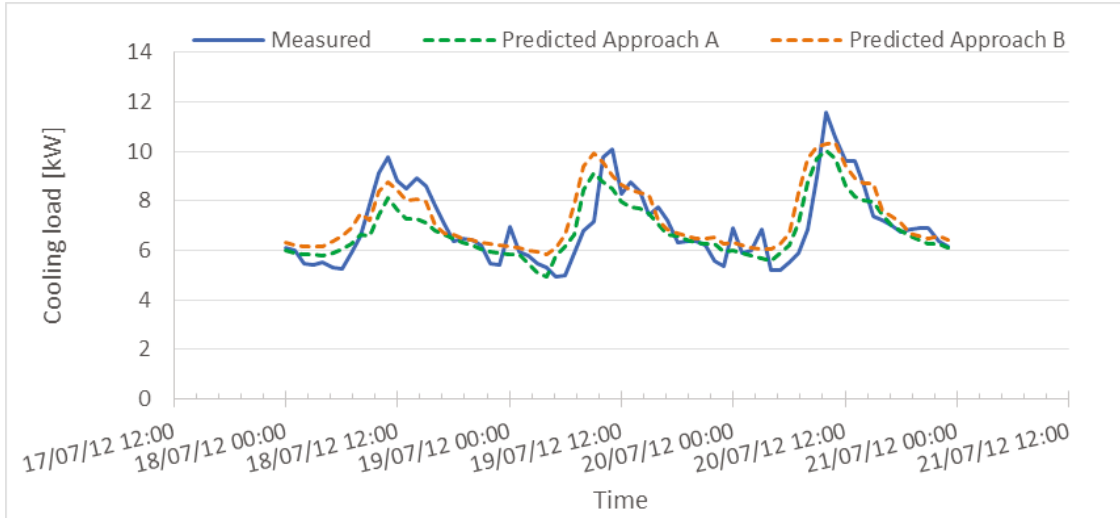


Figure D. 9: Measured vs. predicted cooling load in zone 1.5 SE when using equivalent step-change schedules and when using the RP-1093 schedule, from 18th to 20th of July 2012

Zone 1.6 NE

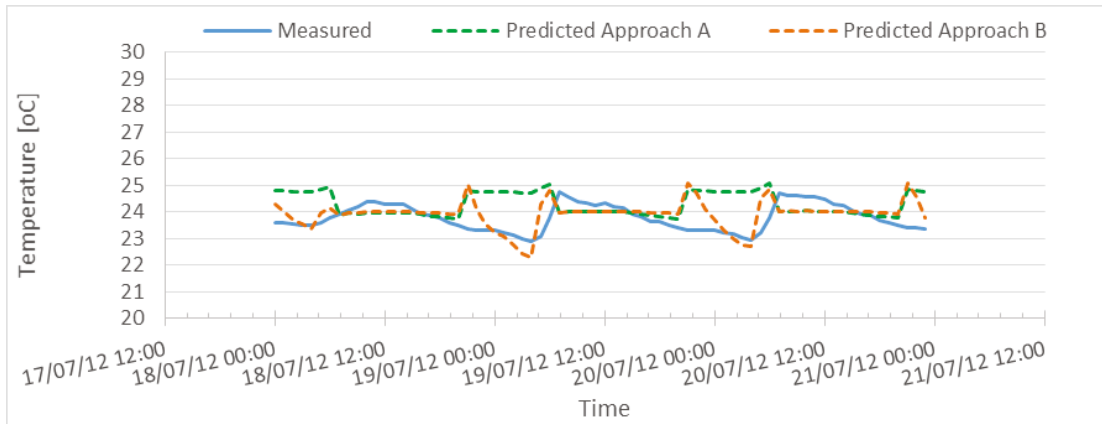


Figure D. 10: Measured vs. predicted indoor air temperature in zone 1.6 NE when using equivalent step-change schedules and when using the RP-1093 schedule, from 18th to 20th of July 2012



Figure D. 11: Measured vs. predicted supply air flow rate in zone 1.6 NE when using equivalent step-change schedules and when using the RP-1093 schedule, from 18th to 20th of July 2012

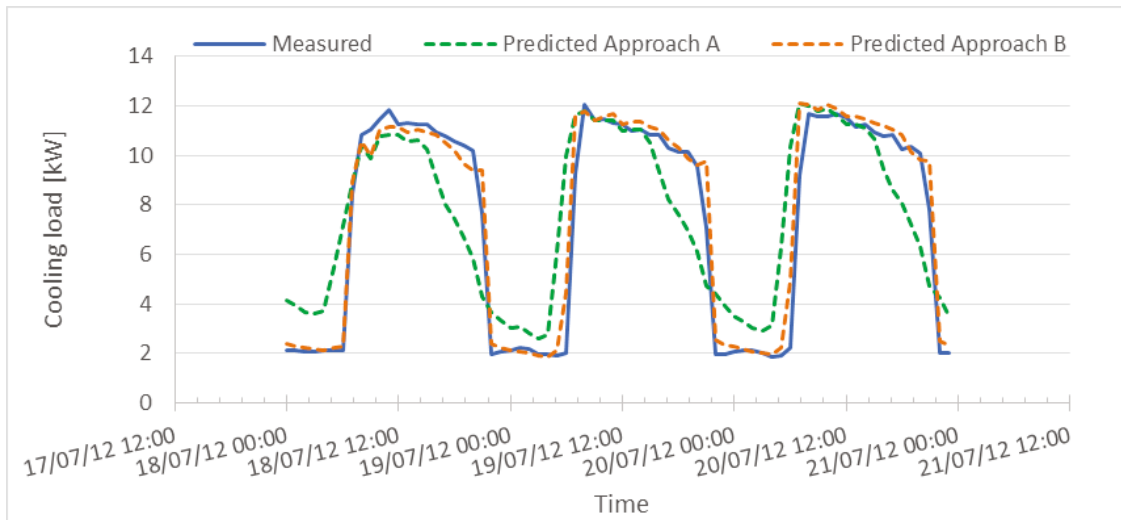


Figure D. 12: Measured vs. predicted cooling load in zone 1.6 NE when using equivalent step-change schedules and when using the RP-1093 schedule, from 18th to 20th of July 2012

Zone 2.1 NE

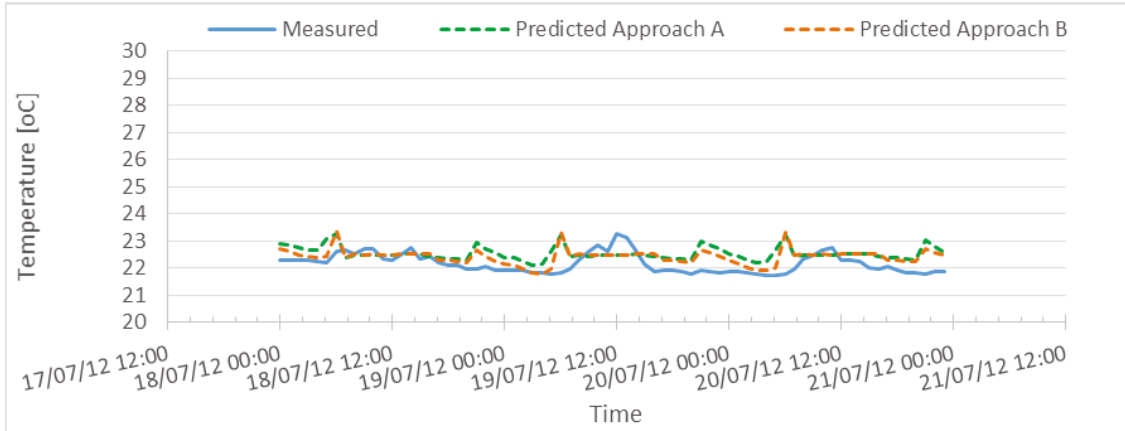


Figure D. 13: Measured vs. predicted indoor air temperature in zone 2.1 NE when using equivalent step-change schedules and when using the RP-1093 schedule, from 18th to 20th of July 2012

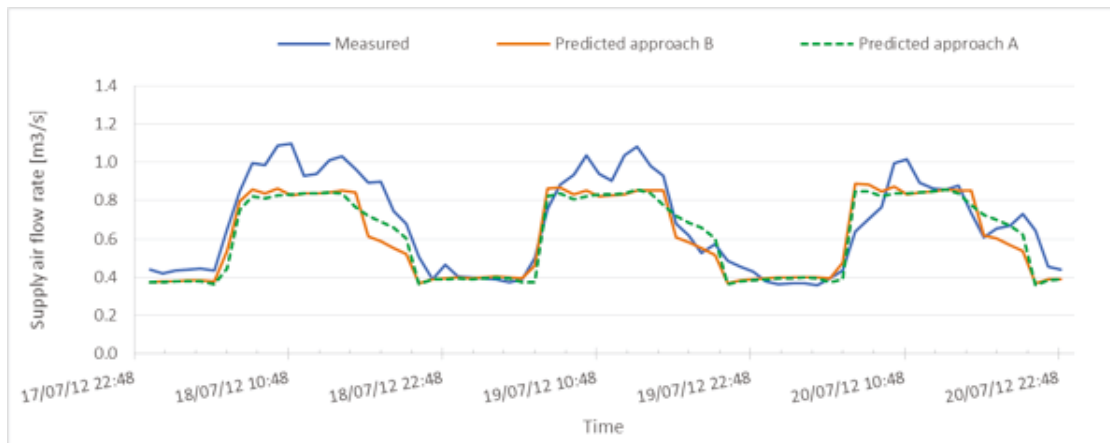


Figure D. 14: Measured vs. predicted supply air flow rate to zone 2.1 NE when using equivalent step-change schedules and when using the RP-1093 schedule, from 18th to 20th of July 2012

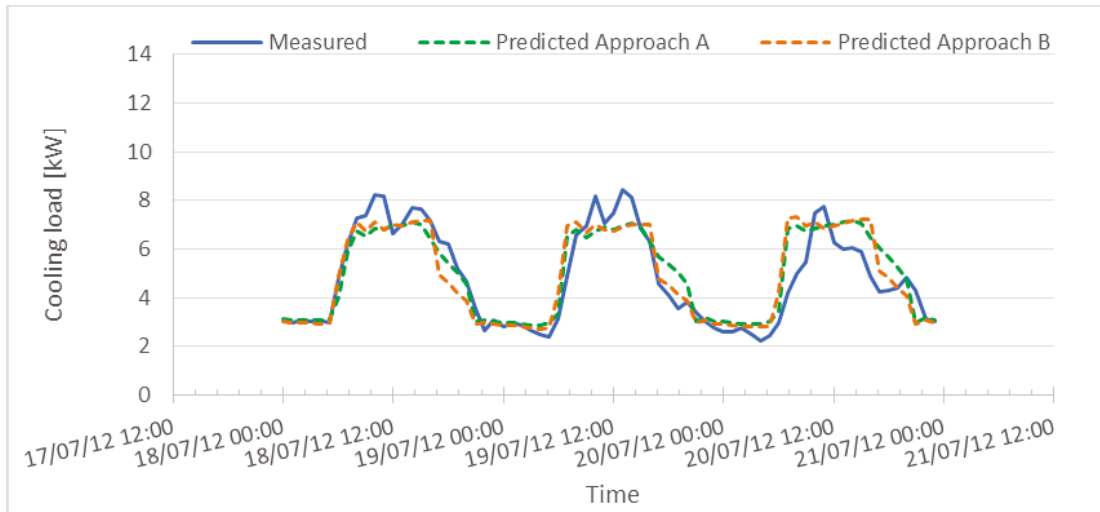


Figure D. 15: Measured vs. predicted cooling load in zone 2.1 NE when using equivalent step-change schedules and when using the RP-1093 schedule, from 18th to 20th of July 2012

Zone 2.3 NW

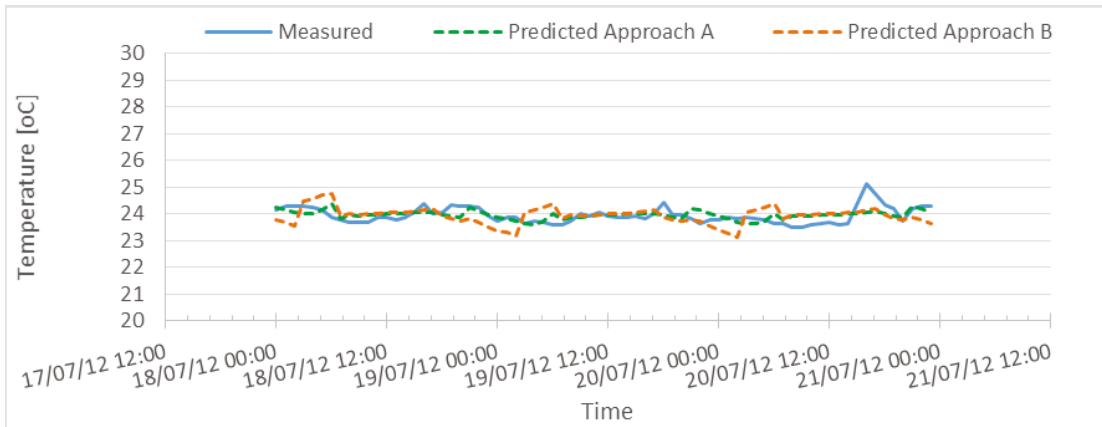


Figure D. 16: Measured vs. predicted indoor air temperature in zone 2.3 NW when using equivalent step-change schedules and when using the RP-1093 schedule, from 18th to 20th of July 2012

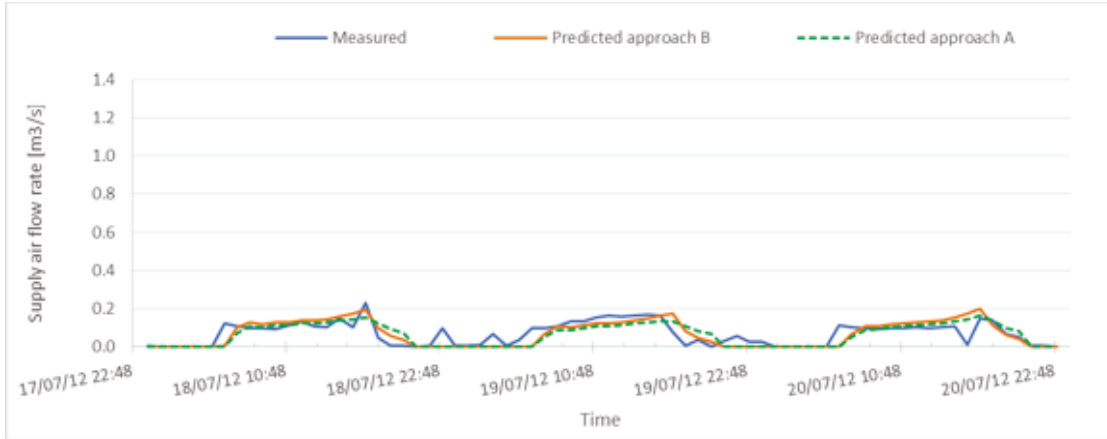


Figure D. 17: Measured vs. predicted supply air flow rate to zone 2.3 NW when using equivalent step-change schedules and when using the RP-1093 schedule, from 18th to 20th of July 2012

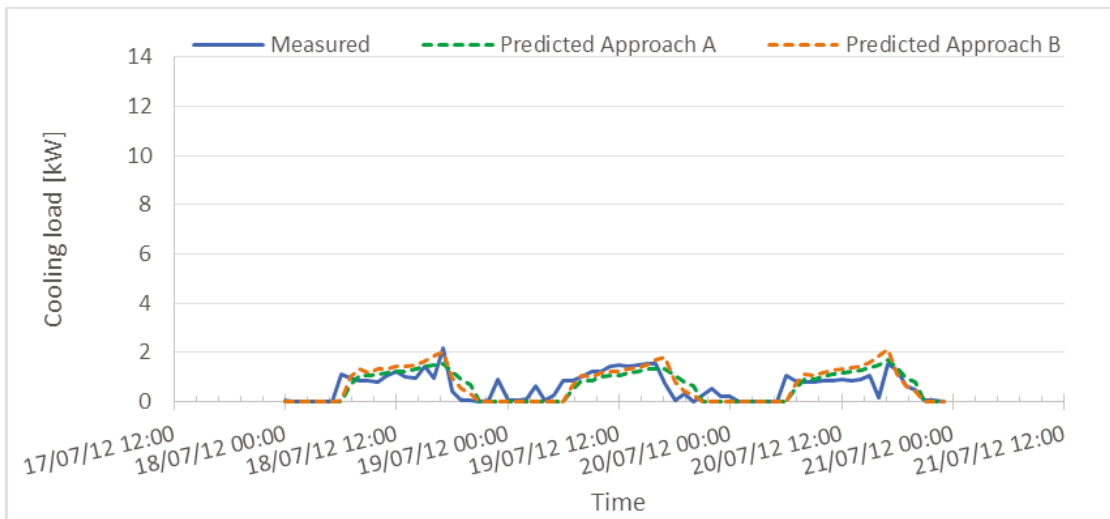


Figure D. 18: Measured vs. predicted cooling load in zone 2.3 NW when using equivalent step-change schedules and when using the RP-1093 schedule, from 18th to 20th of July 2012

Zone 2.4 SW

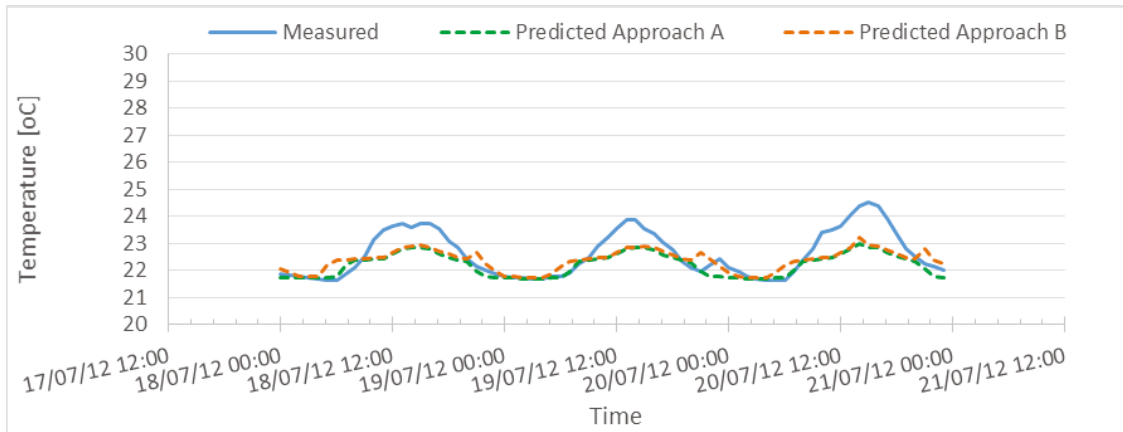


Figure D. 19: Measured vs. predicted indoor air temperature in zone 2.4 SW when using equivalent step-change schedules and when using the RP-1093 schedule, from 18th to 20th of July 2012

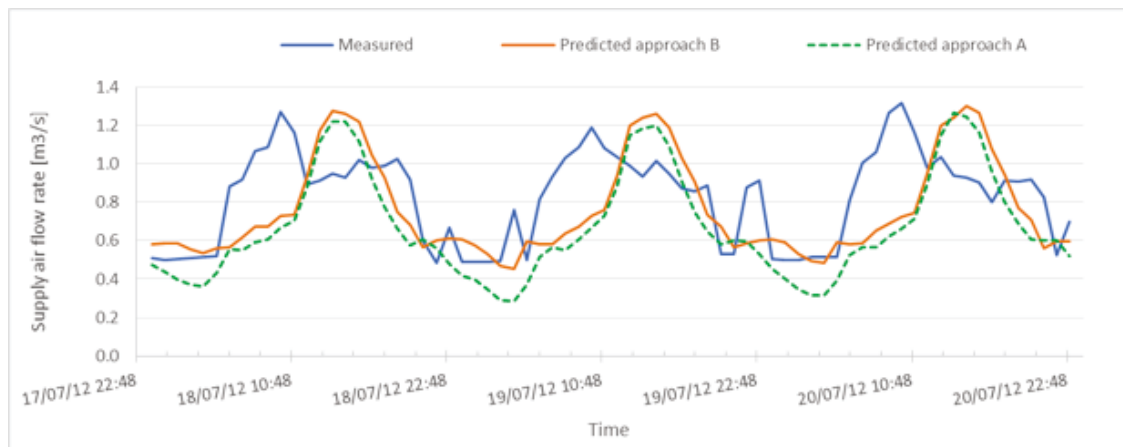


Figure D. 20: Measured vs. predicted supply air flow rate to zone 2.4 SW when using equivalent step-change schedules and when using the RP-1093 schedule, from 18th to 20th of July 2012

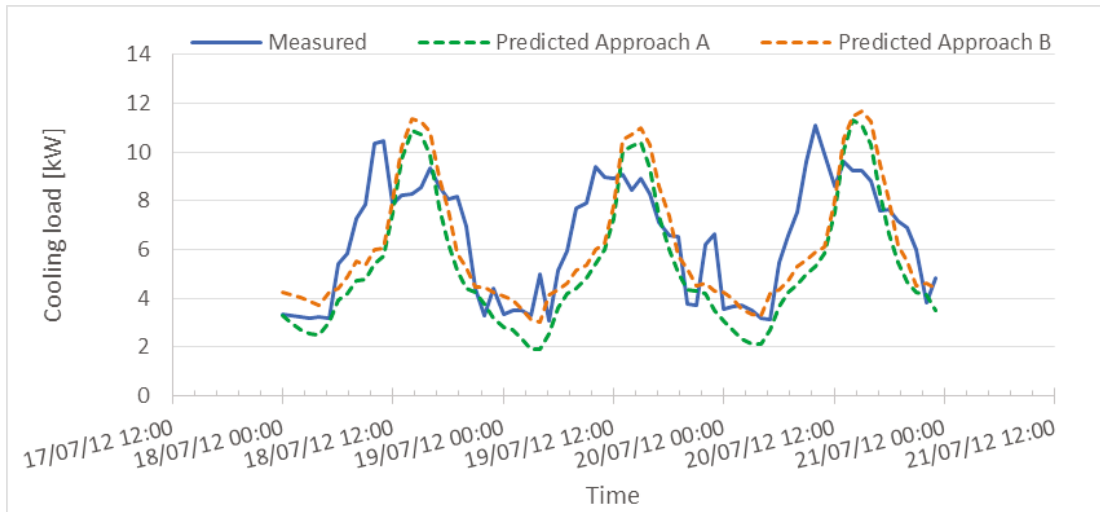


Figure D. 21: Measured vs. predicted cooling load in zone 2.4 SW when using equivalent step-change schedules and when using the RP-1093 schedule, from 18th to 20th of July 2012

Zone 2.5 SE

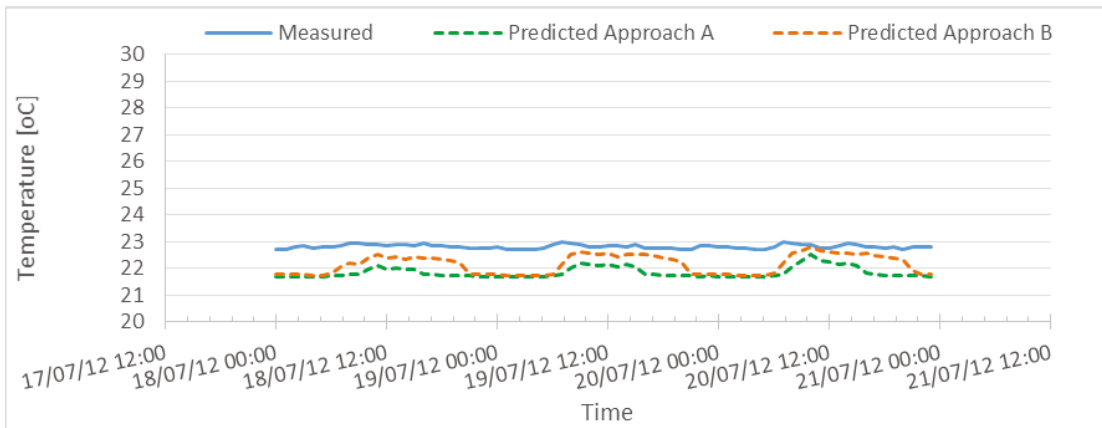


Figure D. 22: Measured vs. predicted indoor air temperature in zone 2.5 SE when using equivalent step-change schedules and when using the RP-1093 schedule, from 18th to 20th of July 2012

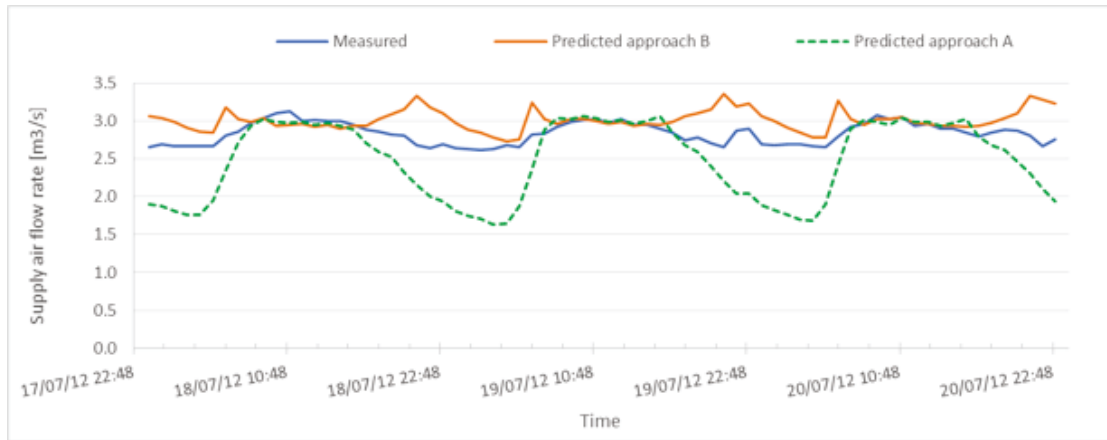


Figure D. 23: Measured vs. predicted supply air flow rate to zone 2.5 SE when using equivalent step-change schedules and when using the RP-1093 schedule, from 18th to 20th of July 2012

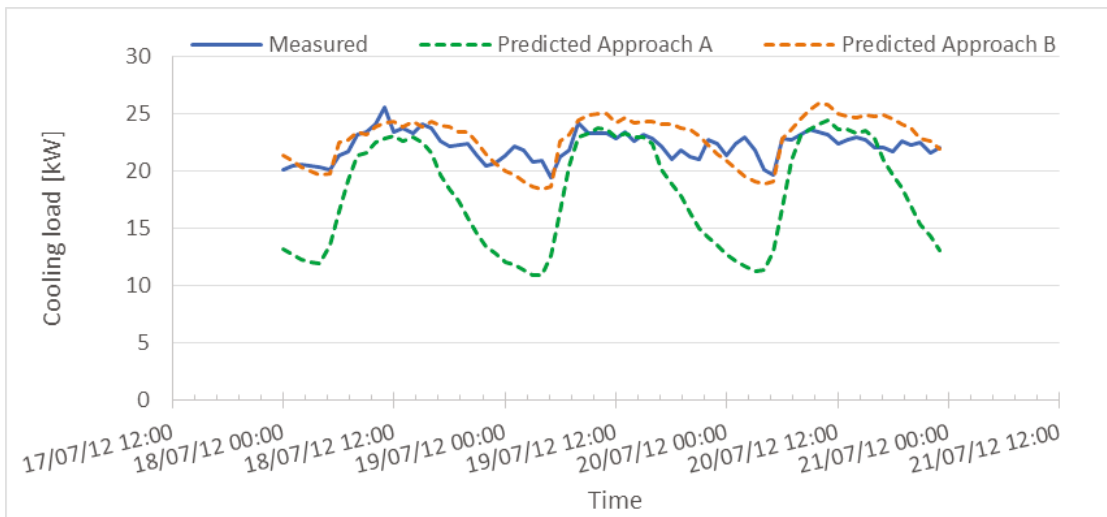


Figure D. 24: Measured vs. predicted cooling load in zone 2.5 SE when using equivalent step-change schedules and when using the RP-1093 schedule, from 18th to 20th of July 2012

Zone 2.6 NE

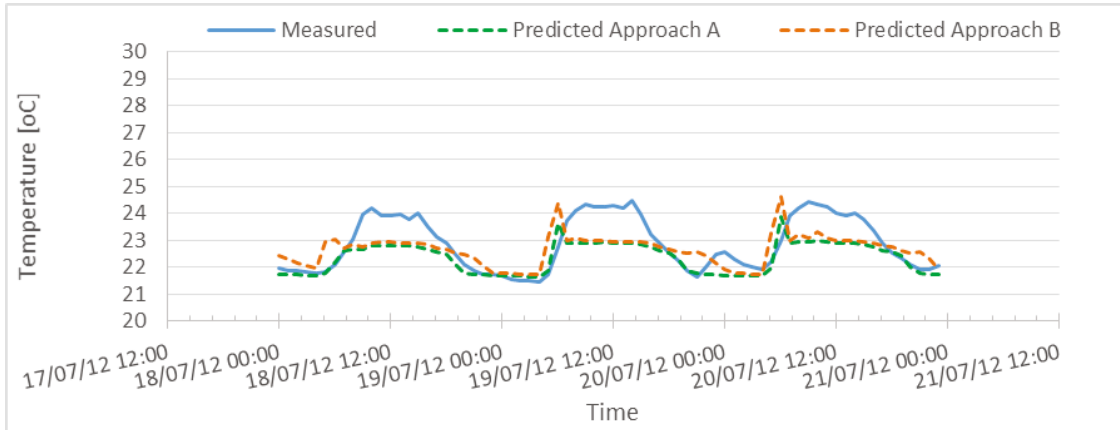


Figure D. 25: Measured vs. predicted indoor air temperature in zone 2.6 NE when using equivalent step-change schedules and when using the RP-1093 schedule, from 18th to 20th of July 2012

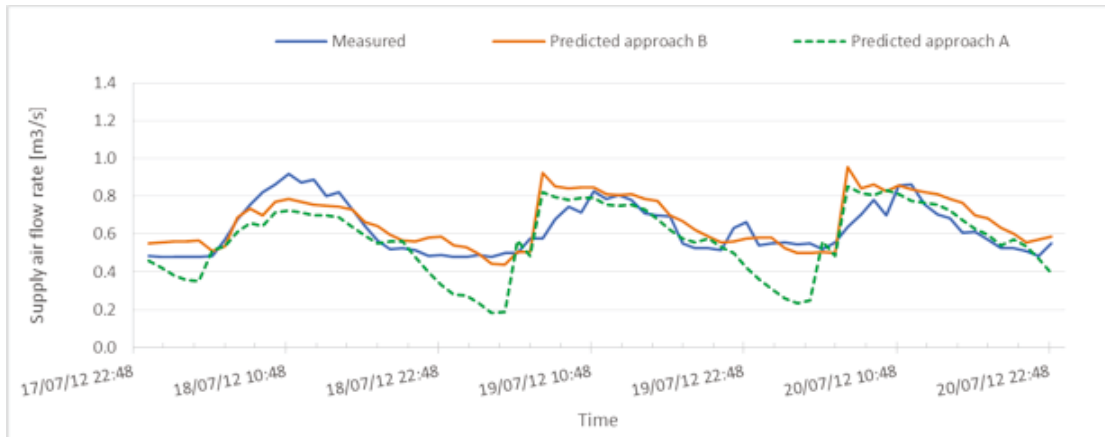


Figure D. 26: Measured vs. predicted supply air flow rate in zone 2.6 NE when using equivalent step-change schedules and when using the RP-1093 schedule, from 18th to 20th of July 2012

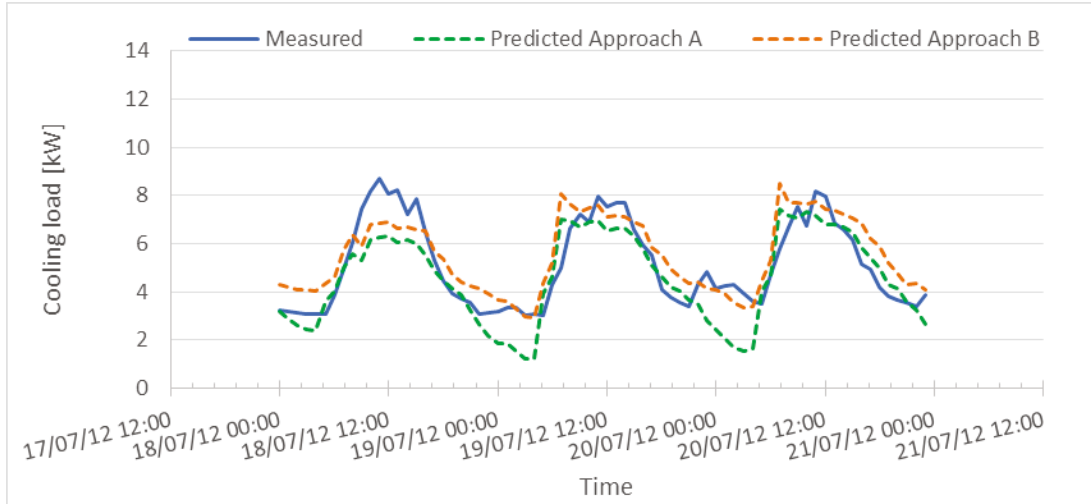


Figure D. 27: Measured vs. predicted cooling load in zone 2.6 NE when using equivalent step-change schedules and when using the RP-1093 schedule, from 18th to 20th of July 2012

Zone 3.1 NE

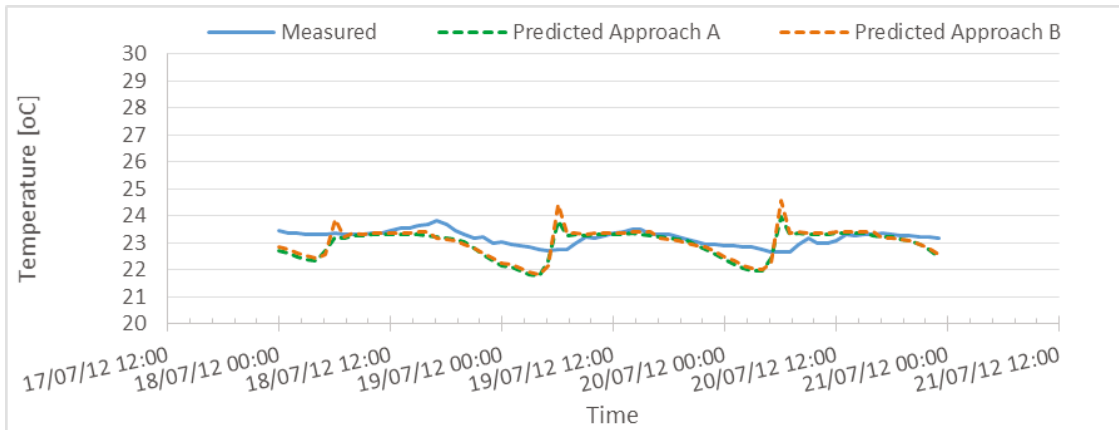


Figure D. 28: Measured vs. predicted indoor air temperature in zone 3.1 NE when using equivalent step-change schedules and when using the RP-1093 schedule, from 18th to 20th of July 2012

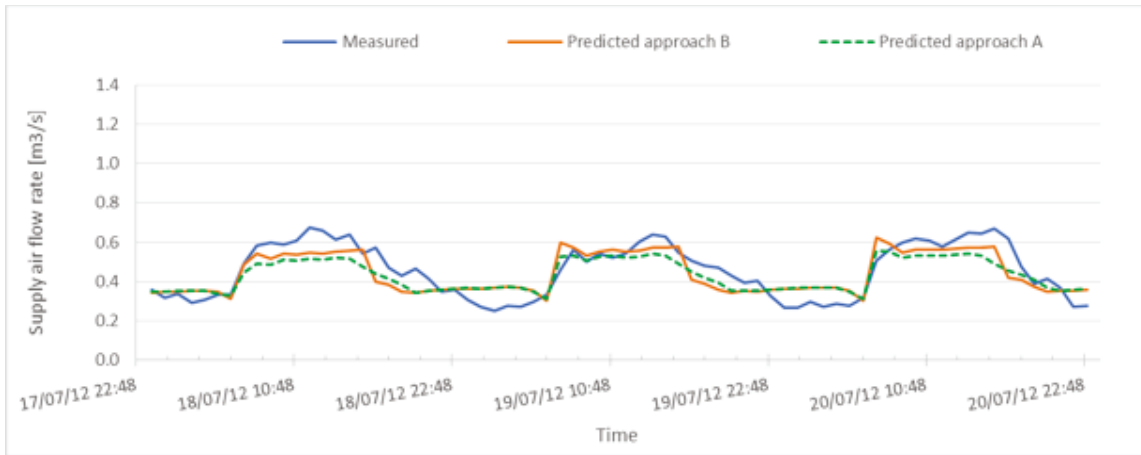


Figure D. 29: Measured vs. predicted supply air flow rate in zone 3.1 NE when using equivalent step-change schedules and when using the RP-1093 schedule, from 18th to 20th of July 2012

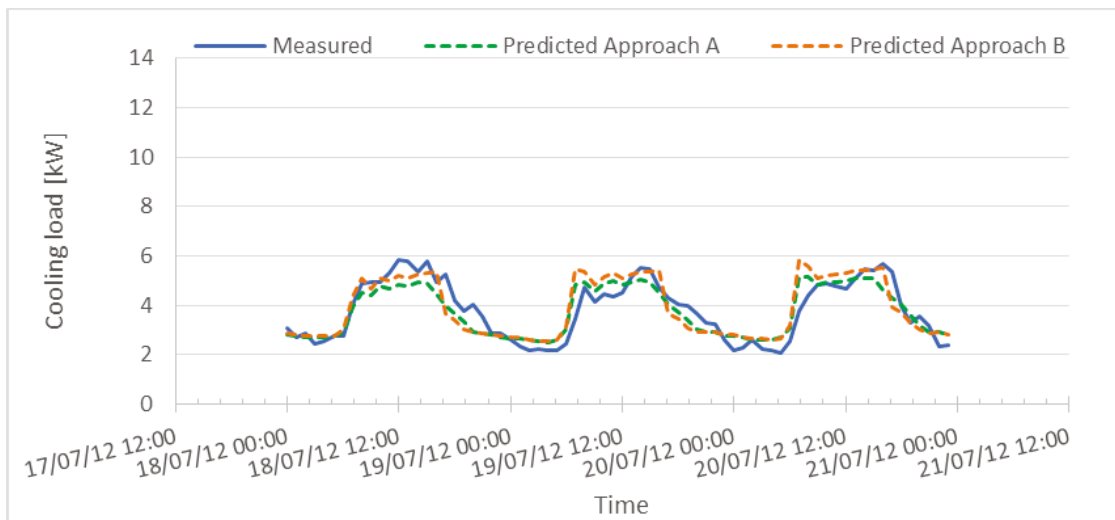


Figure D. 30: Measured vs. predicted cooling load in zone 3.1 NE when using equivalent step-change schedules and when using the RP-1093 schedule, from 18th to 20th of July 2012

Zone 3.2 SW

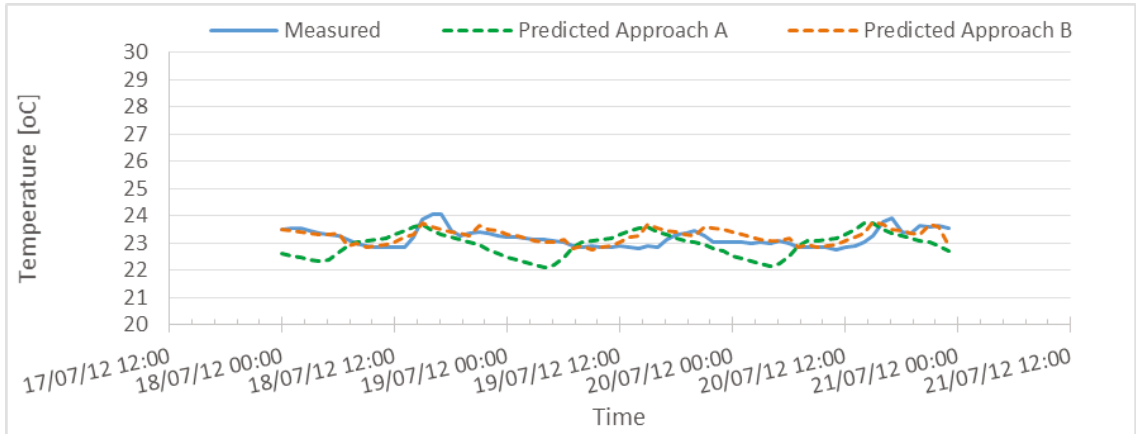


Figure D. 31: Measured vs. predicted indoor air temperature in zone 3.2 SW when using equivalent step-change schedules and when using the RP-1093 schedule, from 18th to 20th of July 2012



Figure D. 32: Measured vs. predicted supply air flow rate in zone 3.2 SW when using equivalent step-change schedules and when using the RP-1093 schedule, from 18th to 20th of July 2012

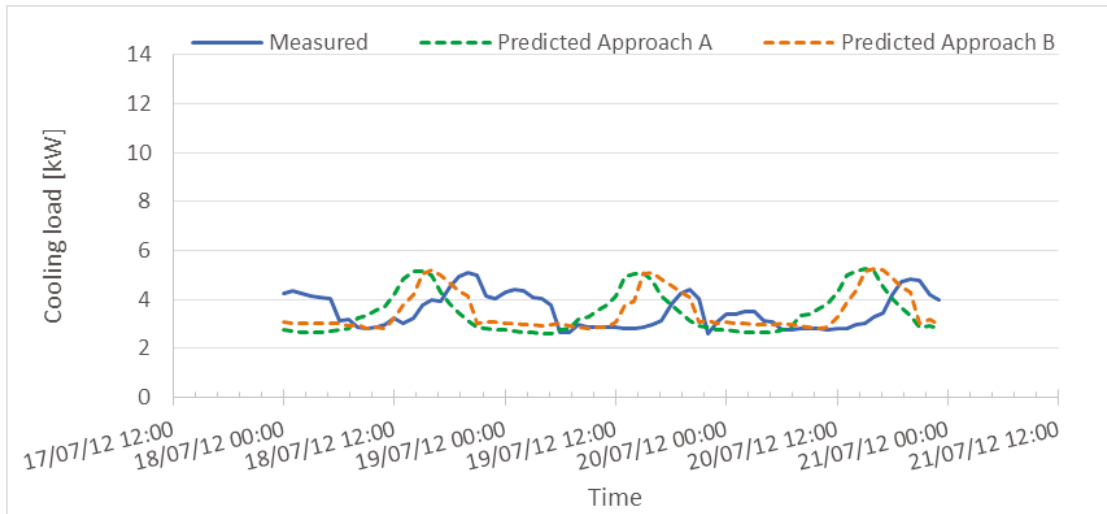


Figure D. 33: Measured vs. predicted cooling load in zone 3.2 SW when using equivalent step-change schedules and when using the RP-1093 schedule, from 18th to 20th of July 2012

Zone 3.3 NW

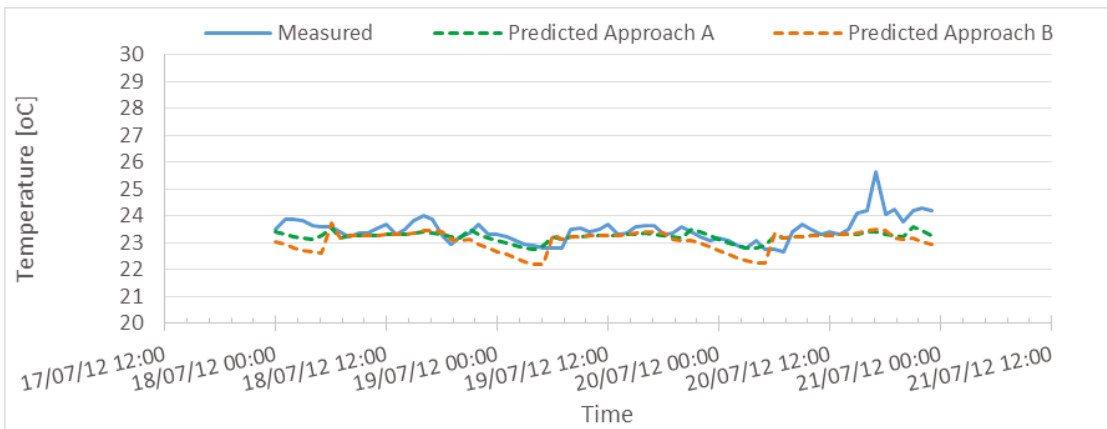


Figure D. 34: Measured vs. predicted indoor air temperature in zone 3.3 NW when using equivalent step-change schedules and when using the RP-1093 schedule, from 18th to 20th of July 2012

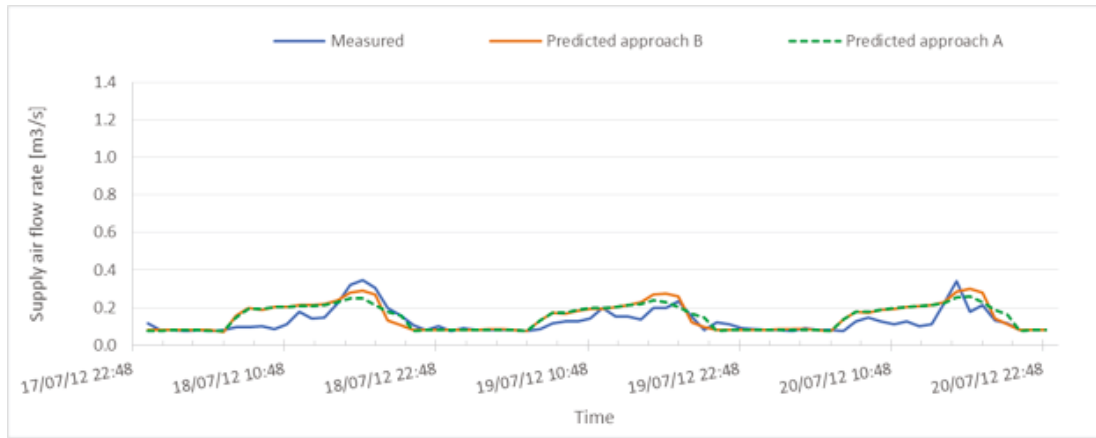


Figure D. 35: Measured vs. predicted supply air flow rate in zone 3.3 NW when using equivalent step-change schedules and when using the RP-1093 schedule, from 18th to 20th of July 2012

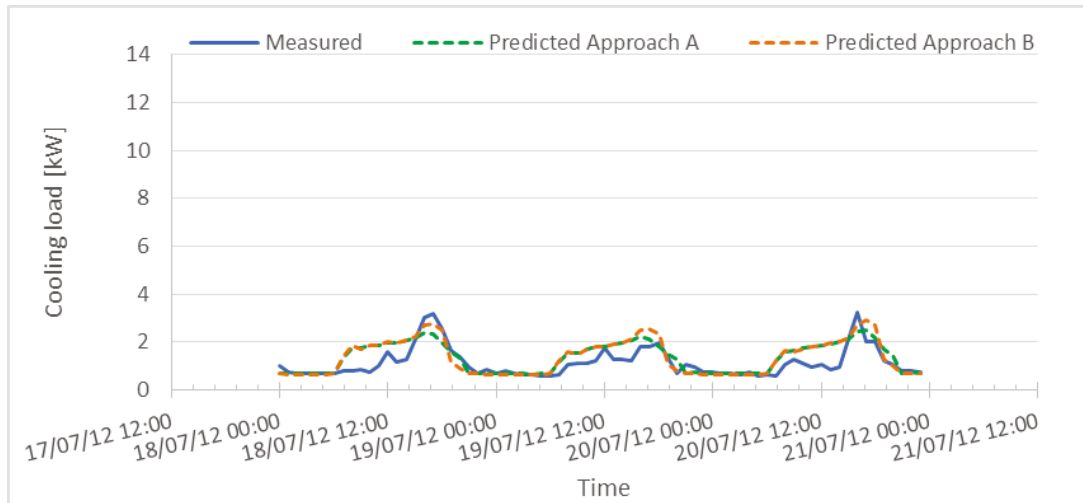


Figure D. 36: Measured vs. predicted cooling load in zone 3.3 NW when using equivalent step-change schedules and when using the RP-1093 schedule, from 18th to 20th of July 2012

Zone 3.4 SW

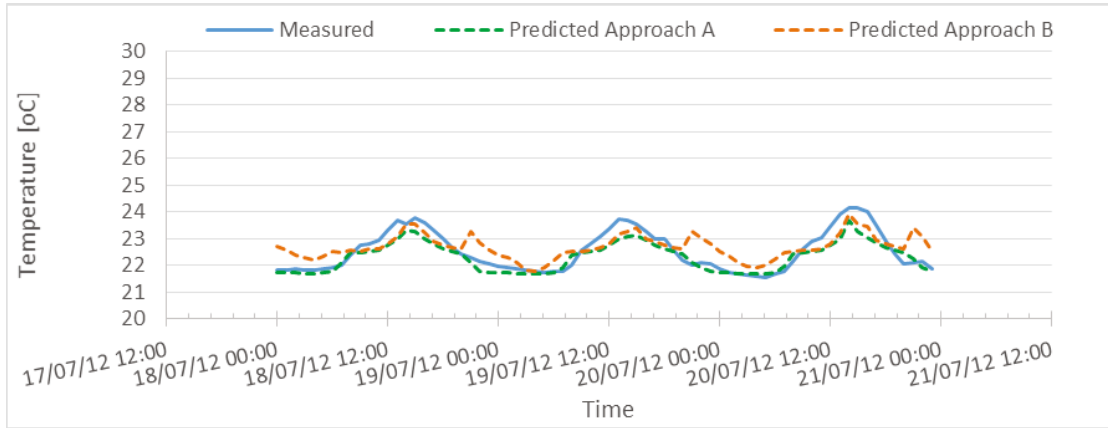


Figure D. 37: Measured vs. predicted indoor air temperature in zone 3.4 SW when using equivalent step-change schedules and when using the RP-1093 schedule, from 18th to 20th of July 2012

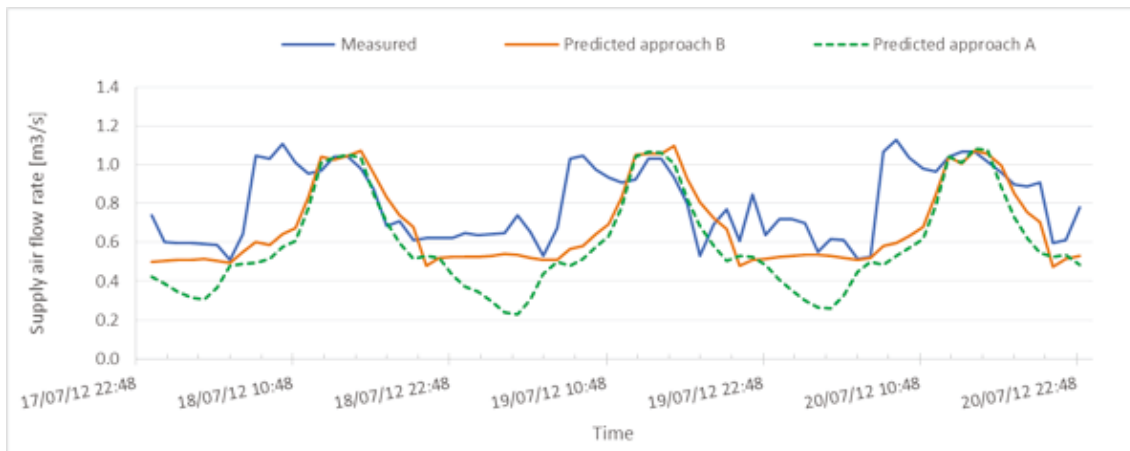


Figure D. 38: Measured vs. predicted supply air flow rate in zone 3.4 SW when using equivalent step-change schedules and when using the RP-1093 schedule, from 18th to 20th of July 2012

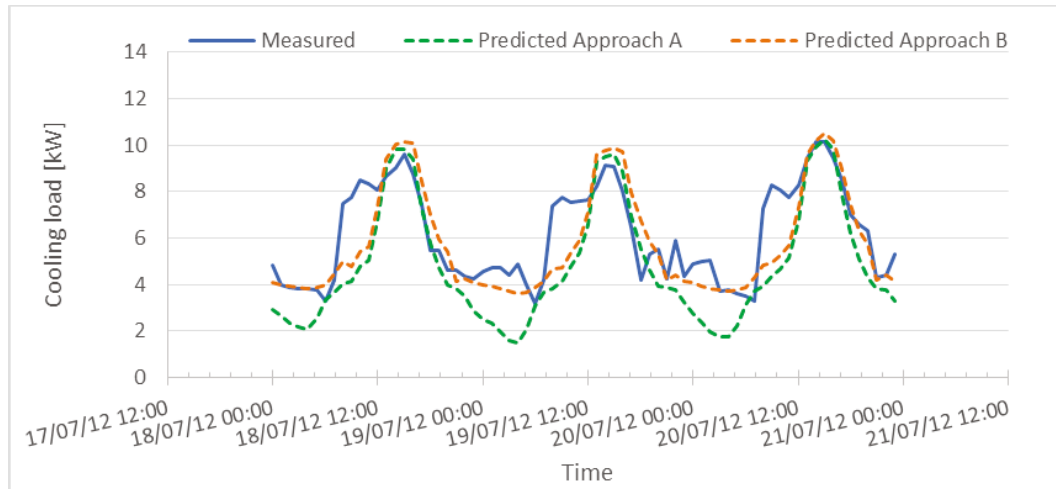


Figure D. 39: Measured vs. predicted cooling load in zone 3.4 SW when using equivalent step-change schedules and when using the RP-1093 schedule, from 18th to 20th of July 2012

Zone 3.5 SE

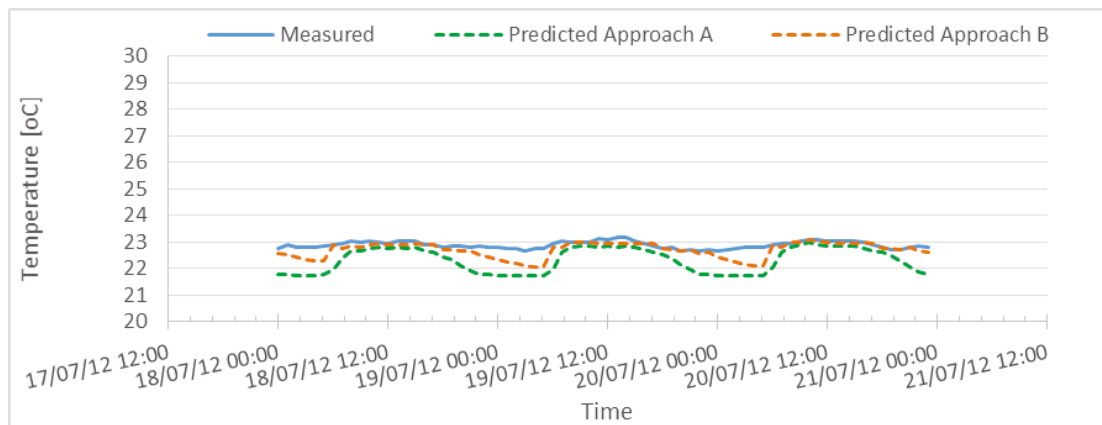


Figure D. 40: Measured vs. predicted indoor air temperature in zone 3.5 SE when using equivalent step-change schedules and when using the RP-1093 schedule, from 18th to 20th of July 2012

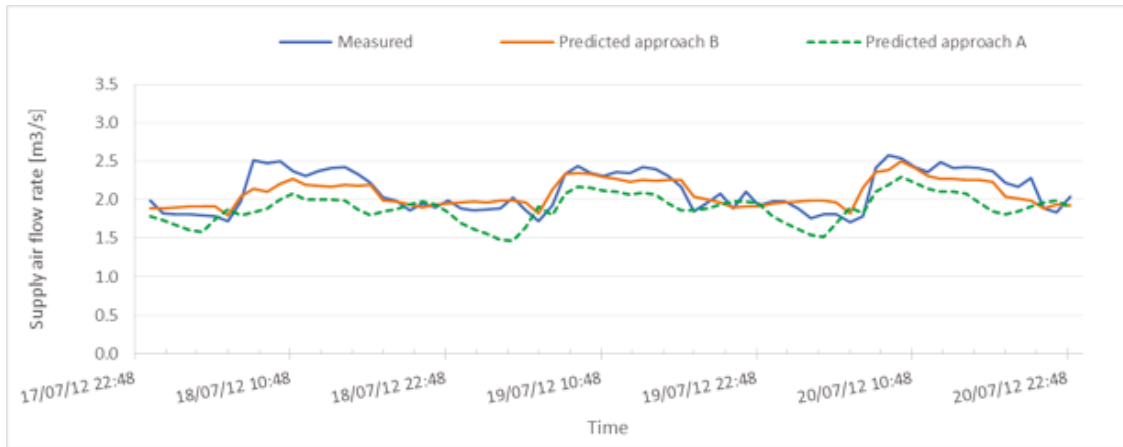


Figure D. 41: Measured vs. predicted supply air flow rate in zone 3.5 SE when using equivalent step-change schedules and when using the RP-1093 schedule, from 18th to 20th of July 2012

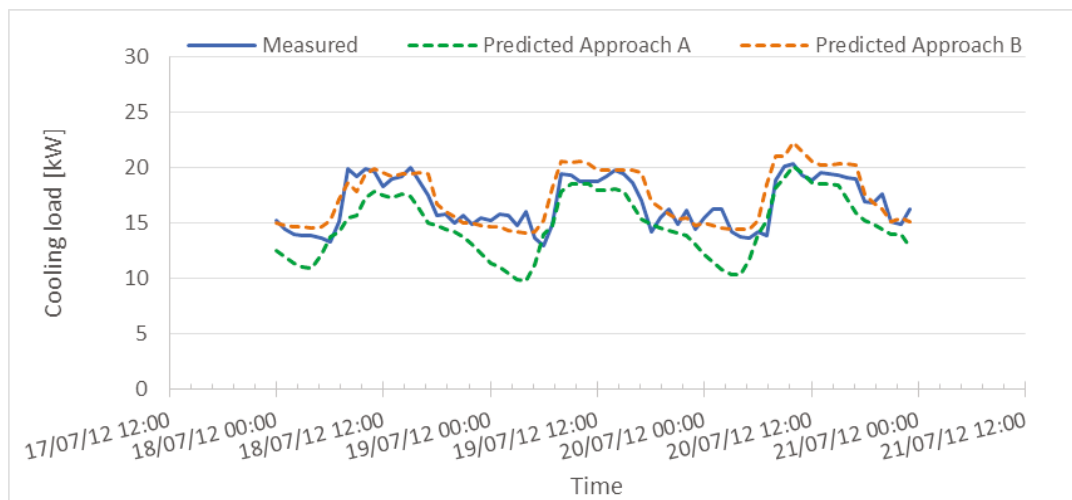


Figure D. 42: Measured vs. predicted cooling load in zone 3.5 SE when using equivalent step-change schedules and when using the RP-1093 schedule, from 18th to 20th of July 2012

Zone 3.6 NE

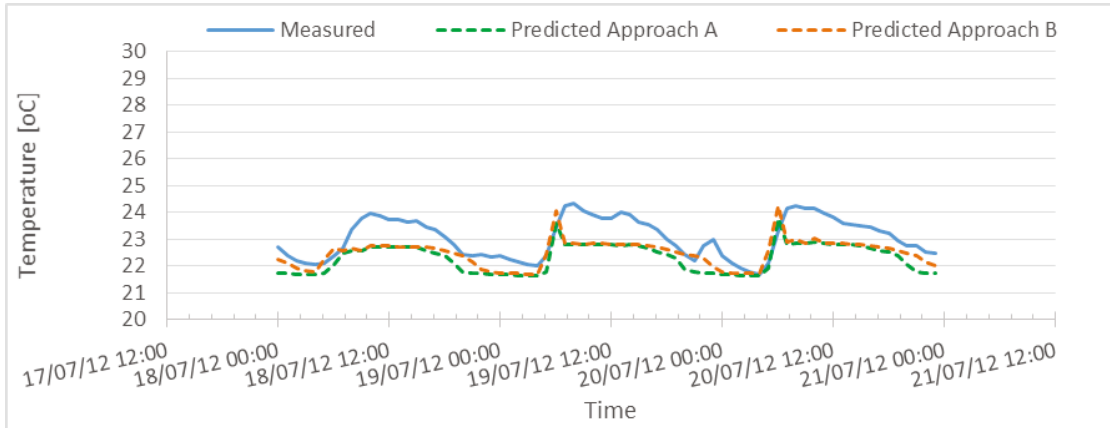


Figure D. 43: Measured vs. predicted indoor air temperature in zone 3.6 NE when using equivalent step-change schedules and when using the RP-1093 schedule, from 18th to 20th of July 2012



Figure D. 44: Measured vs. predicted supply air flow rate in zone 3.6 NE when using equivalent step-change schedules and when using the RP-1093 schedule, from 18th to 20th of July 2012

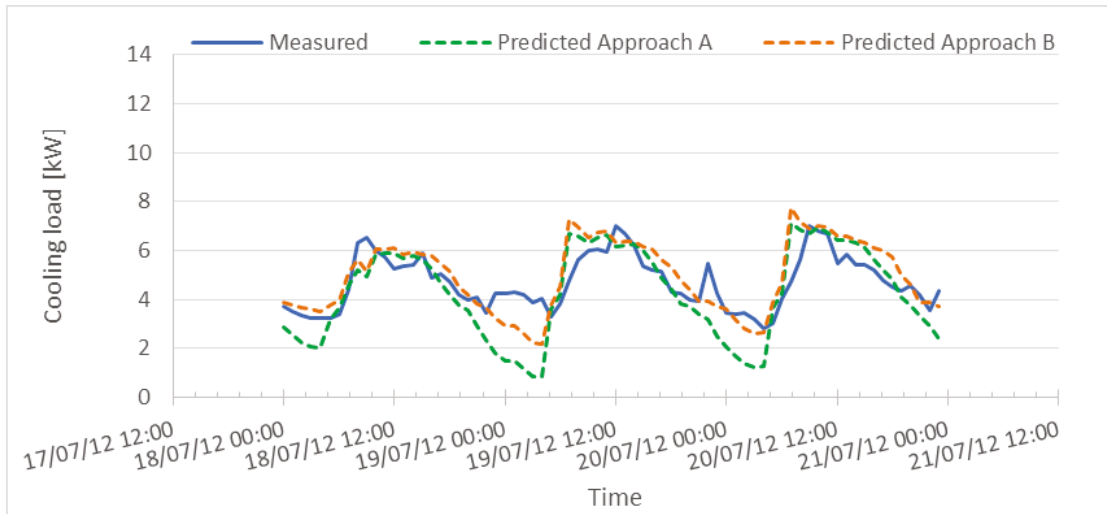


Figure D. 45: Measured vs. predicted cooling load in zone 3.6 NE when using equivalent step-change schedules and when using the RP-1093 schedule, from 18th to 20th of July 2012